TOWARDS THE HYBRID ORGANIC SEMICONDUCTOR FET (HOSFET)

ELECTRICAL AND ELECTROCHEMICAL CHARACTERIZATION OF FUNCTIONALIZED AND UNFUNCTIONALIZED, COVALENTLY BOUND ORGANIC MONOLAYERS ON SILICON SURFACES

The described research has been carried out at the "Miniaturized Systems For Biomedical And Environmental Applications" group (BIOS) of the MESA+ Research Institute at the University of Twente, Enschede, the Netherlands. The research was financially supported by the Dutch Technology Foundation (STW) as project CW/STW 790.35.704.

Samenstelling promotiecommissie:

Voorzitter	
prof. dr. ir. A. J. Mouthaan	Universiteit Twente, EWI
Promotor	
prof. dr. ir. A. van den Berg	Universiteit Twente, EWI
Assistent promotor	
dr. ir. W. Olthuis	Universiteit Twente, EWI
Leden	
prof. dr. ir. P. Bergveld	Universiteit Twente, EWI
prof. dr. ing. D. H. A. Blank	Universiteit Twente, TNW
prof. dr. E. J. R. Sudhölter	Universiteit Wageningen
prof. dr. J. Schmitz	Universiteit Twente, EWI
dr. ir. M. J. M. Pelgrom	Philips

Title: TOWARDS THE HYBRID ORGANIC SEMICONDUCTOR FET (HOSFET) – Electrical and Electrochemical Characterization of Functionalized and Unfunctionalized, Covalently Bound Organic Monolayers on Silicon Surfaces
Cover: Front-side: chips with multiple Field Effect Transistors of which the gates have been modified with Si-C linked monolayers.
Author: Erik Jouwert Faber
ISBN: 90-365-2338-9
Printing: Febodruk B.V. Enschede

TOWARDS THE HYBRID ORGANIC SEMICONDUCTOR FET (HOSFET)

ELECTRICAL AND ELECTROCHEMICAL CHARACTERIZATION OF FUNCTIONALIZED AND UNFUNCTIONALIZED, COVALENTLY BOUND ORGANIC MONOLAYERS ON SILICON SURFACES

PROEFSCHRIFT

ter verkrijging van
de graad van doctor aan de Universiteit Twente,
op gezag van rector magnificus,
prof. dr. W.H.M. Zijm,
volgens besluit van het College voor Promoties
in het openbaar te verdedigen
op donderdag 16 maart 2006 om 13.15 uur

door

Erik Jouwert Faber
geboren op 24 maart 1976
te Leeuwarden

Dit proefschrift is goedgekeurd door:

promotor: prof. dr. ir. Albert van den Berg
assistent promotor: dr. ir. Wouter Olthuis

Aan mijn ouders Rients en Dineke,
mijn broer Chris,
Amber en allen die mij inspireren

"Reality is something that you rise above
We don't see things as they are; we see them as we are
Avoiding danger is no safer in the long run
The fearful fall foul of fate as often as the reckless
…
If you have made mistakes
There is always another chance for you
You can start over again at any moment
Any little time you choose
Talk about failure
To fall is not to fail
Failure is not about falling down
Failure is staying down"

Song: "Rich"
from the album "Marrillion.com" (1999)

Table of Contents

Chapter 1

Chapter 2

Chapter 3

IMPROVEMENT OF ELECTRONIC PROPERTIES OF Si-C LINKED MONOLAYERS ON CHRYSTALLINE SILICON SURFACES: ALKENES VS. ALKYNES 49

Chapter 4

THE USE OF MOTT SCHOTTKY MEASUREMENTS TO DETERMINE THE pH RESPONSES OF ELECTROLYTE-INSULATOR-SILICON STRUCTURES 69

Chapter 7

Chapter 1

General Introduction

Abstract: In this chapter a brief introduction to this thesis is given. After an introduction to the background of this project, a brief overview of the class of Si-C linked monolayers on silicon is provided together with some points of attention for incorporation of such layers into sensing structures. Next the FET based sensors and the newly proposed Hybrid Organic Semiconductor FET (HOSFET) are introduced. Finally, the contents of this thesis are outlined.

1.1 Introduction

The BIOS, lab-on-a-chip group of the university of Twente has a long standing tradition in developing chemical sensors since its former chairholder, prof. Bergveld, invented the Ion Selective FET (ISFET) sensor more than 35 years ago [1]. Besides various FET-based sensors, such as the ChemFET [2], and ImmunoFET [3], also chemical sensors based on new materials, were developed recently, like a hydrogel based CO_2 sensor [4]. As new technologies emerged and miniaturization of devices and structures became more and more applicable, in the last decade the focus of this group was also more on integration of different functionalities into so-called lab-on-a-chips, such as the μdialysis system [5] and the Amina-Chip [6]. More recently, the research field of the BIOS-group has expanded to the fields of micro- and nano-fabrication and nano-fluidics. The core competence has nowadays been divided into 4 different sub-groups, namely: microreactors, micro-/nanofluidics, BioMEMs, and Analysis Systems and Sensors.

In a joint project proposal by prof. Sudhölter, chair holder of the organic chemistry group at the Wageningen University and prof. Bergveld, former chairholder of the BIOS-group at the University of Twente, the idea towards new functionalities and lay-out of the original FET based sensor was suggested. The new technology consists of replacing the inorganic, oxide gate insulators by a directly Si-C linked monolayer. Thereby, a new derivative with interesting new possibilities of the original ISFET is created, the Hybrid Organic Semiconductor FET or HOSFET [7]. The reason to do so is explained in section 1.2. This has led to a research carried out by two PhD students, one in each group. The research carried out in the Wageningen University was focused on the chemical surface modification of silicon surfaces and the physical characterization of such surfaces [8]. The research carried out at the BIOS group was focused on the electrical and electrochemical characterization of silicon samples modified with such monolayers and on the incorporation of functionalized monolayers into FET based sensors and the characterization thereof. This thesis contains the results of the latter study.

A short introduction on modification of silicon surfaces with Si-C linked monolayers and application fields of such layers is given in section 1.2. A short introduction on the FET based sensor and the HOSFET can be found in section 1.3 and finally the outline of this thesis is listed in section 1.4.

1.2 Si-C linked monolayers on silicon surfaces

The full control over surface properties is an ideal in the advancement of materials science. Organic monolayers have been investigated for many years and are a strong candidate to achieve this highly desired control [9]. Much of the research on organic monolayers is based on monolayers prepared by the Langmuir-Blodgett technique, the self-assembly of monolayers of thiols on gold and the chemisorption of organosilicon derivatives on silicon oxide.

An important step forward in the area of organic monolayers includes the covalent attachment of 1-alkenes and 1-alkynes onto hydrogen-terminated silicon surfaces (Figure 1.1), which has continued to attract attention ever since the first reports of Linford and Chidsey in 1993 and 1995 [10, 11].

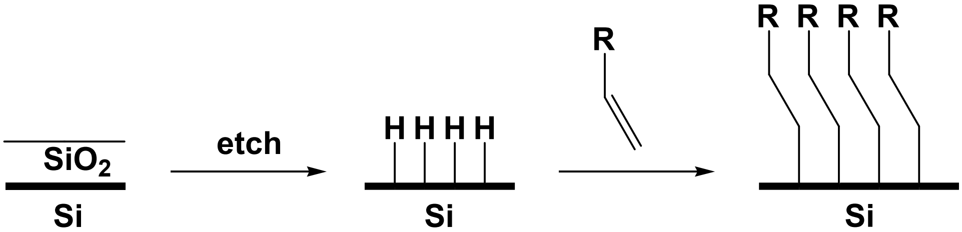

Figure 1.1. Scheme of monolayer formation on crystalline flat silicon [12].

The first step is the etching of native oxide-covered silicon surface yielding an oxide-free hydrogen-terminated surface. The most common surface orientations of silicon are the Si <100> and Si<111> facets. Interfacial Si atoms on the Si<100> surface are occupied with two hydrogen atoms (SiH_2), while the Si<111> surface is mainly occupied with Si-H groups (Figure 1.2). In the case of Si<111> an atomically flat surface is formed with terraces on the scale of ~10^2 by ~10^4 nm^2 [13, 14].

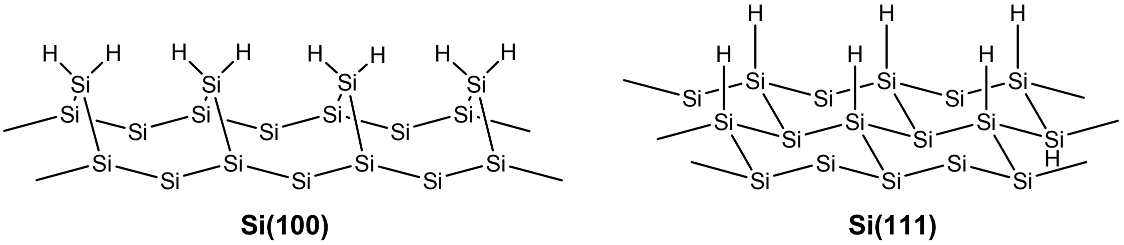

Figure 1.2. Schematic representations of the hydrogen-terminated <100> and <111> silicon surface.

Next, upon reacting with 1-alkenes or 1-alkynes a densely packed organic monolayer is formed on the surface [11]. The monolayer surface groups R (Figure 1.1) can, if desired, be further functionalized with sensing moieties. For R = H chemically inert monolayers are obtained. New synthesis routes for obtaining such layers have emerged [15-18] and the chemical and physical properties of such layers have been extensively studied and several reviews have appeared [13, 19-22]. At present time these monolayers are being applied in a variety of application fields such as passivation layers in solar cells [23, 24], anti-stiction coating films for nano-, and micro-electromechanical systems (NEMS/MEMS) [22], masking layers in lithographic processing [25], insulating films in hybrid molecule-silicon electronics [26], memory devices via incorporation of redox sites inside the monolayer [27-29] and even DNA sensing structures via functionalization of the end groups R in Figure 1.1 [30-32]. Since in this project these monolayers are to be used in sensory structures their behavior in the most likely environmental conditions, i.e. contacted via aqueous solutions, needs to be investigated. A study complemented with detailed literature overview of the electrochemical behavior of silicon electrodes modified with such monolayers is given in Chapter 5.

FET based sensors normally have (stacked) oxides as gate insulators (see section 1.3). The possible advantages of application of such monolayers as replacements of oxide insulators in FET based sensors are amongst others:

1) Si-C linked monolayers on both <100> and <111> silicon form densely packed layers, inhibiting oxidation of the underlying silicon. The surface morphology of these layers can be atomically tuned, i.e. the layers are equally flat or rough as the initial H-terminated silicon surface [11, 20]. Furthermore, chemically inert monolayers are obtained when methyl-terminated monolayers are used, whereas an H-terminated silicon surface gets oxidized in air and in water, resulting in a chemically active surface layer.
2) Such monolayers do not only provide a tremendous flexibility in tuning the surface properties, but also allow the integration of functional groups or biomolecules in monolayers on the silicon surfaces (see Figure 1.3). In this manner the (bio)organic chemistry of the monolayers can be linked to the inorganic chemistry and physical properties of silicon.

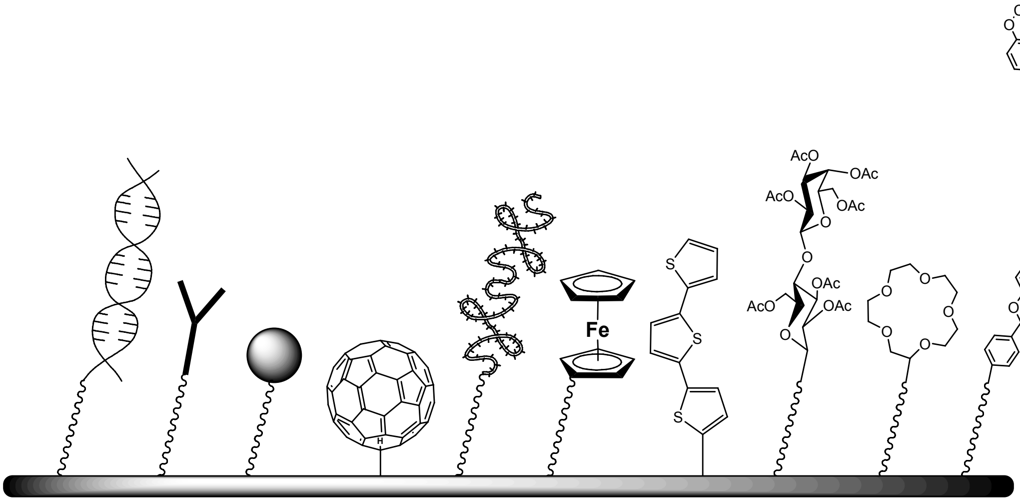

Figure 1.3. A selected number of functional groups that have been covalently attached to H-terminated silicon surfaces directly or indirectly (from left to right): DNA, antibodies, Au nanoparticles, fullerenes, proteins, ferrocene groups, oligothiophenes, carbohydrates, crown ethers, and banana-shaped liquid crystals [33].

This is in contrast to CHEMFETs with inorganic gate insulators, which consist often of complex, stacked sensing structures, necessary to create other functionalities than H^+ sensitive layers [34].

3) The chemistry of monolayer formation is very simple as compared to clean room made gate insulators. Monolayer formation requires merely wet-bench chemistry. The temperatures stay quite low (maximum of 160° C for thermally activated alkylation reactions [17]) as compared to clean room made insulators. Furthermore, no additional process step is required after monolayer formation whereas inorganic insulators require often annealing and curing steps after the initial deposition or growing step of the insulator.
4) Besides these advantages in the chemical domain also advantages are expected with respect to the noise and detection limit of the HOSFET as compared to the ISFET. Since such nm-thin insulators are used the overall insulator capacitance increases as compared to the capacitance of inorganic insulators of which the thickness is in general in the order of 100 nm. A higher capacitance will lead to an increase of the field-effect and also an increase in sensitivity would then be expected. However, due to the construction of most practical ISFET read-out circuitries [34] increasing the insulator capacitance does not lead to a direct increase in sensitivity but it does have a beneficial influence on the detection limit and noise behavior of the FET. This is explained in more detail in Chapter 6.

In summary, via the modification of inorganic, silicon surfaces with organic monolayers hybrid structures are created, which are of particular interest in sensor technology, since it allows one to combine the bioorganic world of, e.g. molecular recognition to the one of semi-conductor technology. One possible strategy to realize the desired transduction of the molecular recognition process into an electrical output is based on field-effect transistors (FETs), in which the conventional SiO_2 layer is replaced by an organic monolayer (see section 1.3). From a chemical point of view the requirements for the design of functional monolayers for sensor applications can be formulated as follows.

1) The ideal modified surface applicable for FET technology has to meet requirements in different areas. First, functional groups (receptors) that have the ability to detect specific molecules or ions should be attached to the surface or the organic layer. This can be realized via the direct attachment of (bio-)functionalized alkenes or via indirect attachment schemes. The first approach requires mild surface modification conditions, while the latter ideally involves a multi-step procedure of well-defined monolayer functionalization.
2) In addition, since a linear response between the ligand concentration and the sensor output is desirable, the ideal functionalized layer probably contains isolated receptor structures that are separated by regions that do not bind to ligand or other ions and molecules present in the detection solution. In other words, heterogeneous monolayers have to be prepared and the compounds used for the latter type of domain should have bio-resistant properties.
3) The sensor is supposed to record only specific receptor-ligand interactions. Consequently the organic monolayers should be as much as possible electrically and chemically insulating. Figure 1.4 summarizes the different desired properties and characteristics of the monolayer in order to make it a feasible sensor interface.

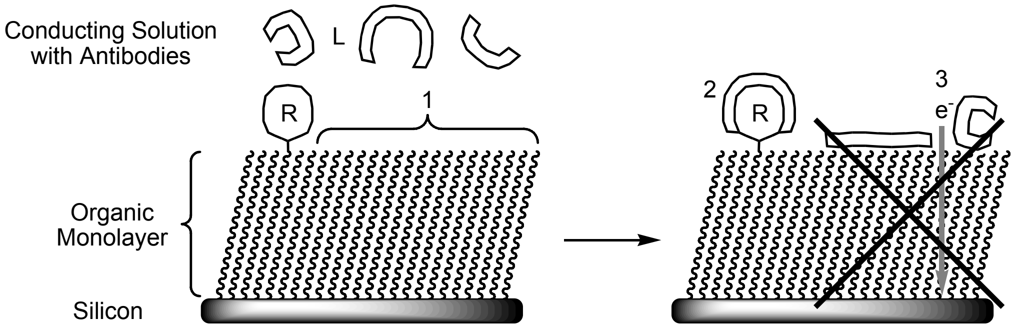

Figure 1.4. Schematic representation of an organic monolayer attached to a surface in order to visualize the desired properties and characteristics of the monolayer. The receptor (R) specifically binds (2) to only one of the ligands (L). None of the ligands binds to other regions (1) of the organic monolayer due to bio-resistant properties. The monolayer should be electrically insulating (3).

1.3 FET-based sensors and the HOSFET

A FET based sensor measures basically changes in electric surface potential on the gate insulator area that occur when specific interaction between bulk species and surface species takes place. In case of an insulator area modified with (bio)molecular receptor groups one could speak of (bio)molecular recognition events taking place; in case of an insulator area modified with simple receptors for ion detection one speaks of simple site-binding events. The simplest site-binding reaction is that of H^+ ions with hydrated surface X-OH (receptor) groups (X = Ta, Al, or Si) on oxide gate insulators as can be found in the ISFET [34]. The result of such specific interactions between protons and charged groups on the insulator surface, i.e. so-called (de)protonation of surface X-OH groups (X = Ta, Al, Si etc.), is depicted in Figure 1.5.

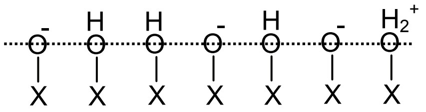

Figure 1.5. Graphical interpretation of (de)protonation of surface X-OH groups (X = Ta, Al, Si etc.).

In case of the HOSFET the oxide gate insulator of the original ISFET (depicted in Figure 1.6A) has been replaced with an organic monolayer to which functional receptor groups R can be attached as desired (depicted in Figure 1.6B). Also indicated in Figure 1.6A is the two-terminal Electrolyte-Insulator-Silicon (EIS) structure, which can be regarded as the functional building block of the FET sensor and which is used to test functionalities and site-binding interactions of silicon samples modified with (un)functionalized monolayers (see Chapters 4, 5, and 6).

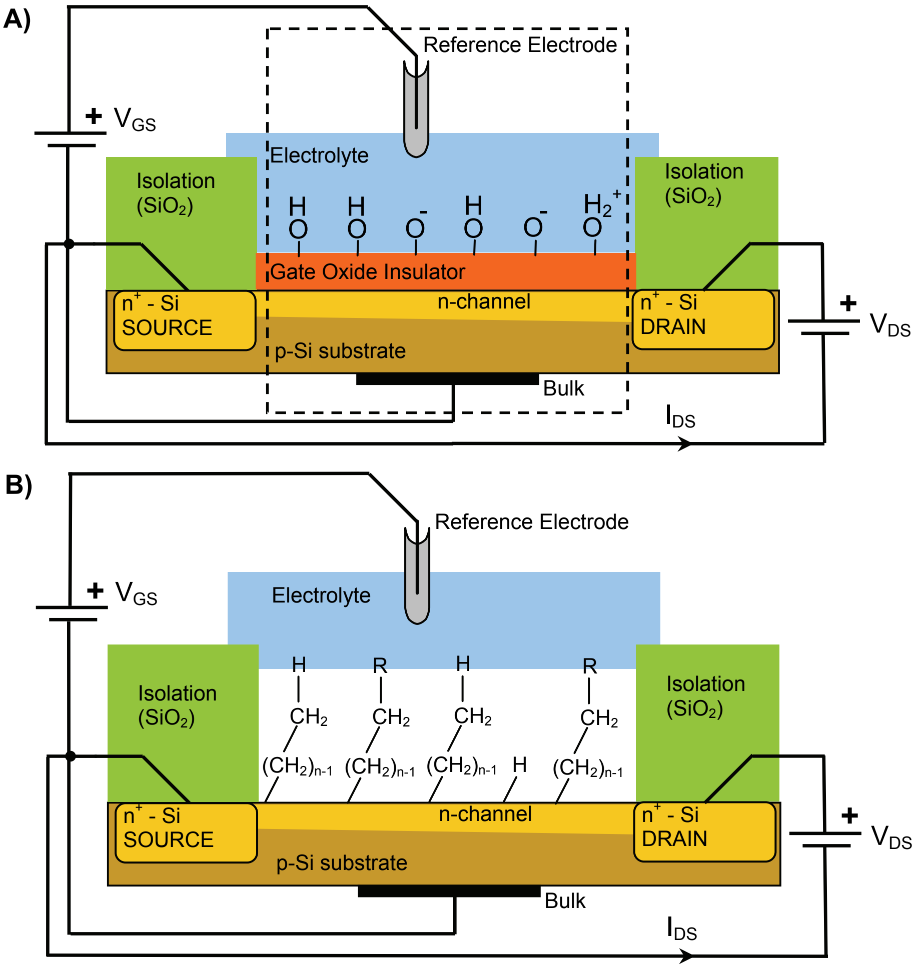

Figure 1.6. Schematic drawings of four terminal n-channel FET devices: A) conventional ISFET and B) HOSFET. The drawing of an EIS-structure is marked via the dashed box in A).

The potential advantages of replacing the oxide insulator have already been mentioned in the previous section together with the demands imposed on the monolayer for creating successful sensors. From an electrical and material point of view the requirements for the design of functional monolayers for sensor applications can be formulated as follows.

1) The FET in Figure 1.6B still requires (clean room made) source and drain regions, as well as source, drain and bulk contacts, and the isolation oxide which masks the gate area. Therefore the most likely fabrication route of the HOSFET is that the complete FET device is manufactured without monolayer, which is consecutively processed in the final stage of the FET fabrication. This is due to the fact that the monolayer will not survive the high temperatures needed for making the source, drain and bulk regions and contacts in the clean room. In the following two process steps for monolayer fabrication as indicated in Figure 1.1 the complete FET on its turn is exposed to the HF and (heated) organic solvents, consecutively [17]. This means that both the FET device should not be negatively affected by the chemicals used in this process and the monolayer on its turn should not suffer from materials at the FET that negatively influence its quality. Preferably, the gate dimensions

should be such that surface characterization techniques can be applied to investigate the monolayer after formation. In case of EIS-test structures (Figure 1.6A) no source, drain and isolation oxide are necessary so site binding reactions at functionalized monolayers can always be measured in this way.

2) The monolayer should be electrically insulating or show low leakage so that a change in species bound to the receptors is sensed by the underlying silicon via the field effect. It can be intuitively understood that a monolayer consisting of longer chains (a larger *n* in Figure 1.6B) shows better insulating properties (see also Chapter 2). A detailed description of FET based sensors and the here discussed issues can be found in Chapter 6.

1.4 Outline of this thesis

Prior to the implementation in FET based sensors the electronic properties of the silicon-monolayer devices need to be understood. This aspect has been studied via the formation of Metal-Insulator-Silicon (MIS) structures and the results of these studies are described in Chapters 2 and 3. Chapter 2 deals with the electronic properties of such monolayers in n-type and p-type <100> Si-C_nH_{2n+1} MIS-devices (n = 10, 12, 16, and 22) and covers current-voltage behavior, capacitance-voltage behavior and the electrical properties of the silicon-monolayer interface. In Chapter 3 the same behavior and properties are investigated of in this case n-type Si-$C_{18}H_{37}$ MIS devices where the parameters of interest were the substrate orientation (<100> vs. <111>) and the molecule type (1-alkyne vs. 1-alkene). This data is complemented with XPS-measurements.

The other chapters concern studies in the electrochemical domain. Chapter 4 deals with a Mott Schottky measurement technique to determine site-binding interactions at EIS-structures with thin insulators such as the organic monolayers. Its usability and validity is compared with commonly used techniques for characterizing EIS-structures with thick (> 10 nm) insulators that can no longer be used for characterizing the EIS-structures with organic monolayers.

In Chapter 5 a detailed study on the electrochemical behavior of EIS-structures with unfunctionalized monolayers is given. Such unfunctionalized monolayers should be chemically inert and upon pH changes no charging of surface groups should occur. However, in the presence of small residual SiO_2 sites a *pH* sensitivity can be expected. This has been measured and the results are compared both with simulations obtained via a site-binding model and measurements on reference EIS-structures with (modified) SiO_2 surfaces. Furthermore, the capacitance-voltage, drift and hysteresis behavior of such EIS-structures is treated. Also their behavior under both anodic and cathodic potentials is investigated via cyclic voltammetry experiments.

In Chapter 6 a collection of measurements on HOSFETs is given. In the first study chips with 24 FETs of which the gate insulators (organic monolayers, 70 nm SiO_2, native oxide, or Si-H) were covered with evaporated aluminum contacts and were characterized via standard $I_{DS} - V_{GS}$, $I_{DS} - V_{DS}$, and $I_{GS} - V_{GS}$ measurements. In the second study the *pH* responses of HOSFETs with unfunctionalized monolayers were determined and compared with the results of Chapter 5 and ISFETs with SiO_2 gates. In the last study ion-sensing (Na^+ and K^+) measurements of HOSFETs and EIS-structures with functionalized monolayers containing the 15-crown-5 crown ether receptor are presented. These results are complemented with simulations via an adapted site binding model describing the theoretical behavior of devices with such functionalized monolayers.

Finally, in Chapter 7 the overall conclusions and an iteration of the conclusions per chapter are given, followed by recommendations for further research.

1.5 References

[1] P. Bergveld, "Development of an Ion-Sensitive Solid-State Device for Neurophysiological Measurements", *IEEE Transactions on Biomedical Engineering* **1970**, *BME-17*, 70.

[2] A. van den Berg, *Ion Sensors based on ISFETs with Synthetic Ionophores*, PhD thesis, University of Twente (Enschede), **1988**.

[3] R. B. M. Schasfoort, *A new approach to ImmunoFET operation*, PhD thesis, University of Twente (Enschede), **1989**.

[4] S. Herber, *Development of a hydrogel-based carbon dioxide sensor*, PhD thesis, University of Twente (Enschede), **2005**.

[5] S. Böhm, *The comprehensive integration of microdialysis membranes and silicon sensors*, PhD thesis, University of Twente (Enschede), **2000**.

[6] B. H. Timmer, *AMINA-chip*, PhD thesis, University of Twente (Enschede), **2004**.

[7] E. J. R. Sudhölter, H. Zuilhof, A. B. Sieval, L. C. P. M. de Smet, G. M. Visser, P. Bergveld, W. Olthuis, E. J. Faber, patent EP 1 363 122 A1, **2003**

[8] L. C. P. M. de Smet, *Covalently Bound Organic Monolayers on Silicon Surfaces: Visible Light Attachment, Characterization and Electrical Properties*, PhD thesis, Wageningen University (Wageningen), **2006**.

[9] A. Ulman, *An Introduction to Ultrathin Organic Films: From Langmuir-Blodgett to Self-Assembly*, Academic Press, New York, **1991**.

[10] M. R. Linford, C. E. D. Chidsey, "Alkyl Monolayers Covalently Bonded to Silicon Surfaces", *Journal of the American Chemical Society* **1993**, *115*, 12631.

[11] M. R. Linford, P. Fenter, P. M. Eisenberger, C. E. D. Chidsey, "Alkyl Monolayers on Silicon Prepared from 1-Alkenes and Hydrogen-Terminated Silicon", *Journal of the American Chemical Society* **1995**, *117*, 3145.

[12] A. B. Sieval, A. L. Demirel, J. W. M. Nissink, M. R. Linford, J. H. van der Maas, W. H. de Jeu, H. Zuilhof, E. J. R. Sudhölter, "Highly stable Si-C linked functionalized monolayers on the silicon (100) surface", *Langmuir* **1998**, *14*, 1759.

[13] D. D. M. Wayner, R. A. Wolkow, "Organic modification of hydrogen terminated silicon surfaces", *Journal of the Chemical Society-Perkin Transactions 2* **2002**, 23.

[14] G. S. Higashi, R. S. Becker, Y. J. Chabal, A. J. Becker, *Comparison of Si(111) Surfaces Prepared Using Aqueous-Solutions of NH_4F Versus HF, Vol. 58*, **1991**.

[15] A. Bansal, X. L. Li, I. Lauermann, N. S. Lewis, S. I. Yi, W. H. Weinberg, "Alkylation of Si surfaces using a two-step halogenation Grignard route", *Journal of the American Chemical Society* **1996**, *118*, 7225.

[16] C. H. deVilleneuve, J. Pinson, M. C. Bernard, P. Allongue, "Electrochemical formation of close-packed phenyl layers on Si(111)", *Journal of Physical Chemistry B* **1997**, *101*, 2415.

[17] A. B. Sieval, V. Vleeming, H. Zuilhof, E. J. R. Sudhölter, "An improved method for the preparation of organic monolayers of 1-alkenes on hydrogen-terminated silicon surfaces", *Langmuir* **1999**, *15*, 8288.

[18] R. Boukherroub, S. Morin, F. Bensebaa, D. D. M. Wayner, "New synthetic routes to alkyl monolayers on the Si(111) surface", *Langmuir* **1999**, *15*, 3831.

[19] J. M. Buriak, "Organometallic chemistry on silicon and germanium surfaces", *Chemical Reviews* **2002**, *102*, 1271.

[20] A. B. Sieval, R. Linke, H. Zuilhof, E. J. R. Sudhölter, "High-quality alkyl monolayers on silicon surfaces", *Advanced Materials* **2000**, *12*, 1457.

[21] S. F. Bent, "Organic functionalization of group IV semiconductor surfaces: principles, examples, applications, and prospects", *Surface Science* **2002**, *500*, 879.

[22] N. Shirahata, A. Hozumi, T. Yonezawa, "Monolayer-derivative functionalization of non-oxidized silicon surfaces", *Chemical Record* **2005**, *5*, 145.

[23] N. S. Lewis, "Frontiers of research in photoelectrochemical solar energy conversion", *Journal of Electroanalytical Chemistry* **2001**, *508*, 1.

[24] N. S. Lewis, "Chemical control of charge transfer and recombination at semiconductor photoelectrode surfaces", *Inorganic Chemistry* **2005**, *44*, 6900.

[25] N. Saito, S. Youda, K. Hayashi, H. Sugimura, O. Takai, "Chemical resistivity of self-assembled monolayer covalently attached to silicon substrate to hydrofluoric acid and ammonium fluoride", *Surface Science* **2003**, *532*, 970.

[26] D. Vuillaume, "Nanometer-scale organic thin film transistors from self-assembled monolayers", *Journal of Nanoscience and Nanotechnology* **2002**, *2*, 267.

[27] Q. L. Li, G. Mathur, M. Homsi, S. Surthi, V. Misra, V. Malinovskii, K. H. Schweikart, L. H. Yu, J. S. Lindsey, Z. M. Liu, R. B. Dabke, A. Yasseri, D. F. Bocian, W. G. Kuhr, "Capacitance and conductance characterization of ferrocene-containing self-assembled monolayers on silicon surfaces for memory applications", *Applied Physics Letters* **2002**, *81*, 1494.

[28] E. A. Dalchiele, A. Aurora, G. Bernardini, F. Cattaruzza, A. Flamini, P. Pallavicini, R. Zanoni, F. Decker, "XPS and electrochemical studies of ferrocene derivatives anchored on n- and p-Si(1 0 0) by Si-O or Si-C bonds", *Journal of Electroanalytical Chemistry* **2005**, *579*, 133.

[29] K. M. Roth, A. A. Yasseri, Z. M. Liu, R. B. Dabke, V. Malinovskii, K. H. Schweikart, L. H. Yu, H. Tiznado, F. Zaera, J. S. Lindsey, W. G. Kuhr, D. F. Bocian, "Measurements of electron-transfer rates of charge-storage molecular monolayers on Si(100). Toward hybrid molecular/semiconductor information storage devices", *Journal of the American Chemical Society* **2003**, *125*, 505.

[30] F. Wei, B. Sun, Y. Guo, X. S. Zhao, "Monitoring DNA hybridization on alkyl modified silicon surface through capacitance measurement", *Biosensors & Bioelectronics* **2003**, *18*, 1157.

[31] W. Liao, F. Wei, M. X. Qian, X. S. Zhao, "Characterization of protein immobilization on alkyl monolayer modified silicon(111) surface", *Sensors and Actuators B-Chemical* **2004**, *101*, 361.

[32] W. Cai, J. R. Peck, D. W. van der Weide, R. J. Hamers, "Direct electrical detection of hybridization at DNA-modified silicon surfaces", *Biosensors and Bioelectronics* **2004**, *19*, 1013.

[33] L. C. P. M. de Smet, *Covalently Bound Organic Monolayers on Silicon Surfaces: Visible Light Attachment, Characterization and Electrical Properties*, PhD thesis, Wageningen University (Wageningen), **2006**, chapter 1, p. 3.

[34] P. Bergveld, A. Sibbald, *Analytical and Biomedical Applications of Ion-Selective Field-Effect Transistors, Vol. XXIII*, Elsevier, **1988**.

Chapter 2

Electronic Properties of Si-C Linked Organic Monolayers on Crystalline Silicon Surfaces*

Abstract: In this Chapter the influence of silicon surface modification via Si-C_nH_{2n+1} (n = 10, 12, 16, and 22) monolayer-based devices on p-type <100> and n-type <100> silicon is studied by forming MIS (metal-insulator-semiconductor) diodes using a mercury probe. From current density - voltage (*J*-*V*) and capacitance - voltage (*C*-*V*) measurements the relevant parameters describing the electrical behavior of these diodes are derived, such as the diode ideality factor (n), the effective barrier height ($q\phi_{eff}$), the flatband voltage (V_{fb}), the barrier height ($q\phi_B$), the monolayer dielectric constant (ε_r), the tunneling attenuation factor (β) and the fixed charge density (N_f). It is shown that the *J*-*V* behavior of these MIS-structures can be precisely tuned via the monolayer thickness. The use of n-type silicon results in lower diode ideality factors as compared to p-type silicon. A similar flatband voltage, independent of monolayer thickness, is found, indicating similar properties for all silicon-monolayer interfaces. An exception is the C_{10}-based monolayer device on p-type silicon. Furthermore, low values of N_f are found for monolayers on p-type silicon (~ $6 \cdot 10^{11}$ cm^{-2}). From stability measurements, performed after months of storage in open air, it is shown that the *J*-*V* curves stay intact for all samples irrespective of their chain length. For p-type silicon the flatband voltage shifts to more negative values over time, indicating the built in of extra positive charges, which is associated with some oxide formation. These results suggest that Si-C linked monolayers on flat silicon may be a viable material for future electronic devices.

---

[*] This Chapter has been published apart from section 2.3.5 as:
E. J. Faber, L. C. P. M. de Smet, W. Olthuis, H. Zuilhof, E. J. R. Sudhölter, P. Bergveld, A. van den Berg, "*Si-C linked Organic Monolayers on Crystalline Silicon Surfaces as Alternative Gate Insulators*", ChemPhysChem **2005**, *6*, 2153.

2.1 Introduction

The focus of this research is on the implementation of organic monolayers in silicon sensor technology. In order to understand the electronic behavior of such monolayers and the properties of the silicon-monolayer interface prior to incorporation in sensors a study on the solid-state behavior of silicon modified with a number of these monolayers has been conducted of which the results are presented in this chapter and in the following chapter.

The ongoing downscaling of MOSFETs in semiconductor industry has strongly stimulated the research of both new insulating materials on silicon and well-controlled Si-insulator interfaces. The demand for new insulators has divided the research into two categories. The demand for thinner gate oxides has driven the SiO_2 gate oxide thickness towards its fundamental limits [1-3], which resulted in a search for a replacement of the thus far commonly used SiO_2 insulator by alternative materials with sometimes opposite, specific requirements. To decrease the leakage currents through the gate, a thicker insulator is required. Since at the same time the capacitance of the gate insulator needs to remain constant, this has resulted in an intensive search for high-K dielectrics [4].

Alternatively, the continuous downscaling of structural dimensions, leading to a higher density of interconnect lines and thinner insulating layers between them, has increased the capacitive coupling between the lines. Replacing the current SiO_2 insulating layer with, in this case, a low-K dielectric layer is imperative to lower this capacitive coupling, resulting in a quest for low-K dielectrics [5, 6].

One of the recently explored, new insulating materials on silicon are covalently bound organic monolayers. Various features of these monolayers such as synthesis routes, comparison with monolayers on other surfaces and electrical properties have already been investigated.

Two categories of other, well-known monolayers on silicon are self-assembled monolayers on oxidized silicon surfaces and those formed by the Langmuir-Blodgett technique. Modification and properties of these types of monolayers have been well studied so far [7, 8]. The third category, organic alkyl monolayers covalently bound to oxide-free hydrogen-terminated silicon surfaces, is under investigation since approximately ten years. Nevertheless, this research field has expanded dramatically since the first papers by Linford et al. [9, 10]. Different preparation methods have been developed [10-14], and the (non-electrical) properties of these monolayers have been investigated and discussed in several reviews [15-18].

From both a chemical and electrical point of view passivation of the silicon surface via directly bound monolayers offers better possibilities as compared to other monolayer preparation techniques. The monolayers are bound via strong, covalent Si-C bonds, which provide a well-defined monolayer, shown to be stable to hot solvents, acids and bases [10, 15]. Thermal stability up to 615 K was observed under ultrahigh vacuum conditions [19]. Chemical, mechanical and thermal stability of this type of layers is thus better as compared to monolayers on silica or gold or monolayers prepared via the Langmuir-Blodgett method [7, 8, 20]. By the construction of MIS-devices (Metal-Insulator-Semiconductor) the electrical behavior of organic monolayers prepared on silicon surfaces with a thin native oxide was studied by the groups of Vuillaume [21-24] and Cahen [25-28]. They showed that the insulating properties of native oxide were greatly improved by the organic monolayer, indicating the outstanding insulating properties of these layers. The Si-O-C bonds, however, are susceptible towards hydrolysis and are thermally labile [10, 29]. Additionally, the presence of a thin oxide layer makes it impossible to investigate the direct influence of the alkyl monolayer on the silicon surface properties.

Organic monolayers on oxide-free surfaces offer a promising alternative due to the formation of real monolayer-silicon interfaces and a well-defined surface morphology, and may serve as new insulating materials in molecular electronic devices. The fabrication method via "wet-bench chemistry" is relatively easy and cheap [15], as compared to insulators made under clean room conditions. Moreover, the Si-C linked monolayer has a similar thickness as currently state-of-the-art gate oxides and has outstanding electrical properties as is explored in a number of studies. One example of such a device is for instance the MIS diode [30, 31], in which the monolayer acts as insulating barrier, and precisely tunes the desired current-voltage behavior [32-34]. The influence of substrate doping on the quality of Si-$C_{18}H_{37}$ | Al MIS-structures was recently investigated by Miramond et al. [35] They found that organic monolayers bound to heavily doped n-type (n^+) wafers showed a lower electrical performance as compared to similar monolayers on p^+-, p- and n-doped wafers. Furthermore, Kar et al. [36] focused on the insulating and passivation properties of these monolayers via the determination of the interface state density, while Sieval et al. [37] and Webb et al. [38] established this via lifetime measurements. Dielectric properties of such monolayers have been studied by Zhao et al. using Current Sensing AFM [39]. They found a dielectric strength of 2.0 $GV \cdot m^{-1}$ for alkyl monolayers on n-type <111> silicon. In a review by Salomon et al. [40] current transport mechanism through such thin monolayers (amongst others alkane thiols on gold and the system described in this paper) is discussed and a comparison of electronic transport measurements on organic molecules has been made. More general examples of metal – monolayer – semiconductor devices and more complex molecular devices are described in the literature [41-45].

The work of Liu and Yu comprises the characterization of n-Si | C_nH_{2n+1} (n = 6, 8, 10, and 12) | Hg MIS-structures [32]; n-Si | $C_{12}H_{25}$ | Hg MIS-structures compared with n-Si | Native Oxide | Hg [33]; p-Si | $C_{12}H_{25}$ | Hg MIS-structures compared with p-Si | Native Oxide | Hg, p-Si | Native oxide-$SiO_3C_{12}H_{25}$ | Hg and pSi-H | Hg [34]. A study concerning thicker monolayers on oxide-free silicon surfaces is still absent, however. The present paper focuses on Si | C_nH_{2n+1} (n = 10, 12, 16, and 22) | Hg structures made on both n-type Si<100> and p-type Si<100>, each with moderate doping (10^{15} cm^{-3}). From Current density -Voltage (*J-V*) and Capacitance-Voltage (*C-V*) measurements the typical parameters describing the electrical behavior of such MIS diodes are derived using the thermionic emission theory. For the longer alkyl chains (n = 16 and 22) a direct analysis from the *C-V* curves is possible resulting in an evaluation of the dielectric constant. It is investigated whether the electrical behavior for longer alkyl chains can still be precisely tuned as a function of the chain length. As a reference we used both H-terminated samples and samples with a thin thermally grown oxide of approximately 2 nm.

Finally, a stability study has been performed in which the *J-V* and *C-V* measurements were repeated for all samples with monolayers. This was done on two occasions after subsequent storage of the samples in ambient air in order to investigate the influence of storage under ambient conditions on the quality of the electronic properties and thus the stability of such silicon electrodes modified with Si-C linked monolayers.

2.2 Theory

The theory section is divided into two parts. The current - voltage behavior is treated in section 2.2.1, and the theory used to analyze the capacitance - voltage behavior is discussed in section 2.2.2.

2.2.1 Current-Voltage behavior

The commonly used transport mechanism that describes the *J-V* behavior of metal – very thin insulator (< 3.5 nm) – moderately doped silicon structures is the thermionic emission theory [30, 31]. In this theory the transport mechanism is governed by a thermionic emission process in which the electrons or holes tunnel directly through the insulator as is generally the case for an insulator thickness < 3.5 nm. An expression for the *J-V* relation, in which the series resistance of the device under test does not play a role yet, is given in Equation 2.1 (for the metal positively biased with respect to n-type silicon) [31]:

$$J = J_0 e^{(\frac{qV}{nkT})}(1-e^{-\frac{qV}{kT}}) = A^*T^2 e^{(\frac{-q\phi_{eff}}{kT})} e^{(\frac{qV}{nkT})}(1-e^{-\frac{qV}{kT}}) \tag{2.1}$$

where J [A·cm^{-2}] is the measured current density, V [V] is the applied bias voltage, A^* is the Richardson constant (110 and 32 A·K^{-2}·cm^{-2} for n-type and p-type silicon, respectively [30]), T [K] is the absolute temperature, kT/q is the thermal voltage (25.7mV at 298K), and n [-] is the diode ideality factor which accounts for the non-idealities in the diode behavior. In the ideal case $n = 1$. If the transport mechanism is not governed exclusively by a thermionic emission process $n > 1$. $q\phi_{eff}$ [eV] is the effective barrier height. In Figure 2.1 an energy band diagram of a n-type Si|insulator|metal structure is drawn to elucidate the formulas used throughout this section. Note that this figure is not to scale and is displayed for illustrative purposes only.

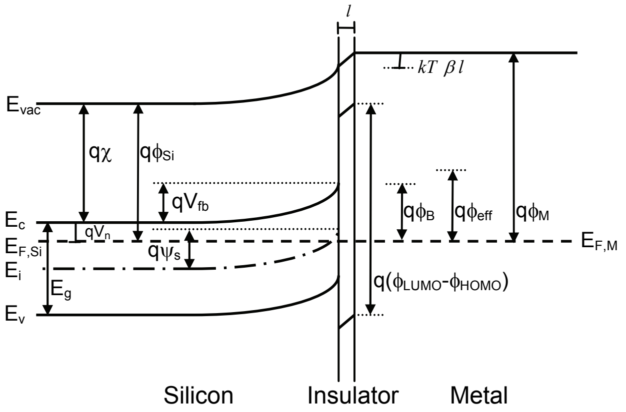

Figure 2.1. Simplified and ideal energy band diagram of n-type silicon, covered with an interfacial thin insulating layer, in thermal equilibrium with a metal. E_{vac} = Vacuum level, E_c = Bottom of conduction band, E_v = Top of valence band, E_g = Bandgap of silicon, E_i = Intrinsic Fermi level, $E_{F,Si}$ (= $q\phi_{Si}$) = Fermi level (work function) of silicon, $E_{F,M}$ (= $q\phi_M$) = Fermi level (work function) of metal, $q\chi$ = electron affinity of silicon, qV_n = Energy difference between E_C and $E_{F,Si}$, $q\psi_S$ = Energy difference between surface and bulk intrinsic Fermi level, ψ_S = surface potential, $q\phi_B$ = Barrier height of metal-semiconductor junction, $q\phi_{eff}$ = Effective barrier height including the contribution of the interfacial layer, qV_{fb} = Amount of band bending due to work function difference between silicon and metal at zero bias (ideal case), $q(\phi_{LUMO}$ - $\phi_{HOMO})$ = Energy difference between Lowest Unoccupied Molecular Orbit and Highest Occupied Molecular Orbit of organic insulator.

For metal-(n-type) semiconductor junctions the barrier height $q\phi_B$ is defined as: $q\phi_B = q\phi_M - q\chi$. $q\phi_M$ is the workfunction of the metal and $q\chi$ is the electron affinity of silicon (4.05eV [30]). In case of a thin insulator an extra barrier term is introduced, hereby increasing the total barrier height $q\phi_{eff}$. Selzer et al. and Liu et al. expressed $q\phi_{eff}$ as given in Equation 2.2 [28, 32-34]):

$$q\phi_{eff} = q\phi_B + kT\beta l \tag{2.2}$$

$kT\beta l$ [eV] describes the additional barrier height imposed by the thin insulator. β [$Å^{-1}$] is the tunneling constant, which is dependent - amongst others - on the type of insulator and charge carrier (holes for p-Si or electrons for n-Si); l [Å] is the thickness of the insulator. We note that this β parameter, which is generally used to describe the efficiency of electronic tunneling through metal – organic monolayer – metal or semiconductor – organic monolayer – metal structures, normally shows a voltage dependency [28, 40]. This is not investigated in this paper since our extraction method in the voltage range of 0 V until 0.2 V (n-type silicon) or 0 V until -0.2 V (p-type silicon) did not give rise to observe and take into account a strong bias dependency of β. Therefore, β determined for all samples modified with a monolayer is thus in fact an "effective" β as compared to literature that brings into account the voltage dependency.

Using Equation 2.1, $q\phi_{eff}$ and n can be derived. Rewriting Equation 2.1 into a function of $\ln(J/(1-e^{-\frac{qV}{kT}}))$ vs. V results in Equation 2.3:

$$\ln\left(\frac{J}{1-e^{-qV/kT}}\right) = \ln(A^*T^2) - \frac{q\phi_{eff}}{kT} + \frac{qV}{nkT} \tag{2.3}$$

A plot of $\ln(J/(1-e^{-\frac{qV}{kT}}))$ vs. *V* should give a straight line from zero bias [31]. The ideality factor *n* can now be derived from the slope and the effective barrier height $q\phi_{eff}$ can be obtained via the $\ln(J/(1-e^{-\frac{qV}{kT}}))$-axis intercept.

For higher forward bias voltages the series resistance R_s plays a role and Equation 2.1 can be adapted to Equation 2.4:

$$J = A^*T^2 e^{(\frac{-q\phi_{eff}}{kT})} e^{(\frac{q(V-JR_s)}{nkT})} \tag{2.4}$$

where R_s [Ω·cm^2] is the total series resistance of the device under test. One way to derive R_s from Equation 2.4 is via Equation 2.5 [31, 34]:

$$\frac{dV}{d\ln J} = JR_s + n\frac{kT}{q} \tag{2.5}$$

A plot of $dV \cdot (d\ln(J))^{-1}$ vs. *J* should give a straight line from which the total series resistance R_s can be derived from the slope.

2.2.2 Capacitance-Voltage behavior

Dielectric properties of the organic monolayer

In ideal *C-V* measurements the capacitance in accumulation equals the insulator capacitance and hence the thickness or dielectric constant of the insulator can be calculated via the well-known formula: $C = \varepsilon_0 \cdot \varepsilon_r \cdot A \cdot l^{-1}$

where ε_0 [F·cm^{-1}] is the permittivity of vacuum, ε_r [-] is the dielectric constant of the insulating layer, *A* [cm^2] is the surface area and l [cm] is the insulator thickness. For a given thickness and area the dielectric constant can be evaluated. In case of thin insulators, however, the capacitance in accumulation often does not reach a constant value, which can be attributed - amongst others - to a voltage dependent accumulation capacitance in series with the insulator capacitance.

If this causes a tilted capacitance in the accumulation regime of the *C-V* curve, the series circuit can be written as Equation 2.6 [46, 47]:

$$\frac{1}{C}=\frac{1}{C_{ins}}+\frac{1}{C_S}=\frac{1}{C_{ins}}-\frac{2kT}{qC_{ins}}\frac{1}{(V_{bias}-V_{fb}-\psi_S)}\approx\frac{1}{C_{ins}}-\frac{2kT}{qC_{ins}}\frac{1}{(V_{bias}-V_{fb})} \tag{2.6}$$

where C_{ins} and C_s are the insulator and accumulation capacitance, respectively; V_{bias} and V_{fb} are the applied voltage and the flatband voltage, respectively and ψ_s is the silicon surface potential (also indicated in Figure 2.1). $q\psi_s$ is the energy difference between the surface intrinsic Fermi level and the bulk intrinsic Fermi Level E_i; $\psi_s = 0$ V denotes the flatband condition. The flatband voltage can be determined from Mott Schottky plots. Under strong accumulation conditions ($V_{bias} - V_{fb}$) >> ψ_s and therefore ψ_s can be neglected. A plot of C^{-1} vs. $(V_{bias} - V_{fb})^{-1}$ should then give a straight line with C_{ins}^{-1} being the C^{-1}-axis intercept. The dielectric constant can consequently be derived from C_{ins}.

Mott Schottky theory

The flatband voltage is a very important parameter in the analysis of MIS- structures since it provides directly measurable, quantitative data on the silicon-insulator interface. The flatband voltage is usually derived from *C-V* curves. However, since *C-V* plots of thin insulators are often distorted, it is often difficult to obtain V_{fb} analytically. Fortunately, the Mott Schottky relation provides a solution since it only considers the silicon in the depletion regime. In this regime the voltage drop over the thin insulator is considered negligibly as compared to the drop over the depletion layer and the dominating depletion capacitance can be expressed in the Mott Schottky form as given in Equation 2.7 (mercury positively biased with respect to n-type silicon) [30]:

$$\frac{1}{C_{sc}^2}=\frac{2(V_{fb}-V_{bias})}{q\varepsilon_0\varepsilon_r N_D A^2} \tag{2.7}$$

where C_{sc} [F] is the measured depletion capacitance; ε_r is now the dielectric constant of silicon and N_D [cm^{-3}] is the doping concentration. In the linear part of the C^{-2} vs. V_{bias} plot the doping N_D can be calculated from the slope and V_{fb} from the *V*-axis intercept.

Since V_{fb} is not influenced by the presence of a very thin insulator (only by the silicon - insulator interface properties) the barrier height $q\phi_B$ (see Figure 2.1) can be evaluated according to Equation 2.8 (for n-type silicon) [48]:

$$q\phi_{B,n}=qV_{fb}+qV_n=qV_{fb}+kT\ln(\frac{N_C}{N_D}) \tag{2.8}$$

where qV_n is the energy difference between the bottom of the conduction band and the Fermi level of silicon (Figure 2.1); N_C is the number of effective states in the conduction band

($2.8\cdot10^{19}$ cm^{-3} for silicon [30]), and N_D [cm^{-3}] is the silicon donor doping as calculated from Equation 2.7.

With the values for $q\phi_{eff}$ (Equation 2.3) and $q\phi_B$ (Equation 2.8) the barrier height $kT\beta l$ of the insulator (Equation 2.2) can be evaluated and subsequently the tunneling constant β, if the insulator thickness is known. All parameters and their derivation routes mentioned in this section are summarized in Figure 2.2.

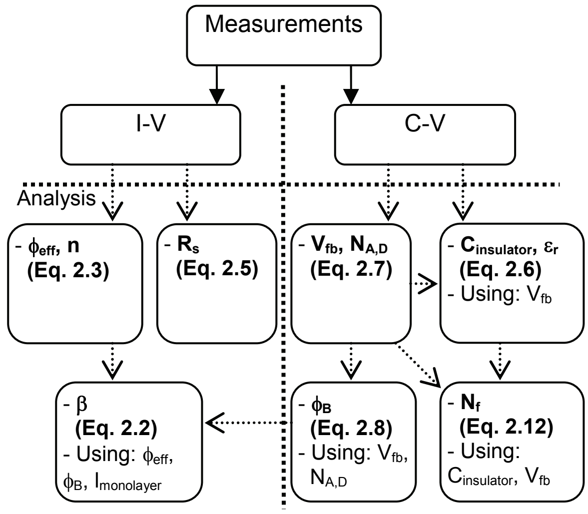

Figure 2.2. Parameter extraction route from *I-V* and *C-V* measurements. The boxes show the parameter and the equation number followed by any additional parameters needed from other extraction routes.

2.3 Results and Discussion

2.3.1 Mercury area verification

The area of the mercury contact on the samples was determined via high frequency *C-V* measurements on several p-type samples with approximately 100 nm thermal oxide (the exact oxide thickness l on each sample was separately measured by ellipsometry). An *I-V* measurement was performed before each *C-V* measurement to make sure the oxide was not leaking. The leakage current of all the samples stayed well below 50 pA. From the measured capacitance in accumulation (see Figure 2.3) the area of the mercury drop was determined. A constant capacitance in accumulation equals the insulator capacitance and hence the area can be simply evaluated via: $C_{acc} = \varepsilon_0 \cdot \varepsilon_r \cdot A \cdot l^{-1}$ [30]. Several spots on different samples gave for the area: $A = (3.7 \pm 0.1)\cdot10^{-3}$ cm^2.

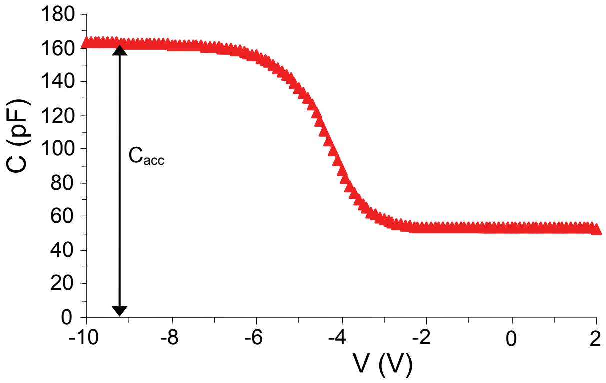

Figure 2.3. Typical example of a High Frequency Capacitance Voltage plot of Hg | SiO_2 (100 nm) | p-Si reference sample.

To investigate the wetting properties of the mercury on the contact area, the area determination was verified by testing samples with a 100 nm thick oxide hydrophobically coated with hexamethyldisilazane (HMDS), showing a static water contact angle of 84°. No significant changes in the calculated area were found. The influence of the wetting properties of the mercury is probably rather small since the mercury is sucked against the insulator using vacuum. Therefore we have assumed a constant area in all our investigated samples. The determination of the silicon doping as shown in Table 2.3 supports this assumption since the doping determination is very sensitive towards fluctuations in the area ($N_{A,D} \sim A^{-2}$ (Equation 2.7)) and the average doping values were all similar except for the nSiO_2 samples.

2.3.2 Current-Voltage data

The average leakage current density *J*-*V* data for different insulators on p-type and n-type silicon samples are displayed in Figure 2.4A and 2.4B, respectively. The curves shown for the C_{10}, C_{12}, C_{16} and C_{22} monolayers and for bare hydrogen-terminated Si and oxidized Si are typical for at least 5 different junctions.

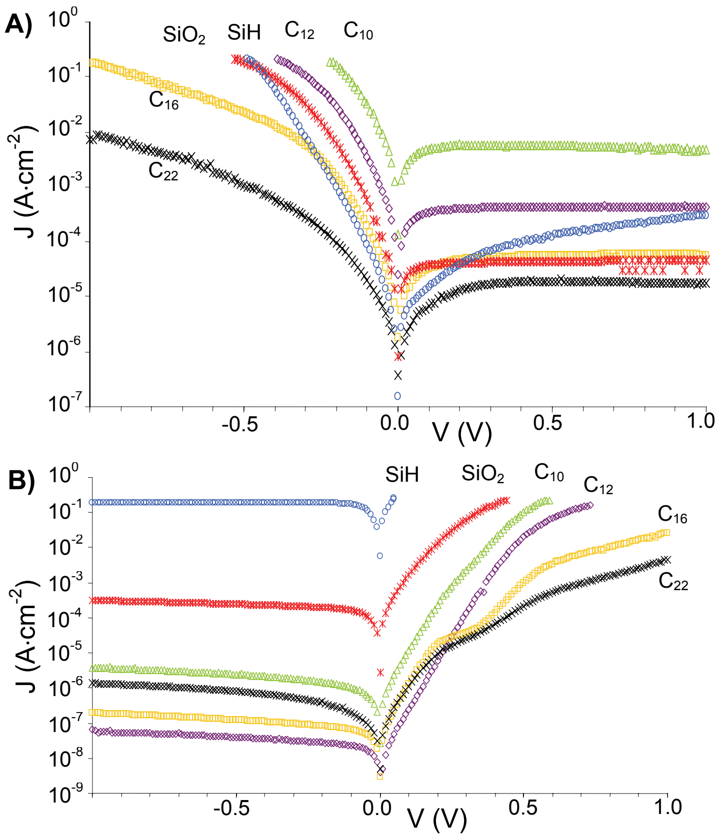

Figure 2.4. Current density vs. bias voltage data for different insulators on A) p-type silicon (left side is accumulation, right side is depletion), and B) n-type silicon (left side is depletion, right side is accumulation).

Starting with the hydrogen-terminated samples, it can be seen that there is an intrinsic difference in *J-V* behavior of mercury in contact with hydrogen-terminated n- or p-type silicon. This can be rationalized by considering the difference in barrier heights for a metal in contact with n- or p-type silicon. The ideal barrier height for n-type silicon is: $q\phi_B = q\phi_M - q\chi$ and for p-type silicon: $q\phi_B = E_g + q\chi - q\phi_M$ [30]. Using the literature value of $q\phi_M$ = 4.49eV as the workfunction of mercury [49] this results in: $q\phi_{B,n}$ = 0.44eV and $q\phi_{B,p}$ = 0.67eV, i.e. the workfunction of mercury is closer to the bottom of the conduction band than to the top of the valence band. This gives a huge difference in *J-V* behavior. As an example the ideally J_0 (the diode reverse current density) for n- and p-type silicon is calculated via Equation 2.1. This gives: $J_{0,n} \approx 60$ A·cm^{-2} and $J_{0,p} \approx 2{\cdot}10^{-3}$ A·cm^{-2}. Obviously, it concerns ideal values, since in real case $q\phi_B$ is also influenced by surface states and imperfections in the (surface of the) silicon lattice [30], but nevertheless it gives a good indication in the expected difference in current densities. Mercury in contact with n-Si gives a very poor Schottky diode or even an Ohmic contact [32, 50, 51], while via mercury in close contact with p-type silicon good Schottky diodes, in terms of rectifying behavior, are obtained [34, 50-53]. This is in agreement with the data of Figure 2.4 where the nSiH samples show a much worse diode behavior than the pSiH samples. A distinct feature that can be seen immediately in Figure 2.4A is the low current density measured for pSiH as compared to the pSi samples with different insulators. Several studies on mercury-silicon interfaces have been reported in which it is shown that mercury forms an atomically flat contact to the silicon surface and that mercury does not chemically interact with the silicon [50-53]. This rules out the existence of any defects at the mercury interface and indicates that electronic behavior of these junctions is totally determined by the surface structure of the silicon and the number of defects at this surface. $q\phi_{B,p}$ values over 0.9 eV have been reported for mercury in contact with p-type <111> silicon [52, 53].

Next, the influence of the 2 nm thick SiO_2 layer is discussed. It can be seen that passivating the p-type silicon surface with a thin oxide layer does not alter its *J-V* characteristics in a dramatic way. This behavior was observed before on *I-V* measurements of mercury in close contact with hydrogen-terminated p-type silicon and with p-type silicon with an interfacial, chemically prepared oxide [51]. The behavior is, however, more like a Schottky diode since a more constant value of J_0 is now obtained in the reverse bias regime. An explanation for the high forward currents at the $pSiO_2$ samples may be due to a cancellation of the extra energy barrier introduced by the oxide as a result of additionally induced interface states at the silicon-SiO_2 interface. For the n-type silicon samples passivation of the nSiH surface with a 2 nm oxide changes its *J-V* behavior dramatically. This is also observed in literature where a thin interfacial layer can change the behavior of mercury – n-type silicon structures from Ohmic to Schottky contacts [32, 50, 51]. Here the oxide does provide an additional barrier that lowers the current density through the structure.

The effect of the modification of p-type silicon surfaces with an organic monolayer on the *J-V* behavior is clearly visible. The *J-V* curves all have the same Schottky diode characteristic shape, indicating a similar transport mechanism through all alkyl insulators. The magnitude of the current density can be precisely tuned by varying the length of the 1-alkene as was also observed by various other researchers via electrical means [28, 32, 34]. Despite the fact that the C_{16} layer is thinner than the oxide layer (1.78 ± 0.02 nm vs. 1.99 ± 0.06 nm) the organic monolayer displays better insulating behavior. This is a clear indication for the good insulating properties of these layers. As compared to the pSiH data, however, the formed MIS-structures with organic monolayers apparently also had net lower barrier heights just as the oxide had. For layers > C_{12} the current density values are lower than for pSiH.

The modification of n-type silicon surfaces with an organic monolayer results in a complete other trend. As compared to both the bare H-terminated and the oxidized samples all monolayers clearly display better insulating properties. Even the thinnest monolayer under present study -C_{10} (1.21 nm)- insulates better than the $nSiO_2$ samples (layer thickness: 2.03 ± 0.11 nm). For the C_{10} and C_{12} monolayers the *J-V* curves have their usual shape. Also the trend in current density magnitude is in accordance with expectations. The C_{12} layer is a better insulator than the C_{10} layer.

The nC_{16} and nC_{22} samples, however, showed an unanticipated result. Two different regimes can be distinguished in the *J-V* plot of the n-type silicon data: $V < 0.4$ V and $V > 0.4$ V. In the first-mentioned regime - reverse and small forward bias voltages - the current densities of both the nC_{16} and nC_{22} layer are higher as compared to the nC_{12} and nC_{16} layers. In other words, the order of J for the different monolayers on n-type silicon is $C_{10} > C_{22} > C_{16} > C_{12}$. This is –in contrast to the data of p-type silicon were we observed $C_{10} > C_{12} > C_{16} > C_{22}$– not in line with the monolayer thickness. For higher forward bias voltages (> 0.4 V) the insulating properties of the longer chains changed and were more in line with the expectations. In this voltage regime the series resistance of the monolayer starts to play a significant role (Equation 2.4) and this could be the reason for the strong current decrease that is observed.

Four possible reasons are now discussed to explain the observed J-V behavior of the nC_{16} and nC_{22} layer in the regime of $V < 0.4$ V. The first one is related to the presence of charges at the monolayer – silicon interface (e.g. surface states). Effects arising from the silicon-monolayer interface, however, are believed to be of no significant influence on the shape of the J-V curves since the delay time between voltage step and actual voltage measurement was 0.2 s, thereby excluding the effect of measuring a charging current due to interface states with short lifetimes.

The second explanation focuses on the properties of the monolayer, since a change in the geometry of the monolayers during the voltage scan could explain the observed relative high current densities. The monolayer tilt angle dependency on current transport is investigated by Yamato and Waldeck by investigating systems with a variety of alkane thiols on different semiconductor substrates [54]. They found an increase in tunneling current with increased tilt angle. If the C_{16} and C_{22} monolayers on n-type silicon are more tilted as compared to C_{12} and C_{10} during the voltage scan due to for instance electrostatic interactions this could give an explanation of the increase in tunneling current. However, a bias voltage induced tilting of monolayers > C_{14} is in contrast with findings of Selzer et al. [28]. They investigated the current transport through alkane thiols on mercury in contact with oxidized p-type silicon and showed that only thinner (< C_{14}) layers are likely to tilt under applied bias voltages. Furthermore, for C_{12} and C_{16} layers on Si<100> tilt angles of 26° are reported [55], and also the reported value of the C_{22} layer (15-26°) is comparable [56].

The third explanation is related to the mechanism of the transport of current and can to some degree be associated with the aspect of geometry. Different mechanisms are extensively treated in a review by Salomon et al. [40]. In order to say something about the most likely current transport mechanism through the nC_{16} and nC_{22} layers, more detailed structural information of the used monolayers is required, like the degree of packing and defects.

The fourth explanation for the deviating J-V results of nC_{16} and nC_{22} may be related to leakage currents. If pinholes are present the mercury can directly contact the silicon surface. If this would be the case this would suggest that in our study thinner layers (nC_{10} and nC_{12}) were more densely packed than the thicker layers (nC_{16} and especially nC_{22}) and form blocking layers for the mercury.

To conclude, if the different J-V behavior of the nC_{16} and nC_{22} samples can be explained by deviating structural layer properties as discussed in the last two explanations, the J-V data in its totality (both n-type and p-type) reveal different structural properties for C_{16} and C_{22} layers on n-type and p-type silicon. More research is needed to explore the observations of the *J*-*V* data.

It is noted on forehand that there is some parallel in the analysis presented below and the studies performed in the nineteen-seventies on metal-oxide-silicon structures with oxides of comparable thickness as the organic monolayers [57-61]. The analysis of the *J*-*V* plots starts by deriving the diode ideality factor *n* and effective barrier height $q\phi_{eff}$ (Equations (1) and (3)) from $\ln(J/(1-e^{-qV(kT)^{-1}}))$ vs. *V* plots (Figure 2.5). In order to exclude any influence of the series resistance R_s only the linear parts from 0 V until 0.2 V (all samples on n-type silicon apart from nSiH of which data from 0 V until only 0.05 V was available) or 0 V until -0.2 V (all samples on p-type silicon) are considered for this analysis.

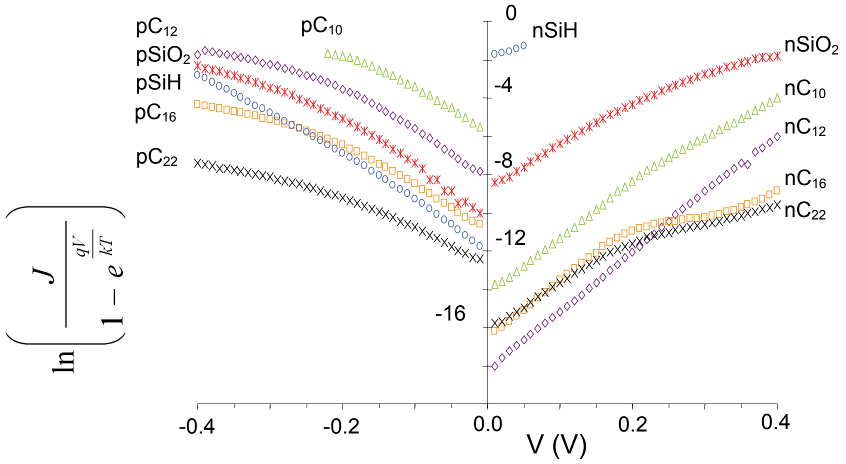

Figure 2.5. $\ln(J/(1-e^{-\frac{qV}{kT}}))$ vs. *V* for all insulators. The plots on the left side are for insulators on p-silicon. Plots for insulators on n-silicon are depicted on the right side.

Subsequently, the series resistance R_s is derived from $dV\cdot(d\ln(J))^{-1}$ vs. *J* plots (Equations 2.4 and 2.5). Now the *J*-*V* data for $V > |0.2|$ V is used for analysis to include the effects of the series resistance. This analysis was, however, not possible for C_{16} and C_{22} monolayers on n-type silicon, due to the non-exponential behavior in the forward direction (see above). The results are given in Table 2.1.

Table 2.1. Parameters derived from thermionic emission theory.

Insulator	n [-]	$q\phi_{eff}$ [eV]	R_s [Ω·cm^2]
pSiH	1.49 ± 0.05	0.695 ± 0.003	-
pC$_{10}$	1.78 ± 0.05	0.528 ± 0.002	0.49 ± 0.04
pC$_{12}$	1.57 ± 0.01	0.593 ± 0.001	0.99 ± 0.03
pC$_{16}$	1.69 ± 0.02	0.663 ± 0.001	4.14 ± 0.05
pC$_{22}$	2.16 ± 0.07	0.709 ± 0.002	22.84 ± 0.05
pSiO$_2$	1.43 ± 0.04	0.649 ± 0.007	1.31 ± 0.03
nSiH	3.40 ± 0.30	0.461 ± 0.003	-
nC$_{10}$	1.22 ± 0.07	0.806 ± 0.005	-
nC$_{12}$	1.34 ± 0.04	0.880 ± 0.003	-
nC$_{16}$	1.34 ± 0.02	0.837 ± 0.001	-
nC$_{22}$	1.63 ± 0.03	0.827 ± 0.002	-
nSiO$_2$	1.67 ± 0.07	0.644 ± 0.003	-

The observed difference in ideality factor (n) for pSiH (n = 1.49 ± 0.05) and nSiH (n = 3.40 ± 0.30) can be explained by the different barrier heights (both $q\phi_{eff}$ and $q\phi_B$) for the two types of contact. Consequently, it can be concluded that mercury in contact with p-type silicon gives much better Schottky diodes as compared to n-type silicon. A more qualitative examination of the diode ideality factor for samples with modified surfaces can be given via Equation 2.9. In the case of an ideal metal – interfacial layer – silicon structure (i.e. no surface states) the ideality factor n is [57]:

$$n = 1 + \frac{l\varepsilon_{r,Si}}{W\varepsilon_{r,insulator}} \quad \text{with: } W = \sqrt{{}^{2\varepsilon_0\varepsilon_{r,Si}}\!\big/\!{}_{qN_D}\,(V_{fb} - V_{bias})} \tag{2.9}$$

Two things can be noticed from this equation. Firstly, the ideality factor n increases with increasing length l of the insulator, i.e. worse diodes are expected when the interfacial layer gets thicker. Secondly, n is dependent on the bias voltage. In Table 2.1 it can be noticed that n increases indeed with monolayer thickness for both n- and p-type silicon. Exception is pC$_{10}$ which shows a worse diode behavior than pC$_{12}$ and pC$_{16}$. Modification of the pSiH surface with a thin oxide leads to a similar ideality factor, whereas modification of this surface with organic monolayers renders less good diodes in this case. This is in contrast with results reported by Liu et al. [34] who obtained lower values for C$_{12}$ layers on p-type <111> silicon (1.33 ± 0.10 vs. 1.57 ± 0.01 in this case). A direct comparison is not possible, since n generally varies over the J-V range of a diode (Equation 2.9) and a different current regime and different method for the derivation of n are used in this study (see above). We used a low current regime for our analysis in which n is normally higher than for high forward currents. Modifying the nSiH surface with a thin oxide layer obviously leads already to a much better diode [50, 51]. All monolayers on nSi gave better diode ideality factors than the oxidized nSi samples. Another trend visible in Table

2.1 is that modifying n-type silicon surface with an organic monolayer renders a more ideal diode behavior as compared to p-type silicon.

The calculated effective barrier height $q\phi_{eff}$ increases with increasing monolayer thickness on p-type silicon, which is in line with expectations (Equation 2.2). Quite remarkable is the high $q\phi_{eff}$ of the pSiH samples as compared to the modified samples. This would indicate that the charge carriers have to cross a lower barrier for p-type silicon modified with an organic monolayer as compared to pSiH junctions. On n-type silicon, however, the silicon surfaces with organic monolayers give higher barriers than nSiH and $nSiO_2$ samples. The calculated effective barrier heights of the monolayers are in line with observations in the *J-V* curves. The barrier height increases from nC_{10} until nC_{12}. Then it decreases for nC_{16} and nC_{22} but still remains larger than for $nSiO_2$. If the deviations for the longer alkyl chains are not caused by leakage of mercury through the layer than the apparent lowering of $q\phi_{eff}$ can have two origins according to the used model. Equation 2.2 shows that $q\phi_{eff}$ depends on a barrier term that is a function of the monolayer thickness, and also on the barrier height $q\phi_B$, which is influenced by the interface properties but not by the monolayer thickness. In the next section $q\phi_B$ and its possible influence on the observed $q\phi_{eff}$ values are investigated.

The series resistance as calculated for p-type silicon samples shows a very clear exponential increase with monolayer thickness as depicted in Figure 2.6. It must be noted, however that only four data points are concerned in this analysis.

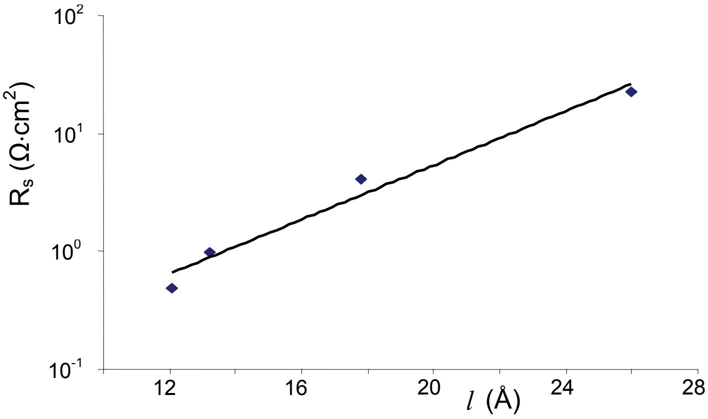

Figure 2.6. Series resistance as a function of monolayer thickness on p-type silicon. The exponential best-fit function is: $R_s = 2.7\cdot10^{-2}e^{0.27l}$ (R^2 = 0.973).

This exponential dependency of R_s on the monolayer thickness clearly indicates that the forward current at high bias voltages is not only influenced by the effective barrier height, $q\phi_{eff}$ (Equation 2.2) but also by the length of the insulator path through which the charge carriers have to travel in the form of the series resistance R_s. Both $q\phi_{eff}$ and R_s are influenced by the monolayer thickness. This also correlates to the trend seen in Figure 2.4A. The *J-V* plots of the pSiH samples have a much steeper slope until higher bias voltages than the pSi samples with insulators. This also indicates that the series resistance is mainly determined by the interfacial layer and not by the (back) contact resistance, since all samples on p-type silicon had the same back contact.

2.3.3 Capacitance-Voltage data

The results for the *C-V* measurements are depicted in Figure 2.7. The figure shows typical curves from at least 5 different junctions.

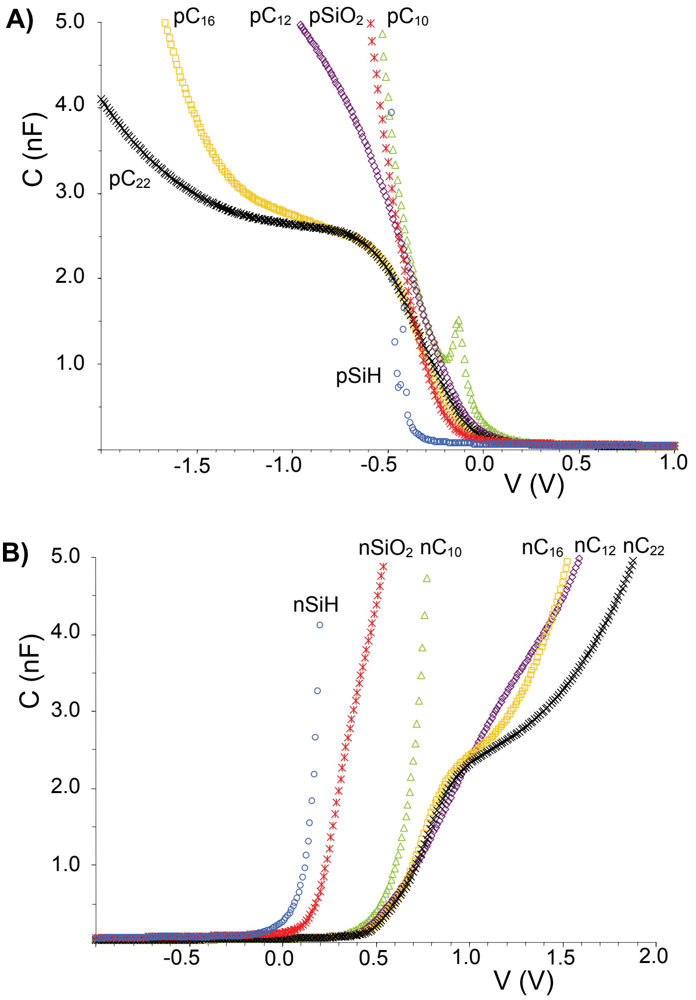

Figure 2.7. Capacitance voltage plots of different insulators on A) p-type silicon and B) n-type silicon.

The *C-V* curves for all H-terminated samples and samples with C_{10}, C_{12}, and SiO_2 insulators on both types of silicon are typical for metal-semiconductor junctions where the capacitance in accumulation increases sharply with the applied voltage [31]. In contrast to $pSiO_2$, pC_{12}, pC_{16}, and pC_{22} an additional peak at -0.2 V is observed for pC_{10}. The origin of this peak might be related to the presence of interface charges that are present at the silicon-monolayer interface of pC_{10}. In that case, the interface charge is contributing to the total charging current and consequently a peak appears in the *C-V* plot. The presence of a larger amount of interface charge at the pC_{10} sample correlates with the deviating flatband voltage for pC_{10} as compared to the flatband voltage for layers > C_{10}. A larger amount of interface states may also be a cause of the higher diode ideality factor n of pC_{10} (1.78 ± 0.05) as compared to pC_{12} and pC_{16} (1.57 ± 0.01 and 1.69 ± 0.02, respectively) since a large amount of interface states will lead to an increase in *n* [57]. The *C-V* curves for samples with C_{16} and C_{22} insulators on both types of silicon display a plateau in the accumulation regime around |1 V| and increase strongly again for higher voltages. This plateau indicates the formation of a real capacitance. The tilted capacitance in the plateau of the accumulation regime is further analyzed in the next section.

Dielectric properties of the organic monolayer

At first it was verified whether the measured capacitance in the *C-V* curves displayed any frequency dependency. During the measurements R_s was compensated for according to a procedure mentioned in [62], in order to exclude frequency distortion in the *C-V* curve as a result of the series resistance. A frequency distortion can occur when measuring on samples with high series resistance while a parallel circuit of a capacitor and resistor is used as *C-V* impedance model [31]. Figure 2.8 gives the typical *C-V* curves for a pC_{22} sample measured at 10, 40, 100, and 400 kHz. No significant capacitance shift occurred in the accumulation regime at any of the samples.

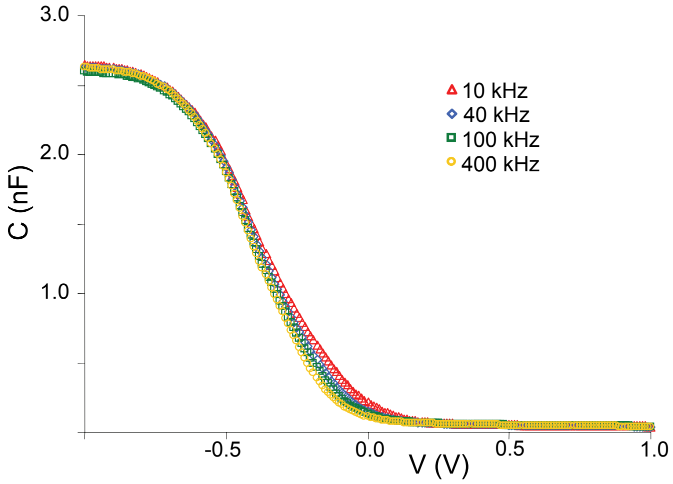

Figure 2.8. *C-V* curves of a $pSi|C_{22}H_{45}|Hg$ MIS-structure at different frequencies. No frequency dispersion was observed in the accumulation regime.

Next the *C-V* data measured at 400 kHz is used for analysis. A typical plot of C^{-1} vs. $(V_{bias} - V_{fb})^{-1}$ for pC_{16} and pC_{22} samples is depicted in Figure 2.9. The linear extrapolation of the curve with the C^{-1} axis intercept yields the inverse insulator capacitance C_{ins}^{-1}, as can be seen from Equation 2.6.

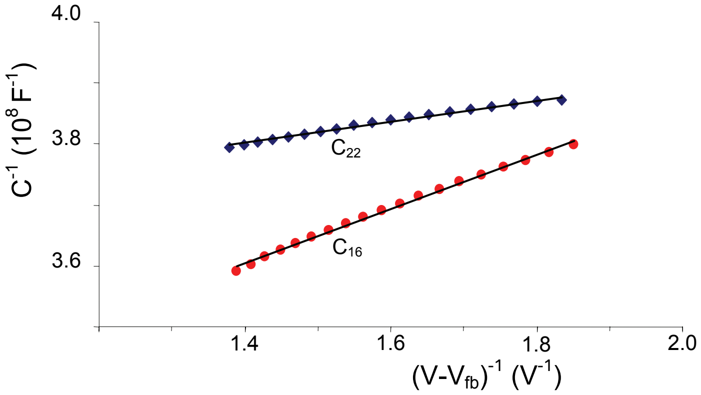

Figure 2.9. C^{-1} vs. $(V-V_{fb})^{-1}$ plot for C_{22} and C_{16} insulators on p-type silicon.

With the thickness and area known the dielectric constant can be graphically evaluated (Table 2.2).

Table 2.2. Dielectric constant for C_{16} and C_{22} monolayers.

Insulator	C [nF]	ε_r [-]
pC_{16}	3.2 ± 0.2	1.7 ± 0.1
pC_{22}	2.8 ± 0.2	2.2 ± 0.2
nC_{16}	3.6 ± 0.2	1.9 ± 0.1
nC_{22}	3.5 ± 0.1	2.8 ± 0.1

These values are in close agreement with value $\varepsilon_r = 2$ found for alkane thiol monolayers on mercury hanging drop electrodes and $\varepsilon_r = 2.7 \pm 0.3$ for Hg-alkane thiol/alkane thiol-Hg junctions [63, 64]. Kar et al. reported a value of 2.13 for a C_{18} monolayer on Al|$C_{18}H_{37}$|p- and n-Si devices [36], which is within the experimental error of the value for the pC_{22} samples (2.2 ± 0.2). The values are, however, much lower than the reported value of $\varepsilon_r = 3.3 \pm 0.6$ from Yu et al. [65], apart from the nC_{22} samples. It is expected that a large amount of oxide would increase the effective dielectric constant, since $\varepsilon_r = 3.9$ for SiO_2. This implies that there is more oxide present inside the C_{22} layers than the C_{16} layers, which could be an indication for the lower static water drop contact angles on these layers (100-102° for C_{22} and 108-109° for C_{16}). Also the low water drop contact angles, 90.6 ± 3.0° up to 101 ± 7.5°, combined with the high dielectric constant found in [65] are in line with these observations.

Mott Schottky measurements

The *C-V* data plotted in the Mott Schottky form is given in Figure 2.10. The measurements shown here were performed at 400 kHz. The measurements were also carried out at 10, 40, and 100 kHz to check whether there is a large frequency dependency on the calculated doping and flatband voltage. A frequency dependency in the Mott Schottky plots is often encountered in electrochemistry on semiconductors and can be attributed to numerous causes, like -amongst others- surface states [66]. The calculated doping did not show any frequency dependency for all organic monolayers. The flatband voltage showed a maximum difference of 17% between 10 kHz and 400 kHz for the C_{12} layer on p-type silicon. Flatband voltages compared between 10 kHz and 400 kHz for the other monolayers showed a difference less than 10%.

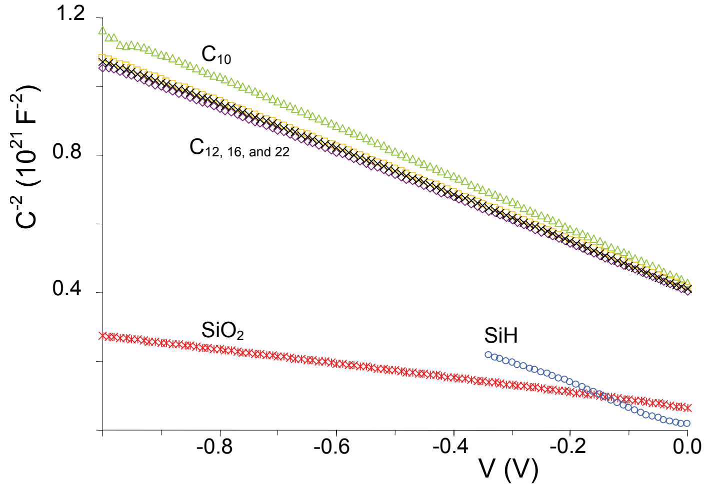

Figure 2.10. Mott Schottky plots for different insulators on n-type silicon.

The plots are linear in the region –1.0 V to +0.2 V for n-type silicon samples, except for the SiH samples, which gave deviations for voltages more negative than –0.35 V. The plots for the insulators on p-type silicon are all linear in the region +1.0 V to +0.2 V. The flatband voltage V_{fb} and doping density are calculated using Equation 2.7 and the barrier height $q\phi_B$ using Equation 2.8. Hereafter, the barrier term $kT\beta l$ from the insulator are calculated via Equation 2.2. The results are given in Table 2.3. The theoretical flatband voltage for ideal cases is shown in the third column for comparison.

Table 2.3. Parameters derived from the Mott Schottky analysis.

Insulator	V_{fb} [V]	$V_{fb,\ theory}$ [V]	*Doping* [10^{15} cm^{-3}]	$q\phi_B$ [eV]	$kT\beta l$ [eV]
pSiH	-0.58 ± 0.01	-0.45	2.0 ± 0.1	0.80 ± 0.01	-
pC_{10}	-0.22 ± 0.01	-0.45	2.2 ± 0.1	0.44 ± 0.01	0.09 ± 0.01
pC_{12}	-0.34 ± 0.03	-0.45	2.3 ± 0.2	0.56 ± 0.03	0.04 ± 0.03
pC_{16}	-0.34 ± 0.02	-0.45	2.0 ± 0.1	0.56 ± 0.02	0.10 ± 0.02
pC_{22}	-0.32 ± 0.04	-0.45	2.1 ± 0.2	0.53 ± 0.04	0.18 ± 0.04
$pSiO_2$	-0.36 ± 0.01	-0.45	1.9 ± 0.1	0.58 ± 0.01	0.07 ± 0.01
nSiH	0.05 ± 0.03	0.18	1.6 ± 0.2	0.30 ± 0.03	-
nC_{10}	0.61 ± 0.01	0.18	1.2 ± 0.1	0.87 ± 0.01	-0.06 ± 0.01
nC_{12}	0.63 ± 0.02	0.18	1.3 ± 0.1	0.88 ± 0.02	0.00 ± 0.02
nC_{16}	0.63 ± 0.01	0.18	1.3 ± 0.1	0.89 ± 0.01	-0.05 ± 0.01
nC_{22}	0.63 ± 0.01	0.18	1.3 ± 0.1	0.88 ± 0.01	-0.06 ± 0.01
$nSiO_2$	0.34 ± 0.01	0.18	2.9 ± 0.1	0.58 ± 0.01	0.07 ± 0.01

The flatband voltages for C_{12}, C_{16} and C_{22} layers on p-type silicon and for all the organic monolayers on n-type silicon are in close agreement with each other. This indicates that the properties of the silicon-monolayer interfaces are influenced in a similar way for all these monolayers. A similar flatband voltage for different monolayer thickness was also noticed by Yu et al. [67] and Bansal et al. [68] who observed this in their electrochemical experiments on n-type <111> Si electrodes covered with organic monolayers. They ascribed such independence of V_{fb} towards monolayer thickness to the neutral character of an adsorbate bound to the silicon surface involving covalent Si-C bonds. The deviating flatband voltage for the pC_{10} sample indicates a change in surface properties, which correlates with the deviating value of n and the peaks in the C-V curve (Figure 2.7A) for pC_{10}.

All the calculated doping levels were in line with the specifications given by the wafer supplier (p-type silicon: $1.4 \cdot 10^{15}$ cm^{-3} $\leq N_A \leq$ $2.8 \cdot 10^{15}$ cm^{-3} and n-type silicon: $4.3 \cdot 10^{14}$ cm^{-3} $\leq N_D$ $\leq$ $4.3 \cdot 10^{15}$ cm^{-3}). The doping levels for all pSi samples were similar whereas at the nSi samples $nSiO_2$ gave a twice as high N_D as compared to the other nSi samples. The calculated doping results indicate that the area of the mercury dot is not influenced strongly by the wetting properties of the different surfaces, since the doping $N_{A,D}$ scales with A^{-2}, as can be seen from Equation 2.7.

Regarding the barrier height it is noticed that $q\phi_B$ for pSiH is very high (0.80 ± 0.01 eV) as compared to theory (0.67 eV). $q\phi_B$ values over 0.9 eV have been reported for Hg-pSiH junctions [52, 53]. The barrier height for the nSiH sample (0.30 ± 0.03 eV) is lower than expected (0.44 eV). A validation of the used method, however, is the fact that for a given combination of a metal and semiconductor, the barrier heights for both (n-type) semiconductor – metal and (p-type) semiconductor – metal junctions are related according to: $q\phi_{B,n} + q\phi_{B,p} = E_g$ where E_g is the semiconductor bandgap energy (for silicon E_g = 1.12 eV) [30]. For the Hg-SiH junctions measured in this study this results in: $q\phi_{B,n} + q\phi_{B,p} =$ 1.10 ± 0.03 eV, which is in perfect agreement with theory. The results for pC_{12} and pSiH samples are in close agreement with the results obtained by Liu et al. [34]. The results showed a similar $q\phi_B$ for the n-type samples modified with an organic monolayer. This is in line with the assumption that the low values of $q\phi_{eff}$ for nC_{16} and nC_{22} (Table 2.1) are not caused by a difference in interface properties for these layers as compared to the thinner layers.

2.3.4 Evaluation of insulator properties, $q\phi_{eff}$, and tunneling constant

Table 3 gives the calculated values for the barrier $kT\beta l$ imposed by the insulators. These values are far too low or even negative as compared to values found in literature of 0.16 eV for <111> nSi-$C_{10}H_{21}$ samples [33], and 0.24 eV for <111> pSi-$C_{12}H_{25}$ samples [34]. In the following discussion about the $q\phi_{eff}$ and $q\phi_B$ values it is assumed that a theory normally applied to silicon surfaces covered with thin oxide layers is also applicable to these silicon junctions with organic monolayers [57]. This is rationalized by the fact that the current transport mechanisms through both types of insulators are equal, and both insulators are densely packed structures. Regarding Equation 2.2 a number of things can be said about $q\phi_{eff}$. First, in ideal cases (i.e. the silicon surface structure is not changed by the contact with the insulator) the barrier height $q\phi_B$ determined for modified samples should be equal to the barrier height $q\phi_B$ of SiH samples. Second, $q\phi_B$ and $q\phi_{eff}$ for SiH samples should be equal since they contain no contribution from an insulating layer. This was also noticed by Liu et al. who attributed such deviations to fixed charges located at the silicon-insulator interface [34]. Since mercury forms an atomically flat and chemically stable contact, it is expected to form an ideal contact with the insulator [50-53]; so all fixed charges should be located at the silicon-insulator interface. Fixed charges at Si-SiO_2 systems often originate from ionic silicon near the interface. Together with uncompleted silicon bonds (e.g. Si-Si or Si-O bonds) at the surface they may result in the fixed charge Q_f. For Si-SiO_2 systems the net Q_f is usually positive [30].

In order to give an analysis of the fixed charge, a comparison is needed with the ideal flatband voltage. In an ideal metal-semiconductor interface the flatband voltage equals:

$$qV_{fb} = q\phi_M - q\phi_{Si} = q\phi_{MSi} \tag{2.10}$$

The silicon work function $q\phi_{Si}$ is dopant dependent and equals for n-type silicon [30, 69]:

$$q\phi_{Si} = q\chi + qV_n = q\chi + kT\ln\left(\frac{N_C}{N_D}\right) \tag{2.11}$$

where N_C is the number of effective states in the conductance band ($2.8\cdot10^{19}$ cm^{-3} for silicon [30]). Using the average value of $N_D = 1.2\cdot10^{15}$ cm^{-3} and $q\phi_M = 4.49$ eV for mercury [49], this gives $V_{fb,theory} = \phi_{MSi,n} = 0.18$ V for n-type silicon. In a similar way using $N_A = 2.0\cdot10^{15}$ cm^{-3} it can be calculated that for p-type silicon $V_{fb,theory} = \phi_{MSi,p} = -0.45$ V.

Positive charges in the insulator will shift ideal *C-V* and Mott Schottky curves to more negative values resulting in a more negative V_{fb} and vice versa. If these theoretical values are compared with the measured values (see Table 2.3), the following can be said about p-type silicon. The hydrogen-terminated sample has a more negative value of V_{fb} indicating the presence of positive charges at the Hg|SiH interface. All the insulators, however, have their flatband voltage shifted in the positive direction, even beyond the theoretical V_{fb}, indicating the presence of negative charges at these interfaces. The amount of negative charges is the largest for pC_{10}, followed by the oxidized samples and then comparable values for the other monolayers. For n-type silicon the hydrogen-terminated samples also have a more negative value of V_{fb} indicating the presence of positive charges at the Hg|SiH interface. All the other insulators have again their flatband voltage shifted in the positive direction beyond the theoretical V_{fb}, indicating the presence of negative charges at these interfaces. The nSiO$_2$ samples now give a lower number of fixed charges.

From a comparison between the measured and ideal flatband voltage the total fixed charge at the C$_{16}$ and C$_{22}$ layers can be estimated via Equation 2.12:

$$N_f = \frac{C_{ins}(\phi_{MSi} - V_{fb})}{qA} \tag{2.12}$$

where N_f [cm^{-2}] is the total number of fixed charges; C_{ins} [F] is the insulator capacitance as determined from the C^{1} vs. $(V-V_{fb})^{-1}$ plots; ϕ_{MSi} and V_{fb} are the theoretical and measured flatband voltage, respectively. This gives the following values for N_f (Table 2.4). By definition, however, $N_f = |Q_f \cdot q^{-1}|$ and is always positive. To show that in all the cases listed in Table 2.4 negative fixed charges are concerned, this is denoted by $-Q_f$.

Table 2.4. N_f calculated for different monolayers.

Insulator	Total insulator charge N_f [cm^{-2}]
pC$_{16}$	$(5.8 \pm 1.0)\cdot10^{11}$ ($-Q_f$)
pC$_{22}$	$(6.2 \pm 2.0)\cdot10^{11}$ ($-Q_f$)
nC$_{16}$	$(2.7 \pm 0.2)\cdot10^{12}$ ($-Q_f$)
nC$_{22}$	$(2.7 \pm 0.1)\cdot10^{12}$ ($-Q_f$)

State of the art MOS-structures have values of N_f in the order of $10^9 - 10^{11}$ cm^{-2} for <100> oriented silicon [70]. The samples with monolayers on p-type silicon have a remarkably low amount of fixed charge, especially if one takes into account that these monolayers were fabricated using wet bench chemistry at low temperatures as compared to temperatures that are used in the fabrication of MOS-structures. A distinct influence of dopant type on the amount of fixed charge can be observed in this case. The amount of fixed charges in the n-type silicon samples is more than 4 times higher as compared to p-type silicon samples. Another type of interface charge from which the physical origin is suggested to be similar to Q_f, is the interface trapped charge or surface states charge Q_{it} [70]. Kar et al. studied the density of these interface traps (D_{it}) at p- and n-type Al|C$_{18}$H$_{37}$|Si structures and found also a substantially higher value of D_{it} at n-silicon structures as compared to p-type silicon structures [36]. They attributed this to the influence of the silicon surface potential and the position of the surface Fermi level during monolayer formation.

Next, the J-V data can be compensated for the shift in V_{fb} due to fixed charge in the samples [57]. The influence of the fixed charge can be eliminated by multiplying Equation 2.1 with a normalization factor $\exp(-kTq^{-1}(V_{fb} - \phi_{MSi}))$ and re-plotting the normalized J-V graphs. From these the normalized effective barrier heights can be calculated. The results with normalized values for $q\phi_{eff}$ and the β values can be found in Table 2.5 (see Figure 2.2 for derivation routes; $q\phi_{eff}$ is derived from the J-V curves and $q\phi_B$ is derived from the C-V measurements). β is expressed in two different units in order to facilitate the comparison with values reported in literature.

Table 2.5. Results of the barrier-height analysis via normalized J-V plots.

Insulator	$q\phi_{eff}$ [eV]	$q\phi_B$ [eV]	$kT\beta l$ [eV]	β [Å^{-1}]	β [per CH_2 group]
pSiH	0.563 ± 0.003	0.80 ± 0.01	-0.24 ± 0.01	-	-
pC_{10}	0.751 ± 0.001	0.44 ± 0.01	0.31 ± 0.01	1.00 ± 0.05	1.21 ± 0.06
pC_{12}	0.701 ± 0.001	0.56 ± 0.03	0.15 ± 0.03	0.43 ± 0.09	0.47 ± 0.10
pC_{16}	0.771 ± 0.001	0.56 ± 0.02	0.21 ± 0.02	0.46 ± 0.04	0.52 ± 0.04
pC_{22}	0.840 ± 0.001	0.53 ± 0.04	0.31 ± 0.04	0.46 ± 0.06	0.54 ± 0.07
$pSiO_2$	0.739 ± 0.002	0.58 ± 0.01	0.16 ± 0.01	-	-
nSiH	0.324 ± 0.001	0.30 ± 0.03	0.03 ± 0.03	-	-
nC_{10}	1.230 ± 0.006	0.87 ± 0.01	0.37 ± 0.01	1.18 ± 0.04	1.42 ± 0.04
nC_{12}	1.330 ± 0.003	0.88 ± 0.02	0.44 ± 0.02	1.30 ± 0.06	1.43 ± 0.06
nC_{16}	1.290 ± 0.001	0.89 ± 0.01	0.40 ± 0.01	0.87 ± 0.02	0.97 ± 0.02
nC_{22}	1.270 ± 0.002	0.88 ± 0.01	0.39 ± 0.01	0.58 ± 0.02	0.69 ± 0.02
$nSiO_2$	0.801 ± 0.003	0.58 ± 0.01	0.23 ± 0.01	-	-

It can be seen that the normalized values for the effective barrier height $q\phi_{eff}$ are much higher as compared to Table 2.3. Especially for the n-type samples with the higher amount of fixed charge, a very large increase in effective barrier height is obtained. Starting with the comparison of the values of $q\phi_{eff}$ and $q\phi_B$ for the SiH samples, it can be seen that for the nSiH sample $q\phi_{eff}$ and $q\phi_B$ are similar. The pSiH samples, however, showed a deviation between these two values. The extra barrier term introduced by the SiO_2 was for p-type silicon in the same order as the C_{12} layer whereas for n-type silicon the monolayers yielded much higher barriers. This indicates the good insulating properties of the organic monolayers on n-type silicon.

While discussing the β parameter it must be recalled that the samples with deviating behavior were pC_{10} (high diode ideality factor, shifted V_{fb}), nC_{16} and nC_{22} (deviating J-V curves). When establishing a general view of the behavior of monolayer on n- and p-type silicon they are treated as exceptions. Table 2.5 shows that a larger dependency is found for electron tunneling than for hole tunneling. This has also been found in literature, where hole tunneling is thought to be a more efficient process than electron tunneling [28, 40]. Theoretical values mentioned for hole and electron tunneling through alkyl layers are 0.4-0.8 Å^{-1} and 0.8-1.0 Å^{-1}, respectively [28]. In literature β has been derived for many different metal – monolayer – metal or metal – monolayer – semiconductor systems and the β values all lie in the above mentioned range [40, 71-75]. Apart from pC_{10} all p-type samples modified with an organic monolayer gave low β values. Such low values indicate that hole tunneling through these layers is very efficient [28, 40]. β values determined for nC_{10} and nC_{12} samples, however, are very high, indicating that electrons do not tunnel efficiently through these layers on n-type silicon. Such high values have not been reported before in literature. β values for the nC_{16} and nC_{22} samples are much lower, which is the result that $q\phi_{eff}$ for these samples was derived from already deviating *J-V* curves.

β can also be determined via an alternative route. Plotting of $q\phi_{eff}$ vs. the monolayer thickness leads to a graphical determination of β via Equation 2.2. This is done for the monolayers on p-type silicon. This method presumes that $q\phi_B$ is equal for all samples. pC_{10} was not included in this analysis, given its deviating value of $q\phi_B$. The n-type samples are also not analyzed in this way, since nC_{16} and nC_{22} both showed deviating behavior. Figure 2.11 shows the two graphs of $q\phi_{eff}$ derived from the non-normalized *J-V* plots ($q\phi_{eff1}$) and normalized *J-V* plots ($q\phi_{eff2}$).

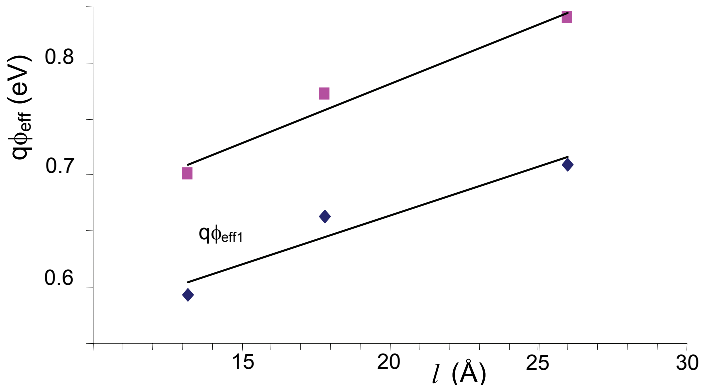

Figure 2.11. $q\phi_{eff}$ vs. monolayer thickness for $q\phi_{eff1}$ and $q\phi_{eff2}$.

From these data the following values for β can be calculated using Equation (2): $\beta_1 = 0.34 \pm 0.10$ Å^{-1} using the $q\phi_{eff1}$ values and $\beta_2 = 0.41 \pm 0.07$ Å^{-1} using the $q\phi_{eff2}$ values, respectively. Repeating this analysis for $q\phi_{eff}$ vs. the thickness expressed as number of carbon atoms gives: $\beta_1 = 0.44 \pm 0.11$ per CH_2-group and $\beta_2 = 0.53 \pm 0.07$ per CH_2-group. The latter results exclude any errors made in the monolayer thickness determination. β_2 is in close agreement with the values derived in Table 2.5. It can be seen that this method is very sensitive towards differences in Si-monolayer interface structure ($q\phi_B$) between the samples, which, if not been taken into account, may lead to an underestimation of the β parameter in this case.

2.3.5 Stability measurements and aging

It is know from literature that H-terminated silicon surfaces as obtained via HF etching are nearly electrically perfect [76] but degrade rapidly in ambient air and in water due to oxidation [77]. Silicon surface passivation via alkylation reactions, such as the ones described in this chapter, offers a good alternative to provide a protection of the silicon against oxidation [10, 15, 55] and to maintain the good electronic properties of the silicon electrodes [37, 38]. However, via alkylation not all Si-H bonds have reacted due to steric hindrance of the attached chains. At Si<111> surfaces about 50-55% [78, 79] and at Si<100> surfaces about 30-35% [80] of the sites have reacted. If a large number of unreacted sites are open to be approached by water or oxygen they can possibly be oxidized. Such oxide formation is thought to degenerate the electrode. To investigate the practical use of the tested monolayers in ambient conditions over a prolonged period of time, two repetition cycles of both *I-V* and *C-V* measurements have been performed to check the stability and aging behavior of all samples with Si-C linked monolayers. The first repetition (situation (B)) was performed after storage in the dark under vacuum for 10 months and then an exposure to ambient air for two months. The second repetition (situation (C)) was performed after a subsequent storage in the dark in ambient air for 2.5 months.

The *J-V* results for the three measurement cycles for all samples on p-type silicon with monolayers are depicted in Figure 2.12. The results from the two repetitions are averaged values of at least three measurements points.

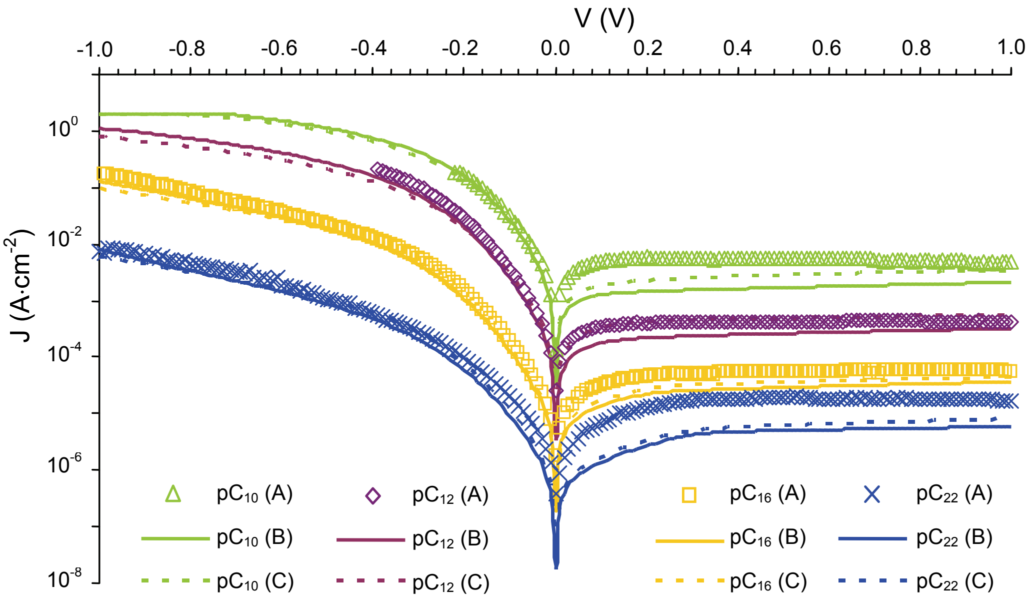

Figure 2.12. *J-V* plots of p-type silicon samples with four different chain lengths measured at three different occasions. (A) is the original data, indicated with markers; (B) is the data of the first repetition, indicated with solid lines; (C) is the data of the second repetition, indicated with broken lines. Left-hand side is accumulation and right-hand side is depletion.

In Figure 2.12 it is shown obviously that the results of three measurement cycles coincide very well for all four chain lengths. This is a clear indication that the monolayer still dictates the current-voltage behavior and that oxidation, if any, is not too such a degree that the samples have degenerated and the chain length dependent behavior is no longer visible. A small current decrease, however, is visible in the depletion regime. In this regime the current is due to minority carriers. The current decrease can be translated into a higher barrier experienced by the minority carriers (see Equation 2.1). A precise cause of the small current decrease in depletion is not clear yet. Partial oxidation may in this case have a beneficial influence on the *J-V* behavior if the oxide provides an extra blocking barrier for the charge carriers.

The results of repeated measurements on n-type silicon electrodes with similar monolayers were in accordance with those of p-type silicon electrodes. The data in accumulation were very reproducible. However, apart from the nC_{10} samples the reverse currents in depletion for nC_{12}, nC_{16}, and nC_{22} increased after every repetition. The strongest increase was observed at the nC_{12} samples as indicated in Figure 2.13.

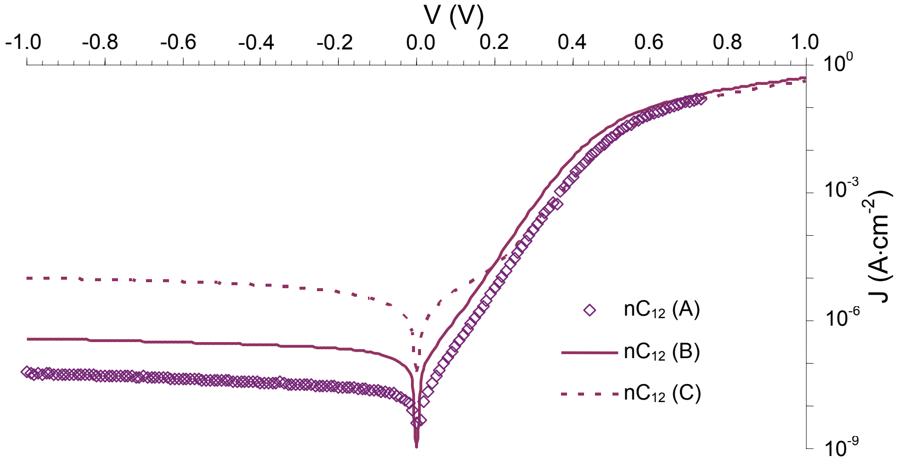

Figure 2.13. *J-V* plots of n-type silicon samples with a C_{12} monolayer measured at three different occasions. (A) is the original data, indicated with markers; (B) is the data of the first repetition, indicated with solid lines; (C) is the data of the second repetition, indicated with broken lines. Right-hand side is accumulation and left-hand side is depletion.

The trend observed at n-type silicon samples in the depletion regime was opposite to the trend observed at p-type silicon samples for which a current decrease was observed at every repeated measurement. The difference in current density between measurement A and C in depletion in Figure 2.13 was nearly three decades. The shape of curve C now resembles the curves of the initial results of the nC_{16} and nC_{22} samples (see Figure 2.4B), in which also large current densities in the reverse bias and low forward bias regime were observed. It was reasoned then that a possible explanation for this behavior was an increase of the amount of surface states possibly due to oxidation or breaking of Si-H bonds. If many surface states are created over time, the minority carriers will experience an easier pathway (lower barrier) from metal to silicon, resulting in larger currents. At high forward voltages the insulator resistive properties play a role again and the currents of all three measurements coincide again. To actually understand the cause of this behavior, more information of the topography of the silicon-monolayer interface is necessary. For instance the amount of extra oxygen in the monolayer, as can be measured via XPS measurements, or a possible increase in surface roughness due to oxidation, as can be measured via STM measurements, can provide crucial answers to clarify the observed phenomena.

Next the *C-V* measurements will be discussed. The data for the pC_{16} and pC_{22} samples is shown in Figure 2.14.

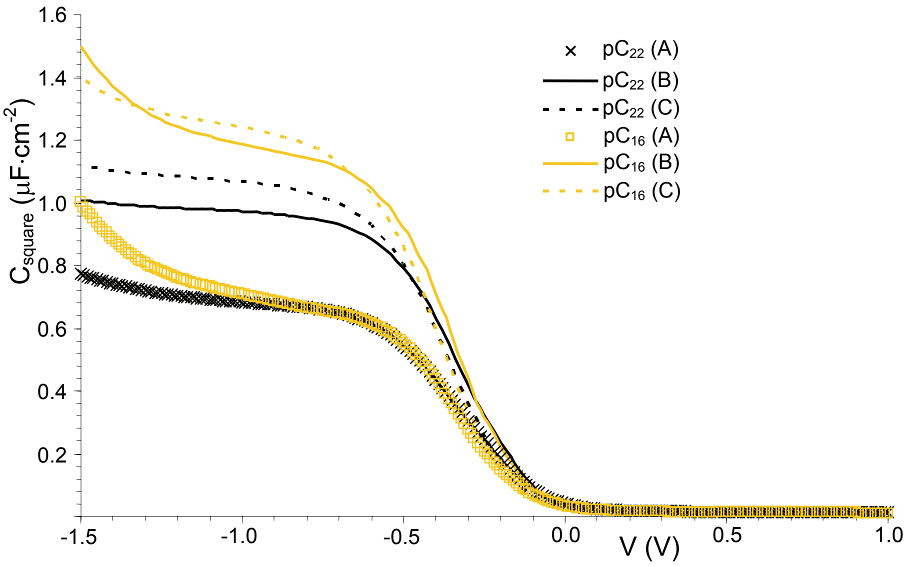

Figure 2.14. *C-V* plots of p-type silicon samples with a C_{16} and C_{22} monolayer measured at three different occasions. (A) is the original data, indicated with markers; (B) is the data of the first repetition, indicated with solid lines; (C) is the data of the second repetition, indicated with broken lines.

Since the areas of the mercury dot were different for subsequent measurements, the capacitance in Figure 2.14 has been normalized, i.e. $C \cdot A^{-1}$ has been plotted. The trend seen in Figure 2.14 is that the capacitance in accumulation increases at each subsequent measurement. The same trend was also observed at the other samples of both p- and n-type silicon. The capacitance in accumulation, which equals the insulator capacitance can be written after normalization for the area as: $C = \varepsilon_0 \cdot \varepsilon_r \cdot d^{-1}$, where ε_r can be taken as an effective dielectric constant and d as an effective thickness of the organic monolayer combined with possible oxide. ε_r is expected not to change much; for a pure monolayer it is calculated in this study to be in between 1.7 ± 0.1 to 2.8 ± 0.2 and for pure SiO_2 this is 3.9 [30, 31], so in the hypothetical case where the whole surface will be oxidized ε_r will increase at most a factor of 2.3. The capacitances have also increased so this is in line with the observations. Upon oxidation the thickness d is expected to increase too. However, this should result in a lower capacitance, which is clearly not the case in Figure 2.14. If oxidation has taken place, the results indicate that the overall thickness increased only a little bit. For instance, the capacitance at the pC_{22} sample increased approximately a factor 1.3 in between measurements A and B. Assuming that in case of the pC_{22} sample ε_r increased from 2.2 (Table 2.2) to 3.9, i.e. a factor of 1.8, then the insulator thickness in case B should have increased only a factor 1.4. Since it is reasonable to assume that ε_r cannot increase so much due to the presence of the monolayer, any thickness increase due to oxidation should be much less.

Finally, the flatband voltages have been derived for all samples via Mott Schottky measurements. The flatband voltage is a sensitive parameter for changes in the monolayer-silicon interface since every extra parasitic charge due to for instance built in of charges as a result of oxidation leads to a change in flatband voltage. For convenience the Equation for the flatband voltage in MIS devices with parasitic charges is given in Equation 2.13 [30]:

$$V_{fb} = \phi_{MSi} - \frac{Q_f}{C_{ins}} - \frac{Q_{it}}{C_{ins}} \tag{2.13}$$

The first term on the right is already defined in Equation 2.10, the second term denotes an additional voltage shift due to fixed charge in the monolayer or at the monolayer-silicon interface, and the last term denotes an additional voltage shift due to interface states at the monolayer-silicon interface. This amount of interface states is actually related to the applied bias voltage. Upon oxidation normally net positive charges are built in [30]. However, if in this case the extra charges due to oxidation or breaking of Si-H bonds are of the same sign, i.e. either positive or negative, charge compensation can occur and no shift will be detected (see Equation 2.13). A case in between is when both positive and negative charges are created which are located at different depths in the insulator. This will lead to shifts in flatband voltages [30] but not as much as the case for charges of one sign. So, care should be taken in interpreting any flatband voltage shifts from repetitive measurements since the origin of any shifts is not precisely known. In Table 2.6 an overview is given of the flatband voltages for subsequent measurements at all samples.

Table 2.6. Results of the Mott Schottky analysis of subsequent measurements.

insulator	$V_{fb,theory} = \phi_{MSi}$ [V]	V_{fb} (A) [V]	V_{fb} (B) [V]	V_{fb} (C) [V]
pC_{10}	-0.45	-0.22 ± 0.01	-0.40 ± 0.02	-0.74 ± 0.04
pC_{12}	-0.45	-0.34 ± 0.03	-0.78 ± 0.04	-0.94 ± 0.03
pC_{16}	-0.45	-0.34 ± 0.02	-0.78 ± 0.02	-1.15 ± 0.02
pC_{22}	-0.45	-0.32 ± 0.04	-0.87 ± 0.03	-1.18 ± 0.03
nC_{10}	0.18	0.61 ± 0.01	0.46 ± 0.01	0.47 ± 0.01
nC_{12}	0.18	0.63 ± 0.02	0.48 ± 0.01	0.51 ± 0.01
nC_{16}	0.18	0.63 ± 0.01	0.50 ± 0.01	0.54 ± 0.01
nC_{22}	0.18	0.63 ± 0.01	0.55 ± 0.01	0.56 ± 0.02

In Table 2.6 a clear trend is visible for all p-type silicon samples. The flatband voltage shifts to more negative values, indicating the presence of more positive charges. Although in measurement (A) V_{fb} was more positive than the theoretical flatband voltage (first column in Table 2.6), indicating negative charges at the silicon-monolayer interface, for measurements (B) and (C) V_{fb} shifted towards more negative values, indicating now positive charges present at the interface. Since oxidation is known to be associated with the built-in of net positive charges [30] the results in Table 2.6 indicate that some degree of oxidation has taken place for all p-type silicon samples. Via XPS measurements this potential explanation can be verified. If the shifts in V_{fb} are now associated with fixed charges as done in the analysis in section 2.3.4 the amount of fixed charges per area can be calculated for each measurements cycle via Equation 2.12. The results are shown in Table 2.7.

Table 2.7. N_f calculated for pC_{16} and pC_{22} samples for three subsequent measurements.

insulator	N_f (A) [10^{11} cm^{-2}]	N_f (B) [10^{12} cm^{-2}]	N_f (C) [10^{12} cm^{-2}]
pC_{16}	-5.8 ± 1.0	+2.8 ± 0.2	+6.6 ± 0.3
pC_{22}	-6.2 ± 2.0	+2.7 ± 0.2	+5.2 ± 0.3

For both samples the fixed charges have become positive in cases B and C and increased to approximately $5\text{-}7\cdot10^{12}$ cm^{-2} in case C. This quantity can be visualized in the following way. The atomic density of the <100> silicon surface is $6.78\cdot10^{14}$ atoms·cm^{-2} [77]. Assume that all charge originates from surface atoms with single charge q then in case C one out of approximately 100 surface atoms would be charged.

In case of the n-type silicon samples this line of reasoning cannot be followed. V_{fb} shifts to more negative directions in case B but shifts then towards slightly more positive values again in case C. A direct indication of oxidation via extra positive charges such as in the case of all p-type silicon samples can thus not be given. However, the *J-V* results and the *C-V* results of the samples of n-type silicon indicate changes. Perhaps, less oxidation took place for the n-type silicon samples of silicon-monolayer interface changed in such a way that both positive and negative charges were created, which would then lead to little change in V_{fb}.

2.4 Conclusions

Organic monolayers covalently bound to p- and n-type silicon were successfully characterized via *J-V* and C-V measurements and the results were compared with H-terminated samples and samples with 2 nm SiO_2. It was demonstrated that all layers showed insulating behavior and behaved as Schottky diodes. All monolayers on n-type silicon and monolayers > C_{12} on p-type silicon showed better insulating properties than silicon oxide.

Results from *J-V* measurements for p-silicon samples showed that the effective barrier height $q\phi_{eff}$ increased clearly as a function of monolayer thickness. Not only the effective barrier height is affected by the chain length, but also the series resistance R_s was strongly affected in an exponential way. Samples of n-type silicon modified with alkyl monolayers did not display this clear dependence. It was found that $q\phi_{eff}$ increased for nC_{10} and nC_{12} as compared to nSiH and $nSiO_2$, but a decrease was found for the longer chains. An unambiguous explanation for this phenomenon can as of yet not be given and has to be further investigated. Organic alkyl monolayers on n-type silicon form more ideal diodes than these monolayers on p-type silicon.

Results from *C-V* measurements showed typical metal-semiconductor *C-V* behavior for SiH, SiO_2, C_{10}, and C_{12} covered silicon. For C_{16} and C_{22} layers a plateau in accumulation was observed and this indicated the formation of a real capacitance. Analysis of this plateau yielded the dielectric constant, which varied from 1.7 ± 0.1 to 2.8 ± 0.2. Mott Schottky analysis gave similar values for the flatband voltage for different chain lengths apart from pC_{10} samples. This suggests similar interface properties for all investigated monolayers other than pC_{10}. For the C_{16} and C_{22} layers the amount of fixed charge has been evaluated. This gave remarkably low values of fixed charge density for monolayers on p-type silicon (~ $6 \cdot 10^{11}$ cm^{-2}) as compared to samples on n-type silicon (~ $3 \cdot 10^{12}$ cm^{-2}). Evaluation of the tunneling constant β gave higher values for n-type silicon, $\beta = 0.58\text{-}1.30$ $Å^{-1}$, as compared to p-type silicon, $\beta = 0.43\text{-}0.46$ $Å^{-1}$ excluding the pC_{10} samples. This confirms that holes tunnel more efficient as compared to electrons.

From stability measurements it was shown that the *J-V* characteristics stayed intact for all samples. For all n-type silicon samples the current in depletion had increased, whereas for p-type silicon the current in depletion had decreased. The capacitance in accumulation had increased in all cases, indicating that ε_r of the insulator may have increased due to oxidation. For p-type silicon samples V_{fb} shifted, following a clear trend, for subsequent measurements towards more negative values. This is in line with oxidation, which usually involves the incorporation of net positive charges. For n-type silicon samples V_{fb} did not shift in a clear way and no conclusions could be drawn from that data, other than that changes have taken place given the changed *J-V* and *C-V* curves.

From the above results we conclude that from the electronic point of view, organic monolayers covalently bound to silicon offer a promising insulating and passivating material for molecular electronic devices. Moreover, given the numerous possibilities for chemical modification of the properties of the organic monolayers and the formation of true silicon-molecule interfaces, we believe that such layers are very promising for future nano-dimensioned silicon devices.

2.5 Experimental

2.5.1 Materials.

Silicon <100> 4” wafers (p-type: 5-10 Ω·cm and n-type: 1-10 Ω·cm) from Okmetic, Finland were used. PE 40/60, EtOH, and CH_2Cl_2 were distilled prior to use. Mesitylene (Fluka, 99%) was distilled and dried over $CaCl_2$. The dried mesitylene was filtered to remove traces of $CaCl_2$. 1-Decene (Fluka, 97%), 1-dodecene (Aldrich, 95%), and 1-hexadecene (Sigma, ~99%) were distilled twice at reduced pressure. 1-Docosene (TCI, 99+%), acetone (Acros, 99+%) and n-hexane (Acros, 99+%) were used as received. HF (Fluka, 50% p.a.-plus) was diluted with demineralized H_2O. Nitrogen was dehydrated over KOH and H_2SO_4, respectively. Mercury (Merck, 99.9999% Suprapur) was used as received. HexaMethylDiSilazane (HMDS) (Merck, VLSI grade) and photoresist (OLIN 907/12) (Fuji Foto Film) were used as received.

2.5.2 Sample preparation.

Oxidation

A number of wafers, both n- and p-type, were thermally oxidized with two different oxide thicknesses. The first batch had a target thickness of approximately 100 nm thermal oxide and was made to determine and verify the area of the mercury dot (batch 1). The second batch had a target thickness of a few nm and was made to check the insulating properties of SiO_2 insulators with similar thickness as the monolayer (batch 2). The wafers of both batches were first cleaned using a standard wafer cleaning (5 min. in 100% HNO_3, copious rinsing in demi water, 10 min. in boiling (69%) HNO_3 at 95°C and again copious rinsing in demi water). Just prior to oxidation the wafers received a HF-dip (1%) and were again rinsed in demi water and spinned dry. The wafers of batch 1 were oxidized in a Tempress Oven using a dry oxidation process in an O_2/N_2 mixture and a subsequent anneal step in a N_2 atmosphere. The wafers of batch 2 were inserted via the automatic transport rail into the same Tempress Oven, which was kept at a constant temperature of 700° C. After the wafer carrier was completely inserted it was immediately driven outward again. In this way a very thin SiO_2 layer of approximately 2 nm was thermally grown. Before oxidation the oven was cleaned with a *trans*-LC (*trans*-1,2-dichloroethylene) cleaning procedure. After oxidation the oxide thickness was measured with ellipsometry. Finally, these oxidized samples were rinsed with hexane before measurements to remove any organic contaminants.

Back contact fabrication and dicing

Before back contact manufacturing wafers without thermal oxide underwent the standard cleaning as described above and the front side was subsequently covered with HMDS and photoresist. After that the wafers were pre-baked at 120° C for 30 minutes. A similar procedure was used for oxidized wafers except that they were processed without cleaning after removal from the oven. Then the wafers received a 1% HF dip to remove the native oxide from the backside. A metal contact was made to the wafer via sputtering. On n-type wafers an interfacial layer of 50nm Ti/W alloy was deposited before a 1000 nm layer aluminum was sputtered. This Ti/W layer lowered the Ohmic resistance of the contact. On p-type wafers a 1000 nm aluminum layer was directly sputtered. Next, a chromium layer was sputtered onto the aluminum on both type wafers to protect it from being etched in HF prior to monolayer formation. This was followed by an annealing step at 450° C in a N_2 atmosphere. The photoresist was removed with acetone. Finally, the samples were diced into pieces of 18 mm x 25 mm. Before monolayer modification the samples are placed in a plasma cleaner to remove all organic contaminants. Possible traces of HMDS and photoresist (if any) are hereby removed from the oxide surface.

Preparation of the organic monolayer

The Si samples were first wiped with tissue that was saturated with chemically pure acetone. After that, the samples were sonicated for at least 15 min in demineralized H_2O and acetone, respectively. Then the samples were dried in a stream of nitrogen and placed in a plasma cleaner/sterilizer (Harrick PDC-32G) for 1 min. Subsequently the samples were etched in 2.5% HF for 2 minutes. After removal from the HF solution the sample was dry, indicating that the surface was oxide-free.

A 1-alkene solution in mesitylene (12.5 ml, 0.2 M) was placed in a small, three-necked flask fitted with a nitrogen inlet, a condenser with a $CaCl_2$ tube, and a stopper. The solution was deoxygenated for at least 45 min, by refluxing it, while slowly bubbling dry nitrogen through the solution. Subsequently a freshly etched Si sample was added to the refluxing solution by removing and replacing the stopper quickly. After 2 h the solution was allowed to cool and the sample was removed and rinsed extensively with distilled PE 40/60, EtOH, and CH_2Cl_2, respectively.

Preparation of the hydrogen-terminated samples

The samples were sonicated for at least 10 min in demineralized H_2O and acetone, respectively. Then the samples were placed in a plasma cleaner/sterilizer (Tepla 300E) for 1 minute. Subsequently the samples were etched in 1% HF for 1 minute, rinsed with demi water and dried using a nitrogen gun.

Preparation of the samples for verification of the mercury dot area

In order to check the area of the mercury dot both hydrophobic and hydrophilic SiO_2 surfaces of batch 1 were used. This was done to exclude any wetting effects of the mercury and hence a possible change in effective contact area. Some of the samples of batch 1 of the oxidized wafers were therefore put in a Lab-Line vacuum oven to let the silicon oxide surface react with HMDS to make it more hydrophobic. HMDS is normally used as a primer to make the hydrophilic SiO_2 surface hydrophobic for a better adhesion of photoresist. At a pressure of 25 cmHg and at a temperature of 140° C the samples were put in the oven for 100 minutes under a constant HMDS flow. Afterwards both the contact angle and the thickness of the HMDS-treated as well as the non-HMDS treated SiO_2 surfaces were determined. The thickness of the HMDS-treated SiO_2 surface increased 0.2 nm as compared to prior to HMDS treatment indicating that only a small layer of HMDS was on the surface. It is not expected that HMDS-treatment of the 100 nm thick SiO_2 layer negatively influences its isolating properties and hence normal *C-V* measurements are equally possible as for the non-HMDS treated SiO_2 samples to determine the mercury dot area.

2.5.3 Contact angle and thickness measurements

Directly after cleaning static water contact angles of the monolayers on the silicon samples were obtained using an Erma Contact Angle Meter G-1 (volume of the drop of demineralized H_2O = 3.5 μl). Two or three drops of water were placed near one of the short edges of the sample. This wetted area was not studied in the electrical measurements. The error of the contact angles is ± 1°. After removal of the water drops the samples were cleaned with EtOH and CH_2Cl_2. The samples were stored under a nitrogen atmosphere or vacuum until the electrical measurements took place.

The thickness of oxide layers was measured with an ellipsometer (Plasmos SD 2002) using a fixed refractive index of 1.465 for the SiO_2 layers. The thickness of the organic monolayers was determined earlier via X-ray reflectivity. The thickness of the C_{10} layer was too thin to be determined via X-ray reflectivity measurements and was therefore calculated using a model mentioned in [10]. Table 2.8 gives an overview of the results.

Table 2.8. Results of static water contact angle and thickness measurements on samples modified with different insulators.

Sample	Abbreviation	Water contact Angle [°]	Thickness [Å]	Thickness determined via:
pSi-SiO_2 (2nm)	pSiO_2	Not measured	19.9 ± 0.6	Ellipsometry
nSi-SiO_2 (2nm)	nSiO_2	Not measured	20.3 ± 1.1	Ellipsometry
pSi-$C_{10}H_{21}$ / nSi-$C_{10}H_{21}$	pC_{10} / nC_{10}	107 / 107	12.1	Calculated [81]
pSi-$C_{12}H_{25}$ / nSi-$C_{12}H_{25}$	pC_{12} / nC_{12}	109 / 108	13.2 ± 0.1	X-ray reflectivity [55]
pSi-$C_{16}H_{33}$ / nSi-$C_{16}H_{33}$	pC_{16} / nC_{16}	109 / 108	17.8 ± 0.2	X-ray reflectivity [55]
pSi-$C_{22}H_{45}$ / nSi-$C_{22}H_{45}$	pC_{22} / nC_{22}	102 / 100	26.0 ± 1.0	X-ray reflectivity [56]
pSi-SiO_2 (100nm)	(used for Hg-dot area verification)	< 20	1003 ± 1	Ellipsometry
pSi-SiO_2 (100nm)-HMDS	(used for Hg-dot area verification)	84	1008 ± 2 (1006 ± 1) [a]	Ellipsometry

[a] Thickness measured before HMDS treatment.

2.5.4 Electrical characterization

I-V and *C-V* measurements were performed using a mercury probe (Material Development Corporation (MDC) MDC811-150) connected to an HP4140B pA meter and an HP4275A C-V meter. A schematic picture of the mercury probe and the sample structure is given in Figure 2.15. Note that the figure is not to scale and serves only to indicate all the layers and positions of the sample in the set-up.

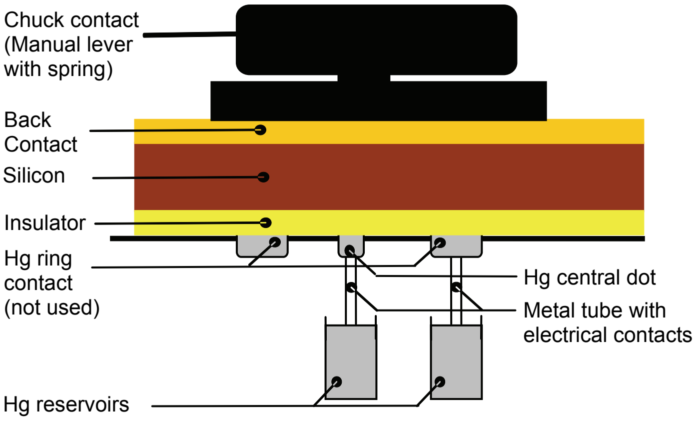

Figure 2.15. Schematic view of the measurements set-up. Only the central mercury dot was used for measurements. The outer mercury ring was not electrically connected.

The sample is placed with the insulator faced down in the probe. Via a manually operated lever the chuck-contact is pressed down on the back contact of the sample and fixed via a spring. As the lever is pressed down, a vacuum valve is opened and mercury in the reservoirs is sucked via the tubes against the insulator. Before the start of the measurements the mercury was renewed. The set-up is computer controlled by the MDC software package CSM/Win. For the *I-V* measurements the bias voltage was swept from +1.0 V to –1.0 V for p-type silicon or vice versa for n-type silicon. The mercury is positively biased with respect to the bulk silicon. The voltage was swept with a step size of 0.01 V at long integration time and a delay time of 0.2 s to measure exclusively the leakage current. All measurements were repeated at least once and in this voltage range none of the samples with organic monolayers showed breakthrough or increase in current during subsequent measurements. For the *C-V* measurements the DC-voltage was swept in the same way as in the *I-V* measurements with a step size of 0.01 V. The ac-amplitude was 50 mV and the measurement frequency was chosen at 400 kHz. This frequency should not be too low to prevent quasistatic behavior and to prevent possible interface states from following the ac-signal. At half of the spots *C-V* measurements were repeated at 10 kHz, 40 kHz and 100 kHz for comparison purposes. The impedance model chosen was a parallel (C_p – G_p) model. The C_p data was automatically corrected for the series resistance according to a procedure in [62].

2.5.5 Stability measurements

In case of the stability study mentioned in section 2.3.5 the following procedures were followed. Before the measurement the samples were rinsed thoroughly with CH_2Cl_2 to remove any loose organic contaminants. Next, *I-V* and *C-V* measurements were performed using the same mercury probe (type: MDC811-150 from Material Development Corporation (MDC), USA) connected to a HP4140B pA meter and a HP4284A C-V (LCR) meter. Before the start of the measurements the mercury was renewed. Both *I-V* meter and *C-V* meter are connected to a HP E5250A low leakage switch mainframe. The set-up is computer controlled by the Metrics software package ICS. For the *I-V* (HP4140B) measurements the bias voltage was swept from 0 V to +1.0 V and from 0 V to –1.0 V (for the p-type silicon; the mercury is positive with respect to the bulk) or vice versa (for the n-type silicon). The voltage was swept with a step size of 0.01 V at medium integration time and a delay time of 0.2 s to measure solely the leakage current. The current limit of the 4140B was set to 10 mA. All measurements were repeated once. For the *C-V* (HP4284A) measurements the DC-voltage was swept in the same way as in the *I-V* measurements with a step size of 0.02 V. The ac-amplitude was 50 mV and the measurement frequency was chosen 400 kHz. Before the measurements of the samples with monolayers were started, reference measurements as described above to check the mercury dot area were done via *C-V* measurements on a p-type silicon sample with a 100 nm SiO_2 insulator (thickness was precisely determined via ellipsometry). Throughout the measurements the under-pressure of the mercury contact was measured and kept constant to prevent fluctuations in contact area. In these cases higher under pressures were used than in the first study mentioned in 2.5.4 and consequently a higher area was used: $A = (5.2 \pm 0.1)\cdot 10^{-3}$ cm^{-2}.

2.6 References

[1] M. Schulz, "The end of the road for silicon?" *Nature* **1999**, *399*, 729.

[2] M. Hirose, M. Koh, W. Mizubayashi, H. Murakami, K. Shibahara, S. Miyazaki, "Fundamental limit of gate oxide thickness scaling in advanced MOSFETs", *Semiconductor Science and Technology* **2000**, *15*, 485.

[3] D. A. Muller, T. Sorsch, S. Moccio, F. H. Baumann, K. Evans-Lutterodt, G. Timp, "The electronic structure at the atomic scale of ultrathin gate oxides", *Nature* **1999**, *399*, 758.

[4] A. I. Kingon, J. P. Maria, S. K. Streiffer, "Alternative dielectrics to silicon dioxide for memory and logic devices", *Nature* **2000**, *406*, 1032.

[5] R. D. Miller, "Device physics - In search of low-k dielectrics", *Science* **1999**, *286*, 421.

[6] P. S. Peercy, "The drive to miniaturization", *Nature* **2000**, *406*, 1023.

[7] A. Ulman, *An Introduction to Ultrathin Organic Films: From Langmuir-Blodgett to Self-Assembly*, Academic Press, New York, **1991**.

[8] A. Ulman, "Formation and structure of self-assembled monolayers", *Chemical Reviews* **1996**, *96*, 1533.

[9] M. R. Linford, C. E. D. Chidsey, "Alkyl Monolayers Covalently Bonded to Silicon Surfaces", *Journal of the American Chemical Society* **1993**, *115*, 12631.

[10] M. R. Linford, P. Fenter, P. M. Eisenberger, C. E. D. Chidsey, "Alkyl Monolayers on Silicon Prepared from 1-Alkenes and Hydrogen-Terminated Silicon", *Journal of the American Chemical Society* **1995**, *117*, 3145.

[11] A. Bansal, X. L. Li, I. Lauermann, N. S. Lewis, S. I. Yi, W. H. Weinberg, "Alkylation of Si surfaces using a two-step halogenation Grignard route", *Journal of the American Chemical Society* **1996**, *118*, 7225.

[12] C. H. deVilleneuve, J. Pinson, M. C. Bernard, P. Allongue, "Electrochemical formation of close-packed phenyl layers on Si(111)", *Journal of Physical Chemistry B* **1997**, *101*, 2415.

[13] A. B. Sieval, V. Vleeming, H. Zuilhof, E. J. R. Sudhölter, "An improved method for the preparation of organic monolayers of 1-alkenes on hydrogen-terminated silicon surfaces", *Langmuir* **1999**, *15*, 8288.

[14] R. Boukherroub, S. Morin, F. Bensebaa, D. D. M. Wayner, "New synthetic routes to alkyl monolayers on the Si(111) surface", *Langmuir* **1999**, *15*, 3831.

[15] A. B. Sieval, R. Linke, H. Zuilhof, E. J. R. Sudhölter, "High-quality alkyl monolayers on silicon surfaces", *Advanced Materials* **2000**, *12*, 1457.

[16] D. D. M. Wayner, R. A. Wolkow, "Organic modification of hydrogen terminated silicon surfaces", *Journal of the Chemical Society-Perkin Transactions 2* **2002**, 23.

[17] J. M. Buriak, "Organometallic chemistry on silicon and germanium surfaces", *Chemical Reviews* **2002**, *102*, 1271.

[18] S. F. Bent, "Organic functionalization of group IV semiconductor surfaces: principles, examples, applications, and prospects", *Surface Science* **2002**, *500*, 879.

[19] M. M. Sung, G. J. Kluth, O. W. Yauw, R. Maboudian, "Thermal behavior of alkyl monolayers on silicon surfaces", *Langmuir* **1997**, *13*, 6164.

[20] G. Roberts, *Langmuir-Blodgett Films*, Plenum, New York, **1990**.

[21] P. Fontaine, D. Goguenheim, D. Deresmes, D. Vuillaume, M. Garet, F. Rondelez, "Octadecyltrichlorosilane Monolayers as Ultrathin Gate Insulating Films in Metal-Insulator-Semiconductor Devices", *Applied Physics Letters* **1993**, *62*, 2256.

[22] C. Boulas, J. V. Davidovits, F. Rondelez, D. Vuillaume, "Suppression of charge carrier tunneling through organic self-assembled monolayers", *Physical Review Letters* **1996**, *76*, 4797.

[23] D. Vuillaume, C. Boulas, J. Collet, J. V. Davidovits, F. Rondelez, "Organic insulating films of nanometer thicknesses", *Applied Physics Letters* **1996**, *69*, 1646.

[24] J. Collet, S. Lenfant, D. Vuillaume, O. Bouloussa, F. Rondelez, J. M. Gay, K. Kham, C. Chevrot, "High anisotropic conductivity in organic insulator/semiconductor monolayer heterostructure", *Applied Physics Letters* **2000**, *76*, 1339.

[25] R. Cohen, N. Zenou, D. Cahen, S. Yitzchaik, "Molecular electronic tuning of Si surfaces", *Chemical Physics Letters* **1997**, *279*, 270.

[26] L. Chai, D. Cahen, "Electric signal transfer through nm-thick molecular bilayers", *Materials Science & Engineering C-Biomimetic and Supramolecular Systems* **2002**, *19*, 339.

[27] Y. Selzer, A. Salomon, D. Cahen, "Effect of molecule-metal electronic coupling on through-bond hole tunneling across metal-organic monolayer-semiconductor junctions", *Journal of the American Chemical Society* **2002**, *124*, 2886.

[28] Y. Selzer, A. Salomon, D. Cahen, "The importance of chemical bonding to the contact for tunneling through alkyl chains", *Journal of Physical Chemistry B* **2002**, *106*, 10432.

[29] M. CalistriYeh, E. J. Kramer, R. Sharma, W. Zhao, M. H. Rafailovich, J. Sokolov, J. D. Brock, "Thermal stability of self-assembled monolayers from alkylchlorosilanes", *Langmuir* **1996**, *12*, 2747.

[30] S. M. Sze, *Semiconductor Devices: Physics and Technology*, Wiley, New York, **1985**.

[31] D. K. Schroder, *Semiconductor Material and Device Characterization*, 2nd ed., Wiley, New York, **1998**.

[32] Y. J. Liu, H. Z. Yu, "Alkyl monolayer-passivated metal-semiconductor diodes: Molecular tunability and electron transport", *ChemPhysChem* **2002**, *3*, 799.

[33] Y. J. Liu, H. Z. Yu, "Alkyl monolayer passivated metal-semiconductor diodes: 2: Comparison with native silicon oxide", *ChemPhysChem* **2003**, *4*, 335.

[34] Y. J. Liu, H. Z. Yu, "Molecular passivation of mercury-silicon (p-type) diode junctions: Alkylation, oxidation, and alkylsilation", *Journal of Physical Chemistry B* **2003**, *107*, 7803.

[35] C. Miramond, D. Vuillaume, "1-octadecene monolayers on Si(111) hydrogen-terminated surfaces: Effect of substrate doping", *Journal of Applied Physics* **2004**, *96*, 1529.

[36] S. Kar, C. Miramond, D. Vuillaume, "Properties of electronic traps at silicon/1-octadecene interfaces", *Applied Physics Letters* **2001**, *78*, 1288.

[37] A. B. Sieval, C. L. Huisman, A. Schonecker, F. M. Schuurmans, A. S. H. van der Heide, A. Goossens, W. C. Sinke, H. Zuilhof, E. J. R. Sudhölter, "Silicon surface passivation by organic monolayers: Minority charge carrier lifetime measurements and Kelvin probe investigations", *Journal of Physical Chemistry B* **2003**, *107*, 6846.

[38] L. J. Webb, N. S. Lewis, "Comparison of the electrical properties and chemical stability of crystalline silicon(111) surfaces alkylated using grignard reagents or olefins with Lewis acid catalysts", *Journal of Physical Chemistry B* **2003**, *107*, 5404.

[39] J. W. Zhao, K. Uosaki, "Dielectric properties of organic monolayers directly bonded on silicon probed by current sensing atomic force microscope", *Applied Physics Letters* **2003**, *83*, 2034.

[40] A. Salomon, D. Cahen, S. Lindsay, J. Tomfohr, V. B. Engelkes, C. D. Frisbie, "Comparison of electronic transport measurements on organic molecules", *Advanced Materials* **2003**, *15*, 1881.

[41] R. L. Carroll, C. B. Gorman, "The genesis of molecular electronics", *Angewandte Chemie-International Edition* **2002**, *41*, 4379.

[42] G. Ashkenasy, D. Cahen, R. Cohen, A. Shanzer, A. Vilan, "Molecular engineering of semiconductor surfaces and devices", *Accounts of Chemical Research* **2002**, *35*, 121.

[43] C. Joachim, J. K. Gimzewski, A. Aviram, "Electronics using hybrid-molecular and mono-molecular devices", *Nature* **2000**, *408*, 541.

[44] R. M. Metzger, "Electrical rectification by a molecule: The advent of unimolecular electronic devices", *Accounts of Chemical Research* **1999**, *32*, 950.

[45] D. Vuillaume, "Nanometer-scale organic thin film transistors from self-assembled monolayers", *Journal of Nanoscience and Nanotechnology* **2002**, *2*, 267.

[46] D. K. Schroder, *Semiconductor Material and Device Characterization*, 2nd ed., Wiley, New York, **1998**, p. 401.

[47] E. Vincent, G. Ghibaudo, G. Morin, C. Papadas, in *IEEE 1997 International Conference on Microelectronic Test Structures, Vol. 10*, **1997**, pp. 105.

[48] The barrier height for p-type silicon is: $q\phi_{B,p} = qV_p - qV_{fb} = kT\ln(N_V(N_A)^{-1}) - qV_{fb}$, where qV_p is the energy difference between the top of the valence band and the silicon Fermi level; N_V is the number of effective states in the valence band (1.04x10^{19} cm^{-3} for p-type silicon [30], and N_A is the acceptor (doping) concentration.

[49] R. C. Weast, M. J. Astle, W. H. Beyer, *CRC Handbook of Chemistry and Physics*, 65th ed., CRC Press, Boca Raton, Florida, **1984**.

[50] D. K. Donald, "Experiments on Mercury-Silicon Surface Barriers", *Journal of Applied Physics* **1963**, *34*, 1758.

[51] P. J. Severin, G. J. Poodt, "Capacitance-Voltage Measurements with a Mercury-Silicon Diode", *Journal of The Electrochemical Society* **1972**, *119*, 1384.

[52] M. Wittmer, J. L. Freeouf, "Ideal Schottky Diodes on Passivated Silicon", *Physical Review Letters* **1992**, *69*, 2701.

[53] M. Wittmer, J. L. Freeouf, "Interface States and the Barrier Height of Schottky Diodes", *Physics Letters A* **1993**, *173*, 190.

[54] H. Yamamoto, D. H. Waldeck, "Effect of tilt-angle on electron tunneling through organic monolayer films", *Journal of Physical Chemistry B* **2002**, *106*, 7469.

[55] A. B. Sieval, A. L. Demirel, J. W. M. Nissink, M. R. Linford, J. H. van der Maas, W. H. de Jeu, H. Zuilhof, E. J. R. Sudhölter, "Highly stable Si-C linked functionalized monolayers on the silicon (100) surface", *Langmuir* **1998**, *14*, 1759.

[56] Q.-Y. Sun, L. C. P. M. d. Smet, B. v. Lagen, M. Giesbers, P. C. Thüne, F. A. Wolf, H. Zuilhof, E. J. R. Sudhölter, "Covalently Attached Monolayers on Crystalline Hydrogen-Terminated Silicon: Extremely Mild Attachment by Visible Light", *Journal of the American Chemical Society* **2005**, *127*, 2514.

[57] H. C. Card, E. H. Rhoderick, "Studies of tunnel MOS diodes I. Interface effects in silicon Schottky diodes", *Journal of Physics D: Applied Physics* **1971**, *4*, 1589.

[58] H. C. Card, E. H. Rhoderick, "Conductance associated with interface states in MOS tunnel structures", *Solid-State Electronics* **1972**, *15*, 993.

[59] S. Kar, W. E. Dahlke, "Interface states in MOS structures with 20-40 A thick SiO_2 films on nondegenerate Si", *Solid-State Electronics* **1972**, *15*, 221.

[60] S. Kar, W. E. Dahlke, "Potentials and direct current in Si-(20 to 40 A)SiO_2-metal structures", *Solid-State Electronics* **1972**, *15*, 869.

[61] E. H. Nicollian, J. R. Brews, *MOS Physics and Technology*, Wiley, New York, **1982**, p. 232.

[62] E. H. Nicollian, J. R. Brews, *MOS Physics and Technology*, Wiley, New York, **1982**.

[63] K. Slowinski, R. V. Chamberlain, C. J. Miller, M. Majda, "Through-bond and chain-to-chain coupling. Two pathways in electron tunneling through liquid alkanethiol monolayers on mercury electrodes", *Journal of the American Chemical Society* **1997**, *119*, 11910.

[64] M. A. Rampi, O. J. A. Schueller, G. M. Whitesides, "Alkanethiol self-assembled monolayers as the dielectric of capacitors with nanoscale thickness", *Applied Physics Letters* **1998**, *72*, 1781.

[65] H. Z. Yu, S. Morin, D. D. M. Wayner, P. Allongue, C. H. de Villeneuve, "Molecularly tunable "organic capacitors" at silicon/aqueous electrolyte interfaces", *Journal of Physical Chemistry B* **2000**, *104*, 11157.

[66] S. R. Morrison, *Electrochemistry at Semiconductor and Oxidized Metal Electrodes*, Plenum Press, New York, **1980**.

[67] H. Z. Yu, R. Boukherroub, S. Morin, D. D. M. Wayner, "Facile interfacial electron transfer through n-alkyl monolayers formed on silicon (111) surfaces", *Electrochemistry Communications* **2000**, *2*, 562.

[68] A. Bansal, N. S. Lewis, "Electrochemical properties of (111)-oriented n-Si surfaces derivatized with covalently-attached alkyl chains", *Journal of Physical Chemistry B* **1998**, *102*, 1067.

[69] For p-type silicon, the workfunction equals: $q\phi_{Si} = q\chi + E_g - qV_p = q\chi + E_g - kT\ln(N_V(N_A)^{-1})$.

[70] J. D. Plummer, M. D. Deal, G. P.B., *Silicon VLSI Technology, Fundamentals, Practice and Modeling*, Prentice Hall, New Yersey, **2000**.

[71] D. J. Wold, R. Haag, M. A. Rampi, C. D. Frisbie, "Distance dependence of electron tunneling through self-assembled monolayers measured by conducting probe atomic force microscopy: Unsaturated versus saturated molecular junctions", *Journal of Physical Chemistry B* **2002**, *106*, 2813.

[72] W. Y. Wang, T. Lee, M. A. Reed, "Mechanism of electron conduction in self-assembled alkanethiol monolayer devices", *Physical Review B* **2003**, *68*.

[73] J. Cheng, D. B. Robinson, R. L. Cicero, T. Eberspacher, C. J. Barrelet, C. E. D. Chidsey, "Distance dependence of the electron-transfer rate across covalently bonded monolayers on silicon", *Journal of Physical Chemistry B* **2001**, *105*, 10900.

[74] R. E. Holmlin, R. Haag, M. L. Chabinyc, R. F. Ismagilov, A. E. Cohen, A. Terfort, M. A. Rampi, G. M. Whitesides, "Electron transport through thin organic films in metal-insulator-metal junctions based on self-assembled monolayers", *Journal of the American Chemical Society* **2001**, *123*, 5075.

[75] K. Slowinski, H. K. Y. Fong, M. Majda, "Mercury-mercury tunneling junctions. 1. Electron tunneling across symmetric and asymmetric alkanethiolate bilayers", *Journal of the American Chemical Society* **1999**, *121*, 7257.

[76] E. Yablonovitch, D. L. Allara, C. C. Chang, T. Gmitter, T. B. Bright, "Unusually Low Surface-Recombination Velocity on Silicon and Germanium Surfaces", *Physical Review Letters* **1986**, *57*, 249.

[77] X. G. Zhang, *Electrochemistry of Silicon and its Oxide*, Kluwer Academic Publishers, New York, **2001**.

[78] A. B. Sieval, B. van den Hout, H. Zuilhof, E. J. R. Sudhölter, "Molecular Modeling of Alkyl Monolayers on the Si(111) Surface", *Langmuir* **2000**, *16*, 2987.

[79] A. B. Sieval, B. van den Hout, H. Zuilhof, E. J. R. Sudhölter, "Molecular Modeling of Covalently Attached Alkyl Monolayers on the Hydrogen-Terminated Si(111) Surface", *Langmuir* **2001**, *17*, 2172.

[80] A. B. Sieval, *Covalently Bound Organic Monolayers on Hydrogen-Terminated Silicon Surfaces*, PhD thesis, Wageningen University (Wageningen), **2001**, chapter 3, p. 44.

[81] For this calculation the model proposed by Linford et al. [10], note 40 was used.

Chapter 3

Improvement of Electronic Properties of Si-C Linked Organic Monolayers on Crystalline Silicon Surfaces: Alkenes vs. Alkynes[*]

Abstract: In this chapter the influence of silicon surface modification via Si-$C_{18}H_{37}$ devices on n-type silicon is studied by forming MIS (metal-insulator-silicon) diodes via a mercury-probe. Both the influence of the monolayer molecule (1-octadecene/1-octadecyne) and substrate orientation (<100>/<111>) are investigated. Via multiple *J-V* and *C-V* measurements relevant parameters are derived to obtain information on both reproducibility and monolayer and silicon-monolayer interface properties. It is found that 1-alkynes, which are able to make 2 Si-C bonds, have superior insulating properties as compared to 1-alkenes, which make only a single Si-C bond. There is no noticeable influence of substrate orientation, which indicates the broad usability of such monolayers. XPS measurements confirm the higher degree of oxidation at samples of both substrates with monolayers made from 1-alkenes. However, in contrast to findings from electrical characterization XPS measurements also show an overall higher amount of oxide on the <111> orientated samples as compared to <100> samples. Nonetheless, the ease of fabrication together with the outstanding electrical properties show the potential of monolayers of preferably 1-alkynes in creating hybrid molecular-silicon devices.

---

[*] This Chapter pertains to a manuscript in preparation:
E. J. Faber, L. C. P. M. de Smet, P. C. Thüne, W. Olthuis, H. Zuilhof, E. J. R. Sudhölter, P. Bergveld, A. van den Berg, *Manuscript in preparation*.

3.1 Introduction

Over the last decennia the ever-decreasing size of active semiconductor elements as used in e.g. microprocessors has placed a concomitantly higher demand on the quality of insulator layers on Si. Given the overall decreasing size, thinner and thinner SiO_2 insulator layers have been used, and these currently approach the fundamental limit [1-3]. As a result, increased interest has arisen in new insulating materials.

One of the candidates is the class of covalently attached monolayers on crystalline silicon surfaces. These can be obtained via reaction of 1-alkenes or 1-alkynes with hydrogen-terminated Si surfaces [4-7], as schematically depicted in Figure 3.1 for attachment onto an idealized Si<100> surface.

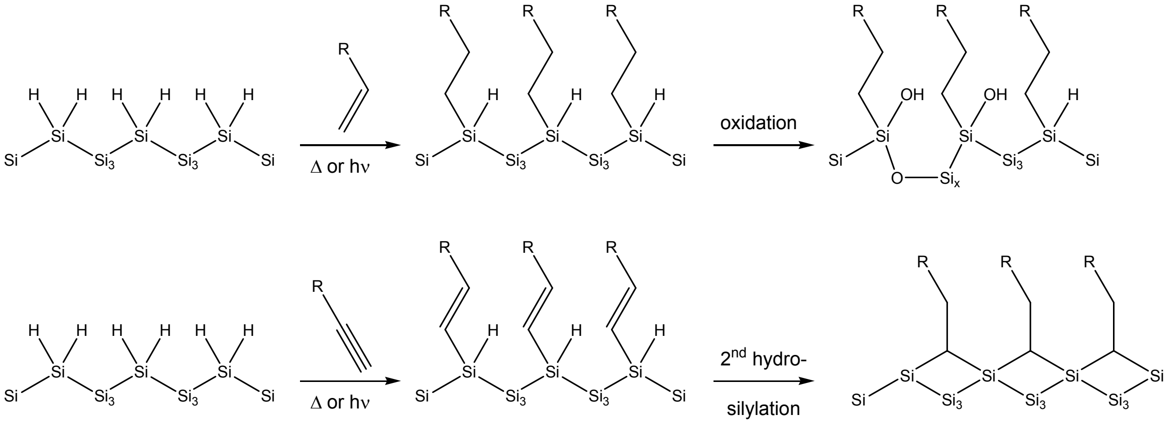

Figure 3.1. Attachment and partial oxidation of monolayers derived from 1-alkenes (top) and 1-alkynes (bottom) on crystalline hydrogen-terminated silicon surfaces.

Upon reaction of a 1-alkene with the H-terminated surface, a very stable Si-C bond is formed, and chain-wise formation [8, 9] of such bonds yields a densely packed monolayer, both on Si<111> and Si<100> [10, 11]. Characteristic of such monolayers is that the molecular cross-section of the attached alkyl chain prevents reaction of all individual Si-H bonds, i.e. upon formation of a densely packed monolayer on Si<111> about 50-55% of the Si-H sites has reacted [10, 11], while on Si<100> this is about 30-35%. The remaining surface Si-H bonds can in principle react with oxygen, yielding a structure such as depicted in Figure 3.1 top right, in which both the formation of silanol groups and incorporation of oxygen atoms are illustrated. XPS analysis of such monolayers has shown that the amount of oxygen being incorporated after formation of densely packed monolayers is very small even after storage for months under ambient conditions [4], but never completely absent. This is of specific importance for the electrical properties of such surfaces, which are determined to a large degree by surface defects such as caused by (partial) oxidation.

The previous chapter comprises the results of electrical measurements on MIS-structures of 1-alkene-derived monolayers ($Si-C_nH_{2n+1}$ with n = 10, 12, 16, and 22) on n and p-type <100>

silicon [12]. These measurements showed that such devices had outstanding silicon-interface properties and that the electrical behavior could be precisely tuned via the chain length. Other comparable electrical investigations of MIS-structures with Si-C linked monolayers as insulators were carried out by the groups of Yu [13-15], Vuillaume [16-18] and Kar [19], in which also the good insulating and passivating properties of these layers were showed. However, while the insulating properties of such monolayers were clearly superior to those of a thermal oxide layer of comparable thickness [12], it would be of significant interest to further improve these. Therefore, in this chapter we present the comparison of the electrical properties of monolayers derived from 1-alkenes and 1-alkynes. The reason to study 1-alkyne-derived monolayers is that previous work in our labs [20] and those of others [8, 21], has shown that 1-alkynes can react with H-terminated Si surface with formation of 2 Si-C bonds. For an idealized hydrogen-terminated Si<100> surface formation of two Si-C bonds with the terminal C atom of the alkyne (as depicted in Figure 3.1, bottom) was calculated to be slightly more stable than formation of one Si-C bond with the terminal C atom, and another Si-C bond involving the adjacent C atom of the alkyne moiety [20]. As a result, upon formation of a densely packed 1-alkyne derived monolayer, the number of unreacted Si-H sites is lower than upon formation of a 1-alkene-derived monolayer (*vide supra*). Therefore we hypothesized that this will lead to a reduction of the number of surface defects, and a concomitant increase in insulating properties. Furthermore, the influence of the silicon substrate orientation (<100>/<111>) is investigated. The <111> oriented silicon surface is used in many scientific studies, also in the above mentioned research of Yu [13-15], Vuillaume [16, 17] and Kar [19], since this orientation has a well-defined surface, which is atomically flat [5]. However, the <100> oriented silicon surface is of more interest for practical applications as this orientation is mainly used in semiconductor industry, since its Si-SiO_2 interface is electrically superior as compared to the same interface on Si<111> [22]. As stated above monolayers bound to both surface orientations form densely packed, high quality layers. Regarding future practical applications, it is of interest to investigate if there are differences in electrical properties of the same monolayer on different surface orientations.

This chapter presents data on the two above mentioned research topics by study of the metal-insulator-semiconductor (MIS) structures using a mercury probe as reported in Chapter 2 and in [12]. These are complemented by XPS measurements to correlate the electrical properties with the amount of oxygen present at such samples.

3.2 Results and Discussion

3.2.1 Current-Voltage data

Before the measurement of the samples the area of the mercury dot was determined following a procedure mentioned in Chapter 2, section 2.3.1. The vacuum that sucks the mercury towards the sample was measured and kept constant throughout all experiments. In this study the mercury area was: $A = (5.2 \pm 0.1)\cdot 10^{-3}$ cm^2. Figure 3.2 shows the averaged results from the *I-V* measurements for all tested samples.

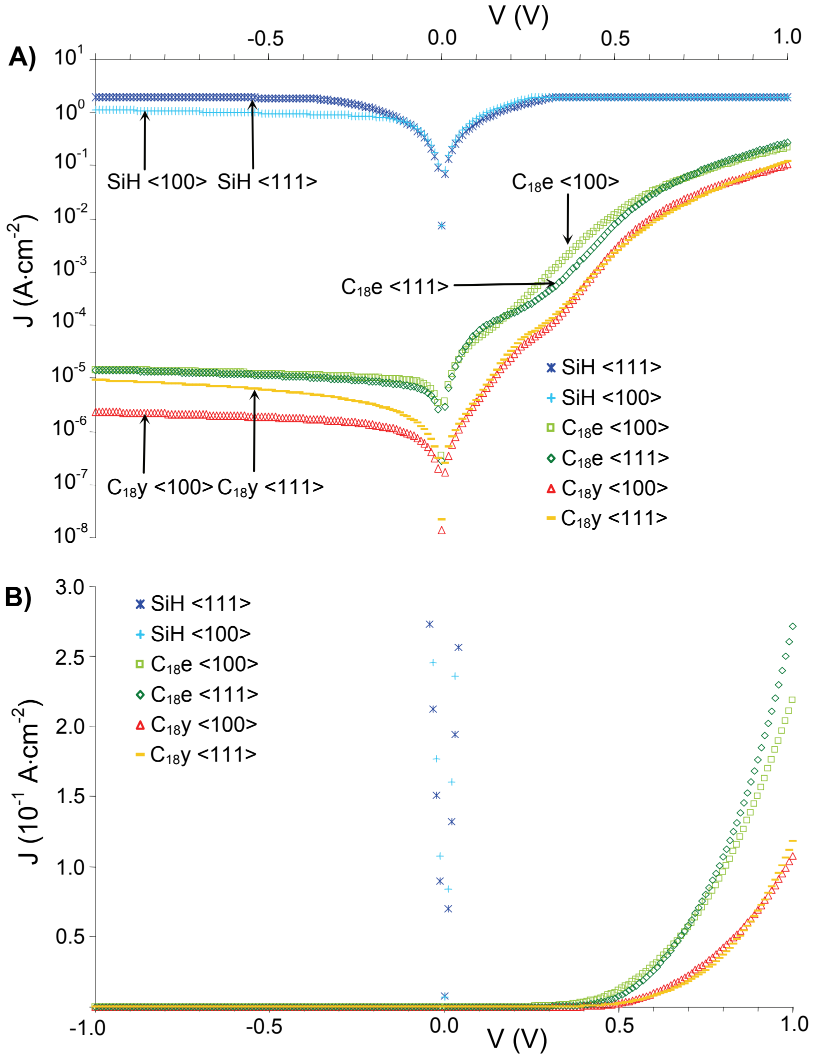

Figure 3.2. *J-V* plots of all tested samples with different insulators, where *J* is plotted both on (A) a logarithmical scale and (B) linear scale. Accumulation or forward direction is on the right-hand side (0 through 1.0 V) and depletion or reverse direction is on the left-hand side (0 through -1.0 V) of the plot. The current density values of the Si-H samples in the top figure clip at 1.95 A·cm^{-2} due to the current compliance of the I-V meter. C_{18}e and C_{18}y stand for samples modified with a monolayer derived from 1-octadecene and 1-octadecyne, respectively.

Modifying the H-terminated silicon surface with an organic monolayer drastically changes its behavior from Ohmic to Schottky diode, as reported before [12, 13, 23]. A distinct feature in Figure 3.2 is that samples modified with 1-octadecyne showed at least a two times lower leakage current in forward direction as compared to all samples modified with 1-octadecene. All samples modified with organic monolayers, however, do not show a straight line in the forward low bias regime as theory predicts [24] but are curved between approximately 0.3 V and 0.5 V. These curves were also observed with monolayers on n-type Si<100> made of 1-hexadecene (C_{16}) and 1-docosene (C_{22}) (see Chapter 2, Figure 2.4 and [12]). A precise origin of these curves can not be given. Interface states, which have their origin at defects at the silicon-monolayer interface, can be a possible cause for the curves in Figure 3.2. To investigate these, a total number of 12 *I-V* or *C-V* measurements were performed. Cycles 1, 2 and 10 of the *I-V* measurements were performed with T_{delay} = 0.2 s, cycle 11 with T_{delay} = 1.0 s and cycle 12 with T_{delay} = 5.0 s (see experimental section 3.5). These repetitive measurements were, however, very reproducible irrespective of measurement delay times. This indicates that the curves do not originate from charging currents of interface states with small life times τ (i.e. $\tau << 5$ s).

One of the characteristic parameters describing the influence of the monolayer on the current density magnitude is the effective barrier height $q\phi_{eff}$. In case of semiconductors modified with nm-thin insulators this can be written as [12-15, 25]: $q\phi_{eff} = q\phi_B + kT\beta l$ where $q\phi_B$ [eV] is the energy difference between semiconductor electron affinity $q\chi$ and metal work function $q\phi_M$; $kT\beta l$ [eV] describes the extra energy height due to the organic monolayer with kT [eV] being the thermal energy, l [Å] the monolayer thickness and the β [Å^{-1}] the characteristic tunneling factor. Another parameter of interest is the series resistance R_S which accounts for all resistive elements in the device such as contact resistance, silicon bulk resistance and the extra series resistance by the monolayer. Since contact resistance and silicon bulk resistance are assumed to be similar for all samples made on Si <100> and Si <111> any changes found in series resistance stem from changes in monolayer structure and monolayer-silicon interface.

Both $q\phi_{eff}$ and R_S can be analytically derived via the Schottky theory, albeit that each parameter is derived from a different forward bias regime. Equation 3.1 gives the *J-V* relation of a Schottky diode in the low forward bias regime ($V < 0.2$ V), i.e. without influence of series resistance [12-14, 24]:

$$J = A^* T^2 e^{(\frac{-q\phi_{eff}}{kT})} e^{(\frac{qV}{nkT})} (1 - e^{-\frac{qV}{kT}}) \tag{3.1}$$

where J [A·cm^{-2}] is the measured current density, V [V] is the applied bias voltage, A^* is the Richardson constant (110 A·K^{-2}·cm^{-2} for n-type silicon [22, 24]), $kT \cdot q^{-1}$ is the thermal voltage (25.7mV at 298K), n [-] is the diode ideality factor which accounts for the non-idealities in the diode behavior and $q\phi_{eff}$ [eV] is the effective barrier height.

For higher forward bias voltages the term $(1-\exp(-qV(kT)^{-1})$ can be neglected and the series resistance R_S starts to play a role. Equation 3.1 can then be adapted to Equation 3.2 [12, 15]:

$$J = A^{*}T^{2}e^{\left(\frac{-q\phi_{eff}}{kT}\right)}e^{\left(\frac{q(V-JR_{s})}{nkT}\right)} \tag{3.2}$$

where R_S [$\Omega{\cdot}\mathrm{cm}^2$] is the total series resistance of the device under test. The derivation routes of both $q\phi_{eff}$ and R_S from Equations 3.1 and 3.2, respectively, can be found in Chapter 2.

Figure 3.3A shows $q\phi_{eff}$ as derived from all the *J*-*V* data in the regime from 0 V through 0.2 V via Equation 3.1 and Figure 3.3B shows R_S as derived from all the *J*-*V* data in the regime from 0.7 V through 0.8 V via Equation 3.2.

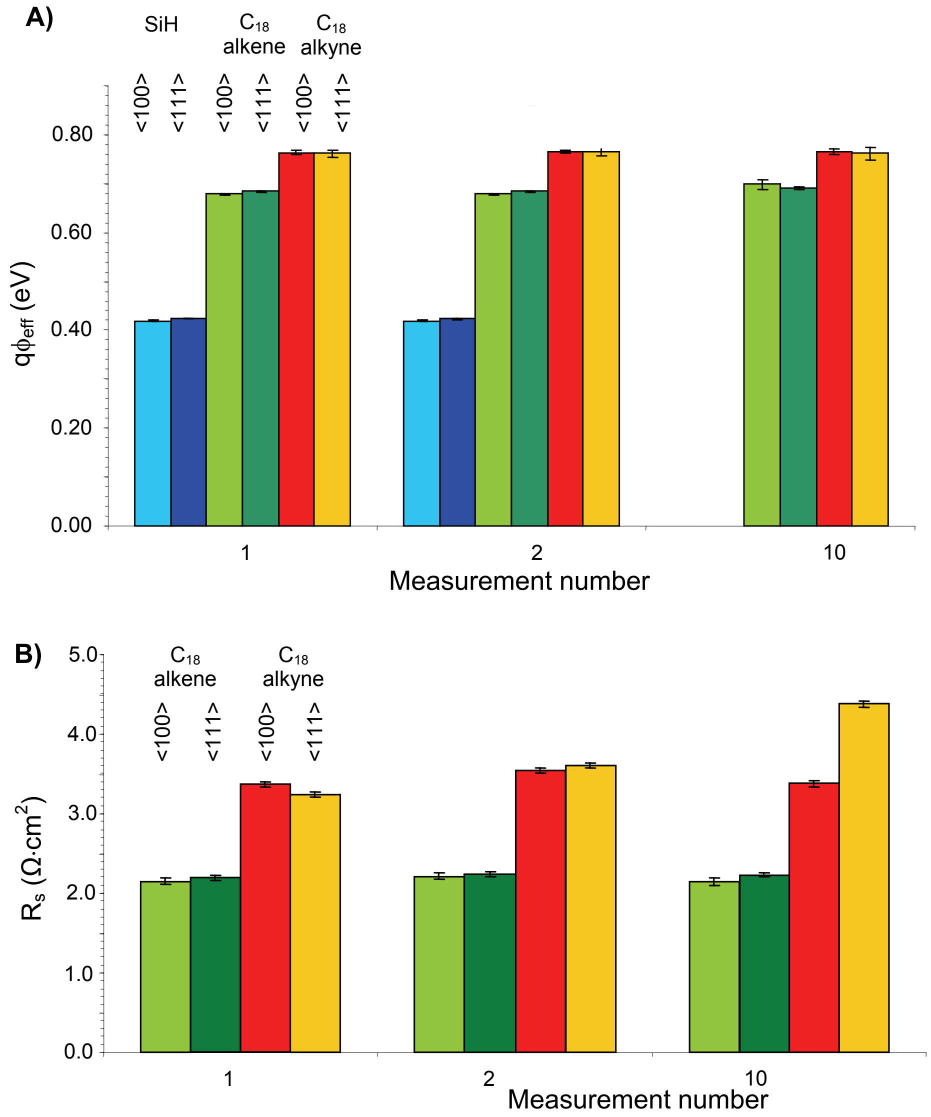

Figure 3.3. (A) $q\phi_{eff}$ vs. measurement number and (B) R_S vs. measurement number.

The H-terminated samples gave the lowest barrier height and these values are in close relation with the theoretical value of ($q\phi_M$ - $q\chi$) 0.44eV for n-type silicon [12]. The total series resistance R_S of the Si-H samples could not be derived via Equation 3.2 due to the Ohmic behavior of the devices. However, to be able to make a comparison R_S was simply estimated via Ohms law. For SiH<100> and SiH<111> R_S was found to be 0.134 and 0.163 $\Omega\cdot\text{cm}^2$, respectively. These low values suggest that back contact resistance and silicon bulk resistance have only a small influence on the total device series resistance and that the monolayer resistance has the most dominant influence on R_S.

Modifying the H-terminated n-type silicon surface with an organic monolayer gives rise to a drastic increase in $q\phi_{eff}$ [12, 13]. There is furthermore a significant difference of 0.08 eV between the samples modified with alkenes ($q\phi_{eff} \approx$ 0.68 eV) and the samples modified with alkynes ($q\phi_{eff}$ $\approx$ 0.76 eV). $q\phi_{eff}$ (ideal case: $q\phi_{eff} = q\phi_B + kT\beta l$) can be influenced by the silicon-monolayer defects [13-15, 24], especially when $q\phi_{eff}$ is extracted from *I-V* measurements. These will consequently lower $q\phi_{eff}$ derived from *I-V* measurements [24]. This indicates that modifying Si-H surfaces with 1-octadecyne renders devices with better interface properties (i.e. lesser defects) and hence improved performances. The total series resistance R_S shows the same trend. Devices modified with 1-octadecyne gave a substantially higher series resistance as compared to those modified with 1-octadecene.

Figures 3.3A and 3.3B show both the apparent absence of the influence of the substrate orientation. This indicates that a certain type of molecule (alkene/alkyne) passivates both types of surface orientations equally well. This is in strong contrast with oxidized surfaces. SiO_2 grown on <111> oriented silicon is known to have a substantial higher number of surface defects as compared to oxidized <100> oriented silicon surfaces [22].

In these figures it can also be seen that the sample properties remained constant over 10 consecutive measurements. An exception was the 1-octadecyne sample on Si<111> in the 10th measurement in Figure 3.3B. It can be seen that R_S had increased. A precise explanation for this can not be given.

3.2.2 Capacitance-Voltage data

In Figure 3.4 the averaged results from the *C-V* measurements performed at a frequency of 400 kHz are plotted. The figure shows typical curves from at least 5 different junctions.

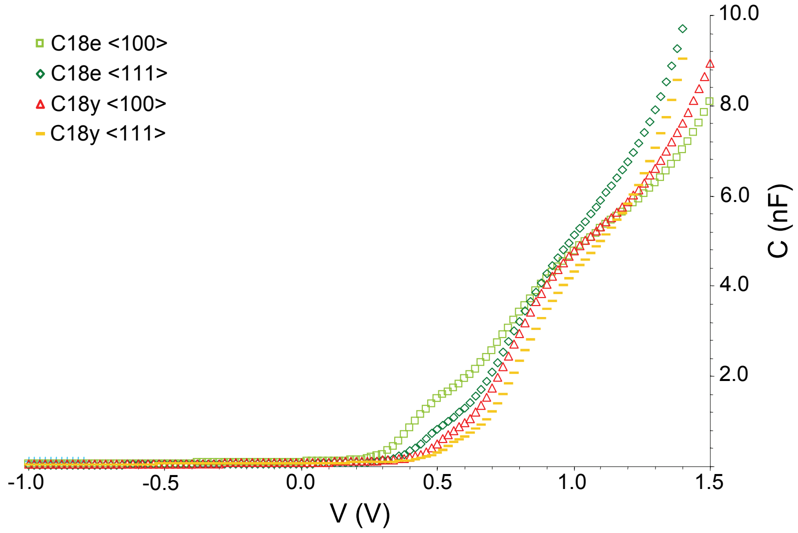

Figure 3.4. Capacitance voltage plots of different insulators.

The *C*-*V* curves for the Si-H <111> samples could not be determined due to their Ohmic character. For the Si-H <100> samples capacitance behavior was only observed in the regime of -1.0 V to -0.8 V and is not shown in Figure 3.4 since that data coincides with the other curves. The *C*-*V* curves for all samples with C_{18} insulators display a weak indication of a plateau in the accumulation regime around 1 V and increase strongly again for higher voltages. As was stated in Chapter 2 this plateau indicates the formation of a real capacitance. However, as compared to the C_{16} and C_{22} insulators on n-type Si<100> described in Chapter 2, the plateaus are in this case less wide or even hardly visible as is the case for C_{18}e <100> samples. Furthermore, the *C*-*V* curves of both samples with 1-alkenes show a knee around 0.5 V. These may indicate the presence of interface charges at these samples as was also observed at the MIS-structure of p-type silicon with $–C_{10}H_{21}$ monolayer in Chapter 2. The tilted capacitance in the plateau of the accumulation regime, although very small, is further analyzed in the next section.

Dielectric properties of the organic monolayer

In the previous chapter the dielectric properties of the organic monolayer in the form of the dielectric constant ε_r were derived from the monolayer capacitance C_{ins} [F], which was on its turn obtained via a method by Vincent et al. [26] and demonstrated in [27]. Unfortunately, this theory was not applicable to these samples since they had such small plateaus in accumulation. Recently, Kar published a powerful and quick, alternative method to derive the insulator capacitance C_{ins} from distorted *C*-*V* curves in accumulation of high-K dielectrics [28]. The only assumption in the proposed model is that both the space charge capacitance C_{sc} and the capacitance associated with interface charges C_{it} are exponential functions of the surface potential ψ_s as is the case in ideal operating situations [29]. In such cases C_{sc} and C_{it} can be written as Equations 3.3a and b, respectively (for a detailed description of the above mentioned parameters see Chapter 2):

$$C_{sc} = a_1 e^{\beta_{acc}\psi_s} \tag{3.3a}$$

$$C_{it} = a_2 e^{\beta_{acc}\psi_s} \tag{3.3b}$$

Where a_1 and a_2 are constants, β_{acc} is in this case a constant pre-factor of the exponent. In ideal cases it is equal to $\beta_{acc,theory} = q\cdot(2kT)^{-1} = 19.38\ \mathrm{V}^{-1}$ at 300K [28, 29]. The total measured capacitance C is made up of C_{ins}, C_{sc} and C_{it}. In case of equilibrium situation and via some mathematical rewriting an expression of this total C from which C_{ins} can be derived, is given in Equation 3.4:

$$\sqrt{\left|\frac{1}{C}\frac{dC}{dV}\right|} = \frac{\sqrt{|\beta_{acc}|}}{C_{ins}}(C_{ins} - C) = \frac{-\sqrt{|\beta_{acc}|}}{C_{ins}}C + \sqrt{|\beta_{acc}|} \tag{3.4}$$

A plot of $sqrt(\left|C^{-1}dC(dV)^{-1}\right|)$ vs. the total capacitance C in accumulation should give a straight line from which the insulator capacitance C_{ins} can be derived from the C-axis intercept and β_{acc} can be derived from the $sqrt(\left|C^{-1}dC(dV)^{-1}\right|)$ -axis intercept.

This method was successfully applied by Kar et al. on a large number of high-K dielectrics on silicon substrates [28, 30]. In all cases β_{acc} deviated strongly from $q\cdot(2kT)^{-1}$ and this deviation depended strongly on the physical properties of the high-K dielectrics [30]. Since the only two criteria for successful application of this method are mentioned in Equations 3.3a and b, which are expected to also hold for the silicon electrodes modified with Si-C linked monolayers, this method will be used for analysis of the devices tested here. In a different paper Kar also suggests this method for use as insulator capacitance extraction of silicon electrodes modified with Si-C linked monolayers [19].

In Figure 3.5 the $sqrt(\left|C^{-1}dC(dV)^{-1}\right|)$ vs. C plots are depicted for two different types of samples. The C-V data measured at 400 kHz is used for this analysis.

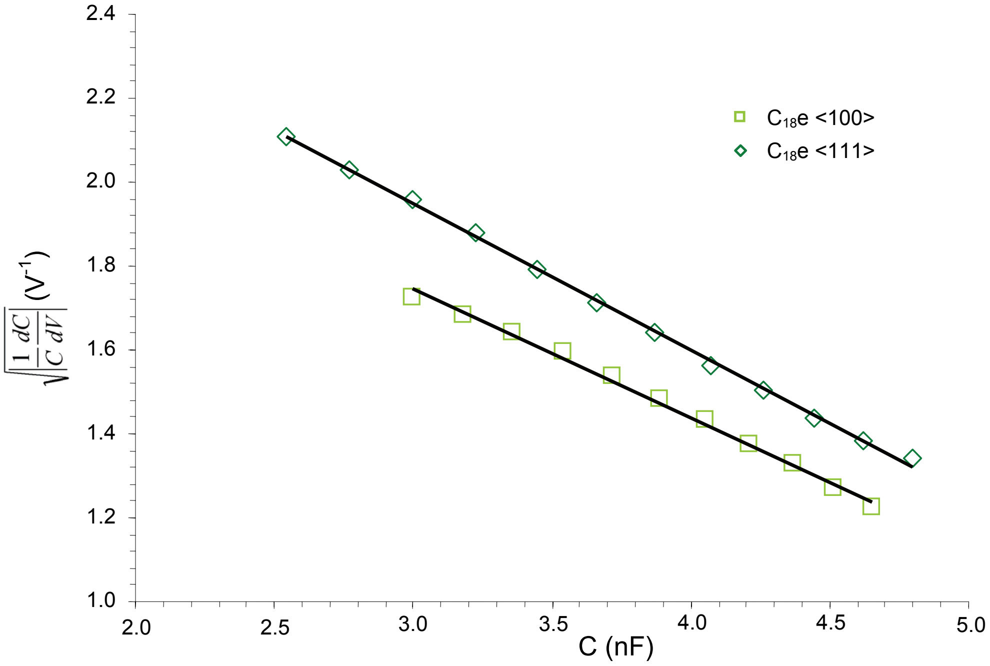

Figure 3.5. $\sqrt{\left|\frac{1}{C}\frac{dC}{dV}\right|}$ vs. C curves for the samples modified with 1-alkenes.

Via Equation 3.4 C_{ins} and β_{acc} have been derived. From the C_{ins} values the insulator dielectric constant can simply be derived via $C_{ins} = \varepsilon_0\cdot\varepsilon_r\cdot A\cdot d^{-1}$, where A [cm^2] is the area and d [cm] is the insulator thickness. For the thickness of the C$_{18}$ monolayers the value of $d = 1.95\cdot10^{-7}$ cm determined in another study [31] was taken. In order to provide a fair comparison with the data of Chapter 2, this data has also been analyzed via the model by Kar. Finally, in order to compare the different insulator capacitance values these have been normalized with respect to the area so $C\cdot A^{-1}$ is given. The data from the analysis is collected in Table 3.1.

Table 3.1. Insulator capacitance and dielectric constants of the C$_{18}$ monolayers compared with the C$_{16}$ and C$_{22}$ monolayers of Chapter 2.

	Method of Kar			Method of Chapter 2	
Insulator	$C\cdot A^{-1}$ [μF·cm^{-2}]	ε_r [-]	$\beta_{acc}\cdot\beta_{acc,theory}^{-1}$ [-] [a]	$C\cdot A^{-1}$ [μF·cm^{-2}]	ε_r [-]
C$_{18}$e <100>	1.8 ± 0.1	3.9 ± 0.3	0.37 ± 0.01	-	-
C$_{18}$e <111>	1.7 ± 0.1	3.7 ± 0.1	0.46 ± 0.01	-	-
C$_{18}$y <100>	1.4 ± 0.1	3.0 ± 0.1	0.63 ± 0.01	-	-
C$_{18}$y <111>	1.3 ± 0.1	2.8 ± 0.1	0.66 ± 0.01	-	-
pC$_{16}$	0.84 ± 0.03	1.6 ± 0.1	0.94 ± 0.01	0.86 ± 0.05	1.7 ± 0.1
pC$_{22}$	0.73 ± 0.05	2.4 ± 0.1	0.96 ± 0.01	0.76 ± 0.05	2.2 ± 0.2
nC$_{16}$	0.89 ± 0.05	1.7 ± 0.1	0.98 ± 0.01	0.97 ± 0.05	1.9 ± 0.1
nC$_{22}$	0.81 ± 0.03	2.4 ± 0.1	0.94 ± 0.01	0.95 ± 0.03	2.8 ± 0.1

[a] $\beta_{acc,theory} = q\cdot(2kT)^{-1}$ = 19.38 V^{-1} at 300 K [28, 29]

First the comparison is made between the data of Chapter 2 (last four rows in Table 3.1) according to an analysis of the two mentioned methods. Apart from the nC_{22} sample the two methods give the same outcome within the experimental uncertainties, which is a clear indication of the validity of the method of Kar. It is also expected that monolayers with same chain lengths give the same capacitances on both n-type and p-type silicon, provided that the monolayers are not degenerated. This is the case if the analysis method by Kar is used, indicating that this method may even be more accurate than the one used in Chapter 2, provided that both layers of course have the same physical properties. Additional information on the electronic behavior of such monolayers obtained via the method of Kar is given by the factor $\beta_{acc}\cdot\beta_{acc,theory}^{-1}$ (where $\beta_{acc,theory}$ is $q\cdot(2kT)^{-1}$), which is very close to unity in all four cases. This indicates that the space charge capacitance C_{sc} and any interface trap capacitance C_{it} are neat exponential functions of the surface potential ψ_s. These samples thus in fact behave nicely in accordance with theory, which was never observed to such a close degree for any of the high-K dielectrics examined by Kar et al. [28, 30]. This again shows the good electronic properties of silicon electrodes modified with Si-C linked monolayers.

Next, the data of the C_{18} modified n-type silicon electrodes is discussed. An obvious point is the large insulator capacitance per unit area as compared to the data of Chapter 2, in some cases it was even more than a factor of two higher. This may be an indication that the samples have degraded in some way or that they were of poor quality from the start. After all, from the stability study in Chapter 2.3.5 it was shown that the capacitance increased for n-type Si<100> electrodes modified with C_{16} and C_{22} monolayers upon prolonged storage under ambient conditions. The accompanying dielectric constants are thus very high of these samples as compared to the data of Chapter 2. It is expected that the dielectric constant of the C_{18} layer was somewhere between that of the nC_{16} and nC_{22} layer, i.e. 1.7 ± 0.1 to 2.4 ± 0.1. In all cases ε_r was much higher, even up to $\varepsilon_r = 3.9 \pm 0.3$, which is the theoretical upper limit if the complete monolayer would be replaced by SiO_2. However, in these calculations the thickness was assumed to be fixed and a value was chosen, which was determined from good quality monolayers. In Chapter 2.3.5 it was also shown that upon degradation also the thickness is likely to increase too and thus the values in Table 3.1 are thus in fact overestimated. They can be regarded as an indication for the amount of possible degradation due to oxidation. In that case it can be seen that the samples modified with 1-alkenes degrade faster than the samples modified with 1-alkynes. Within the experimental uncertainties there is no influence observed of the substrate orientation for both 1-alkynes and 1-alkenes derived monolayers. The fact that the samples modified with 1-alkenes are of lower quality than the ones modified with 1-alkynes is also indicated by the lower ratio of $\beta_{acc}\cdot\beta_{acc,theory}^{-1}$ and thus less ideal behavior for the samples modified with 1-alkenes.

In conclusion, this capacitance analysis method gives rise to the assumption that all samples modified with C_{18} monolayers in this study are of lower quality and are thus possibly slightly oxidized as compared to the samples analyzed in Chapter 2.

Mott Schottky measurements

In Figure 3.6 the averaged results from the *C-V* measurements are plotted in Mott Schottky form ($C^{-2} - V$). A more detailed discussion on the theory of Mott Schottky measurements can be found in Chapters 2 and 4.

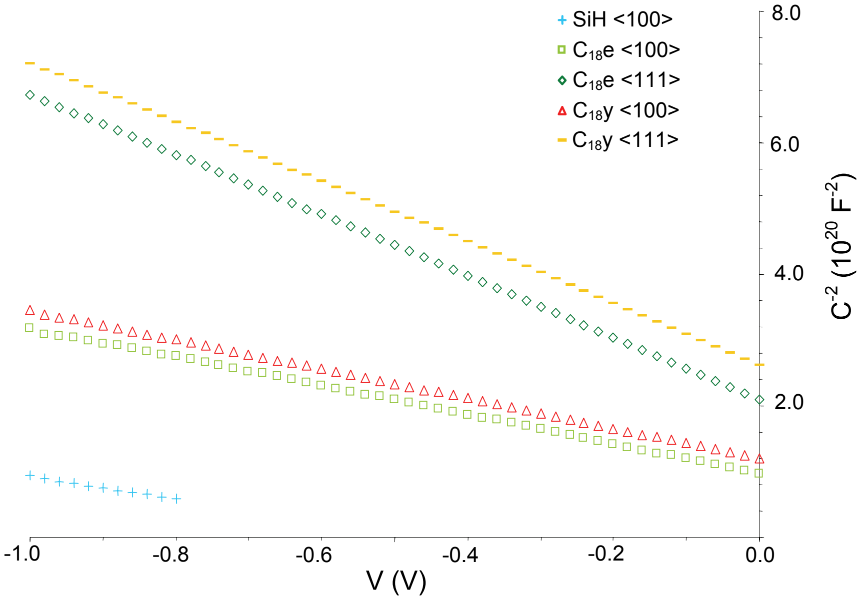

Figure 3.6. Mott Schottky plots for different insulators.

The Mott Schottky plots of the samples with monolayers were all linear in the region from -1.0 V to 0 V. The results of the extrapolation of the flatband voltage V_{fb} and the doping N_D from the Mott Schottky plots, following a procedure given in Chapter 2 and mentioned in [12, 22], is given in Table 3.2:

Table 3.2. Parameters derived from the Mott Schottky analysis.

Insulator	V_{fb} [V]	$V_{fb,\ theory}$ [V]	N_D [10^{15} cm^{-3}]	$N_{D,min}$ - $N_{D,max}$ [a] [10^{15} cm^{-3}]
SiH <100> [b]	-0.46 ± 0.07	0.20	2.6 ± 0.2	0.42 – 4.2
SiH <111> [c]	-	0.18	-	0.83 – 1.4
C_{18}e <100>	0.45 ± 0.01	0.20	2.0 ± 0.1	0.42 – 4.2
C_{18}e <111>	0.46 ± 0.01	0.18	(9.6 ± 0.4) ·10^{-1}	0.83 – 1.4
C_{18}y <100>	0.54 ± 0.01	0.19	2.0 ± 0.1	0.42 – 4.2
C_{18}y <111>	0.58 ± 0.01	0.18	(9.7 ± 0.4) ·10^{-1}	0.83 – 1.4

[a] Range of doping values calculated from the specifications of the wafer supplier.
[b] The Mott Schottky analysis for nSiH<100> could only be performed for the data from -1.0V through -0.8V.
[c] The Mott Schottky analysis for nSiH<111> could not be carried out since no depletion layer was formed on this sample due to its Ohmic behavior.

All calculated doping values stayed within the range given by the wafer supplier (see last column in Table 3.2), validating the procedure. A similar V_{fb} was found for the samples modified with 1-octadecene, irrespective of substrate orientation. The samples modified with 1-octadecyne showed a much more positive V_{fb}. Comparing the values of all samples modified with monolayers with the theoretical V_{fb} [12] it can be noticed that these values are more positive than $V_{fb,theory}$, indicating the presence of negative charges as was also found before for 1-alkenes of C_{10}, C_{12}, C_{16} and C_{22} on n-Si <100> [12]. Oxide formation on Si is generally accompanied with the built in of positive charges [22] and these, consequently, shift V_{fb} towards more negative values. The fact that samples modified with 1-octadecyne have approximately 0.1 V more positive values of V_{fb} than 1-octadecene samples may indicate that more oxidation has occurred on the latter. This outcome correlates with the findings from the *I-V* measurements, which also showed the superior behavior of the samples modified with 1-octadecyne. No strong influence of the substrate orientation is also witnessed in the analysis of the Mott Schottky data.

Charges at the silicon-monolayer interface

Following a procedure used in Chapter 2 the amount of fixed charges at the silicon-monolayer interface N_f has been estimated via Equation 3.5:

$$N_f = \frac{C_{ins}(\phi_{MSi} - V_{fb})}{qA} \tag{3.5}$$

where N_f [cm^{-2}] is the total number of fixed charges; C_{ins} [F] is the insulator capacitance as determined from the $sqrt(\left|C^{-1}dC(dV)^{-1}\right|)$ vs. C plots; ϕ_{MSi} and V_{fb} are the theoretical and measured flatband voltage, respectively. The data is shown in Table 3.3. By definition $N_f = |Q_f \cdot q^{-1}|$ and is always positive. To show that in all the cases in Table 3.3 negative fixed charges are concerned, this is denoted by $-Q_f$. Also the data of Chapter 2 is given to provide a comparison. The latter has been calculated via two routes since for these calculations the insulator capacitance C_{ins} is necessary, which is obtained for the latter case via two ways (see Table 3.1).

Table 3.3. N_f calculated for different monolayers.

	Method of Kar	Method of Chapter 2
Insulator	Total insulator charge N_f [cm^{-2}]	Total insulator charge N_f [cm^{-2}]
C_{18}e <100>	$(2.8 \pm 0.1)\cdot 10^{12}$ $(-Q_f)$	-
C_{18}e <111>	$(2.9 \pm 0.1)\cdot 10^{12}$ $(-Q_f)$	-
C_{18}y <100>	$(3.0 \pm 0.1)\cdot 10^{12}$ $(-Q_f)$	-
C_{18}y <111>	$(3.2 \pm 0.1)\cdot 10^{12}$ $(-Q_f)$	-
pC_{16}	$(5.7 \pm 1.0)\cdot 10^{11}$ $(-Q_f)$	$(5.8 \pm 1.0)\cdot 10^{11}$ $(-Q_f)$
pC_{22}	$(5.9 \pm 2.0)\cdot 10^{11}$ $(-Q_f)$	$(6.2 \pm 2.0)\cdot 10^{11}$ $(-Q_f)$
nC_{16}	$(2.5 \pm 0.2)\cdot 10^{12}$ $(-Q_f)$	$(2.7 \pm 0.2)\cdot 10^{12}$ $(-Q_f)$
nC_{22}	$(2.3 \pm 0.1)\cdot 10^{12}$ $(-Q_f)$	$(2.7 \pm 0.1)\cdot 10^{12}$ $(-Q_f)$

First the comparison is made again between the data of Chapter 2 (last four rows in Table 3.3) according to an analysis of the two mentioned methods. Apart from the nC_{22} sample the two methods give the same outcome within the experimental uncertainties. The value of N_f for the nC_{22} sample is still in the same order of magnitude for both methods. The conclusions drawn in Chapter 2 can be regarded as justified.

The values of N_f for all C_{18} samples are all in the range $(2.8 - 3.2)\cdot10^{12}$ cm^{-2} and thus no clear trend can be observed from this data. The stability study on C_{16} and C_{22} monolayers on n-type <100> silicon mentioned in section 2.3.5 showed that V_{fb} did not change much upon storage under ambient conditions. This was in contrast with the samples of p-type <100> silicon, which all showed a shift of V_{fb} due to additional positive charges upon longer storage. Since N_f is directly proportional to the shift in V_{fb} with respect to the theoretical V_{fb} (see Equation 3.5) this means that N_f is expected to change not much as a function of time and that the amount of sample degradation can not be determined via N_f. These values of N_f for the C_{18} samples are in the same order of magnitude as the nC_{16} and nC_{22} samples (N_f = $(2.3 – 2.5)\cdot10^{12}$ cm^{-2}) of the study in Chapter 2 but it can thus not be unambiguously determined that the nC_{18} samples are either degraded or in good condition. Therefore no solid conclusions can be drawn from the N_f data.

In summary, the electrical characterization of all C_{18} samples showed via analysis of both the *J*-*V* and *C*-*V* data that samples modified with alkynes show superior electrical behavior in terms of higher barrier heights $q\phi_{eff}$, higher series resistances R_s, and lower insulator dielectric constant ε_r. No direct correlation of the electrical properties and substrate orientation was found. Via calculation of the fixed charges N_f no clear difference was observed between the samples. Comparison of the data of the C_{18} samples with the data of Chapter 2 leads to the assumption that all samples have degraded to a certain degree. The results thus show clear superiority of the samples modified with 1-alkynes but no guarantee can be given that all monolayers are perfectly intact.

3.2.3 X-ray photoelectron measurements

In order to measure the degree of oxidation, modified silicon samples were subjected to X-ray photoelectron spectroscopy (XPS). The Si_{2p} regions of two samples are given in Figure 3.7. From the Si_{2p} region of the resulting XPS data the surface area of the Si_{2p}(ox) and Si_{2p}(non-ox) contributions were obtained. Table 3.4 presents the complete set of data on the XPS measurements.

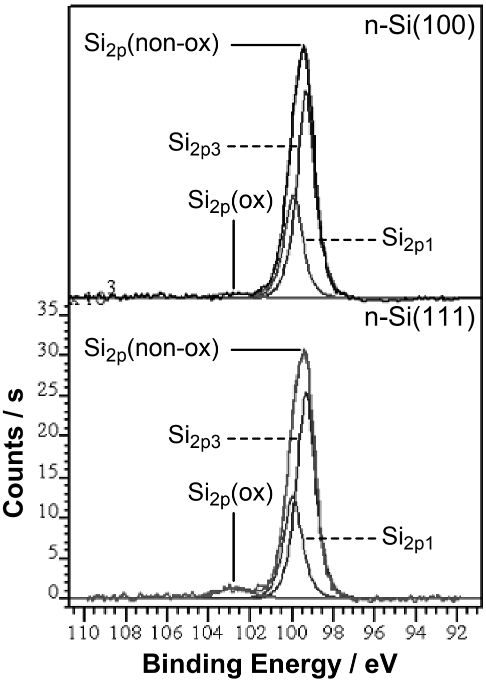

Figure 3.7. Si_{2p} regions of 1-octadecyne-derived monolayers on n-Si <100> (top) and n-Si <111> (bottom). The data is indicated by labels via solid lines, while the fit of the Si_{2p3} and Si_{2p1} peaks are indicated by labels via dashed lines. The scaling on the y-axis of the top figure is the same as of the bottom figure.

Table 3.4 Averaged values for $Si_{2p}(Ox)/(Si_{2p1} + Si_{2p3})$, which reflect the degree of oxidation on the Si samples modified with 1-octadecene and 1-octadecyne.

Type of Compound	Type of Silicon	$Si_{2p}(Ox)/(Si_{2p1} + Si_{2p3})$
1-octadecyne	n-Si <100>	0.030 (±0.003)
1-octadecene	n-Si <100>	0.049 (±0.002)
1-octadecyne	n-Si <111>	0.060 (±0.005)
1-octadecene	n-Si <111>	0.093 (±0.002)

For both types of silicon, the degree of oxidation - calculated via $Si_{2p}(Ox)/(Si_{2p1} + Si_{2p3})$ -of 1-octadecene-derived structures is higher as compared to those of 1-octadecyne-derived structures. This is in line with the trend found in the values of V_{fb}, $q\phi_{eff}$, and ε_r.

Despite the higher amount of Si-H bonds that is present on the Si <100> surface, the degree of oxidation of the modified Si <111> surface is higher as compared to the Si <100> surface, as follows from Table 3.4. It is known that substrate conditions play an important role in the growth of native oxide on the silicon surface and it has been reported that the oxide growth rate on Si <111> is higher as compared to Si <100> [32, 33], both for native oxide as well as for thermal oxide. Also the type of doping and its concentration [32, 34, 35] affect the oxide growth, but in this study these two parameters are similar for Si <100> and Si <111>. In contrast to the XPS data, the results of every electrical characterization method do not indicate a different behavior for the two substrate orientations. Nonetheless, XPS proves to be a powerful surface characterization method to determine the amount of oxide in these layers.

3.3 Conclusions

An electrical study on the influence of molecule type (1-octadecene/1-octadecyne) and silicon substrate orientation (<100>/<111>) has been carried out on Hg | C_{18} monolayer | n-type silicon structures. Both *J-V* and *C-V* measurements have been performed and repeated a number of times to investigate the reproducibility of the samples. The outcome was compared with XPS measurements. A number of clear trends were observed from both *J-V* and *C-V* results. The current densities of the samples modified with alkynes were at least two times lower than those modified with alkenes. The effective barrier heights were approximately 0.08 eV higher for the samples modified with alkynes as compared to those modified with alkenes, indicating a better quality of silicon-monolayer interface for the former. Also the series resistance was significantly higher for the samples modified with alkynes. The values of ε_r of the monolayer made from 1-alkynes were significantly lower than those made from 1-alkenes, indicating a higher degree of oxide present at the monolayers of 1-alkenes. The values of the flatband voltage were approximately 0.1 V more positive for the samples modified with alkynes with respect to those modified with alkenes, which may be again attributed to a higher degree of oxide present at the latter. Concerning the substrate orientation, no clear influence of this was observed in both *J-V* and *C-V* results. This apparent lack of influence of substrate orientation on device behavior and silicon-monolayer interface properties as compared to a SiO_2 insulator is quite remarkable. Nonetheless, this can be seen as a proof for the broad usability of these monolayers in creating stable devices with the desired, precisely tunable interface properties.

The results of the XPS measurements correlated with the differences observed between monolayers made of 1-alkynes or 1-alkenes. More oxygen was present at the monolayers made from 1-alkenes. However, XPS showed that the C_{18} monolayers on Si <111> contained overall more oxygen as compared to all Si <100> samples. This finding could not be correlated in any way to the findings from the electrical characterization and a clear explanation for this is so far not known.

In conclusion, XPS and electrical characterizations provide a powerful combination to determine the electronic properties of such MIS-structures with organic insulators. This study showed via both methods the preferred use of 1-alkynes over 1-alkenes in creating metal-insulator-silicon devices. The ease of fabrication together with the outstanding electrical properties shows the potential applications of the monolayers made from 1-alkynes in hybrid molecular-silicon electronics. Furthermore, given the numerous possibilities for chemical modification of such layers the properties of such electronic devices can be precisely tuned.

3.4 Experimental

3.4.1 Sample preparation.

The sample modification and preparation is described in Chapter 2 and will therefore not be repeated here. Only the etch-step to create H-terminated <111> silicon surfaces is not included there. This was done by etching the sample for 15 minutes in an aqueous 40% NH_4F solution, deoxygenated with argon. All samples were made from moderately doped ($\approx 1 \cdot 10^{15}$ cm^{-3}) n-type silicon wafers. The list of all tested samples can be found in Table 3.5. This includes also the static water contact angle measurements done in a similar procedure as mentioned in Chapter 2.

Table 3.5. Overview of tested samples.

Sample structure (alkene/alkyne, substrate orientation)	Sample abbreviation	Water contact angle (°)
1-octadecene, <100>	C_{18}e <100>	105 ± 1
1-octadecene, <111>	C_{18}e <111>	106 ± 1
1-octadecyne, <100>	C_{18}y <100>	107 ± 1
1-octadecyne, <111>	C_{18}y <111>	107 ± 1
H-term. , <100>	SiH<100>	-
H-term. , <111>	SiH<111>	-

3.4.2 Electrical characterization

Electrical characterization was performed with a HP4140B pA meter for *I-V* measurements and a HP4284A LCR meter for *C-V* measurements. Both devices were connected to a HP E5250A low leakage switch mainframe. The set-up was computer controlled via the Metrics software package ICS. For the *I-V* measurements the voltage was swept from 0 V to -1.0 V (reverse direction) and from 0 V to +1.0 V (forward direction). The step size was 10 mV and the delay time T_{del} was 0.2 s. The current limit was set to 10 mA. For the *C-V* measurements the voltage was swept from -1.0 V (depletion/inversion) to +1.5 V (accumulation) with a step size of 10 mV. The amplitude and frequency of the superimposed ac-signal were 20 mV and 400 kHz, respectively. The impedance model chosen was a parallel (C_p - G_p) model. The C_p data was automatically corrected for the series resistance according to a procedure in [29].

On each measurement point a series of both *I-V* and *C-V* measurements with different settings were performed to obtain both information on the reproducibility of the measurements and the influence of the varied parameters. The followed measurement routine is listed in Table 3.6.

Table 3.6. Measurements sequence per point.

Meas nr.	Type	Settings
1	I-V	As mentioned in text
2	I-V	As 1
3	C-V	As mentioned in text
4	C-V	As 3, $C_s - R_s$ circuit
5	C-V	As 3, $f = 1$ MHz
6	C-V	As 3, $f = 100$ kHz
7	C-V	As 3, $f = 40$ kHz
8	C-V	As 3, $f = 10$ kHz
9	C-V	As 3, $f = 4$ kHz
10	I-V	As 1
11	I-V	As 1, $T_{del} = 1$ s
12	I-V	As 1, $T_{del} = 5$ s

3.4.3 XPS measurements

The samples for the XPS measurements were taken from the same type of wafers as for the electrical characterization only without any back contact. Details on the wafers and monolayer fabrication can be found in 3.4.1 and in Chapter 2. The XPS measurements were performed on a VG Ionex system equipped with a Clam II analyzer and a standard aluminum K(α) X-ray source. Spectra were taken in normal emission at 10^{-9} mbar within 10 minutes. All C_{1s} peaks corresponding to hydrocarbons were calibrated to a binding energy of 285.0 eV to correct for the energy shift caused by charging. The data in the Si_{2p} region was fitted using the three different contributions: Si_{2p3}, Si_{2p1}, and Si_{2p}(Ox), at 99.33, 99.93, and 102.47 eV, respectively. For each combination of reagent/substrate facets two independent samples were prepared and studied with XPS.

3.5 References

[1] M. Schulz, "The end of the road for silicon?" *Nature* **1999**, *399*, 729.

[2] M. Hirose, M. Koh, W. Mizubayashi, H. Murakami, K. Shibahara, S. Miyazaki, "Fundamental limit of gate oxide thickness scaling in advanced MOSFETs", *Semiconductor Science and Technology* **2000**, *15*, 485.

[3] D. A. Muller, T. Sorsch, S. Moccio, F. H. Baumann, K. Evans-Lutterodt, G. Timp, "The electronic structure at the atomic scale of ultrathin gate oxides", *Nature* **1999**, *399*, 758.

[4] A. B. Sieval, R. Linke, H. Zuilhof, E. J. R. Sudhölter, "High-quality alkyl monolayers on silicon surfaces", *Advanced Materials* **2000**, *12*, 1457.

[5] D. D. M. Wayner, R. A. Wolkow, "Organic modification of hydrogen terminated silicon surfaces", *Journal of the Chemical Society-Perkin Transactions 2* **2002**, 23.

[6] J. M. Buriak, "Organometallic chemistry on silicon and germanium surfaces", *Chemical Reviews* **2002**, *102*, 1271.

[7] S. F. Bent, "Organic functionalization of group IV semiconductor surfaces: principles, examples, applications, and prospects", *Surface Science* **2002**, *500*, 879.

[8] M. R. Linford, P. Fenter, P. M. Eisenberger, C. E. D. Chidsey, "Alkyl Monolayers on Silicon Prepared from 1-Alkenes and Hydrogen-Terminated Silicon", *Journal of the American Chemical Society* **1995**, *117*, 3145.

[9] B. J. Eves, Q.-Y. Sun, G. P. Lopinski, H. Zuilhof, "Photochemical attachment of organic monolayers onto H-terminated Si(111): Radical chain propagation observed via STM studies", *Journal of the American Chemical Society* **2004**, *126*, 14318.

[10] A. B. Sieval, B. van den Hout, H. Zuilhof, E. J. R. Sudhölter, "Molecular Modeling of Covalently Attached Alkyl Monolayers on the Hydrogen-Terminated Si(111) Surface", *Langmuir* **2001**, *17*, 2172.

[11] A. B. Sieval, B. van den Hout, H. Zuilhof, E. J. R. Sudhölter, "Molecular Modeling of Alkyl Monolayers on the Si(111) Surface", *Langmuir* **2000**, *16*, 2987.

[12] E. J. Faber, L. C. P. M. de Smet, W. Olthuis, H. Zuilhof, E. J. R. Sudhölter, P. Bergveld, A. van den Berg, "Si-C Linked Organic Monolayers on Crystalline Silicon Surfaces as Alternative Gate Insulators", *ChemPhysChem* **2005**, *6*, 2153.

[13] Y. J. Liu, H. Z. Yu, "Alkyl monolayer-passivated metal-semiconductor diodes: Molecular tunability and electron transport", *ChemPhysChem* **2002**, *3*, 799.

[14] Y. J. Liu, H. Z. Yu, "Alkyl monolayer passivated metal-semiconductor diodes: 2: Comparison with native silicon oxide", *ChemPhysChem* **2003**, *4*, 335.

[15] Y. J. Liu, H. Z. Yu, "Molecular passivation of mercury-silicon (p-type) diode junctions: Alkylation, oxidation, and alkylsilation", *Journal of Physical Chemistry B* **2003**, *107*, 7803.

[16] S. Kar, C. Miramond, D. Vuillaume, "Properties of electronic traps at silicon/1-octadecene interfaces", *Applied Physics Letters* **2001**, *78*, 1288.

[17] C. Miramond, D. Vuillaume, "1-octadecene monolayers on Si(111) hydrogen-terminated surfaces: Effect of substrate doping", *Journal of Applied Physics* **2004**, *96*, 1529.

[18] D. K. Aswal, S. Lenfant, D. Guerin, J. V. Yakhmi, D. Vuillaume, "Self assembled monolayers on silicon for molecular electronics", *Analytica Chimica Acta*, *In Press, Corrected Proof.*

[19] S. Kar, "Study of silicon-organic interfaces by admittance spectroscopy", *Applied Surface Science*, *In Press, Corrected Proof.*

[20] A. B. Sieval, R. Opitz, H. P. A. Maas, M. G. Schoeman, G. Meijer, F. J. Vergeldt, H. Zuilhof, E. J. R. Sudhölter, "Monolayers of 1-alkynes on the H-terminated Si(100) surface", *Langmuir* **2000**, *16*, 10359.

[21] M. R. Linford, C. E. D. Chidsey, "Alkyl Monolayers Covalently Bonded to Silicon Surfaces", *Journal of the American Chemical Society* **1993**, *115*, 12631.

[22] S. M. Sze, *Semiconductor Devices: Physics and Technology*, Wiley, New York, **1985**.

[23] P. J. Severin, G. J. Poodt, "Capacitance-Voltage Measurements with a Mercury-Silicon Diode", *Journal of The Electrochemical Society* **1972**, *119*, 1384.

[24] D. K. Schroder, *Semiconductor Material and Device Characterization*, 2nd ed., Wiley, New York, **1998**.

[25] Y. Selzer, A. Salomon, D. Cahen, "The importance of chemical bonding to the contact for tunneling through alkyl chains", *Journal of Physical Chemistry B* **2002**, *106*, 10432.

[26] E. Vincent, G. Ghibaudo, G. Morin, C. Papadas, in *IEEE 1997 International Conference on Microelectronic Test Structures, Vol. 10*, **1997**, pp. 105.

[27] D. K. Schroder, *Semiconductor Material and Device Characterization*, 2nd ed., Wiley, New York, **1998**, p. 401.

[28] S. Kar, "Extraction of the capacitance of ultrathin high-K gate dielectrics", *Electron Devices, IEEE Transactions on* **2003**, *50*, 2112.

[29] E. H. Nicollian, J. R. Brews, *MOS Physics and Technology*, Wiley, New York, **1982**.

[30] S. Kar, S. Rawat, S. Rakheja, D. Reddy, "Characterization of accumulation layer capacitance for extracting data on high-κ gate dielectrics", *Electron Devices, IEEE Transactions on* **2005**, *52*, 1187.

[31] A. B. Sieval, A. L. Demirel, J. W. M. Nissink, M. R. Linford, J. H. van der Maas, W. H. de Jeu, H. Zuilhof, E. J. R. Sudhölter, "Highly stable Si-C linked functionalized monolayers on the silicon (100) surface", *Langmuir* **1998**, *14*, 1759.

[32] S. I. Raider, R. Flitsch, M. J. Palmer, "Oxide Growth on Etched Silicon in Air at Room Temperature", *Journal of the Electrochemical Society* **1975**, *122*, 413.

[33] X. G. Zhang, *Electrochemistry of Silicon and its Oxide*, Kluwer Academic Publishers, New York, **2001**.

[34] M. Morita, T. Ohmi, E. Hasegawa, M. Kawakami, M. Ohwada, "Growth of Native Oxide on a Silicon Surface", *Journal of Applied Physics* **1990**, *68*, 1272.

[35] M. Morita, T. Ohmi, E. Hasegawa, M. Kawakami, K. Suma, "Control Factor of Native Oxide-Growth on Silicon in Air or in Ultrapure Water", *Applied Physics Letters* **1989**, *55*, 562.

Chapter 4

The use of Mott Schottky measurements to determine the *pH* responses of Electrolyte – Insulator – Silicon structures

Abstract: This chapter contains theoretical and some practical aspects on Mott Schottky measurements. Electrolyte-Insulator-Silicon (EIS) structures can be used for sensing purposes by determining the shift in flatband voltage ΔV_{fb}. Three methods are discussed for determining the *pH* sensitivity at EIS-structures. Two of them involve the capacitance – voltage (*C*-*V*) curves as starting point, namely a graphical method in which the shifts of the *C*-*V* curves upon *pH* changes along the *V*-axis is measured and the second one involves an analytical determination of V_{fb} from ideal *C*-*V* curves. However, in case of nm-thin insulators, such as Si-C linked monolayers, *C*-*V* curves are often distorted, which makes it impossible to derive the sensory response via the two mentioned methods. Via the third method, Mott Schottky measurements, it is still possible to derive the sensory response. The three methods are tested with success on EIS-structures with thick insulators, resulting in a similar *pH* sensitivity for all three methods. The non-idealities encountered during Mott Schottky measurements will be discussed as well as how to deal with these non-idealities in EIS-structures with thin insulators. Al those findings lead to the conclusion that Mott Schottky measurements provide a good tool for investigating the *pH* responses at EIS-structures with thin insulators.

4.1 Introduction

Silicon can be found in all kind of devices in our direct environment and is widely studied over a large variety of devices and disciplines, ranging from solid-state devices [1, 2] to solar cells and electrochemistry [3, 4]. Silicon also forms the basic material of FET based sensors [5]. The most important functional element of the FET based sensors is formed by the Electrolyte-Insulator-Silicon (EIS) structure [5]. This is the electrochemical analogue of the solid-state Metal-Insulator (or Oxide)-Silicon (MIS or MOS) structure [1, 2], which on its turn is the functional element of the MOSFET device. Schematic pictures of both MIS- and EIS-structures are shown in Figure 4.1.

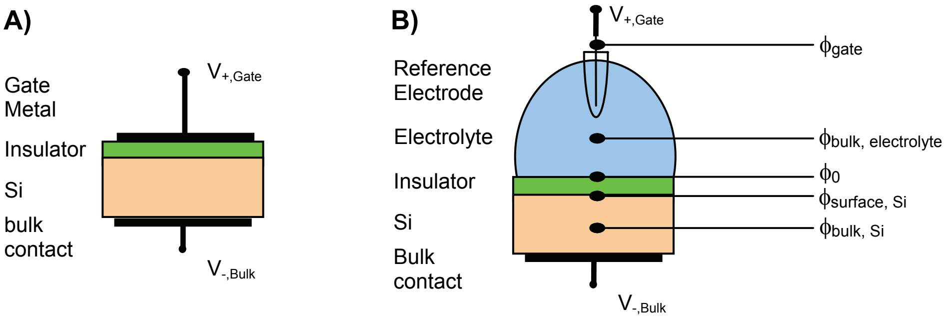

Figure 4.1. Schematic setup of A) a MIS-structure and B) an EIS-structure with a two-electrode connection. Also indicated in B) are the potentials at different locations in the EIS-structure.

EIS-structures can be used as sensory elements due to the fact that the surface layer of the gate insulator (mostly oxides) shows specific interactions with protons in the bulk of the solution. The result of such specific interaction between those protons and charged groups on the insulator surface, i.e. so-called (de)protonation of surface Si-OH groups, is depicted in Figure 4.2 for SiO_2.

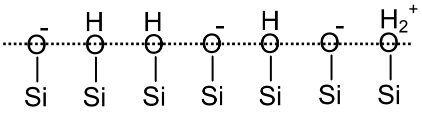

Figure 4.2. Graphical interpretation of (de)protonation of surface Si-OH groups on the surface layer of SiO_2.

Other inorganic insulators than SiO_2 that show similar *pH* dependent interactions between surface groups and bulk protons are Si_3N_4, Al_2O_3 and Ta_2O_5 [5]. The gate insulators can also be surface modified to be receptive to other species. Examples of such FET-based sensors are the ISFET, which has H^+ sensitive receptor groups [5-7], and the CHEMFET, which has receptor groups for detection of other ions [5, 8-11]. As a result of the charge on the surface there is a potential difference between the insulator surface and the bulk of the solution. The *pH* dependent potential on the surface is called ϕ_0 and the potential in the bulk is called ϕ_{bulk}. Since the latter is constant and can be taken zero as a reference, the potential difference between surface and bulk will simply be written as ϕ_0. ϕ_0 is located within the device as depicted in Figure 4.1B and can thus not be determined directly. However, via external connections as shown in Figure 4.1B ϕ_0 can be determined. The characteristic voltage of the EIS-structure is the so-called flatband voltage V_{fb}, which can be written as Equation 4.1 [5]:

$$V_{fb} = E_{ref} - \phi_0 + \chi_{sol} - \frac{\Phi_{Si}}{q} - \frac{Q_{ins} + Q_{ss}}{C_{ins}} \tag{4.1}$$

where E_{ref} is the contribution of the reference electrode; χ_{sol} is the surface dipole potential of the solution; Φ_{Si} is the silicon workfunction; Q_{ins} and Q_{ss} are the insulator charge and surface states charge, respectively and these are zero in ideal cases; C_{ins} is the insulator capacitance. Except for ϕ_0 all the other terms are constant and *pH* independent. Although in the early days of FET based sensor research, surface states were also thought to display a *pH* dependent influence on V_{fb} the work of Diot et al. [12] showed that this was not the case.

The flatband voltage V_{fb} is the externally applied voltage needed to make all energy bands in the silicon flat from bulk to the surface [1]. This is a quantity that can easily be measured via special FET electronic read-out circuitry [5]. Although the derivation of the absolute value of V_{fb} can sometimes be questioned due to the large number of uncertainties encountered during practical situations, which are also mentioned in the following sections, relative measurements can result in the proper responses. After all, if Equation 4.1 for analyte 1 is rewritten to: V_{fb1} = Const. - $\phi_{0,1}$ and for analyte 2: V_{fb2} = Const. - $\phi_{0,2}$ the measured response is $\Delta V_{fb} = V_{fb,1} - V_{fb,2} = -(\phi_{0,1} - \phi_{0,2}) = -\Delta\phi_0$. This is all under the condition that the non-idealities described in the next sections and any unknown parameters in Equation 4.1 remain constant during the experiments. A more detailed description of the relation of ϕ_0 and bulk *pH* can be found in the site binding theory, originally described by Yates et al. [13], later adapted by Bousse [14] and finally modified into a compactly notated model by van Hal et al. [15, 16].

The characterization of EIS-structures and especially their *pX* responses occurs commonly via capacitance voltage (*C-V*) measurements [5], which will now be briefly introduced. Two types of capacitance-voltage (*C-V*) measurements are used for MIS [2] and EIS characterizations. The quasi-static (QS) *C-V* technique that uses a voltage ramp to characterize the device or the high-frequency (HF) *C-V* technique that uses a combined ac and dc potential to characterize the system. Since only the latter is used in this project, no attention will be paid to the QS technique. The QS technique is very sensitive towards leakage currents [2] and the thin insulators used in this project were prone to such leakage currents, thereby hindering proper use of the QS *C-V* technique.

The HF *C-V* technique consists basically of a DC potential with a superimposed ac-signal. The DC-potential is swept over a certain range and is used to excite the different states of the system (e.g. accumulation, inversion and depletion). The ac potential is a sinusoidal voltage with a certain amplitude and frequency. The ac potential is used as the exciting voltage for an impedance measurement. However impedance is not the quantity looked for here, but the capacitance has to be calculated from it. To state it simply, MIS- and EIS-structures can in ideal cases be visualized as being a series circuit of two capacitors, namely the insulator C_{ins} and the space charge capacitance of the silicon, C_{sc}. The total capacitance is $C^{-1} = C_{ins}^{-1} + C_{sc}^{-1}$. In accumulation C_{sc} will be very large and C_{ins} will dominate the total capacitance. In depletion C_{sc} becomes smaller as function of the bias voltage and will therefore decrease the total capacitance. In inversion two scenarios can occur. The different states of a *C-V* curve can be visualized via a standard *C-V* plot in Figure 4.3.

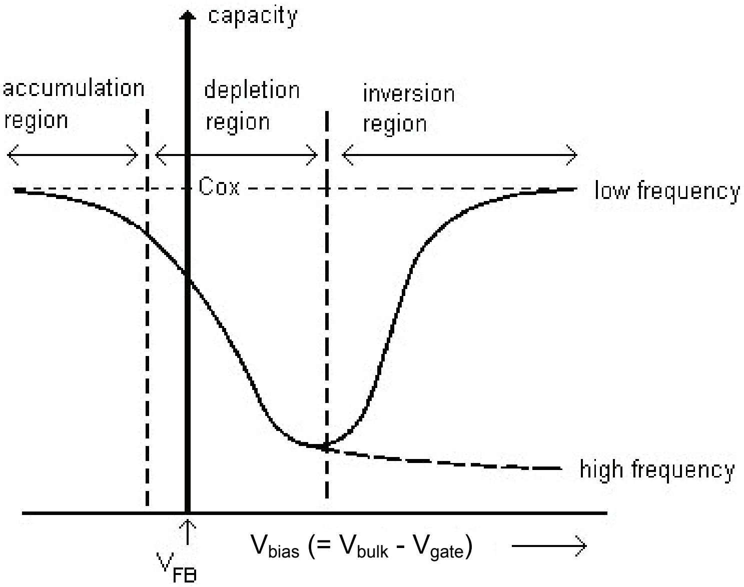

Figure 4.3. Theoretical *C – V* plot for n-type silicon with an insulator. Note that the bulk silicon is in this case positively biased with respect to the gate. Such polarity convention is normally encountered in electrochemical experiments. If the gate was to be positively biased with respect to the bulk, this plot would correspond to a p-type silicon sample.

This figure shows that the capacitance in accumulation is large and approximately equal to C_{ins}. In depletion the space charge capacitance will decrease as the bias voltage increases and thus the total capacitance will also decrease. The two scenarios in inversion depend on the frequency of the ac-signal. For low frequencies (≈ < 1kHz) an inversion layer will be formed near the surface, thereby making C_{sc} very large once again so only C_{ins} makes up for the total capacitance. In that case the *C-V* plots are nearly the same as a plot made via the QS *C-V* technique. For high frequencies, the inversion charge is not able to follow the ac-signal. The space charge capacitance therefore approaches a constant value and also the total capacitance stays now constant. To measure the capacitance correctly always a high-frequency (>1 kHz) ac voltage will be used.

From ideal *C-V* measurements V_{fb} can be directly derived via two quite straightforward methods. The first one is based on an analytical derivation of V_{fb} from *C-V* curves and this technique is commonly used for MIS-structures [1, 2]. However, it requires that *C-V* curves have nearly ideal shapes and that the capacitance in accumulation reaches a constant value, a requirement mostly not fulfilled when measuring on very thin insulators. The second method is a graphical method. It is commonly used for deriving the V_{fb} shifts upon *pH* changes from *C-V* plots for EIS-structures [5]. An example of a collection of *C-V* curves measured on an EIS-structure is shown in Figure 4.4.

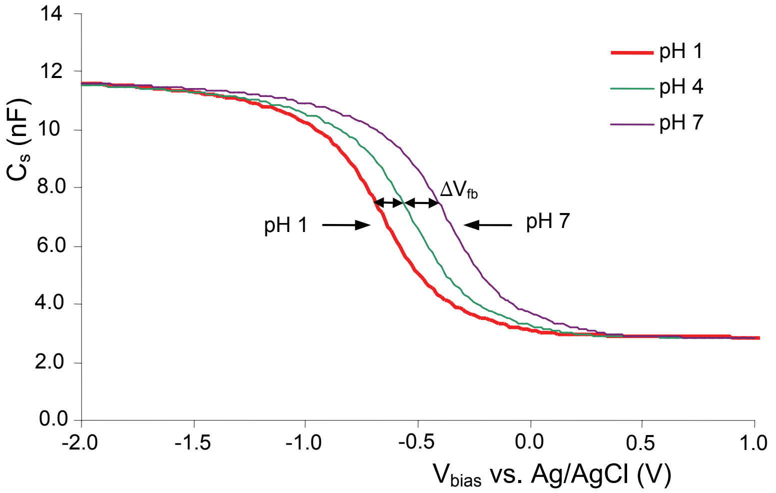

Figure 4.4. High Frequency *C-V* plots made at three different *pH* values in 0.1 M electrolyte of TetraButylAmmonium Chloride. The tested EIS-structure consisted of a 52.6 nm SiO_2 insulator with on top a 64.6 nm Ta_2O_5 insulator.

The *C-V* curves in Figure 4.4 can be regarded as ideal curves, i.e. no or negligible leakage current flows through the gate insulators and the resulting *C-V* curves show constant plateaus in the accumulation regime from which the insulator capacitance can be derived. The *pH* responses can easily be derived from such curves. Since the insulators block charge transfer very well and upon *pH* changes only V_{fb} will change, all curves will then show an equal shape but have shifted over the *V*-axis with the amount ΔV_{fb} due to the *pH* change.

However, in case of thin insulators *C-V* plots do not look like Figure 4.4 and can be heavily distorted, which hinders the determination of the *pH* responses. In this project Si-C linked, organic insulators are used, which have a thickness of a few nanometers. They are so thin that direct tunneling of electrons through such layers can take place. Although it was found that the use of such layers in MIS-structures suppressed the direct tunneling current as a function of monolayer chain length to a large degree [17], the longest alkyl chain used in this study (2.60 nm for $-C_{22}H_{45}$ [18]) was still shorter than the upper limit of direct tunneling of 3.5 nm [2].

Besides direct tunneling over the monolayer, several other unwanted processes can occur at such electrodes. In Figure 4.5 a number of such processes are schematically visualized.

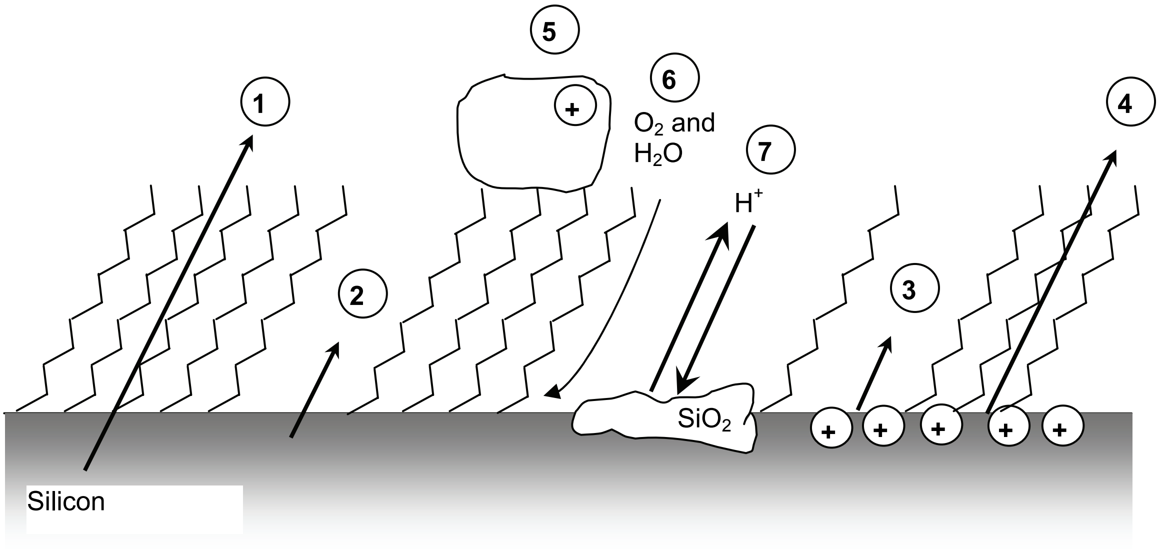

Figure 4.5. Schematic view of an EIS-structure with a non-perfect organic monolayer as insulator. The unwanted processes are explained in the text below. The processes are not to scale and are exaggerated to illustrate their working mechanism.

The seven processes drawn in Figure 4.5 are:

1) Direct tunneling of charges over the monolayer from the silicon bulk to species in the electrolyte or vice versa. The amount of charge carriers able to tunnel directly over the monolayer can be reduced to a large degree by increasing the monolayer chain length but this process can not be prevented given the reasons mentioned above.
2) The leakage of charge carriers from the bulk of the silicon directly to species in the electrolyte or vice versa via pinholes in the monolayer.
3) The leakage of charge carriers from surface states at the surface of the silicon directly to species in the electrolyte or vice versa via pinholes in the monolayer. In this case positively charged surface states are drawn, but neutral or negatively charged states are likewise possible. Surface states are electronic energy levels in the bandgap. These states are located at the surface and are capable of transferring charges with species in the solutions. Most surface states result from the termination of the bulk structure at the surface. They can be passivated via –H or alkyl termination. A large contribution on the total amount of surface states is due to the breaking of Si-H bonds, resulting in dangling surface bonds [4].
4) Direct tunneling of charges over the monolayer from surface states at the surface of the silicon directly to species in the electrolyte or vice versa. In this case positively charged surface states are drawn, but neutral or negatively charged states are likewise possible. In studies on MIS-structures with these kind of monolayers it was found that the amount of surface states was very low, especially on p-type silicon the amount found was 1.7 - $3.0 \cdot 10^{11}$ $cm^{-2}V^{-1}$ over an energy range of 0.22 - 0.73 eV over the valence band edge on Si-$C_{18}H_{37}$ – Al devices [19]. Also Liu et al. found a very low number of surface state density on MIS-structures of alkylated samples as compared to oxidized silicon samples and alkoxilated, oxidized samples [20].

5) (Non-)specific adsorption of neutral or charged species onto the monolayer. Even neutral, adsorbed species are expected to have an influence on the electrical properties of the monolayer. The capacitance associated with such a thin monolayer is quite large and any change in thickness due to for instance tight adsorption of neutral or charged species will lower the total insulator capacitance. When a large number of charged species is adsorbed, accompanied with the formation of a large surface charge, this can lead to a large shift in the flatband voltage. Finally, when the surface gets covered with a large amount of non-specifically adsorbed species these can hinder site-binding reactions of receptors on the surface with desired species in the electrolyte. More information on (non)-specific adsorption onto Si-C linked monolayers can be found in [21]. It should also be mentioned that OH^- adsorption might occur at such layers since in literature it is mentioned that such process occurs at hydrophobic monolayer – electrolyte interfaces [22], amongst which organic monolayers on Au surfaces [23-25].
6) Oxidation of the remaining Si-H sites in pinholes as a result of reaction with water or oxygen. If this process occurs during measurements this will lead to structural changes of the silicon electrode both in terms of morphology and electronic properties. Electrochemically created oxide is often very porous and can contain a significant amount of water, hydroxyl ions and other species which are present in the electrolyte [4]. Also the electrical properties of anodic oxide are of very poor quality due to high concentration of charges and states associated with the loose structure and high levels of impurities in anodic oxides [4]. Severe oxidation of the silicon electrode is thus expected to deteriorate the electrode properties and will certainly make the properties of the electrode vary during the formation of the oxide.
7) Interaction of charged species with SiO_2 formed at the surface. Charged species, mostly cations such as H^+ and to a lesser degree alkali ions such as Na^+ and K^+, can interact with Si-OH groups in oxidized spots [13, 16, 26] and can consequently charge these groups. Such interactions are unwanted when for instance *pH* sensitive receptors are anchored to the monolayer and should thus be taken into consideration when choosing certain receptors.

Of all mentioned processes only number 1 can not be prevented as it is a result of the limited thickness of the monolayer. Although upon monolayer formation a densely packed layer is created, not all Si-H sites have reacted, amongst other due to steric hindering [27]. It was shown via simulations that on Si<111> about 50-55% of all Si-H sites have reacted [28, 29] and it is estimated that on Si<100> surfaces about 30-35% have reacted [30]. Therefore, the other six processes are very likely to occur to some degree, depending on a variety of parameters such as monolayer density, anodic potentials, choice of species in the electrolyte etc. It is thus of importance to keep their influence as small as possible. Process 1, on its turn, is already dominant enough to make a proper investigation of *pH* or *pX* responses via regular *C-V* measurements, and thus determination of V_{fb}, nearly impossible. Mott Schottky measurements can provide an outcome here.

Mott Schottky measurements can be used to analyze all *pX* responses of EIS-structures with both functionalized and unfunctionalized monolayers. In the theory section the theory of ideal Mott Schottky measurements is described, followed by a discussion on the non-idealities that can be encountered and in fact have been partly encountered during measurements. Since the Mott Schottky analysis starts with choosing proper impedance networks special attention has also been paid to choosing the proper networks in the right situations. This is followed by the results section in which first the representation and discussion on measurements on ideally behaving EIS-structures are discussed. This serves the purpose to show that the *pH* response analysis via both methods, *C-V* and Mott Schottky, leads to the same outcome. In the second part of the results section the Mott Schottky analysis of EIS-structures with thin insulators such as Si-C linked monolayers is treated. Also the non-idealities encountered during practical measurements and how to deal with these will be discussed. Next the conclusions will be drawn and finally the experimental settings are given.

4.2 Theory

4.2.1 The Mott Schottky relation in ideal situations

The Mott Schottky relation describes the relation of the space-charge (differential) capacitance of silicon in depletion (see Figure 4.6) and the applied polarization ($V_{fb} - V_{bias}$).

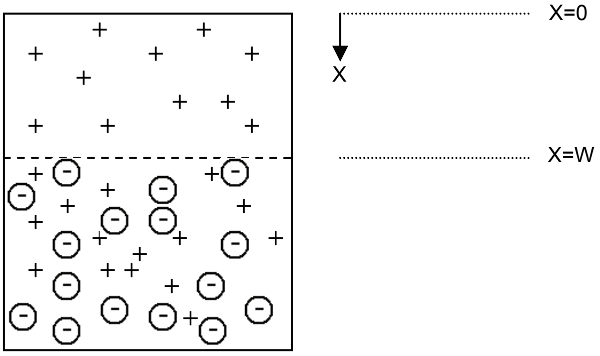

Figure 4.6. Schematic picture of n-type silicon in depletion.

The depletion thickness is denoted by *W* and the distance from the surface ($x = 0$) is denoted by *x*. For $x < W$ the silicon is fully depleted from mobile charge carriers and only ionized, immobile donor atoms are left. The charge density in this region $x < W$ can thus be estimated to be $\rho_{x<W} \approx q{\cdot}N_D$ [C·cm^{-3}] with N_D being the doping concentration in the case of n-type silicon. For p-type silicon voltage signs should be reversed and N_D should be replaced by N_A. Furthermore, it will be assumed that for $x > W$ there is charge neutrality because the charge of every immobile donor atom is compensated by a mobile electron, so $\rho_{x>W} \approx 0$. The depletion layer thickness can be described as a function of applied bias voltage [1] (Equation 4.2):

$$W = \sqrt{\frac{2\varepsilon_0 \varepsilon_{r,Si}(V_{fb} - V_{bias})}{qN_D}} \tag{4.2}$$

The space charge Q_{SC} per unit area of the semiconductor can then be described by Equation 4.3:

$$Q_{SC} = \rho_{x<W} W = qN_D W = \sqrt{2q\varepsilon_0 \varepsilon_{r,Si} N_D (V_{fb} - V_{bias})} \tag{4.3}$$

Now the space charge capacitance per unit area C_{sc} [F·cm^{-2}] associated with this charge can simply be written as Equation 4.4a:

$$C_{SC} = \left|\frac{dQ_{SC}}{dV}\right| = \sqrt{\frac{q\varepsilon_0 \varepsilon_{r,Si} N_D}{2(V_{fb} - V_{bias})}} = \frac{\varepsilon_0 \varepsilon_{r,Si}}{W} \tag{4.4a}$$

This equation can be rewritten into the Mott Schottky relation in order to obtain a linear dependence of V_{bias} (Equation 4.4b):

$$C_{SC}^{-2} = \frac{2(V_{fb} - V_{bias})}{q\varepsilon_0 \varepsilon_{r,Si} N_D} \tag{4.4b}$$

Plotting C_{sc}^{-2} vs. V_{bias} should then yield a linear plot from which the flatband voltage V_{fb} can be obtained via the V–axis intercept and the doping N_D can be obtained via the slope of the plot. As an example the typical Mott Schottky plot of Si-$C_{12}H_{25}$ | Hg MIS-structures is given in Figure 4.7.

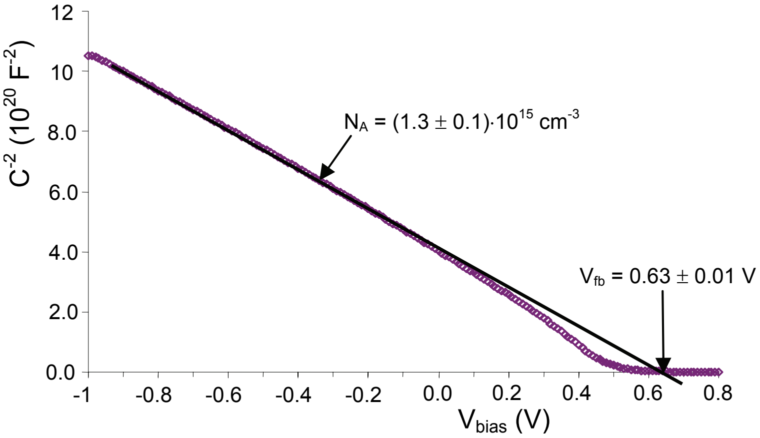

Figure 4.7. Example of a Mott Schottky curve as shown in Chapter 2 (Figure 2.10). The doping as derived from the slope and the flatband voltage as derived from the *V*-axis intercept are also indicated.

4.2.2 Non-idealities in Mott Schottky measurements

Many non-idealities can occur in the Mott Schottky plots. Such non-idealities are extensively described in a report by Gomes et al. [31]. The errors described here are some of the ones they also mentioned in their work. Some errors can be easily corrected for, and some not. The errors described here are grouped into two categories: modeling errors and solid-state related errors.

A) Modeling errors

C_{sc} has to be derived from high frequency *C-V* measurements, which are in fact impedance measurements under varying bias voltages. In the simplest cases the impedance can be modeled via a 2-element model of either a parallel circuit of a capacitor and a resistor, $C_p – R_p$, or a series circuit of a capacitor and a resistor, $C_s – R_s$. In practical cases, the models are often more complicated and when such complicated model is fitted by a 2-element model, errors are easily made in the estimation of C_{sc} from either C_p or C_s. A more elaborate discussion about modeling can be found in section 4.2.3.

B) Solid-state related errors

Several parasitic processes or non-idealities can occur inside the semiconductor or near the semiconductor surface, which can cause deviations in Mott Schottky plots. Some of them are listed in this subsection.

B-1) Surface states

Surface states are electronic energy levels located in the forbidden bandgap [3]. They are physically located at the surface and are able to transfer charges with other solids and solutions. Dangling bonds that are caused by the termination of the bulk phase are intrinsic surface states. At steps on the surface there will be more surface states which will increase the reactivity of the surface at these sites. Many researchers have studied the behavior of surface states. The following references provide some good information on the electrochemical behavior of surface states at the semiconductor-electrolyte interface and how they contribute in *I-V* and *C-V* behavior [31-40].

Together with surface states the concept of Fermi level pinning can be introduced. Fermi level pinning stems from a very high density of surface states [3, 41, 42]. In the following example it is assumed there is a high density of mono-energetic acceptor-like surface states (i.e. the surface states are positively charged when empty or neutral upon capturing an electron) in a n-type semiconductor (i.e. they all have an energy close to E_{ss} in the bandgap and E_{ss} is positioned above the intrinsic Fermi Level E_i). Furthermore, they are all filled at a certain bias voltage (i.e. $E_{F,Si}$ is positioned above E_{ss}). This is illustrated in Figure 4.8.

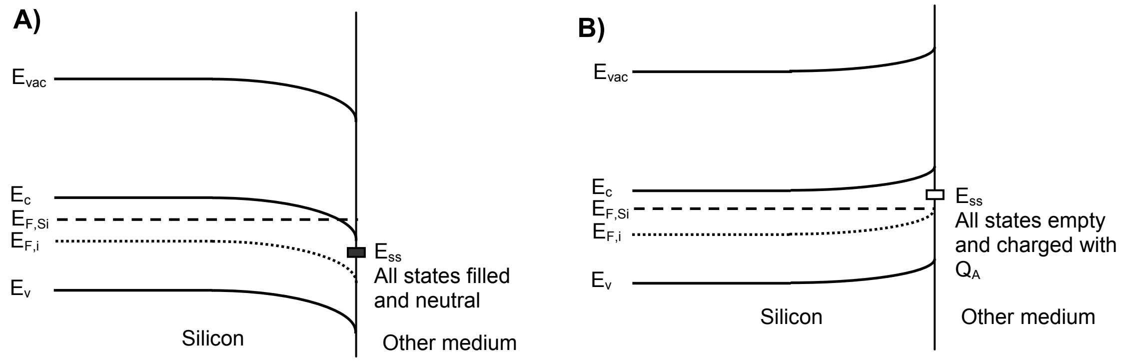

Figure 4.8. Two energy band diagrams of n-type silicon with mono-energetic acceptor-like surface states. In A) the bands are bent in such a way that all the states are filled and neutral. In B) the bands are bent in such a way that all the states are empty, resulting in a total silicon surface state charge Q_A.

If the bias voltage is changed in such a way that the bands start to bend upward in the direction of depletion and the Fermi level moves up to the E_{ss} level, only the surface states will be charged. Upon further increasing of the bias voltage the bands can not be bend further since the surface states are being charged until they are fully charged with charge Q_A. This situation is depicted in Figure 4.8B. While charging the surface states, their charge will be compensated by a counter charge on the gate metal in case of MIS-structures, i.e. C_{ins} will be charged. In case of EIS-structure the counter charge will be in the electrolyte, leading to either a charging of C_{dl} and / or a charging of C_{ins} depending on the magnitudes of C_{dl} and C_{ins}. This means that during the surface states charging none of the applied bias voltage drops over the space charge capacitance, i.e. the depletion region will not increase and is at these bias voltages no longer a function of V_{bias}. After the surface states are emptied, any further increase of voltage will further increase the band bending and that voltage will drop over the space charge region again [3]. When the surface states are being charged, the surface Fermi level is thus in fact pinned, i.e. over a certain voltage range independent of bias voltage.

It suffices here to say that surface states that are energetically located in the forbidden bandgap will increase the conduction over the interface. Because charge processes at surface states are known to have a certain time constant (τ_{ss} [s]), they can be modeled by a resistance in series with a capacitance. τ_{ss} is defined in Equation 4.5:

$$\tau_{ss} = R_{ss} \cdot C_{ss} \tag{4.5}$$

where the combination of R_{ss} [Ω] and C_{ss} [F] describe a time dependent charging/discharging process. C_{ss}, however, has no length associated with it as most capacitances do but is just described by the relation given by Equation 4.6:

$$C_{ss,dif} = \frac{\partial \sigma}{\partial V} \tag{4.6}$$

where $\partial\sigma$ [C] is the charge difference in the capacitor; ∂V [V] is the difference in potential drop over the capacitor; and $C_{ss,dif}$ [F.m^{-2}] is the differential capacitance.

The values of C_{ss} and R_{ss} are frequency dependent. For higher frequencies, the surface states are not able to follow the ac-signal. So increasing the frequency leads to a diminished influence of the C_{ss} and R_{ss}. If the surface states then still have a dominant influence on the impedance data the relationship between C^{-2} and V can even be non-linear for a surface state density distributed over the semiconductor bandgap. Since the surface states can be modeled by simple impedance elements, they will be discussed more elaborately in section 4.2.3.

B-2) Frequency dependence in the Mott Schottky plots

In practice, a common non-ideality found in Mott Schottky plots is the frequency dependence of the slope of the plots. Two types of frequency dependence can be observed.

The first case shows frequency dependent slopes of the plots which all go to different V-axis intercepts. So both the doping and the flatband voltage cannot be properly derived.

The second case shows frequency dependent slopes of the plots which all go to one single V-axis intercept, so only the doping can not be derived from the slopes. The flatband voltage, however, can still be derived from this V-axis intercept. For the ideal Mott Schottky relation given by Equation 4.4b the semiconductor dielectric constant ε_r is assumed to be constant. The latter case can now be modeled by a frequency dependent ε_r and Gomes et al. [31] derived an analytical expression for this phenomenon.

The origin of the frequency dependent ε_r of the semiconductor is believed to be due to dipolar relaxation in a region underneath the surface and at least extending as far as the space-charge layer itself [31]. It has been shown that the effects of this frequency dependency are smaller at electrodes with more perfect surfaces. The occurring of frequency dependent behavior is therefore related to surface roughness [31, 43, 44]. Oskam et al. [44] investigated this phenomenon by testing n-GaAs semiconductor samples with either a gold contact or a contact via an electrolyte. In the latter case they deliberately roughened some of the surfaces of their samples to investigate the influence of this roughening. The samples with gold contact did not show any frequency dependence in the slopes of the Mott Schottky plots whereas the samples contacted via an electrolyte did show a frequency dependency, in fact they found both types of the above mentioned dispersions. These depended both on the surface roughness and also on the specific conductivity of the electrolyte. At flat electrodes, almost no frequency dependency was observed and increasing the electrolyte conductivity diminished the frequency dependency. Since their findings could be closely related to the same phenomena occurring at metal electrodes, they argued that the frequency dependency is related due to relaxation phenomena at the electrolyte side of the interface and not in the semiconductor. So in literature dielectric relaxation phenomena in the double layer (depletion layer) at the semiconductor side as well as the double layer in the electrolyte side are named as the cause for the frequency dependency. One distinct feature from literature is that the frequency dependency has a clear relation with surface roughness.

B-3) Presence of deep-lying localized levels

This phenomenon can occur when the electronic defect structure of the semiconductor is not limited to one single type of completely ionized donor or acceptor level. Gomes et al. [31] have analytically discussed the example of a semiconductor with two types of donor centers present, one being completely ionized at flatband situation (density N_D), the other one completely filled (density N_D’). In some cases it was shown that frequency dependency can be expected. Mott Schottky plots can then, depending on the frequency, have multiple slopes. One can be associated with doping density N_D, from which V_{fb} can be determined. For large band bending (i.e. corresponding to relatively large C^{-2} values), hereby effectively emptying the deeper donor levels N_D’, still a linear slope may be observed. For low voltages and very high frequencies this second slope correlates to a doping value of $N_D + N_D$’. In such cases, however, care should be taken in interpreting the right flatband voltage. A good practical example can be found in [45]. In case of Si-wafers with a single type of dopant atoms, such as P and B, it can be expected that all these dopant atoms are completely ionized at room temperature [1] and that this phenomenon will not occur.

In practice, non-idealities may not be limited to one of the above mentioned situations but can be caused by a number of these effects.

4.2.3 Impedance models to derive the space charge capacitance

Total impedance model

In order to give a good circuit for C_{sc} derivation from Mott Schottky measurements, an impedance circuit model incorporating most non-idealities encountered in literature [3] is first discussed (see Figure 4.9).

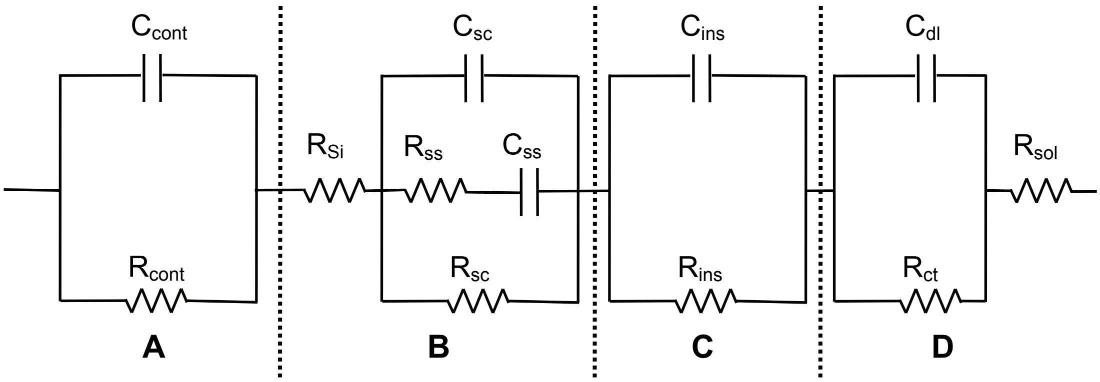

Figure 4.9. Extended Impedance model of the EIS-structure. Region A = (Back) Contact impedance, B = Silicon bulk resistance and space charge impedance, C = Insulator Impedance, and D = Electrolyte Impedance formed by double layer impedance and solution resistance. In case of MIS-structures this scheme is still valid with the simplification that region D can be replaced by a short-circuit.

Region A is the back contact to the semiconductor. This parasitic impedance should be as low as possible, so Ohmic contacts are preferred. In case of moderately doped silicon, Ohmic contacts can be made either by aluminum deposition and sintering [46] or by scratching the silicon and deposit a small drop of liquid Ga/In eutectic. This simplifies the contact impedance to a simple resistor which can be added to the silicon bulk resistance. A study on the impedance of three types of back contacts, Al, Ga/In, and direct wire contact, can be found in Appendix C.

Region B describes the bulk silicon and space charge layer. The silicon bulk resistance can be described by a resistor. The space charge layer can be modeled by the space charge capacitance C_{sc}. In case of constant surface reactions taking place in depletion, it means some leakage is present in the depletion layer, modeled by a space charge resistance R_{sc}. The surface states, also mentioned in section 4.2.2, can be modeled in parallel to C_{sc} as a resistance R_{ss} and capacitance C_{ss} in series.

Region C describes the insulator impedance. It can be modeled for perfect insulators (mostly oxides) by a capacitor C_{ins}. For leaky insulators an extra resistor R_{ins} comes in parallel.

Region D is the impedance in the electrolyte. The solution bulk can be modeled by a resistor R_{sol}. The electrolyte double layer (analogous to the space charge layer in the semiconductor) can be modeled by the double layer capacitance C_{dl} and a charge transfer resistance R_{ct}. The double layer capacitance C_{dl} is a series circuit of two capacitors: the Helmholtz capacitance C_H and the diffuse layer capacitance C_{diff}. The first one is considered to be constant in electrochemical experiments but nonetheless its value differs in literature from 10 - 40 $\mu F \cdot cm^{-2}$ at metal electrodes [47] to 3 - 4 $\mu F \cdot cm^{-2}$ at semiconductor electrodes that are H-terminated [48] or modified with Si-C linked monolayers [49, 50]. The value of C_{diff} is concentration and bias voltage dependent. It increases for higher bias voltages and higher electrolyte concentrations, thereby diminishing its influence. For high electrolyte concentrations (approximately > 0.1 M) the influence of C_{diff} is negligible and C_{dl} can be approximated by C_H.

The model in Figure 4.9 is far too complicated to use as a practical fitting model for the impedance data and luckily, in most practical cases it can be severely simplified.

Two-element models

As stated above, C_{sc} has to be derived from impedance measurements. First, the concept of impedance is explained in order to make a smooth transition to modeling. This can be done by plotting the impedance Z in a so-called polar diagram or Nyquist diagram, in which Z is then pictured as a vector. This is illustrated in Figure 4.10.

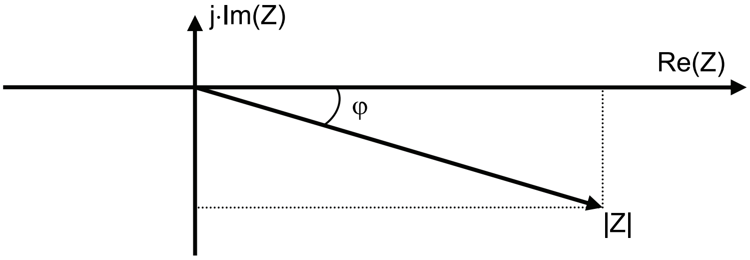

Figure 4.10. Polar diagram of the impedance *Z*. *Z* is pictured as vector with a certain length and a certain phase angle.

The X-axis of a Nyquist plot is called the real axis and the Y-axis is called the imaginary axis. From Figure 4.10 it can be seen that Z can be written as (Equation 4.7):

$$Z = \mathrm{Re}(Z) + j\,\mathrm{Im}(Z) \tag{4.7}$$

The impedance can also be written in two other, frequently encountered parameters: the modulus: $|Z| = \sqrt{\mathrm{Re}(Z)^2 + \mathrm{Im}(Z)^2}$, which is the length of the vector in Figure 4.7 and the phase angle $\varphi = \arctan(\mathrm{Im}(Z)\cdot\mathrm{Re}(Z)^{-1})$, which is the angle with the positive real axis. It can be seen that the impedance is known if any two of the four parameters $|Z|$, φ, Re(Z), or Im(Z) are known. More background information on impedances can be found in [51].

Most frequency analyzers give their output data in the form of Re(Z) (also called: the in-phase component) and Im(Z) (also called: the out-phase component). An equivalent circuit of two elements can easily and directly be fitted using these two quantities without any complicated fitting routine. The first element is of course C_{sc}. The other element can be a resistor R_s in series with C_{sc} or a resistor R_p in parallel with C_{sc}. The equivalent circuits are depicted in Figure 4.11.

Figure 4.11. A) Series ($C_s - R_s$) and B) parallel ($C_p - R_p$) equivalent circuit.

The series circuit is useful when the measurements suffer from a high series resistance in the form of either contact resistance R_{cont}, silicon bulk resistance $R_{Si,bulk}$ or electrolyte resistance R_{sol} (see Figure 4.9). R_s is simply the sum of all these resistances.

Both R_s and C_{sc} can simply be derived from the total impedance (Equation 4.8):

$$Z = R_S - j\frac{1}{\omega C_s} \tag{4.8}$$

where $R_S = \mathrm{Re}(Z)$ and $C_S = -(2\pi f\,\mathrm{Im}(Z))^{-1}$

The parallel circuit is useful when the measurement suffers from large leakage currents in depletion. R_p is thus R_{sc} in Figure 4.9. The impedance can then be written as (Equation 4.9):

$$Z = \frac{R_P}{1+\omega^2 C_P^2 R_P^2} - j\frac{\omega C_P R_P^2}{1+\omega^2 C_P^2 R_P^2} \tag{4.9}$$

This is a rather complex description and it is more convenient when dealing with parallel circuits to write down the admittance $Y = Z^{-1} = R_P^{-1} + j\omega C_P$. After some rewriting R_p and C_p can be found (Equation 4.10):

$$C_P = \frac{-\mathrm{Im}(Z)}{2\pi f(\mathrm{Re}^2(Z) + \mathrm{Im}^2(Z))} \quad \text{and} \quad R_P = \frac{\mathrm{Re}^2(Z) + \mathrm{Im}^2(Z)}{\mathrm{Re}(Z)} \tag{4.10}$$

All four fitting parameters C_p, C_s, R_s and R_p can now be derived in a glance from Re(Z) and Im(Z). In case of a dominant behavior of C_{sc} in the impedance both circuits will show the same C, so $C_p = C_s$. A large discrepancy between these two indicates the use of a wrong model.

If the frequency dependence of C_{sc} in the Mott Schottky plots is strong, one can try to incorporate this effect in a constant phase element (CPE). The CPE is discussed in detail in Appendix A.

Three or more element models

In practice, two element models may be insufficient for proper data fitting. Since at each frequency the impedance data gives two quantities, namely Re(Z) and Im(Z) or $|Z|$ and φ, a model of more than two elements results in complex fitting routines. Using the data at multiple frequencies may be an outcome, albeit that this increases the time for analysis significantly. On the other hand, if complete impedance spectra are present of several frequency decades, a linear least-squares fitting program, such as "Equivalent Circuit" [52] can provide an easy route for finding the proper model. As stated before, Mott Schottky measurements are commonly performed at one frequency, so a two-element model is preferred. When a model is more complex, there are still possibilities to fit it via a two-element model, but some precautions have to be made then. Two of such more complex, but practical models will be treated now.

The first model is the combination of the serial and parallel *C*-*R* model, when both series resistance and parallel leakage resistance play a non-negligible role. The circuit diagram is depicted in Figure 4.12.

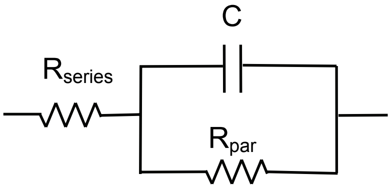

Figure 4.12. Three element model consisting of $R_{series,}$, R_{par}, and C.

If this model is fitted by a C_p-R_p model, C_p is [2]:

$$C_p = \frac{C}{(1+{R_{series}}/{R_{par}})^2 + (\omega R_{series} C)^2} \tag{4.12}$$

It can be seen from Equation 4.12 that C_p depends both on R_{series} and R_{par}, so for minimal influence of these two R_{series} should be as small as possible and R_{par} should be as large as possible. In most practical cases the term $1+ R_{series}\cdot R_{par}^{-1} \approx 1$ and then the influence of frequency can be clearly illustrated. For low frequencies, the term $(\omega R_{series}C)^2 << 1$ and can be neglected and C_p equals the desired capacitance C. For higher frequencies, however, the term $(\omega R_{series}C)^2$ starts to dominate and $C_p << C$. So, if this model suits the practical situation, care should be taken that the measurement frequency is not too high.

If this model is fitted by a C_s-R_s model, C_s is [2]:

$$C_s = C(1+(\omega R_{par}C)^{-2}) \tag{4.13}$$

In case of the series model, C_s depends solely on R_{par} and series resistance has no influence. The influence of frequency can also be easily illustrated. In contrast to the parallel model a high frequency is now preferred since then $(\omega R_{par}C)^{-2} << 1$ and C is correctly measured. For lower frequencies C_s will increase sharply with frequency.

This model can be useful for both the semiconductor in depletion where $C = C_{sc}$, $R_{par} = R_{sc}$ and $R_{series} = R_{series}$, as long as C_{ins} and C_{dl} can be neglected (see Figure 4.9). It can also be useful for measurements when the semiconductor is operated in accumulation where $C = C_{ins}$, $R_{par} = R_{ins}$ and $R_{series} = R_{series}$, as long as C_{dl} can be neglected. Given the large value of C_{ins} for thin insulators, deviations in the latter case can easily occur if the parallel model is used since the term $(\omega R_{series}C)^2$ now increases. The series model, on the other hand, favors a large C_{ins}.

Another practical model is given in Figure 4.13.

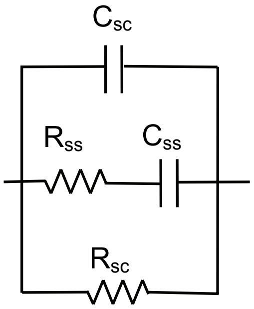

Figure 4.13. Impedance model incorporating parasitic impedances in the space charge layer [3].

This model consists only of the space charge impedance and contains three branches in parallel, namely C_{sc}, R_{sc} and the series circuit of R_{ss} and C_{ss}. This model should be used if both space charge leakage resistance and the influence of surface states are non negligible. Via some mathematics the data can be fitted via a parallel $C_p - R_p$ model and C_p is found to be [3]:

$$C_p = C_{sc} + \frac{C_{ss}}{1 + (\omega R_{ss} C_{ss})^2} \tag{4.14}$$

C_p now is an unmanageable combination of C_{sc}, C_{ss} and R_{ss}. Equation 4.14, however, also shows that for sufficient high frequencies the second term will be zero and C_{sc} can be properly derived. It must be noted that a parallel model is used for this derivation and the series resistance must thus be negligibly low, otherwise errors will still be made in the derivation of C_{sc}. Equations 4.13 and 4.14 give rise to opposite demands if both surface states and large series resistances are present. The first equation disfavors high frequencies, whereas the latter favors the use of high frequencies. In practice, one needs to try different frequencies to find the optimal result. In summary, in Table 4.1 all of the discussed circuits and the value of the capacitances in C_p or C_s for the case of two element models are listed. The circuit code is written in the Circuit Description Code (CDC) by Boukamp [52].

Table 4.1. C_s and C_p values obtained via different fitting models.

Circuit code	Figure	C_s value	C_p value
$[R_sC_s]$	4.11A	C_s	$\frac{C_S}{1+(\omega R_S C_S)^2}$
(R_pC_p)	4.11B	$C_p(1+(\omega R_s C_p)^{-2})$	C_p
$R_{series}(R_{par}C)$	4.12	$C_s = C(1+(\omega R_{par} C)^{-2})$	$C_p = \frac{C}{(1+R_{series}/R_{par})^2 + (\omega R_{series} C)^2}$
$(C_{sc}R_{sc}[C_{ss}R_{ss}])$	4.13	-	$C_p = C_{sc} + \frac{C_{ss}}{1+(\omega R_{ss} C_{ss})^2}$

Finally, it is mentioned that also the impedance analyzer itself can have a large influence on the measurement results and proper choice of measurement settings. Some considerations on this topic are given in Appendix B.

4.2.4 The influence of C_{dl} on the determination of C_{ins} from the capacitance in accumulation

In most EIS-structures relatively thick insulators are used. Relatively thick means in this case that the capacitance of these insulators is much smaller than the electrolyte double layer capacitance C_{dl}. In the case of nm-thin insulators this no longer holds and the influence of C_{dl} on the total capacitance has to be taken into account. For this explanation the model in Figure 4.9 has been simplified to a series model of three perfect capacitors, namely the space charge capacitance C_{sc}, insulator capacitance C_{ins} (or C_{ox} in case of an oxide insulator), and the double layer capacitance C_{dl}. In other words, no leakage path in the space charge region is assumed, the insulator is assumed to be perfect and no electrochemical reactions occur. Three capacitance in series can be replaced by a single capacitance via $C_{total}^{-1} = C_{sc}^{-1} + C_{ins}^{-1} + C_{dl}^{-1}$.

Some estimations are now made on the series circuit of C_{ins} and C_{dl}, which equals the total capacitance in accumulation. In this project very thin organic insulators are considered. According to [18] the longest monolayer in this project, obtained via alkylation of 1-dodocesene (C_{22}), is only 2.6nm thin. The capacitances associated with such monolayers can be quite large. This insulator capacitance is in series with C_{dl}, which equals the Helmholtz capacitance for electrolytes with high ionic concentrations. However, as stated above values of C_H differ in literature from 10-40 μF·cm^{-2} at metal electrodes [47] to 3-4 μF·cm^{-2} at semiconductor electrodes that are H-terminated [48] or modified with Si-C linked monolayers [49, 50]. As compared to the insulator capacitance the Helmholtz capacitance can not be neglected. As an example the capacitance per surface area is calculated for four different chain lengths in Table 4.2. In the last column the series capacitance of C_H and C_{ins} is calculated to show the influence of C_H on the (ideal) accumulation capacitance. Here the value of C_H = 3.5 μF·cm^{-2} was taken since this is the value found for silicon electrodes modified with Si-C linked monolayers. The lowest value of C_H has the largest influence on the series capacitance of C_H and C_{ins}.

Table 4.2. Si-C linked organic monolayers, their thickness and estimated capacitance per unit area.

Monolayer	Thickness [17] [cm]	Insulator Capacitance [a] $[\mu F\cdot cm^{-2}] = \varepsilon_0\varepsilon_r l^{-1}$	Total Capacitance [b] $[\mu F\cdot cm^{-2}]$
C_{10}	$1.2\cdot 10^{-7}$	1.84	1.21 (34%)
C_{12}	$1.32\cdot 10^{-7}$	1.68	1.14 (32%)
C_{16}	$1.78\cdot 10^{-7}$	1.24	0.92 (26%)
C_{22}	$2.60\cdot 10^{-7}$	0.85	0.68 (20%)

[a] for the dielectric constant $\varepsilon_r = 2.5$ was taken since this is an average value found in literature [17]

[b] this is the series capacitance of insulator and Helmholtz Capacitance: $C^{-1} = C_{ins}^{-1} + C_H^{-1}$. C_H was 3.5 $\mu F\cdot cm^{-2}$. Between brackets is the percentage decrease of measured C_{ins} as a result of C_H.

If the monolayer capacitance is to be estimated from *C-V* measurements in the accumulation regime, the influence of the Helmholtz layer has to be incorporated otherwise this leads to large errors. Especially for electrolytes with low ionic concentrations, C_{diff} starts to play a role, thereby effectively lowering C_{dl} and thus lowering the series capacitance of C_{ins} and C_{dl} even more. If one wants to derive C_{ins} via *C-V* measurements it is desirable to use concentrated electrolytes.

There are cases mentioned in literature where the double layer capacitance or the insulator capacitance has a non-negligible influence on the space charge capacitance and then care should be taken in the derivation of V_{fb} from Mott Schottky plots. This can occur on semiconductors with a very large dielectric constant, such as TiO_2 [53, 54]. It was demonstrated that the doping could still be properly derived from the Mott Schottky plot but that the flatband voltage as derived from the *V*-axis intercept has been shifted with an amount of $qN_D\varepsilon_0\varepsilon_r(8\pi C_X^2)^{-1}$ for n-type semiconductors [3, 53, 54]. C_X is here the ideal series circuit of C_{dl} and C_{ins}. Smit extended this model further to more complex cases [55]. Since the dielectric constant of silicon is rather small (ε_r = 11.7 [1]), this effect is not expected to occur at the experiments mentioned in this thesis.

4.3 Results and Discussion

Prior to electrochemical characterization a study was performed on the influence of three types of back contacts on the total impedance of the electrodes. The results of this study can be found in Appendix C. It was shown that both clean-room made, annealed Al contacts and at room temperature made Ga/In contacts gave low Ohmic contacts to p-type silicon electrodes.

Characterizing the sensory response of EIS –structures via Mott Schottky measurements can be a very time-consuming task. At different analytes the response has to be determined and in most cases multiple points are taken per analyte. This can easily lead to more than 100 files of measurement data and analyzing these by hand would take days of work. Therefore, an automatic doping and V_{fb} extraction routine for multiple sets of data was developed in the computer program Matlab^{TM} and used for analysis. This routine is explained in Appendix D.

4.3.1 Analysis of EIS-structures with thick insulators

EIS-structures with thick insulators should behave ideally and therefore it is expected that investigation of the *pH* response via both *C-V* curves and Mott Schottky measurements should give the same outcome. This is investigated in this section.

Capacitance-Voltage measurements

The measurements in this section are made on p-type silicon samples covered with a stacked insulator of 52.6 nm SiO_2 with on top 64.6 nm Ta_2O_5. This is the current insulator and sensing element of the ISFET sensor as developed and made in the BIOS group. In Figure 4.14 the results are shown of *C-V* measurements done at seven *pH* values ranging from 1 to 7.

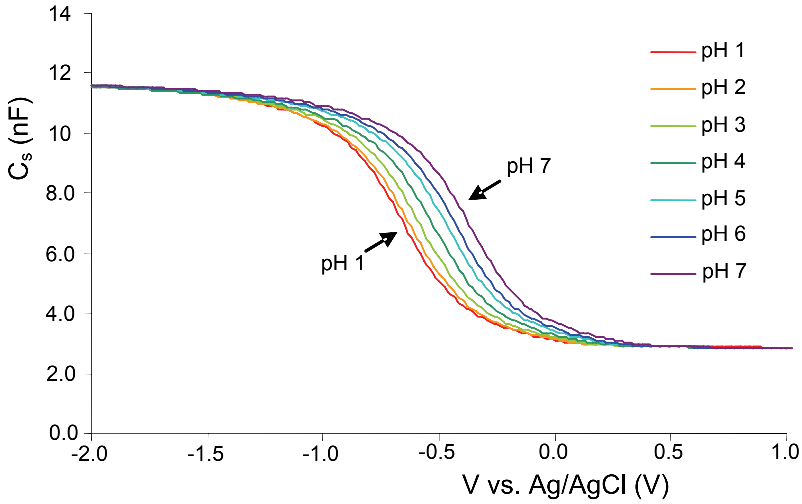

Figure 4.14. High Frequency *C-V* plots made at seven different *pH* values in 0.1 M electrolyte of TetraButylAmmonium Chloride. The tested EIS-structure had a 52.6 nm SiO_2 insulator with on top a 64.6 nm Ta_2O_5 insulator. The capacitance values are calculated via a series model (see section 4.2.3 for details).

The curves in Figure 4.14 resemble school-book *C-V* curves. The capacitances in accumulation and inversion are constant. Via the capacitance in accumulation the insulator properties, such as dielectric constant and thickness can be derived. Upon a *pH* increase the curves shift over the *V*-axis with an amount ΔV_{fb} corresponding to this *pH* increase as expected from theory [5]. The data in Figure 4.14 have been analyzed in two ways.

Method 1 is according to a graphical analysis [5]. A fixed capacitance value is chosen in the depletion regime, in which the shifts upon *pH* changes are large so that the shifts can be easily measured. In this case the data was obtained by reading the *V*-data at each *pH* belonging to a capacitance value of 7.0 nF in Figure 4.14. These shifts correspond to ΔV_{fb}. In this way not the absolute value of V_{fb} can be determined but that does not matter since only the relative response, i.e. the *pH* sensitivity, is of interest here.

Method 2 is an analytical determination of V_{fb} from the *C*-*V* curves [2]. The relation between oxide capacitance, i.e. the capacitance in accumulation, and the capacitance at which the flatband situation, C_{fb}, occurs can be described by Equation 4.15:

$$\frac{C_{fb}}{C_{ox}} = \frac{1}{1 + \frac{136\sqrt{T/300}}{d_{ox}\sqrt{N_A}}} \tag{4.15}$$

where T [K] is the absolute temperature, d_{ox} [cm] is the oxide thickness of a SiO_2 insulator, and N_A [cm^{-3}] is the doping. The value for the doping is taken as $2.0 \cdot 10^{15}$ cm^{-3}, a value found for similar wafers via Mott Schottky measurements on MIS-structures [17] and d_{ox} is calculated from ellipsometry measurements. However, Equation 4.15 assumes a SiO_2 insulator and in this case the insulator is a combination of SiO_2 and Ta_2O_5. Therefore the thickness of the Ta_2O_5 layer has been recalculated to an equivalent SiO_2 layer thickness via the equivalent oxide thickness [56]. The total layer thickness is after recalculation $77.2 \cdot 10^{-7}$ cm. This gives the relation $C_{fb} = 0.718 \cdot C_{ox}$. For C_{ox} the accumulation capacitance value at -2.0 V vs. Ag/AgCl was taken. Next, via linear interpolation from the data of Figure 4.14 the accompanying voltage value can be derived, which equals V_{fb}. The results of both methods are discussed in the next paragraph.

Mott Schottky measurements

In Figure 4.15 the Mott Schottky plots ($C^{-2} - V$) plots of the data of Figure 4.14 are shown.

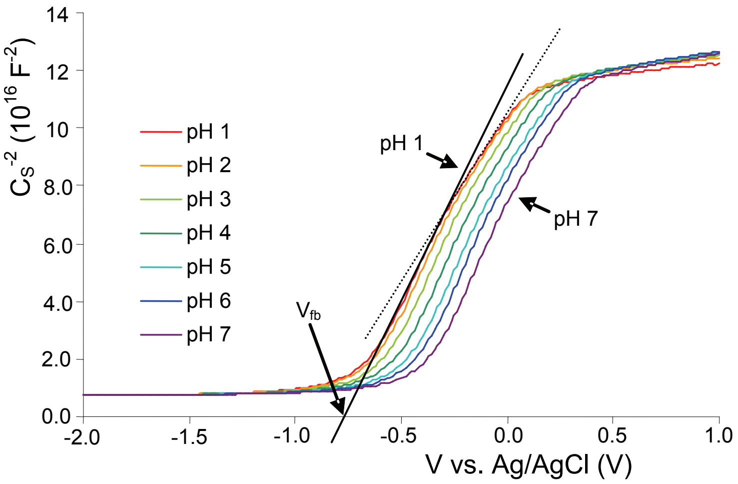

Figure 4.15. Mott Schottky representation of the data of Figure 4.14.

The Mott Schottky plots are linear over approximately 0.2 V. A linear fit through this region will reveal V_{fb} via the V-axis intercept. However, a second linear region indicated with a dashed fit line can also be observed. The cause of this second slope is unclear and this line has not been investigated further. Two slopes in the Mott Schottky plots were also observed for EIS-structures with thin insulators and in those cases the slope closest to the accumulation regime (the left-hand slope in this case) was used to calculate the pH sensitivity. The existence of two slopes is treated in detail in the next paragraph. For $V > 0.4$ V vs. Ag/AgCl it can be seen that inversion has been reached and a quite steady capacitance and thus C^{-2} value has been achieved. V_{fb} has been derived from Figure 4.15 via the Mott Schottky relation (see Equation 4.4b) and for comparison purposes this method is called method 3. The results of all three methods can now be graphically compared in Figure 4.16.

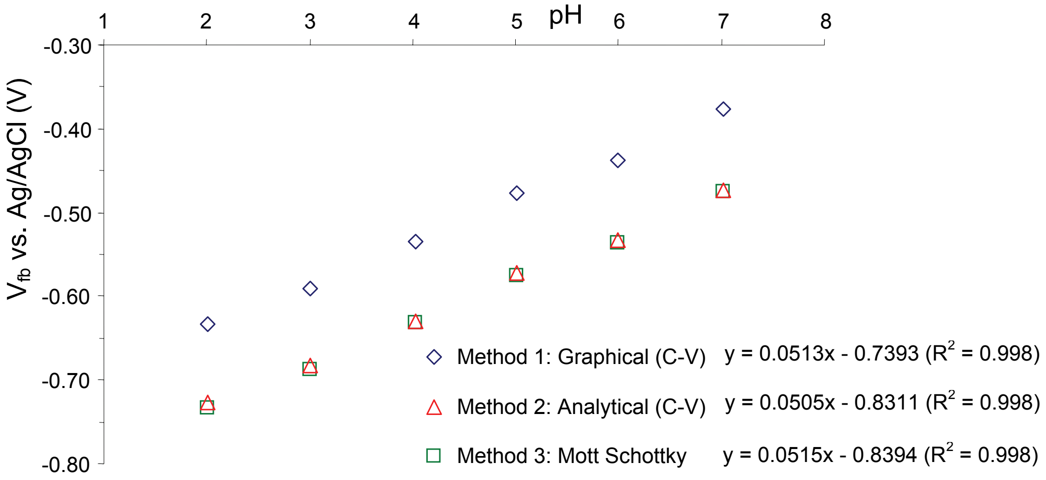

Figure 4.16. The results of the *pH* responses determined via the three methods.

The first clear observation is the remarkable similarity between V_{fb} derived via the analytical *C-V* method and via the Mott Schottky measurements. This is not expected since the oxide insulator is expected to give some shift in the flatband voltage as derived from Mott Schottky measurements. De Grijse et al. [53] investigated the effect of a potential drop over the Helmholtz layer on the derivation of V_{fb} from Mott Schottky plots. It is assumed here for simplicity that a thick insulator will have the same effect, i.e. the potential drops partly over the space charge region and partly over the insulator and consequently V_{fb} will shift. The influence of the Helmholtz capacitance, C_H, is neglected in this case since its value is much larger than C_{ins}. Calculating the correction term according to De Grijse et al. the error in this case in V_{fb} from Mott Schottky measurements is approximately 0.1 V. However, the absolute value of V_{fb} is not of direct interest in this case, since the *pH* sensitivity is needed in these experiments.

The results of the three linear fit functions through the data are listed in Figure 4.16. The fit functions all show the same, high $R^2 = 0.998$, indicating good linear fits. The graphical method and Mott Schottky method give almost the same sensitivity in the *pH* 2 - 7 range, 51.3 ± 1.1 and 51.5 ± 1.1 $mV \cdot pH^{-1}$, respectively. The analytical method via *C-V* analysis revealed a sensitivity of 50.5 ± 1.1 $mV \cdot pH^{-1}$. All methods revealed the same sensitivity within the experimental uncertainties. Therefore, it is concluded that the use of Mott Schottky measurements for deriving *pH* or *pX* sensitivities at EIS-structures with thick insulators is adequate and accurate. Although it can not be verified via methods 1 and 2, the use of the Mott Schottky method is assumed to be also well applicable for analyzing EIS-structures with thin insulators. There are on forehand no reasons or indications why this method should not work on EIS-structures with thin insulators. In the next section this is elaborately discussed.

4.3.2 Analysis of EIS-structures with thin insulators

The focus in this section is on the analysis and the difficulties encountered during this analysis on EIS-structures with thin insulators. An elaborate electrochemical characterization of such EIS-structures and the conclusions drawn from that characterization can be found in Chapter 5. First of all, a suitable impedance model as discussed in the theory section was chosen together with the optimal measurement frequency. The two two-element models are preferred to keep the measurements and analysis quick and simple. After an analysis of the Mott Schottky data of EIS-structures with Si-C linked monolayers via the series (C_s) and parallel (C_p) model it was found that the Mott Schottky plots via both models were similar in shape but the absolute values of V_{fb} derived from them were different. However, the absolute value was not of direct interest. The sensitivities on the other hand were equal for both models. The series model was chosen as most suitable model because it gave the most realistic values for the capacitance in accumulation. Next, the measurement frequency should be determined. A high frequency is favorable to prevent the influence of surface states on the capacitance values. The optimal frequency was chosen to be 10 kHz. Lower frequencies were avoided given the reasons above. Higher frequencies gave rise to errors in the measured capacitance values which are thought to originate from instrumental limitations (see also Appendix B). Therefore all measurements on EIS-structures with thin insulators were performed at a frequency of 10 kHz and analyzed via the series ($C_s - R_s$) model.

Capacitance-Voltage measurements

In Figure 4.17 *C-V* curves are shown for a p-type silicon electrode modified with a C_{22} monolayer, measured at different *pH* values. The shape of these *C-V* curves was typical for most of the tested electrodes with Si-C linked monolayers.

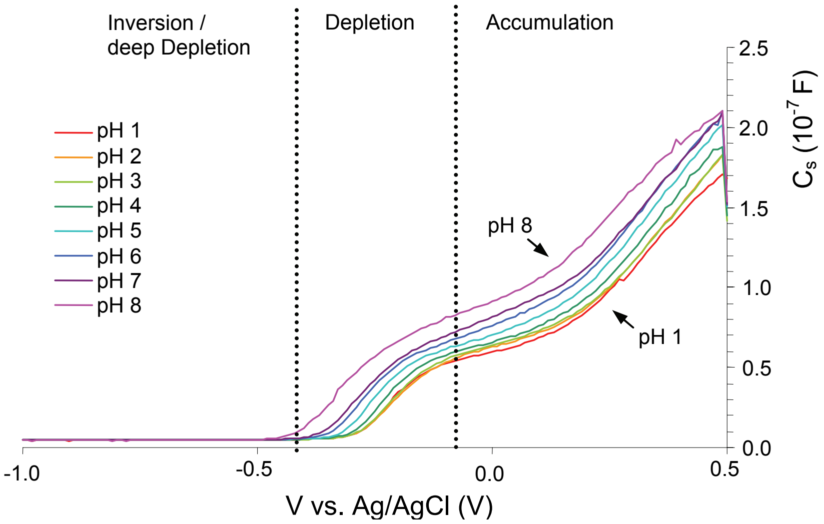

Figure 4.17. Typical high-frequency *C-V* curves (measured at 10 kHz) of p-type silicon electrodes modified with a C_{22} monolayer. The *C-V* plots are shown for up going *pH* values ranging from 1 to 8. The background electrolyte was 0.1 M TetraButylAmmoniumChloride (TBACl) The capacitance values are calculated via a series model (see section 4.2.3 for details).

In Figure 4.17 the three operating regimes of the silicon-electrode are indicated, namely inversion, depletion, and accumulation. The regimes are indicated for the plot made at *pH* 8. It can be seen that the accumulation capacitances do not reach a constant level but increase as a function of bias voltage. At voltages higher than 0.2 - 0.3 V vs. Ag/AgCl an even sharper increase occurs. Such non-constant capacitances were typical for silicon electrodes modified with organic monolayers and consequently a detailed analysis of the insulator properties and silicon-monolayer interface properties could not be carried out. As for the investigation of the *pH* sensitivity it can already be seen in Figure 4.17 that the *C-V* curves shift along the *V*-axis to more negative values for increasing *pH* values.

It was stated before that for a proper determination of the *pH* sensitivity the flatband voltage V_{fb} has to be known. In case of ideal *C-V* curves with constant accumulation capacitances V_{fb} can be determined analytically (method 1) from these plots [2] but this can not be done in this case. Another possibility to estimate the V_{fb} shifts between the curves is to measure graphically the shifts along the *V*-axis between the curves (method 2), provided that the curves are identical irrespective of the *pH* value [5]. There is, however, a trend that the capacitances in accumulation increase for increasing *pH* values. To illustrate this assumption a calculation has been made in Table 4.3.

Table 4.3. Influence of *pH* on the estimation of C_{acc}.

pH	C_{acc} (V = 0 V vs. AgAgCl) [nF]	V_{fb} [V vs. Ag/AgCl]	$\Delta V_{fb} = V_{fb} - V_{fb}$(pH 1 up) [V vs. Ag/AgCl]	C_{acc} ($V = 0 - \Delta V_{fb}$ V vs. Ag/AgCl) [nF]
1 up	59.6	-0.253	0	59.6
3 up	63.9	-0.257	0.004	63.2
5 up	70.4	-0.291	0.038	66.8
7 up	81.5	-0.333	0.078	72.3

Table 4.3 gives an overview of the measured capacitance at a bias voltage in the accumulation regime, in this case 0 V vs. Ag/AgCl for 4 different *pH* values was chosen. It can be seen that C increases indeed for increasing *pH* values. The shift in V_{fb}, however, has not been taken into account and therefore these values can not be compared since at 0 V vs. Ag/AgCl a shifted curve to the left gives already a higher capacitance (see Figure 4.17). Therefore, the amount of shift has been calculated via V_{fb} as determined via Mott Schottky plots. The third column lists V_{fb} and the fourth column lists the shift in V_{fb} with respect to V_{fb} measured at *pH* 1. In the fifth column C_{acc} has been determined again now taking the V_{fb} shift into account. Still, C_{acc} is higher for higher *pH* values and C_{acc} decreases for decreasing *pH* values. The data in Table 4.3 illustrates that the C-V curves for different *pH* values are thus not identical and graphical determination of the *pH* sensitivity is therefore thought to be not correct. The third option to determine (the shifts in) V_{fb} is via the use of Mott Schottky plots, which will be discussed in detail in the next paragraph.

Mott Schottky measurements

Two non-idealities encountered in practice are discussed in this section to decide their influence on interpretation of the derived flatband voltage V_{fb}. This is crucial for the consequent determination of the sensory response from V_{fb}. How to deal with these non-idealities and the consequence on the subsequent derivation of V_{fb} and thus the *pH* sensitivity is discussed.

The first non-ideality encountered is the frequency dependency of the slope of the Mott Schottky plots. A typical example can be found in Figure 4.18.

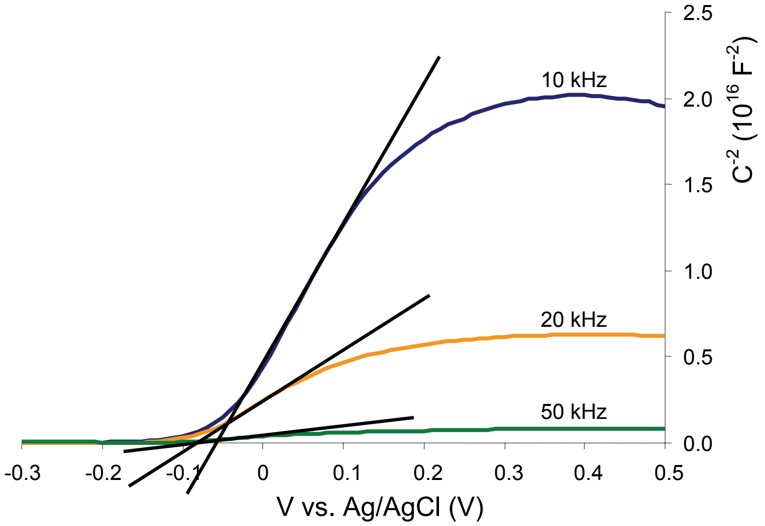

Figure 4.18. Typical example of Mott Schottky plots that exhibit frequency dependency. The sample is a n-type silicon sample covered with a C_{22} monolayer in contact with 0.1M TetraButylAmmoniumChloride (TBACl).

Also frequencies of 5 kHz and 75 kHz were tested and these data fitted in the trend shown in Figure 4.18 indicating the frequency dependence was present over a large frequency range. It is also shown that the frequency dependency is of such a nature that both the doping and V_{fb} can not be properly derived, since both the slopes and the V-axis intercepts are frequency dependent. In literature two types of frequency dependency are known, one in which the slopes are frequency dependent but all converge to a single point on the V-axis and one in which both the slopes and V-axis intercept are frequency dependent [31, 44] as in this case. It is thus impossible to find the absolute value of V_{fb}. This does not have to be a problem since we are interested in the sensory response of the EIS-structures and the absolute value of V_{fb} is not of direct interest. If the effects that cause the deviations remain constant at one frequency during all the experiments on one sample, relative measurements can be used to find the sensory response. It has thus to be decided that the encountered deviation is indeed independent of the different experimental conditions the sample is exposed to. Most experiments are *pH* titrations in which thus the *pH* and maybe the total ionic strength of the analyte will be changed. Since V_{fb} of all tested samples is expected to change with *pH*, the criterion for proper measurements will be related to the slope of the plots. If the slope of the Mott Schottky plots is constant during the titrations at a given frequency the measurements are said to be right for determining the response. This is supported by the fact that to our best knowledge nothing is reported in literature on the correlation between the frequency dependency of the slope and the *pH* of the solution. If the ionic strength, on the other hand, changes to such a degree that it will change C_{dl} one has to be careful because in literature a relation has been found between ionic strength, and thus C_{dl}, and the frequency dependency of the Mott Schottky slopes [44]. Therefore it is tried to keep the ionic strength at all times constant.

Figure 4.19 gives the typical Mott Schottky plots of a p-Si sample modified with 1-docosene ($C_{22}H_{45}$) at 6 *pH* points ranging from *pH* 2 through 7.

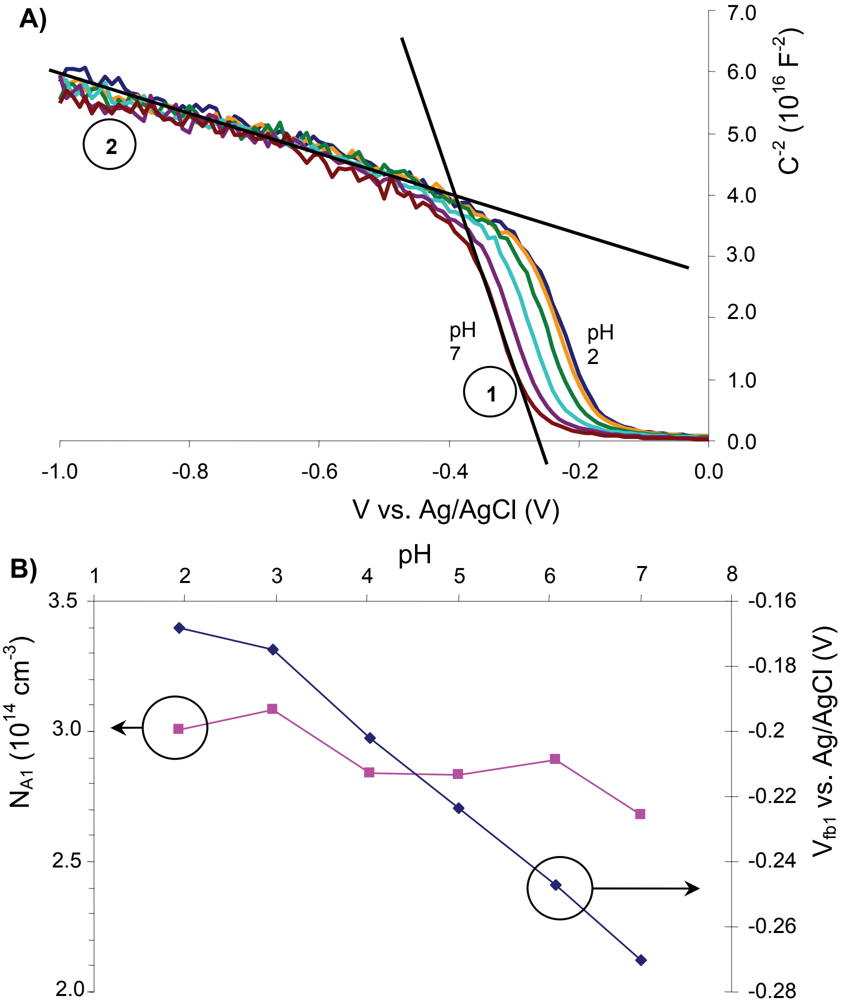

Figure 4.19. A) Mott Schottky plots of a p-type silicon sample with C_{22} monolayer as insulator in contact with 0.1 M TBACl for *pH* values from 2 through 7 and (B) the derived doping and flatband voltage vs. *pH*.

Figure 4.19A gives a typical example of Mott Schottky plots on p-type silicon encountered in this project. It can be seen that in the Mott Schottky plots two slopes can be distinguished. This is in fact the second non-ideality. On forehand, it can be said that only the right-hand slopes (slope 1) seem to shift with *pH* and the left-hand slopes (slope 2) seem to show no sensitivity at all towards *pH*. In case of EIS-structures with thick insulators the Mott Schottky plots went to constant values (see Figure 4.15) indicating that the electrodes operated in the inversion. The presence of slope 2 over such large voltage range at EIS-structures with thin insulators indicates that such electrodes do not reach inversion but in fact go into deep depletion. Such situation can occur if all minority charges generated at the electrode surface are directly carried away (e.g. via direct tunneling over the monolayer) and thus an inversion situation does not occur. Figure 4.19B shows both the doping N_A and V_{fb} derived from slope 1 as a function of *pH*. It can be seen that there is no direct correlation between N_A and the *pH*. The difference between the highest and the lowest found N_A is 13%. Other samples in general showed even smaller differences, so these differences are thought to have random causes. Furthermore, the V_{fb} vs. *pH* values seem to be reasonable on first hand. The sensitivity in the *pH* 4 – 7 region is approximately -23 mV per *pH*, which is less than commonly found for SiO_2 [16]. Since the surface is covered with an organic monolayer, it is expected that very few SiO_2 islands or Si-OH sites are present resulting in a reduced *pH* sensitivity as compared to bare SiO_2. This aspect is treated in depth in Chapter 5, in which the measured sensitivity data is also compared with simulations.

Since the slope of the Mott Schottky plots, derived from single frequency measurements, shows no or negligible correlation with the parameter of interest, *pH* in this case, it is concluded that differential measurements of V_{fb} can be done to find the right response of the samples.

The second non-ideality encountered is visible in Figure 4.19A. Two slopes appear in the Mott Schottky plots. This phenomenon was always encountered for electrodes made from p-type <100> silicon wafers. Electrodes made from n-type <100> silicon wafers did not show this effect to such a large degree.

N_A and V_{fb} derived from slopes of type 1 are already depicted in Figure 4.19B. N_A and V_{fb} derived via the slopes of type 2 can be found in Figure 4.20. These values are called N_{A2} and V_{fb2}.

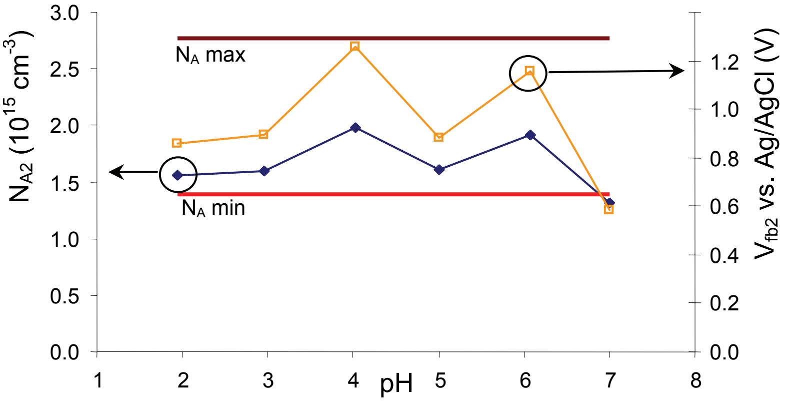

Figure 4.20. N_{A2} and V_{fb2} vs. *pH* as derived from slope 2 in Figure 4.19A.

The first thing noticed is that V_{fb2} is in no way related to the *pH*. On the other hand are the derived doping values in accordance with the specifications of the wafer supplier (indicated with solid lines). The doping values derived from the slope 1 are far too low (Figure 4.19B). In section 4.2.2 one type of non-ideality is described that can lead to more slopes in Mott Schottky plots, namely the presence of deep-lying localized levels. For high-quality silicon wafers it is, however, not expected that this effect can occur. An alternative is that the surface silicon layer contains less doping impurities, say N_{A1} than the bulk layer with doping N_{A2}, so $N_{A1} < N_{A2}$. As the voltage becomes more negative, the depletion layer becomes thicker. At first only the surface region with doping N_{A1} gets depleted, resulting in the right-hand slopes. At a certain voltage the depletion layer enters the bulk zone. This was described as the deep depletion situation in Figure 4.19A. From that point the bulk effect starts dominating the Mott Schottky relation and this results in a less steep slope corresponding with N_{A2}. It can not be ruled out that surface states also have an effect on the shape of the plots, but to our best knowledge no examples exist in literature where such double slopes are caused due to surface states.

In summary, the proper doping should be derived from slope 2, since this region is associated with a homogenously doped bulk layer; to investigate the sensory response of the sample slope 1 should be used to derive V_{fb} since only these slopes respond to pH changes. It is most likely that this is not the correct, absolute V_{fb} but as long as it concerns relative measurements the proper sensory response can be found.

4.4 Conclusions

This chapter showed an overview of theoretical and practical considerations on Mott Schottky measurements for use in the characterization of the sensory responses of EIS-structures with thin insulators. In EIS-structures the sensory response is measured via a change of the so-called flatband potential V_{fb} upon a change in stimulus, such as pH. In most cases relative measurements are concerned, so not the absolute value of V_{fb} is of interest, but instead ΔV_{fb}. Three methods were mentioned for determining the pH sensitivity at EIS-structures. Two of them involve the C-V curves as starting point, namely a graphical method in which upon pH changes the shifts of the C-V curves along the V-axis are measured and the second one involves an analytical determination of V_{fb} from ideal C-V curves. However, in case of nm-thin insulators C-V curves are often distorted, thereby making it impossible to derive the sensory response via the two mentioned methods. A third method, Mott Schottky measurements, was proposed as an alternative to derive the sensory response. The three methods have been tested on ideally behaving EIS-structures with thick insulators. The resulting pH sensitivity was similar for all three methods, indicating the validity of all three methods. Since there were on forehand no reasons or indications why this Mott Schottky method should not work on EIS-structures with thin insulators, it was decided that the sensitivities of EIS-structures with thin insulators could be properly analyzed via this method.

Also discussed were the non-idealities encountered during Mott Schottky measurements on EIS-structures of p-type silicon with nm-thin insulators, such as organic monolayers. The first non-ideality concerned frequency dependency of the slopes and V-axis intercepts. This made it impossible to derive the absolute value of V_{fb}. The second non-ideality concerned double slopes in the Mott Schottky plots giving rise to two possible flatband voltages and two possible doping values. When the silicon entered depletion a very steep slope (slope 1) appeared over a small voltage regime of approximately 0.1 V. When the silicon got further depleted the slope became less steep and this continued over a very large voltage range (slope 2) that was associated with a deep depletion situation of the electrode. Via slope 2 the proper doping values could be derived but V_{fb} derived from this slope was insensitive and not related to different analytes. From slope 1, on the other hand, V_{fb} showed a clear and realistic dependence on the different analytes. Since the region of slope 1 can be associated with the surface region of the silicon electrode it is expected to be the most sensitive to changes in *pH* and it is thus plausible to use this region as basis for the calculation of the sensitivities. On the other hand the doping derived from slope 1 was far too low but nonetheless constant during all experiments.

It is concluded that Mott Schottky measurements provide a good tool for investigating the *pH* responses at EIS-structures with thin insulators. The non-idealities are constant at single frequency measurements and not sensitive towards different analytes and therefore the proper sensory response can still be derived via slope 1 from relative measurements. Via slope 2 the doping can be derived as a routine check.

4.5 Experimental

The experiments described in this chapter have been worked out in detail in Chapter 5. Also the experimental details can be found in that chapter.

4.6 References

[1] S. M. Sze, *Semiconductor Devices: Physics and Technology*, Wiley, New York, **1985**.

[2] D. K. Schroder, *Semiconductor Material and Device Characterization*, 2nd ed., Wiley, New York, **1998**.

[3] S. R. Morrison, *Electrochemistry at Semiconductor and Oxidized Metal Electrodes*, Plenum Press, New York, **1980**.

[4] X. G. Zhang, *Electrochemistry of Silicon and its Oxide*, Kluwer Academic Publishers, New York, **2001**.

[5] P. Bergveld, A. Sibbald, *Analytical and Biomedical Applications of Ion-Selective Field-Effect Transistors, Vol. XXIII*, Elsevier, **1988**.

[6] P. Bergveld, "Development of an Ion-Sensitive Solid-State Device for Neurophysiological Measurements", *IEEE Transactions on Biomedical Engineering* **1970**, *BME-17*, 70.

[7] P. Bergveld, "Development, Operation, and Application of the Ion-Sensitive Field-Effect Transistor as a Tool for Electrophysiology", *IEEE Transactions on Biomedical Engineering* **1972**, *BME-19*, 342.

[8] A. v. d. Berg, *Ion Sensors based on ISFETs with Synthetic Ionophores*, PhD thesis, University of Twente (Enschede), **1988**.

[9] P. v. d. Wal, *The Development of a Durable Potassium Sensor based on FET-Technology*, PhD thesis, University of Twente (Enschede), **1991**.

[10] J. A. J. Brunink, *Sodium-selective CHEMFETs*, PhD thesis, University of Twente (Enschede), **1993**.

[11] W. P. R. V. Stauthamer, *Anion-sensitive CHEMFETs*, PhD thesis, University of Twente (Enschede), **1994**.

[12] J. L. Diot, J. Joseph, J. R. Martin, P. Clechet, "pH dependence of the Si/SiO2 interface state density for EOS systems : Quasi-static and AC conductance methods", *Journal of Electroanalytical Chemistry* **1985**, *193*, 75.

[13] D. E. Yates, S. Levine, T. W. Healy, "Site-binding model of the electrical double layer at the oxide/water interface", *Journal of the Chemical Society, Faraday Transactions 1* **1974**, *70*, 1807.

[14] L. Bousse, *The Chemical Sensitivity of Electrolyte/Insulator/Silicon Structures: Fundamentals of ISFET Operation*, PhD thesis, Universtity of Twente (Enschede), **1982**.

[15] R. E. G. van Hal, J. C. T. Eijkel, P. Bergveld, "A novel description of ISFET sensitivity with the buffer capacity and double-layer capacitance as key parameters", *Sensors and Actuators B: Chemical* **1995**, *24*, 201.

[16] R. E. G. van Hal, J. C. T. Eijkel, P. Bergveld, "A general model to describe the electrostatic potential at electrolyte oxide interfaces", *Advances in Colloid and Interface Science* **1996**, *69*, 31.

[17] E. J. Faber, L. C. P. M. de Smet, W. Olthuis, H. Zuilhof, E. J. R. Sudhölter, P. Bergveld, A. van den Berg, "Si-C Linked Organic Monolayers on Crystalline Silicon Surfaces as Alternative Gate Insulators", *ChemPhysChem* **2005**, *6*, 2153.

[18] Q.-Y. Sun, L. C. P. M. d. Smet, B. v. Lagen, M. Giesbers, P. C. Thüne, F. A. Wolf, H. Zuilhof, E. J. R. Sudhölter, "Covalently Attached Monolayers on Crystalline Hydrogen-Terminated Silicon: Extremely Mild Attachment by Visible Light", *Journal of the American Chemical Society* **2005**, *127*, 2514.

[19] S. Kar, C. Miramond, D. Vuillaume, "Properties of electronic traps at silicon/1-octadecene interfaces", *Applied Physics Letters* **2001**, *78*, 1288.

[20] Y. J. Liu, H. Z. Yu, "Molecular passivation of mercury-silicon (p-type) diode junctions: Alkylation, oxidation, and alkylsilation", *Journal of Physical Chemistry B* **2003**, *107*, 7803.

[21] L. C. P. M. de Smet, *Covalently Bound Organic Monolayers on Silicon Surfaces: Visible Light Attachment, Characterization and Electrical Properties*, PhD thesis, Wageningen University (Wageningen), **2006**, chapter 5, p. 67.

[22] K. G. Marinova, R. G. Alargova, N. D. Denkov, O. D. Velev, D. N. Petsev, I. B. Ivanov, R. P. Borwankar, "Charging of oil-water interfaces due to spontaneous adsorption of hydroxyl ions", *Langmuir* **1996**, *12*, 2045.

[23] H. J. Kreuzer, R. L. C. Wang, M. Grunze, "Hydroxide ion adsorption on self-assembled monolayers", *Journal of the American Chemical Society* **2003**, *125*, 8384.

[24] Y. H. M. Chan, R. Schweiss, C. Werner, M. Grunze, "Electrokinetic characterization of oligo- and poly(ethylene glycol)-terminated self-assembled monolayers on gold and glass surfaces", *Langmuir* **2003**, *19*, 7380.

[25] R. Schweiss, P. B. Welzel, C. Werner, W. Knoll, "Dissociation of surface functional groups and preferential adsorption of ions on self-assembled monolayers assessed by streaming potential and streaming current measurements", *Langmuir* **2001**, *17*, 4304.

[26] L. Bousse, P. Bergveld, "On the impedance of the silicon dioxide/electrolyte interface", *Journal of Electroanalytical Chemistry* **1983**, *152*, 25.

[27] A. B. Sieval, A. L. Demirel, J. W. M. Nissink, M. R. Linford, J. H. van der Maas, W. H. de Jeu, H. Zuilhof, E. J. R. Sudhölter, "Highly stable Si-C linked functionalized monolayers on the silicon (100) surface", *Langmuir* **1998**, *14*, 1759.

[28] A. B. Sieval, B. van den Hout, H. Zuilhof, E. J. R. Sudhölter, "Molecular Modeling of Alkyl Monolayers on the Si(111) Surface", *Langmuir* **2000**, *16*, 2987.

[29] A. B. Sieval, B. van den Hout, H. Zuilhof, E. J. R. Sudhölter, "Molecular Modeling of Covalently Attached Alkyl Monolayers on the Hydrogen-Terminated Si(111) Surface", *Langmuir* **2001**, *17*, 2172.

[30] A. B. Sieval, *Covalently Bound Organic Monolayers on Hydrogen-Terminated Silicon Surfaces*, PhD thesis, Wageningen University (Wageningen), **2001**, chapter 3, p. 44.

[31] W. P. Gomes, F. Cardon, "Electron energy levels in semiconductor electrochemistry", *Progress in Surface Science* **1982**, *12*, 155.

[32] J.-N. Chazalviel, "Electrochemical Transfer via Surface States: A New Formulation for the Semiconductor/Electrolyte Interface", *Journal of the Electrochemical Society* **1982**, *129*, 963.

[33] H. Gerischer, "The role of semiconductor structure and surface properties in photoelectrochemical processes", *Journal of Electroanalytical Chemistry* **1983**, *150*, 553.

[34] H. Gerischer, "The impact of semiconductors on the concepts of electrochemistry", *Electrochimica Acta* **1990**, *35*, 1677.

[35] Z. Hens, "The electrochemical impedance of one-equivalent electrode processes at dark semiconductor vertical bar redox electrodes involving charge transfer through surface states. 1. Theory", *Journal of Physical Chemistry B* **1999**, *103*, 122.

[36] P. M. Hoffmann, G. Oskam, P. C. Searson, "Analysis of the impedance response due to surface states at the semiconductor/solution interface", *Journal of Applied Physics* **1998**, *83*, 4309.

[37] M. J. Madou, B. H. Loo, K. W. Frese, S. R. Morrison, "Bulk and surface characterization of the silicon electrode", *Surface Science* **1981**, *108*, 135.

[38] A. Natarajan, G. Oskam, P. C. Searson, "The potential distribution at the semiconductor/solution interface", *Journal of Physical Chemistry B* **1998**, *102*, 7793.

[39] G. Oskam, P. M. Hoffmann, P. C. Searson, "*In Situ* Measurements of Interface States at Silicon Surfaces in Fluoride Solutions", *Physical Review Letters* **1996**, *76*, 1521.

[40] D. Vanmaekelbergh, A. R. Dewit, F. Cardon, "Recombination in Semiconductor Electrodes - Investigation by the Electrical and Optoelectrical Impedance Method", *Journal of Applied Physics* **1993**, *73*, 5049.

[41] A. J. Bard, A. B. Bocarsly, F.-R. F. Fan, E. G. Walton, M. S. Wrighton, "The Concept of Fermi Level Pinning at Semiconductor/Liquid Junctions. Consequences for Energy Conversion Efficiency and Selection of Useful Solution Redox Couples in Solar Devices", *Journal of the American Chemical Society* **1980**, *102*, 3671.

[42] J.-N. Chazalviel, T. B. Truong, "An Experimental Study of the n-Si/Acetonitrile Interface: Fermi Level Pinning and Surface States Investigation", *Journal of the American Chemical Society* **1981**, *103*, 7447.

[43] J.-N. Chazalviel, "Schottky barrier height and reverse current of the n-Si-electrolyte junction", *Surface Science* **1979**, *88*, 204.

[44] G. Oskam, D. Vanmaekelbergh, J. J. Kelly, "A reappraisal of the frequency dependence of the impedance of semiconductor electrodes", *Journal of Electroanalytical Chemistry* **1991**, *315*, 65.

[45] J. H. Kennedy, K. W. Frese, "Flatband Potentials and Donor Densities of Polycrystalline α-Fe_2O_3 Determined from Mott-Schottky plots", *Journal of the Electrochemical Society* **1978**, *125*, 723.

[46] J. D. Plummer, M. D. Deal, G. P.B., *Silicon VLSI Technology, Fundamentals, Practice and Modeling*, Prentice Hall, New Yersey, **2000**.

[47] A. J. Bard, L. R. Faulkner, *Electrochemical Methods, Fundamentals and Applications*, John Wiley & Sons, **1980**.

[48] G. Oskam, J. C. Schmidt, P. C. Searson, "Electrical Properties of n-Type (III) Si in Aqueous $K_4Fe(CN)_6$ Solution", *Journal of The Electrochemical Society* **1996**, *143*, 2538.

[49] H. Z. Yu, S. Morin, D. D. M. Wayner, P. Allongue, C. H. de Villeneuve, "Molecularly tunable "organic capacitors" at silicon/aqueous electrolyte interfaces", *Journal of Physical Chemistry B* **2000**, *104*, 11157.

[50] P. Allongue, C. H. de Villeneuve, J. Pinson, "Structural characterization of organic monolayers on Si < 111 > from capacitance measurements", *Electrochimica Acta* **2000**, *45*, 3241.

[51] J. W. Nilsson, S. A. Riedel, *Electric Circuits*, sixth ed., Prentice-Hall, New Jersey, **2000**.

[52] B. A. Boukamp, "A Nonlinear Least Squares Fit procedure for analysis of immittance data of electrochemical systems", *Solid State Ionics* **1986**, *20*, 31.

[53] R. De Gryse, W. P. Gomes, F. Cardon, J. Vennik, "On the Interpretation of Mott-Schottky Plots Determined at Semiconductor/Electrolyte Systems", *Journal of the Electrochemical Society* **1975**, *122*, 711.

[54] K. Uosaki, H. Kita, "Effects of the Helmholtz Layer Capacitance on the Potential Distribution at Semiconductor/Electrolyte Interface and the Linearity of the Mott-Schottky plot", *Journal of the Electrochemical Society* **1983**, *130*, 895.

[55] W. Smit, "Application of a Modified Colloid Chemical Site Binding Model to Mott-Schottky Plots Determined at Oxidic Semiconductor/Electrolyte Systems", *Journal of the Electrochemical Society* **1985**, *132*, 2172.

[56] see internet: "http://www.icknowledge.com/misc_technology/Highkgates.pdf"

[57] J. Ross Macdonald, "Note on the parameterization of the constant-phase admittance element", *Solid State Ionics* **1984**, *13*, 147.

[58] C. S. Hsu, F. Mansfeld, "Concerning the conversion of the Constant Phase Element Parameter Y0 into a Capacitance", *Corrosion* **2001**, *57*, 747.

[59] W. H. Mulder, J. H. Sluyters, T. Pajkossy, L. Nyikos, "Tafel current at fractal electrodes : Connection with admittance spectra", *Journal of Electroanalytical Chemistry* **1990**, *285*, 103.

[60] C.-H. Kim, S.-I. Pyun, J.-H. Kim, "An investigation of the capacitance dispersion on the fractal carbon electrode with edge and basal orientations", *Electrochimica Acta* **2003**, *48*, 3455.

[61] C. A. Schiller, W. Strunz, "The evaluation of experimental dielectric data of barrier coatings by means of different models", *Electrochimica Acta* **2001**, *46*, 3619.

[62] J.-B. Jorcin, M. E. Orazem, N. Pebere, B. Tribollet, "CPE analysis by local electrochemical impedance spectroscopy", *Electrochimica Acta*, *In Press, Corrected Proof.*

[63] J. Ross Macdonald, *Impedance Spectroscopy, Emphasizing Solid Materials and Systems*, John Wiley & Sons, **1987**.

Appendix A

Modeling frequency dependency: constant phase elements

In real world electrochemical experiments frequency dependency of the impedance parameters was often observed. In section 4.2.2 it was stated that both the double layer capacitance C_{dl} in the electrolyte and the space charge layer C_{sc} in the semiconductor can show such frequency dependency. Instead of modeling such behavior wrongly via a pure *C*, it can better be modeled via a constant phase element (CPE). The general admittance expression of a CPE [52, 57] is given via Equation 4A.1:

$$Y(\omega) = Y_0(j\omega)^n = Y_0\omega^n(\cos(n\pi/2) + j\sin(n\pi/2)) \tag{4A.1}$$

It must be noted that this is in fact the most general expression of any basic circuit element. All other elements, like *R*, *C*, *L*, and *W*, can be derived from it, as illustrated in Table 4A.1.

Table 4A.1. Special cases of the general admittance expression.

n	Basic element	Y_0
1	Capacitance	*C*
0.5	Warburg	*W*
0	Resistance	R^{-1}
-1	Inductance	L^{-1}

Equation 4A.1 shows that the CPE, general circuit notation *Q*, has a numerical value of the admittance Y_0 in $S\cdot s^n$ or $\Omega^{-1}\cdot s^n$. The phase angle is constant and has a value of -90·*n*°. For instance a value of $n = 0.89$ leads to a constant phase angle of -80°. In contrast to an element like *C* or *R*, a CPE has 2 parameters: *n* and Y_0. In a Nyquist plot a CPE can simply be visualized via a straight line that makes an angle of -90·*n*° with the Real axis (see Figure 4A.1A). One frequently encountered model is a *Q* in parallel to *R*. This is namely an alternative for $C_{dl} - R_{ct}$ parallel branch in Figure 4.9. If C_{dl} suffers from frequency dependency it may be better described by a CPE. As stated before this is not only a phenomenon seen at semiconductor electrodes but also at metal electrodes. Figure 4A.1B shows the Nyquist diagram of both a *C*-*R* parallel model and a *Q*-*R* parallel model.

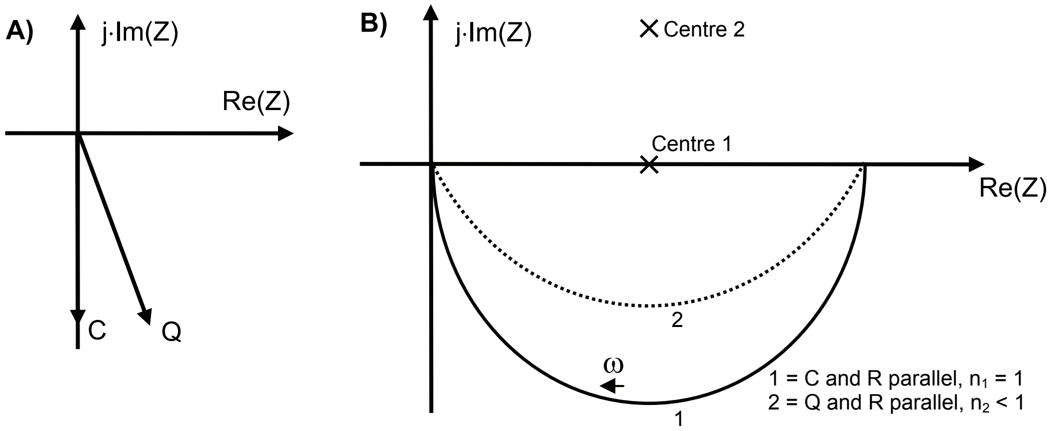

Figure 4A.1. A) Nyquist plots of a pure capacitor and a CPE. In B) the Nyquist plots of a parallel connection of a *C* and *R* and *Q* and *R* are given.

The plot of the *C*-*R* model in Figure 4A.1B is the well-known semi-circle. The centre of the circle is situated on the real axis; *R* can be derived from the point where the right side of the circle reaches the real axis and *C* can be derived from the lowest point of the circle. At this point the frequency is: $\omega_{min} = (RC)^{-1}$. The plots of the *Q*-*R* model are still semi-circles but they are depressed, i.e. the centre is now located not on the real-axis but above it. For decreasing *n*, this centre also shifts further away from the real axis. Only for the case of a *Q*-*R* parallel model a capacitance *C* can be associated with *Q*. At the lowest point of the circle the relation is [58]: $C = Y_0(\omega_{min})^{n-1}$.

As mentioned before in section 4.2.2 surface roughness is thought to be one of the dominant causes of frequency dependent impedance parameters at metal-electrolyte and semiconductor-electrolyte systems. In [59] the surface roughness is linked to CPE behavior. The higher the surface roughness, the more CPE behavior ($n < 1$) was observed. A second cause can be a distribution of reaction rates. This can be seen at polycrystalline metal surfaces or carbon electrodes with a distribution of active sites with varying activation energies on the surface. In [60] it is shown that for a glassy carbon electrode, the CPE exponent correlates with the fraction of exposed edge plane orientation, not with the fractal dimension of the surface. A third cause can be a varying thickness of composition. This was observed at coatings on steel for which CPE behavior was found if the bulk conductivity of the coating changed with distance through the coating [61]. Finally, a non-uniform current distribution can be the cause of CPE behavior. In [62] both local and global impedances were measured at Mg-alloy electrodes in dilute Na_2SO_4. The best fit for the global impedance gave a CPE with $n = 0.91$. For the local impedances, measured with a sub-mm current probe, the CPE values varied from $n = 1.0$ near the centre to $n = 0.83$ at the edges of the sample. This indicated that edge-effects play also a role in the origin of CPEs. Finally, in [63] it is mentioned that, although a particular theory may not give exactly CPE behavior, very often CPE behavior will fit experimental data so well, that deviations are totally masked by experimental noise and uncertainties. So even if the true nature of the system is unknown, CPEs can provide useful modeling elements.

Appendix B

Instrumental demands

In section 4.2.3 different models for data fitting were discussed. Besides choosing a model one should also choose a good measurement frequency. Although this choice is partly based on the chosen model, also the instrument specifications play a role in choosing the proper measurement frequency. There is a trade-off between high and low frequencies.

At high frequencies the advantage is that the measurement results solely contain information of site binding reactions at the insulator-electrolyte interface and not of surface states and polarizing or diffusion effects in the insulator. The disadvantage is that the demands on the impedance analyzer become severe, because the needed phase accuracy increases for increasing frequency.

For low frequencies the advantage is that the demands on the impedance analyzer are less severe. The disadvantage is that all sorts of unwanted charges and charging processes (as mentioned above for the advantage of high frequencies) are measured that obscure the parameter that is to be measured.

Since in most cases in this project a series model of capacitor and resistor is chosen for data fitting of the Mott Schottky measurements, the concept of phase accuracy is illustrated via this model. The absolute value of the impedance of this model is:

$$|Z| = \sqrt{R_{series}^2 + \frac{1}{(\omega C)^2}} \qquad (4B.1a)$$

And the phase angle is:

$$\varphi = -\arctan\left(\frac{1}{\omega R_{series} C}\right) \qquad (4B.1b)$$

For low frequencies the term $(\omega C)^{-2}$ dominates $|Z|$ and $|Z|$ will decrease approximately a factor of 10 per tenfold increase in frequency. In this regime φ is approximately -90°. For high frequencies the impedance of the capacitor will be negligible and $|Z|$ will be approximately equal to R_{series} and $\varphi \approx 0°$. In section 4.2.3 it was stated that a high measurement frequency was preferred for accurate use of the series model. At very high frequencies the impedance, however, is almost equal to R_{series} and $\varphi \approx 0°$. Alternatively, a graphical plot of the complex impedance of the series model, $Z = R_{series} - j(\omega C)^{-1}$, shows that the vector is very close to the real axis (see Figure 4B.1).

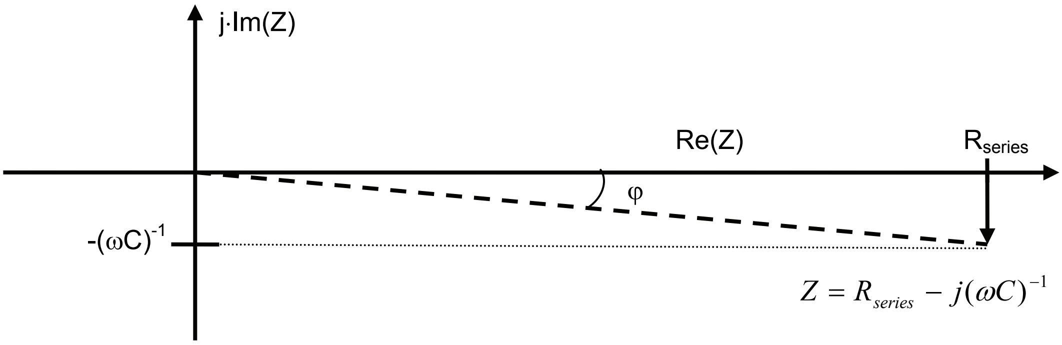

Figure 4B.1. The influence of the resistance (R_{series}), the capacitance (C) and the angular frequency (ω) on the phase angle. Increasing R_{series}, C, and ω all bring the vector closer to the real axis.

If the vector is so close to the real axis that any instrumental phase inaccuracy or noise may cause the vector to jump to the quadrant with positive imaginary axis, this results in a negative value for the fitted C parameter and hence an erroneous analysis. Such negative C indicates then in fact inductive behavior. For most impedance analyzers phase accuracy is in the order of few tens or hundreds of a degree but such values for the phase angle can be reached when measuring at very high frequencies. Equation 4B.1b shows that φ will approach the real axis for increasing frequency, increasing capacitance and increasing resistance. This clearly states again that the series resistance R_{series} should always be kept as low as possible (good back contact, not too lowly doped silicon and well conducting electrolyte). When measuring with the semiconductor in depletion, C can be substituted by the space charge capacitance C_{sc}. Since this is in general a fairly small capacitance φ will be not too small and normal measurements can be done. If the semiconductor is operated in the accumulation regime, however, C should be substituted by C_{ins} or the series capacitance of C_{ins} and C_{dl}. Since C_{ins} is large for thin insulators, phase problems can easily occur in these regimes. Lowering the measurement frequency or series resistance are the solutions.

Another technical reason why unstable or unexpected measurements can be obtained is the high impedance of the reference electrode at high frequencies. Beyond a certain frequency the RC time of the reference electrode and parasitic capacitances in the potentiostat become too large. The consequence is that the measurement becomes unstable and, therefore, unreliable results are obtained. These can be overcome by inserting a second platinum electrode, in the electrolyte, close to the reference electrode and connecting it via a large capacitor to the reference electrode. This change in measurement configuration will (when choosing a proper capacitor) cause low frequency signals to be measured via the reference electrode and high frequency signals to bypass the reference electrode via the secondary platinum electrode.

Appendix C

Back contact impedances

Low impedance, preferably low Ohmic, back contact is crucial for proper characterization of MIS- and EIS-structures (see also Figure 4.9). Impedance measurements, such as *C-V* measurements and Mott Schottky measurements, suffer greatly from poor contacts and such contacts can dominate the total impedance of MIS- or EIS-structures. Three types of back contacts have been tested to verify which one gives the optimal result. The first type is an annealed aluminum (Al) back contact, made via cleanroom techniques. From solid state semiconductor and IC research it is known that this gives a good Ohmic contact to p-type silicon [46]. The second type is a back contact made from a Gallium Indium (GaIn) eutectic. This eutectic is commercially available and is in the liquid phase at room temperature and therefore easy to apply to the semiconductor. It is widely used in semiconductor electrochemistry because if gives reasonably good Ohmic contacts at very few costs, both financially and practically. It is a good alternative if cleanroom made contacts are not available or can not be applied. The third contact is contacting the silicon directly via the contact wire. After cleaning the sample, the backside was only scratched with a diamond pen to remove some of the native oxide. It is expected that this gives a very poor contact. All samples were made from moderately doped (ρ = 5-10 $\Omega\cdot$cm) p-type <100> wafers, sawed in pieces of 10 mm x 10 mm. First *C-V* measurements were performed to check the sample capacitive and resistive behavior at a certain frequency under different bias conditions. These measurements also revealed when the silicon operated in the accumulation regime. In this regime the semiconductor space charge layer does not play a role and one can look solely at the back contact impedance. Therefore impedance measurements were done afterwards with the silicon in accumulation to investigate the frequency behavior of the back contacts, i.e. if they are Ohmic or not for all frequencies.

In Figure 4C.1 the $C_s - V$ and $R_s - V$ plots are depicted. The *C-V* data was fitted with a series model since this series resistance (or impedance) was the parameter of interest in this case.

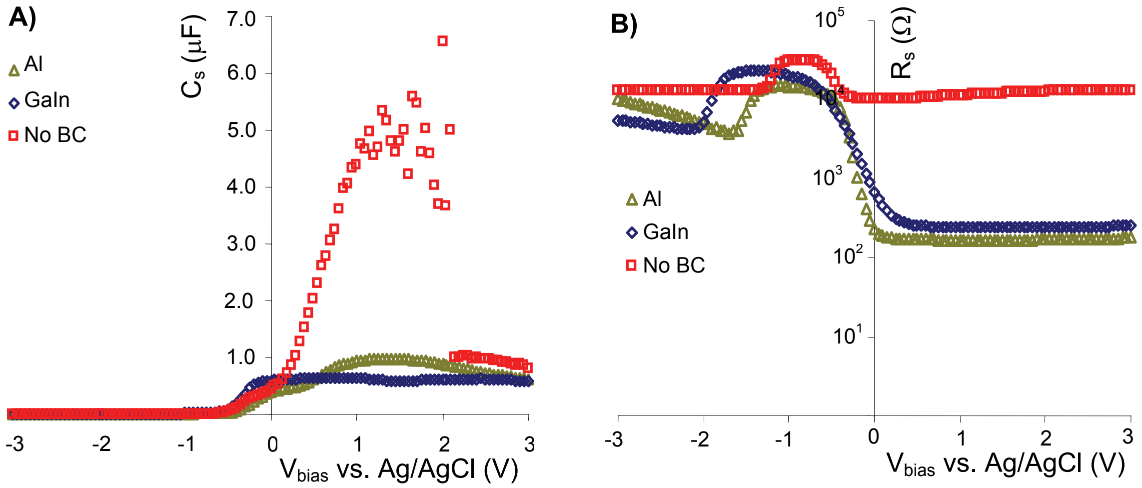

Figure 4C.1. A) $C_s - V$ and B) $R_s - V$ plots of samples with native oxide insulators and different back contacts. The measurement frequency was 1 kHz.

The *C-V* plots are not very illustrative for the back contact impedance. They provide, however, information where the accumulation regime is. For voltages more negative than -0.5 V it can be seen that the capacitance is very small, indicating depletion and inversion regimes. The voltages more positive than -0.5 V can thus be used for the impedance measurements since they are in the accumulation regime. The sample with no back contact gives a very distorted accumulation capacitance, as compared to the other two samples. Since the structure of all samples (bulk silicon and insulator) is expected to be equal, this distortion can be attributed to a very high back contact impedance. The $R_s - V$ plots give more detailed information on the back contact impedance. For $V_{bias} > 0$ V vs. Ag/AgCl R_s seems to be independent of bias voltage, indicating that in that region the real part of the impedance Re(Z) equals the series resistance. The lowest R_s is obtained via the Al back contact: $R_s \approx 170$ **Ω** ($V_{bias} = 1.0$ V vs. Ag/AgCl); the GaIn contact gives a resistance in the same order of magnitude: $R_s \approx 250$ **Ω**; measuring with no back contact results, however, in a very high resistance, as was expected: $R_s \approx 12.0$ k**Ω**. These values are measured at one frequency, so it can not be sure if a pure resistance is measured.

Therefore, impedance measurements were performed using a frequency sweep from 1 MHz to 0.1 Hz at $V_{bias} = 1$ V vs. Ag/AgCl. The results are given in Figure 4C.2.

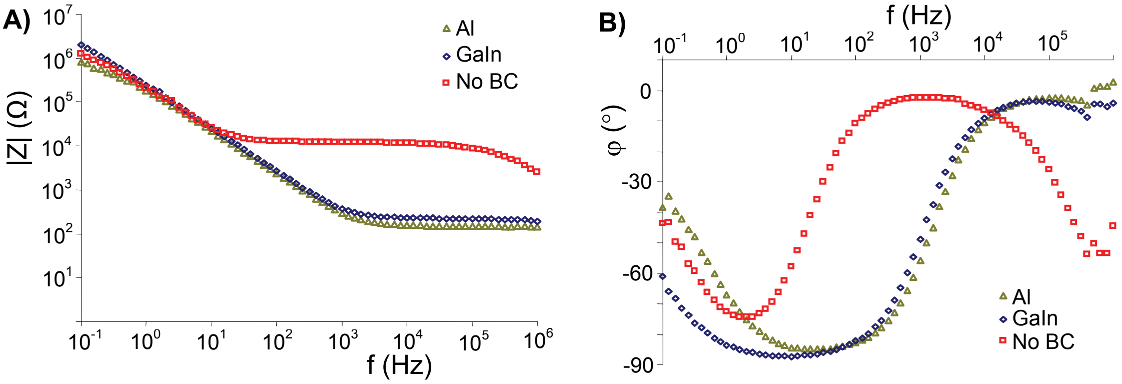

Figure 4C.2. Bode plots: A) |Z| vs. frequency and B) φ vs. frequency of samples with native oxide insulators and different back contacts.

Figure 4C.2A displays capacitive behavior for all samples at low frequencies and consequently a constant plateau arises, which can be associated with the series resistance of the sample. The samples with Al and GaIn contacts have almost identical Bode plots, albeit that the resistive plateau of the sample with GaIn contact is slightly higher. The sample with no back contact shows again a much higher resistance. The formation of a plateau over a broad frequency band also indicates that the series impedance is indeed purely resistive and that the measured R_s obtained via the C-V measurements is correct. The plateau values are similar to the values found from the R_s vs. V_{bias} plots. The rolling off of $|Z|$ at high frequencies, resembling capacitance behavior, cannot be rationalized by the presence of unanticipated extra capacitive elements in the model in Figure 4.14 and is most likely caused by the high impedance of the reference electrode (see Appendix B).

In conclusion, it can be stated that both cleanroom made, annealed Al back contacts and wet-bench made GaIn back contacts on moderately doped (ρ = 5-10 Ωcm), p-type <100> silicon give comparable contact impedances. They are both Ohmic in nature and the resistance is in the same order of magnitude (170 Ω vs. 250 Ω, respectively). Without any back contact the contact impedance is almost 50 times higher as compared to the other two (12 kΩ). It is thus recommended to use always one of the two contact methods for the type of silicon tested in this study. It is reasonable to assume that these findings are also true for other doping concentrations and substrate orientations.

Experimental

The wafers (Silicon <100> 4" wafers (p-type: 5-10 Ωcm) from Okmetic, Finland) that received an aluminum back contact were first cleaned using a standard wafer cleaning (5 min. in 100% HNO_3, copious rinsing in demi water, 10 min. in boiling (69%) HNO_3 at 95°C and again copious rinsing in demi water). The front side was subsequently covered with HMDS and photoresist (Olin 907/12). After that the wafers were pre-baked at 120° C for 30 minutes. Then the wafers received a 1% HF dip to remove the native oxide from the backside. A 1000 nm aluminum contact was made to the wafer via direct sputtering. Next, a chromium layer was directly sputtered onto the aluminum on both type wafers. The reason to do so is given in Chapter 2, section 2.5.2. This was followed by an annealing step at 450° C in a N_2 atmosphere. The photo resist was removed with acetone. Finally, the samples were diced into pieces of 10 mm x 10 mm. The samples for the categories GaIn and No back contact were made from similar wafers that were manually cut in pieces of 10 mm x 10 mm.

Next, a number of samples with aluminum back contact and without back contact was cleaned ultrasonically for 5 minutes in demi water and in acetone, consecutively. Consequently, they were put for 2 minutes in a plasma cleaner (PDC-002, Harrick Scientific Corporation) to remove any organic contaminants from the native oxide and to make sure that all samples had similar, hydrophilic surface properties of the insulator. After that, the samples were fixed in a home-made sample holder in such a way that the front-side of the sample could contact the liquid via an O-ring with an average surface area of 0.489 cm^2. The samples with an aluminum back contact were electrically contacted via a wire without further modification. The back side of the other two types of samples was scratched with a diamond pen to remove the native oxide. After that, the samples of the category No back contact were directly connected to the wire. On the back side of the samples of category GaIn some GaIn (99.99+%; Aldrich) was smeared via a cotton bud and the wire was brought into contact with the GaIn.

The sample holder was placed in a beaker with a 0.1 M KCl (99+%, ACS Reagent; Aldrich) solution and connected via both the Working Electrode and Sense leads to a PARSTAT2263 potentiostat (Princeton Applied Research). A platinum electrode was used as Counter electrode and the reference electrode was an Ag/AgCl (sat'd KCl) electrode (REF200, Radiometer).

First, Capacitance Voltage measurements were carried out. The bias voltage was swept from -3 V to 3 V vs. Ag/AgCl, respectively with steps of 50 mV. The amplitude of the ac-voltage was 20 mV and the frequency was 1 kHz.

Second, impedance measurements were carried out at a various number of bias voltages. The amplitude of the ac-voltage was 20 mV and the frequency was varied from 1 MHz to 0.1 Hz. Such scans were performed at the following bias voltages: -3.0, -2.0, -1.0, -0.5, 0.0, +0.5, +1.0, +2.0, and +3.0 V vs. Ag/AgCl, respectively.

Appendix D

Automatic extraction routine for Mott Schottky analysis

Characterizing the sensory response of EIS-structures can be a very time-consuming task. At different analytes the response has to be determined and in most cases multiple points are taken per analyte. This can easily lead to more than 100 files of measurement data and analyzing these by hand would take days of work. Therefore, an automatic doping and V_{fb} extraction routine for multiple sets of data was developed in the computer program Matlab™. This routine searches for the boundary points of slope 1 in order to detect its position. These points are of course not fixed but change either due to either drift or due to a different analyte composition. Taking Figure 4.19A as starting point, the information of the position of slope 1 can easily be found via the derivative of C^{-2}. This is illustrated in Figure 4D.1.

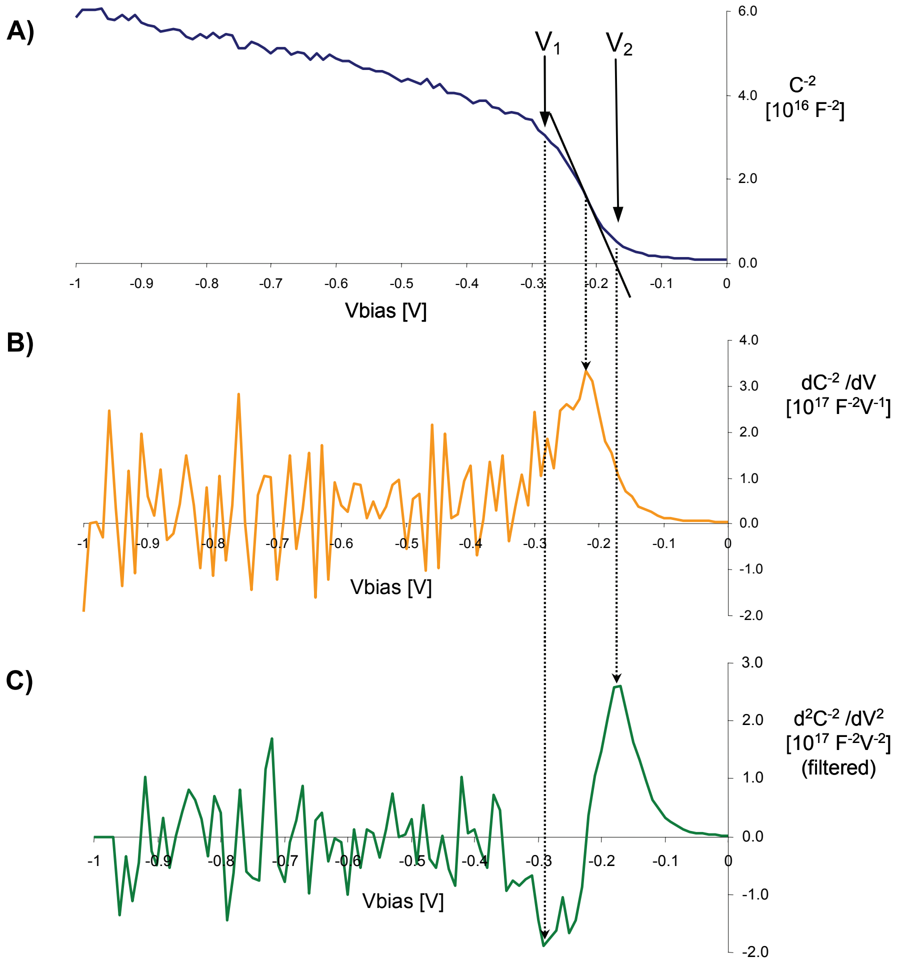

Figure 4D.1. A) C^{-2} – V data of a p-type silicon electrode modified with Si-C linked monolayer; B) is its derivative dC^{-2}/dV and C) its second derivative d^{2}dC^{-2}/dV^2.

At the middle of slope 1, C^{-2} shows the strongest increase and $\mathrm{d}C^{-2}/\mathrm{d}V$ will show a maximum at this point. Figure 4D.1B shows that the maximum of the first derivative $\mathrm{d}C^{-2}/\mathrm{d}V$ indeed coincides with the middle of slope 1. This gives, however, no information on the boundaries of slope 1 but one can even discriminate further. At the boundaries of slope 1 C^{-2} will have its inflection points. In these points $\mathrm{d}^2C^{-2}/\mathrm{d}V^2$ will show a maximum and a minimum. The maximum and minimum of the second derivative coincide with the inflection points of the $C^{-2}-V$ plot. The accompanying values of C^{-2} with these voltage values are, however, not on the fit line in Figure 4D.1A. If the left inflection point occurs at V_1 and the right inflection point is at V_2, all points between one or two points to the right of V_1 and one or two points to the left of V_2 should be taken for fitting (for the cases shown here with V_{step} = 10 mV).

A very crucial fact is illustrated in Figure 4D.1. The C^{-2} data was already very noisy and this noise is amplified in the first derivative and even more in the second derivative (acting as high-pass filters in the frequency domain). Therefore, care should be taken in preventing all noise sources in the measurement set-up. The noise can be somewhat filtered in the software via a moving average with weighing factors. The data of the second derivative has been filtered this way. An example of a moving averaging routine with two weighing factors is given in Equation 4D.1. The averaged value XA_i of sample X_i is:

$$XA_i = \alpha_2 X_{i-2} + \alpha_1 X_{i-1} + X_i + \alpha_1 X_{i+1} + \alpha_2 X_{i+2} \tag{4D.1}$$

Where α_j ($0 \leq \alpha_j \leq 1$) is the weighing scaling factor of the points $X_{i\pm j}$. The dataset of all XA_i data is not precisely scaled and thus not mathematically correct but that does not hinder the derivation of the inflection points. Setting all α values to zero leaves the original data unfiltered. Setting all α values to 1 results in maximum filtering. If this does not filter enough more α_j factors and corresponding $X_{i\pm j}$ values can be introduced. This whole routine can be easily incorporated in an automatic extraction routine in a program like Matlab™.

Chapter 5

Electrochemical Characterization of EIS-structures with Unfunctionalized, Si-C linked Monolayers

Abstract: The work described in this chapter focuses on the electrochemical behavior and characterization of Si-C linked, organic monolayers in electrolyte-insulator-silicon devices prior to incorporation in full sensors. It is shown that p-type silicon electrodes modified with $–C_nH_{2n+1}$ (n = 12, 16, and 22) monolayers become (partially) oxidized when operated under anodic bias voltages. Similar electrodes of n-type silicon do not show oxidative behavior but the formation of hydrogen gas is observed for large cathodic potentials. Under illumination, however, also n-type silicon electrodes become oxidized. The oxide thickness is estimated to be 1 - 2 nm. Oxide formation can lead to a sensitivity of the modified electrode towards *pH* changes due to (de)protonation of Si-OH groups. This is investigated via titration experiments, subsequential data analysis via Mott Schottky analysis and data fitting using a site-binding model to compare such layers with pure SiO_2 layers and SiO_2 layers modified with HMDS. All samples display *pH* sensitivity. In case of samples with Si-C linked monolayers the amount of Si-OH groups is estimated to be 0.32 - 0.64 % of a pure SiO_2 insulator. The pK_a value of all samples with monolayers (4.0 - 4.4), obtained from curve fitting, is lowered as compared to pure SiO_2 (6.0) indicating a more acidic behavior of the Si-OH groups as compared to SiO_2. Long-term drift of approximately 1 $mV\cdot h^{-1}$ for samples with organic monolayers shows that silicon electrodes modified with organic monolayers are in good equilibrium with the solution. The above results indicate that the electrodes modified with functionalized monolayers, sensitive towards other species than H^+ should be very well possible.

5.1 Introduction

The electrochemical behavior of Electrolyte-Insulator-Silicon (EIS) structures, in which the insulator is an unfunctionalized, Si-C linked organic monolayer of a few nanometers thickness, is studied in this Chapter. First a short recapitulation of the fabrication routes and physical properties of such layers is given. Figure 5.1 shows how crystalline, flat silicon surfaces can be modified with Si-C linked organic monolayers [1, 2]. After cleaning the surface, the silicon surface with native oxide is etched in a dilute HF solution to obtain an H-terminated silicon surface. Next, upon reacting with 1-alkenes or 1-alkynes a densely packed organic monolayer is formed on the surface [2]. The monolayer surface groups R can, if desired, be further functionalized with sensing moieties. For R = H chemically inert monolayers are obtained.

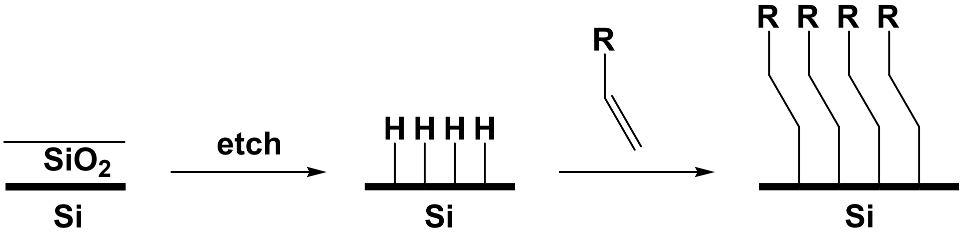

Figure 5.1. Scheme of monolayer formation on crystalline flat silicon [1].

After the first papers by Linford et al. [2, 3], new synthesis routes for creating functionalized surfaces quickly emerged [4-7]. The chemical and physical properties of such layers have been extensively studied and several reviews have appeared [8-12]. H-terminated silicon surfaces are easily passivated via such alkyl chains through covalent linkage [13-15] and are readily fabricated using simple wet-bench chemistry [9] at relatively low temperatures (approximately 160° C in case of thermal activation of the alkylation reaction [6] (see Figure 5.1) or even at room temperature in case of an alkylation reaction via visible light activation [16]). This has led to a variety of application fields of such layers. Examples of such application fields are passivation layers in solar cells [17, 18], anti-stiction coating films for nano-, and micro-electromechanical systems (NEMS/MEMS) [12], masking layers in lithographic processing [19], insulating films in hybrid molecule-silicon electronics [20], memory devices via incorporation of redox sites inside the monolayer [21-23] and even DNA sensing structures via functionalization of the end groups R in Figure 5.1 [24-26]. The behavior of these monolayers in solid-state Metal-Insulator-Silicon (MIS) devices is described in detail in Chapters 2 and 3. It was for example found that MIS-structures with these monolayers incorporated on n-type silicon contacted via mercury, showed electronic behavior from Ohmic for the H-terminated silicon to Schottky diode behavior for the silicon modified with organic monolayers [27, 28]. The magnitude of the current densities through such structures with monolayers can be precisely tuned via the alkyl chain length.

However, tunneling currents through such MIS-structures, although strongly suppressed, are still present since these layers are still thin enough for direct tunneling to take place. The longest alkyl chain used in this study (2.60 nm for -$C_{22}H_{45}$ [16]) is still shorter than the upper limit of direct tunneling of 3.5 nm [29].

Since in this project Si-C linked monolayers are to be used in sensory structures their behavior in the most likely environmental conditions, i.e. contacted via aqueous solutions, needs to be investigated. Therefore, it is necessary to fully understand the electrochemical behavior of EIS-structures with such chemically inert, unfunctionalized monolayers, prior to testing EIS-structures with functionalized monolayers. The characterization and investigation of the electrochemical behavior and sensory responses of EIS-structures with functionalized organic monolayers is treated separately in the next chapter. In order to be useful as insulating layer in such sensing structures an unfunctionalized monolayer should therefore passivate the surface and protect the underlying silicon from oxidation.

It is known from literature that an H-terminated silicon surface, although nearly electrically perfect [30] since all surface dangling bonds are bound and thus passivated by hydrogen, is not stable and gets oxidized both in air [31-39] and aqueous solutions [31, 35, 36, 40]. The H-termination of the surface slows down oxidation as compared to freshly cleaved surfaces but in air the surface is rapidly covered by a film of organic impurities [32, 34, 38] which reduces the initial oxide formation [34]. The formation of a monolayer of oxide on the crystalline, H-terminated silicon surfaces has been reported to take anywhere from 1 hour [36, 37] to a week [33, 39] or even up to a month [38]. After HF treatment small amounts of Si-F terminated groups can be present at the surface, depending on the HF concentration and solution composition [31]. Such Si-F terminated groups are not as stable as Si-H terminated groups. Rinsing in demineralized water already seems to create a slight coverage with Si-OH groups due to an exchange reaction of Si-F groups with water during the water rinse [31, 33]. Both in air and aqueous solutions the native oxide is thought to originate from water and in air the humidity plays thus a crucial role in the oxidation speed [35-37, 39, 40]. In aqueous solutions a higher amount of dissolved oxygen speeds up the oxidation but the oxygen is thought to act as a driving force in the oxidation reaction and not as a reactive species [40]. Other factors that influence the amount of oxide and oxidation speed are doping [34-36], the substrate orientation (<100> or <111> oriented surfaces) [34, 37] and illumination [34]. The electronic superiority of the Si-H surface quickly gets lost over time due to electronic defects as result of oxidation. Also the surface geometry stays not intact since the oxide tends to be amorphous and non-uniform [35]. Modifying the H-terminated silicon surface with an alkyl monolayer may provide a good option to tackle and prevent the phenomena mentioned above.

Bansal and Lewis [41] showed that modifying H-terminated n-type Si<111> electrodes with -C_nH_{2n+1} (n = 1 - 6) monolayers via a two-step chlorination/alkylation method rendered very stable photoanodes. Under illumination and in an 0.35 M $K_4Fe(CN)_6$ – 0.05 M $K_3Fe(CN)_6$ aqueous solution the -CH_3 and -C_2H_5 modified electrodes showed better passivating properties and a better stability against oxidation as compared to the Si-H electrode. High-resolution XP spectra of all electrodes after immersion confirmed this finding. The Si-H samples had approximately three monolayers of oxide and the -CH_3 and -C_2H_5 modified electrodes had less than one monolayer of oxide as compared to the situation before immersion. The electrode series resistance increased with increasing monolayer chain length. In another article [42] they investigated the electrochemical properties of n-type Si<111> electrodes in CH_3OH-1,1' –dimethylferrocene$^{+/0}$ ($Me_2Fc^{+/0}$) solutions. The surfaces of the electrodes were modified with -C_nH_{2n+1} (n = 2, 4, 6, 10, 12, and 18) alkyl chains. Using this organic solvent with $Me_2Fc^{+/0}$ redox couple allowed them to study the current density and differential capacitance vs. voltage behavior without the effects of possible oxidation due to the presence of water. All electrodes remained stable under illumination and the values for both the open circuit voltage V_{oc} and flatband voltage V_{fb} indicated that the electrical properties of the alkyl modified electrodes were not compromised as compared to a sample prepared with a fresh H-terminated surface. The electrode series resistance increased for larger chain lengths until n = 6. For larger chain lengths there was no correlation between chain length and series resistance possibly due to less optimal packing of the longer chain monolayers through which solvents may penetrate as a result of fabrication method. By adding water (until 20% v/v) to the solution they investigated the electrode stability towards oxidation. The Si-H electrodes deteriorated swiftly due to oxidation but all alkylated electrodes showed outstanding resistivity towards oxidation.

Recently, Takabayashi et al. [43] studied the electrochemical behavior of n-type Si<111> electrodes modified with various Si-C linked organic monolayers, amongst others -C_nH_{2n+1} (n = 1, 4, and 6), in 100 mM $LiClO_4$ with 5 mM K_2PtCl_6. Via cyclic voltammetry Pt was electrodeposited in pinholes in the monolayer in order to enhance the stability and increase the performance of the photo electrodes. The Pt deposition rate and amount of deposited Pt depended strongly on the alkyl chain length. The Pt dot size increased in the order from -H, -CH_3, -C_4H_9, to -C_6H_{13}. Pt growth is expected to start at openings in the monolayer and the initially formed Pt contacts the silicon directly. Such openings are more present at -CH_3 terminated silicon as compared to silicon modified with longer chains since the alkyl chains are tilted and hinder Pt deposition. The large Pt islands encountered on the electrodes with longer alkyl chains have grown in diameter and lay on top of the monolayer and are thus anchored to the silicon via relatively small openings in the monolayer. Via XPS the amount of oxygen after Pt nano-deposition was measured and after Pt deposition almost no oxidation could be observed for the alkylated electrodes as compared to the H-terminated electrodes. Pt deposition improved the solar cell characteristics of the electrodes significantly as compared to electrodes without deposited Pt. Stability tests showed that after 24 hours of illumination -CH_3 terminated Si-electrodes with deposited Pt were not or hardly degenerated in contrast to the other electrodes. For the electrodes with longer alkyl chains a considerable number of Pt dots were peeled off during this test.

Yu et al. [44] studied the electron transfer kinetics through -C_nH_{2n+1} (n = 2, 6, 10, and 15) alkyl monolayers on n-type Si<111> electrodes in acetonitrile with anthraquinone (AQ) as electrochemical probe. The advantage of using AQ is that it is a neutral redox species and can give insight into the ability to penetrate into the organic film in the absence of electrostatic effects. Cyclic voltammetry experiments showed that longer chains block the interfacial electron transfer more effectively. Furthermore, for longer chains rectifying behavior was observed, i.e. the reverse current peak of the redox couple is repressed. In the evaluation of the apparent electron transfer rate constant vs. monolayer chain length they found a very weak dependence of 0.05 per mesitylene (CH_2) group. They attributed such low values to a less optimal packing of their layers suggesting that monolayer penetration by species in the solvent takes place. In another article [45] they studied the capacitive behavior of such layers in aqueous solutions. They found a direct relationship between the monolayer capacitance, as derived from the capacitance in accumulation, and the thickness of their layers. From that data the dielectric constant of the monolayers was found to be $\varepsilon_r = 3.3 \pm 0.6$. They attributed this high value to vacancies in the monolayer through which electrolyte might penetrate.

Chidsey and co-workers [46] investigated the influence of the type of monolayer, alkyl, fluorinated alkyl and alkoxy monolayers, on n-type Si<111> electrodes via ellipsometry, XPS, AFM and electrochemical measurements. XPS measurements showed that, given their fabrication route, the alkyl monolayer showed the least amount of oxygen at the monolayer-silicon interface. This was ascribed to the densest packing of the alkyl monolayer. AFM measurements showed that the surface topography of the original silicon surface stays unaffected for each of the monolayer modified surfaces. Cyclic voltammetry measurements in aqueous solutions with a redox couple showed that the alkyl monolayers successfully block redox currents. The Si-H electrodes showed large currents and diffusion-limited current peaks. However, such peaks were absent at the electrodes modified with alkyl monolayers. Subsequent cyclic voltammetry measurements were performed in organic solvents (methanol, acetonitrile, and tetrahydrofuran) with redox couples. In tetrahydrofuran the currents were lowest and most reproducible. This could on one hand be ascribed to the fact that permeation of the monolayer is lowest with this solvent due to its relatively large molecular size which keeps the redox couple at a larger distance from the silicon. On the other hand, surface states could also play a role in the selective behavior of the modified electrodes towards different solvents. Modifying the silicon surface with an organic monolayer slows down oxygen formation but does not completely block it, resulting in traces of oxidized surface spots. If the major part of surface states originates from this oxide, the solvent which is the least polar, in this case tetrahydrofuran, gives rise to the least oxide formation and thus the most reproducible behavior. In a subsequent study [47] they focused on the influence of monolayer chain length of Si-C_nH_{2n+1} (n = 5 - 8) electrodes on the electron transfer kinetics in tetrahydrofuran with a redox couple. The electron transfer rates showed an exponential distance dependence with a decay constant of 1.00 ± 0.05 per CH_2, independent of the bias voltage. This was similar to that of monolayers on gold surfaces in aqueous solutions, indicating that no significant contribution of the electron transfer could be made by transfer via pinhole defects in the monolayer.

Wei and Zhao [48] investigated the formation and characteristics of mixed monolayers of 1-dodecene (DN) and undecylenic acid (MU) on p-type Si<111> silicon electrodes via fluorescence emission intensity measurements and capacitance measurements. Via fluorescent labeling of the acid group and measuring the fluorescence of the monolayer surface, it was found that the mixed monolayer had the same mole fraction as the initial DN and MU mixtures. Pure monolayers of DN had capacitances of 2.5 $\mu F\cdot cm^{-2}$ whereas pure monolayers of MU had capacitances of 1.8 $\mu F\cdot cm^{-2}$. It was not mentioned why a lower capacitance was found for pure MU monolayers as compared to pure DN monolayers. The capacitance of mixed monolayers, however, did not show a linear dependence on mole fraction of DN and MU. Via a model of the surface via effective capacitance per molecules, they successfully modeled their findings and concluded that a strong interaction exists between DN and MU molecules, thereby varying film structure and film dielectric constant. Although there was no linear relation between film capacitance and mole fraction of DN and MU, their study showed that both surface density of desired functional groups and dielectric properties of the film could be precisely tuned.

Allongue et al. modified Si electrodes with functionalized phenyl groups via an electrochemically driven monolayer formation due to the reduction of diazonium salts. In [49] they showed that the monolayers preserved the original surface structure on the atomic scale and protect the surface against oxidation. Furthermore, they were able to functionalize their phenyl layers with a large variety of groups such as Br, NO_2, COOH, CN, and $-C_nH_{2n+1}$ ($n = 1$, 4, and 12). In [50] they showed that such electrochemically derived monolayers via diazonium salts follow the surface profile and are able to withstand HF rinsing. Via capacitance measurements in accumulation they found that the density of defect states at the silicon-monolayer interface is similar to the one of a Si-H surface. Monolayers with large functional groups gave less packed layers and are more prone to re-oxidation. Re-oxidation of the surface does occur at all monolayers and initiates from defects sites and seems to stop at densely packed domains.

From the literature summarized above we draw the following conclusions. From the passivation point of view, i.e. the protection of the underlying silicon against oxidation and the retaining of a low number of surface defects, modifying H-terminated silicon surfaces with organic monolayers through covalent Si-C linkage offers some clear advantages over the use of H-terminated silicon surfaces. The monolayer follows the surface topography of the H-terminated surface, shows very little initial oxide and slows down oxidation of the surface to a very large degree. Although the amount of initial oxygen in these layers is low and subsequent oxidation during experiments is strongly repressed, oxygen is still present. Furthermore, the electrical behavior of such modified silicon electrodes is stable, reproducible and can be precisely tuned by varying monolayer thickness or composition. The surface states at such modified electrodes are in the same order as the H-terminated silicon surfaces. From the insulation point of view, i.e. suppression of charge transport from the silicon to the electrolyte, the monolayers form tunneling barriers and can suppress redox current to a large degree. They are, however, no perfect insulators, simply because given the limited thickness of monolayers, tunneling is always possible. For use as insulating layer in chemically modified sensory structures in aqueous solutions the influence of oxide, although present in minute traces, has to be investigated. The methyl-terminated monolayers are chemically inert but silicon oxide is chemically active and can cause unexpected sensory responses if not taken into account.

In the theoretical section of this chapter the silicon-monolayer-electrolyte interfaces are closely examined to investigate the processes occurring in these regions when exposed to aqueous solutions. After that, the theory of site binding interactions at SiO_2 surfaces is recapitulated from literature and adapted to silicon surfaces modified with monolayers and with possible traces of SiO_2. In the results and discussion section three studies are treated. Firstly, cyclic voltammetry experiments on silicon electrodes modified with organic monolayers are treated in order to investigate the electrochemical and reactive behavior of layers in aqueous solutions under different applied bias voltages. Secondly, results are shown and discussed of capacitance measurements performed on p-type electrodes modified with a number of insulators. Capacitance measurements are for EIS-characterization the most commonly used technique. Thirdly, a study is presented which deals with the pH dependent response of silicon electrodes modified with unfunctionalized, inert monolayers. Since small traces of SiO_2 are expected to be present at the electrode, a certain response of the electrode towards pH changes is expected and investigated in detail. This section is followed by conclusions and finally the experimental details are given.

5.2 Theory

5.2.1 Silicon-oxide-electrolyte interfaces

Elemental semiconductors like silicon and germanium react with water and the surface is covered with a thin layer of oxide when in contact with aqueous solutions. This oxide can consequently interact with protons in the solution. The process occurring at such oxidized semiconductors also apply to semiconductors with thick, well prepared oxides, which are on their turn the building blocks of FET-based sensors [51]. On the electrolyte side the process is to a great extent identical to metal electrodes, in which an electrical double layer forms at the electrolyte-metal interface [52]. This double layer consists of several regions or layers and can be described by the Gouy-Chapman-Stern model [52]. In Figure 5.2 a schematic picture of the build-up of the double layer near a metal electrode is shown.

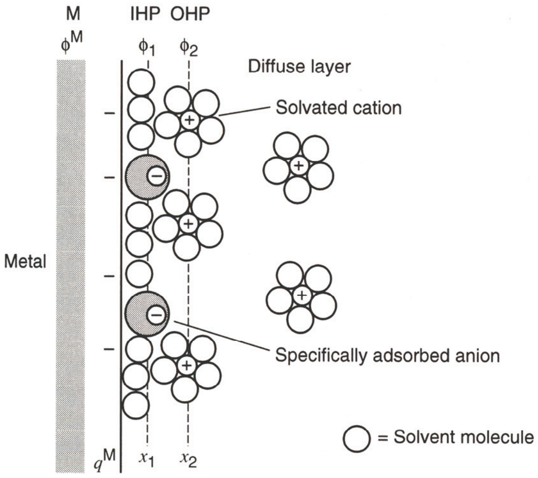

Figure 5.2. Graphical interpretation of the formation of the electrolyte double layer at metal electrodes [52].

The layer closest to the electrode, the inner layer, contains solvent molecules and sometimes other species (ions or molecules) that are said to be *specifically* adsorbed. This inner layer is called the Helmholtz or Stern layer. Two planes can on their turn be distinguished within the Helmholtz layer. The locus of the electrical centers of the *specifically* adsorbed ions is called the inner Helmholtz plane (IHP) which is at distance x_1 in Figure 5.2. Solvated ions can only approach the metal to a distance x_2. The locus of centers of these nearest solvated ions is called the outer Helmholtz plane (OHP). The interaction of the solvated ions with the charged metal involves long-range electrostatic forces, so that their interaction is essentially independent of the chemical properties of the ions. These ions are said to be *non-specifically* adsorbed. Due to Brownian motion in the solution, the *non-specifically* adsorbed ions are distributed in a three-dimensional region, called the diffuse layer, which extends from the OHP into the bulk of the solution. The thickness of this diffuse layer depends on the total ionic strength in the solution and on the potential applied over the double layer. Increasing the total ionic strength of the solution or the potential over the layer will diminish the thickness of this layer.

In the Gouy-Chapman-Stern model two capacitances can now be associated with this double layer. The Helmholtz capacitance C_H corresponds to the capacitance of the charges held at the OHP, i.e. all the charges present from the metal electrode surface until x_2. C_H is independent of electrolyte concentration and applied bias voltage and equals at metal electrodes 10-40 $\mu F \cdot cm^{-2}$ [52]. The diffuse capacitance C_{diff} corresponds to the capacitance from the OHP into the bulk, i.e. all the charges present in the diffuse layer. Its value strongly depends on electrolyte concentration and applied bias voltage. These capacitances are connected in series and the total capacitance is called the double layer capacitance C_{dl} and its value equals $C_{dl}^{-1} = C_H^{-1} + C_{diff}^{-1}$. For solutions with high ionic strengths or high bias voltages C_{diff} becomes very large and C_{dl} is approximately equal to C_H.

In case of semiconductor electrodes with oxidized surfaces the double-layer build-up can be depicted as in Figure 5.3 according to a model by [31].

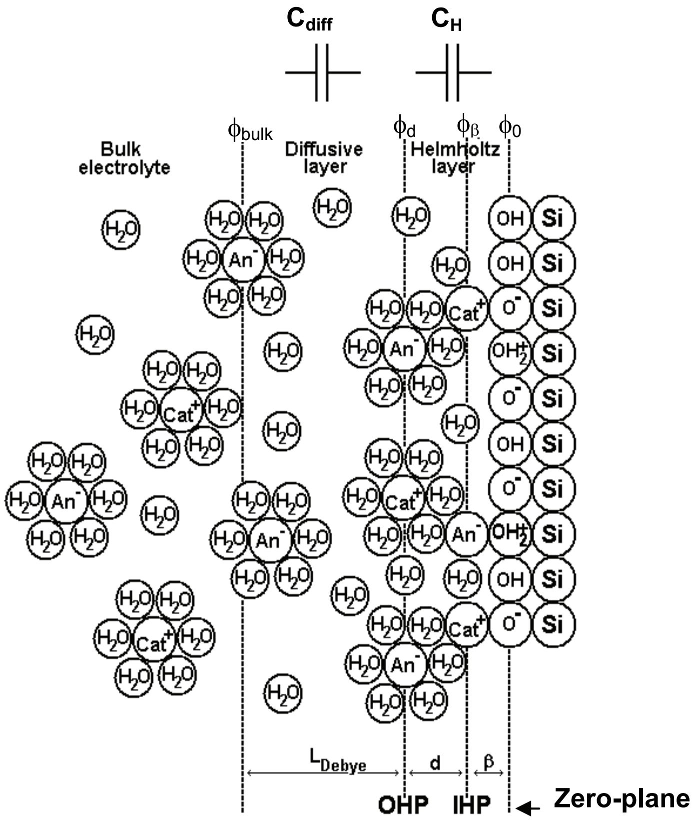

Figure 5.3. Graphical interpretation of a triple layer in the electrolyte at an oxidized silicon surface. In this case not a thick SiO_2 insulator is drawn, but merely a monolayer of Si-OH. This does not change the concept of the site binding reactions and resulting responses.

This model is somewhat more complicated due to fact that this is a triple layer surface complexation model (TLM). An additional plane, the zero plane, is present at this model in between the IHP and the electrode surface. SiO_2 surface groups can become hydrated resulting in Si-OH groups which can on their turn interact with H_3O^+ species in the solution. The hydrogen ions are permitted to coordinate with the unsaturated sites at the innermost layer of oxide sites or zero plane in Figure 5.3. Other ions, denoted by cat$^+$ and an$^-$ in this example, can consequently be adsorbed to the charged oxide sites, making up the IHP. So according to this model there are two planes in which specific adsorption can take place, the zero plane for H^+ adsorption and the IHP for specific adsorption of other ions. The description of the other processes at such electrodes is the same as given for the metal electrodes. The total Helmholtz layer is now thus in fact made up by two different layers. It begins at the zero plane and ends at the OHP. Note that for oxidized semiconductor surfaces C_H can be fully charged without any external charge in the semiconductor. The number of charged Si-OH sites due to protonation or deprotonation is that large that the charge at the zero-plane and the counter charge at the IHP, OHP, and diffuse layer fully charges C_H and C_{diff}. The value for C_H at silicon electrodes is lower than the value for metal electrodes (10-40 $\mu F \cdot cm^{-2}$ [52]). Values in literature vary and are mostly in the range of 3-4 μF·cm^{-2}. Oskam et al. derived a value for C_H of about 3 μF·cm^{-2} via intensity modulated photocurrent spectroscopy using n-type Si<111> electrodes in a 0.1 M $K_4Fe(CN)_6$ + 0.5 M KCl solution [53]. Allongue et al. found a value for C_H of 3.5 μF·cm^{-2} via capacitance measurements in aqueous H_2SO_4/HF solutions using n-type Si<111> electrodes of which the surface was modified with organic monolayers [50]. Yu et al. found a value of (3.7 ± 0.5) μF·cm^{-2} via capacitance measurements in aqueous 0.1 M H_2SO_4 + 2% HF solutions using n-type Si<111> electrodes of which the surface was also modified with organic monolayers [45].

It can already be intuitively understood that the potential at the zero-plane ϕ_0 with respect to the bulk potential ϕ_{bulk} is strongly dependent on the bulk pH of the solution. This relation will be described in the next paragraph.

5.2.2 Site binding theory

A site binding model basically describes the relation between the potential at the zero plane ϕ_0 as a function of bulk pH or pX in case of specific receptor groups sensitive to species X. The relation of ϕ_0 and bulk pH at oxide surfaces was first described by Yates et al. [54] and later adapted by Bousse [55] and van den Berg [56]. The description in this section is based on the most recent model proposed by van Hal et al. [57, 58].

As can be seen in Figure 5.3 a hydrated SiO_2 surface in contact with an electrolyte can take on three forms, in which the ratio of the three different forms depends on pH. The ratio of these neutral (-OH), negatively ($-O^-$) and positively ($-OH_2^+$) charged groups determines the net charge on the surface. This ratio is described by the chemical reactions that occur between the amphoteric sites and the protons in the solution. With the use of reaction or so-called dissociation constants it is possible to describe the relation between the proton concentration (and thus pH) and net charge on the surface in a, for SiO_2 in contact with aqueous electrolytes, unique way. The net number of charged groups per surface unit $[B]$ [m^{-2}] is defined as the number of negatively charged groups minus the number of positively charged groups as given in Equation 5.1.

$$[B] = [SiO^-] - [SiOH_2^+] \tag{5.1}$$

Multiplying $[B]$ by $-q$, the elementary charge, gives the total net charge σ_0 on the surface, i.e. $\sigma_0 = -q[B]$.

If a net charge accumulates on the surface, an equal but opposite charge will be built up at some distance in the electrolyte and this situation can be modeled with a capacitor. In the previous subsection the ability of ions inside an electrolyte to form charged and diffuse layers is treated and modeled as a series combination of C_H and C_{diff}. The total series capacitance is commonly called the double layer capacitance, C_{dl}. The total charge σ_0 now present on the SiO_2 surface due to protonated or deprotonated Si-OH groups, will be compensated by a charge of the opposite sign in the electrolyte side so $\sigma_{dl} = -\sigma_0$. Via C_{dl} and the voltage difference across C_{dl}, namely $\delta\phi_0$ these two charges are related (for small differences) according to Equation 5.2.

$$\frac{\delta\sigma_{dl}}{\delta\phi_0} = -\frac{\delta\sigma_0}{\delta\phi_0} = -C_{dl} \tag{5.2}$$

The relation of interest is how ϕ_0 changes as a function of the bulk pH ($\delta\phi_0 \cdot \delta pH^{-1}$). As mentioned above σ_0 can be described as $-q[B]$. The total charge on the surface σ_0 can at first be described as a function of the pH at the surface by Equation 5.3.

$$\frac{\delta\sigma_0}{\delta pH_S} = -q\frac{\delta[B]}{\delta pH_S} = -q\beta_{\text{int}} \tag{5.3}$$

where pH_S is the surface pH; β_{int} is the chemical intrinsic buffer capacity; the rest of the parameters is defined as above. β_{int} can be described as the ability of the surface to compensate or buffer pH changes at this surface. A high β_{int} denotes a good buffer ability of the surface. A high and constant β_{int} is favorable for use in sensing structures but in real life situations β_{int} does not have to be constant and can be a function of pH_S. This can lead to ranges of pH_S where there can be optimal buffering and ranges of pH_S where there is hardly any buffering and consequently a low response.

Combining the relation of σ_0 and C_{dl} in Equation 5.2 and the relation of σ_0 and pH_S in Equation 5.3 a relation between surface pH and the parameter of interest ϕ_0 can be obtained. This is given in Equation 5.4.

$$\frac{\delta\phi_0}{\delta pH_S} = \frac{\delta\phi_0}{\delta\sigma_0}\frac{\delta\sigma_0}{\delta pH_S} = -\frac{q\beta_{\text{int}}}{C_{dl}} \tag{5.4}$$

A high β_{int} denotes a large change in ϕ_0 upon changes in pH_S and a small C_{dl} gives the largest change in ϕ_0 upon pH_S changes as can be simply understood via Equation 5.4.

Because in an experiment usually the bulk pH, pH_B, instead of pH_S is known, pH_S has to be written as a function of pH_B. This can be done by using the classical Boltzmann equation as given in Equation 5.5.

$$a_{H_S^+} = a_{H_B^+} e^{\frac{-q\phi_0}{kT}} \tag{5.5}$$

where $a_{H_S^+}$ and $a_{H_B^+}$ are the activities of protons at the surface and at the bulk of the electrolyte, respectively, which are linked to the concentration by an activity coefficient; the rest of the parameters is defined above. In most common electrolytes the activity coefficient can be approximated by one so that the activities equal the concentrations. Hence, Equation 5.5 can be written in pH values as in Equation 5.6.

$$pH_S = pH_B + \frac{q\phi_0}{2.303kT} \tag{5.6}$$

Next, substituting Equation 5.6 into Equation 5.4 and rearranging terms leads to Equation 5.7.

$$\frac{\delta\phi_0}{\delta pH_B} = -\frac{1}{\dfrac{C_{dl}}{q\beta_{\text{int}}} + \dfrac{q}{2.303kT}} = -2.303\frac{kT}{q}\alpha, \text{ where } \alpha = \frac{1}{\dfrac{2.303kTC_{dl}}{q^2\beta_{\text{int}}} + 1} \tag{5.7}$$

Equation 5.7 shows the universal description of the site binding theory with only one parameter α. α [-] is a dimensionless sensitivity parameter that varies between 0 and 1 depending on β_{int} and C_{dl}. The fact that a higher β_{int} results in a higher sensitivity is easily understood. The fact that a lower C_{dl} results in a higher sensitivity can be also intuitively understood when realizing that C_{dl} represents the ability of the electrolyte to compensate for changes in surface charge. A low value of C_{dl} leads to a higher ϕ_0 upon the same change in σ_0 (Equation 5.2).

The protonation and deprotonation reactions at the oxide surface are described via material specific association constants and these constants thus determine also the response. Also the total number of oxide reaction sites plays on important role. The effect of these has not been taken into account yet and this can all be accounted for in the intrinsic buffer capacity and hence β_{int} will be further specified. At first the reactions at the silicon hydroxide surface are given in Equation 5.8a and b.

$$SiOH \rightleftharpoons SiO^- + H_S^+ \tag{5.8a}$$

and

$$SiOH_2^+ \rightleftharpoons SiOH + H_S^+ \tag{5.8b}$$

Using the activity coefficients of the different species the dissociation constants of Equations 5.8a and b can be determined via Equations 5.9a and b.

$$\frac{\upsilon_{SiO^-} a_{H_S^+}}{\upsilon_{SiOH}} = K_a \tag{5.9a}$$

and

$$\frac{\upsilon_{SiOH} a_{H_S^+}}{\upsilon_{SiOH_2^+}} = K_b \tag{5.9b}$$

where the activity constants for surface species are represented by υ [mol.m^{-2}]. The *K* values are tabulated intrinsic dissociation constants. The activity of protons is a function of *pH* and the rest of the parameters is dependent on the number of active surface groups, N_S [m^{-2}] as defined in Equation 5.10.

$$N_s = \upsilon_{SiOH} + \upsilon_{SiOH_2^+} + \upsilon_{SiO^-} \tag{5.10}$$

Next, *[B]* can now be rewritten as a function of N_s and K_a and K_b in Equation 5.11.

$$[B] = [SiO^-] - [SiOH_2^+] = N_S\left(\frac{\upsilon_{SiO^-} - \upsilon_{SiOH_2^+}}{\upsilon_{SiOH} + \upsilon_{SiOH_2^+} + \upsilon_{SiO^-}}\right) = N_S\left(\frac{a_{H_S^+}^2 - K_a K_b}{K_a K_b + K_b a_{H_S^+} + a_{H_S^+}^2}\right) \tag{5.11}$$

Via Equation 5.3, in which β_{int} is defined as *[B]* differentiated as a function of pH_S, β_{int} can now be written as an analytical expression of N_S, K_a, K_b, and $a_{H_S^+}$. This is given in Equation 5.12.

$$\beta_{\text{int}} = N_S \frac{K_b a_{H_S^+}^2 + 4K_a K_b a_{H_S^+} + K_a K_b^2}{\left(K_a K_b + K_b a_{H_S^+} + a_{H_S^+}^2\right)^2} 2.303 a_{H_S^+} \tag{5.12}$$

β_{int} can now be elucidated by comparing it with its analogue in chemistry, for instance the buffer capacity of a phosphate buffer as function of the *pH*. For the *pH* values near the dissociation constants pK_x (pK_1 = 2.16, pK_2 = 7.21, and pK_3 = 12.32 [59]) the buffer shows optimal buffering. For *pH* values more than one *pH* unit away from pK_x the buffer gives very poor buffering. All parameters needed to calculate the *pH*-sensitivity via Equation 5.7 are now treated and defined.

Next some simulation results will be treated to show the separate influence of C_{dl}, N_s, K_a and K_b, respectively. In most cases the standard parameters for SiO_2 surfaces are used: $N_s = 5 \cdot 10^{18}$ m^{-2}, $pK_a = 6$, $pK_b = -2$, and $C_H = 20$ µF·cm^{-2} [58] and the concentration C_0 is generally 0.1 M so that the influence of C_{diff} is negligible.

The influence of the *pH* on the number of charged and neutral surface groups

Given such SiO_2 surface as mentioned above, it is first demonstrated in Figure 5.4 how the number of charged and neutral groups are divided as a function of *pH*.

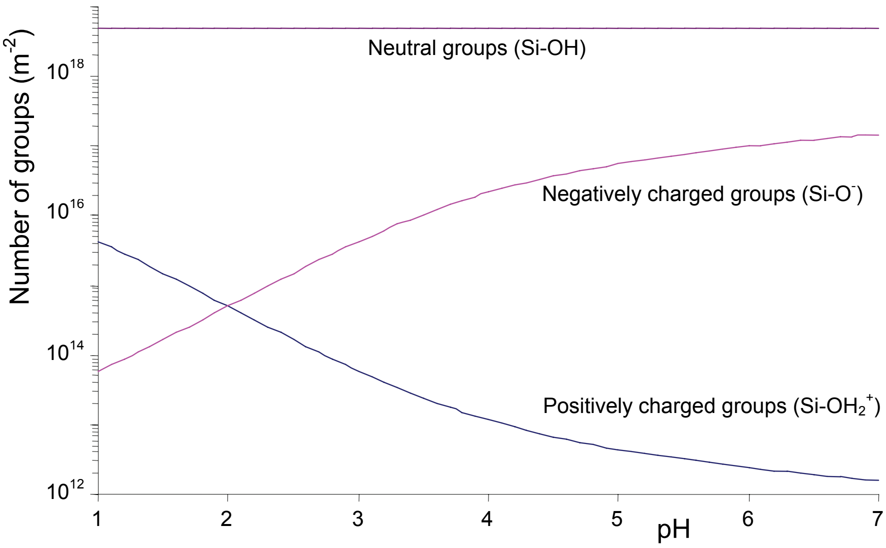

Figure 5.4. Simulation results for the number of different groups on a pure SiO_2 surface; $N_s = 5{\cdot}10^{18}$ m^{-2}, $pK_a = 6$, $pK_b = -2$ and $C_0 = 0.1$ M. Note that the number of groups is plotted on a logarithmic scale.

Figure 5.4 illustrates the fact that only a small fraction of the total surface groups is actually charged and thereby contributing to the overall response. Even at $pH = 7$, at which the largest amount of negatively charged surface groups are present in this figure, their amount is a mere 1% of the total amount of surface groups! Figure 5.4 also illustrates the concept of point of zero charge. At a certain *pH* the number of positively and negatively charged surface are equal and hence, the net surface charge is zero. This *pH* is called the point of zero charge, pH_{pzc}, and for SiO_2 the pH_{pzc} is approximately 2 [58]. The pH_{pzc} is approximately equal to $0.5(pK_a + pK_b)$.

The influence of the total electrolyte concentration and C_{dl}

The total electrolyte concentration C_0 has its influence on C_{dl} as discussed in section 5.2.1 and C_{dl} on its turn, also determines the *pH* response as given in Equation 5.7. In Figure 5.5 the influence of the total electrolyte concentration on the response is given.

In this figure it is illustrated that the response increases indeed for decreasing electrolyte concentration, albeit not significantly for concentrations between 10 mM and 1 M. Again, the influence of the point of zero charge is illustrated in Figure 5.5. The sensitivity is lowest around pH_{pzc} since a very small amount of charged surface groups contributes in that region to the response.

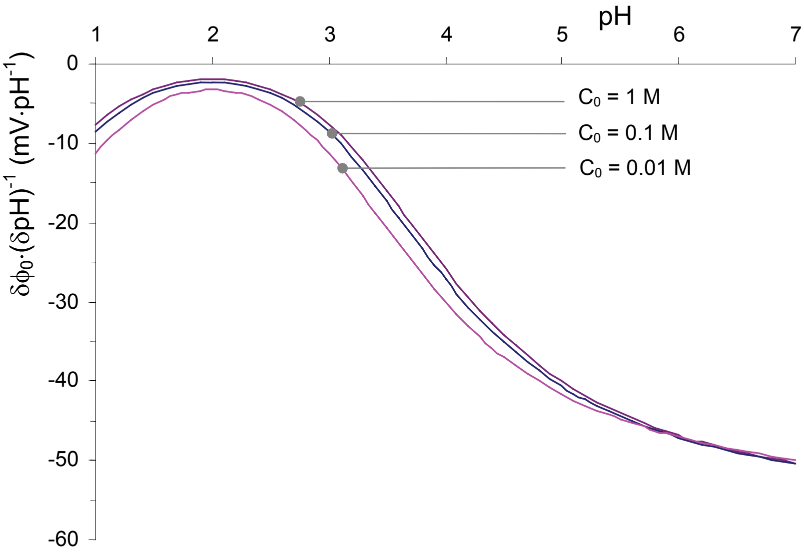

Figure 5.5. The simulated *pH* response for different values of the background concentration C_0; $N_s = 5{\cdot}10^{18}$ m^{-2}, $pK_a = 6$, $pK_b = -2$, and $C_H = 20$ μF·cm^{-2}.

The influence of the total number of surface groups N_S

In Equation 5.12 it can be seen that β_{int} scales proportionally with the total number of surface groups N_s and hence, a lower number of surface groups will cause a lower β_{int} and lower sensitivity. This effect is illustrated in Figure 5.6.

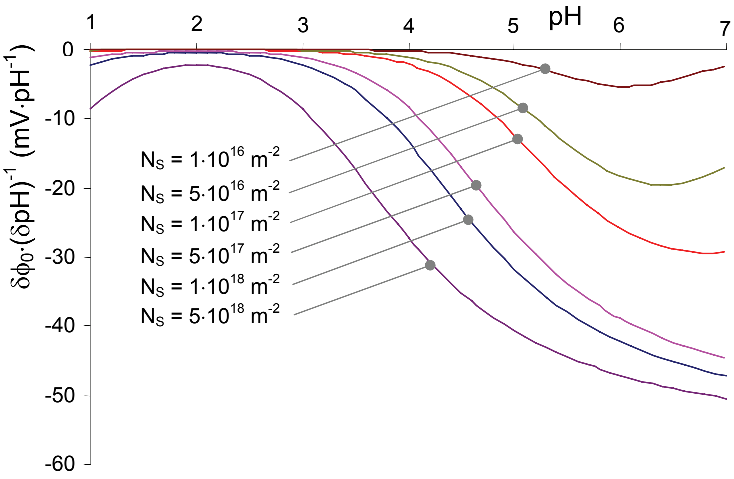

Figure 5.6. The simulated *pH* response for bare SiO_2 for different values of the total number of surface groups; $pK_a = 6$, $pK_b = -2$, $C_H = 20$ μF·cm^{-2}, and $C_0 = 0.1$ M.

In Figure 5.6 it is illustrated that the sensitivity decreases for decreasing N_s. For $N_s = 1{\cdot}10^{17}$ m^{-2} and below, saturation of the charged surface groups can occur for higher *pH* values, causing even a decrease in sensitivity for higher pH values.

The influence of the dissociation constants *pK$_a$* and *pK$_b$*

The dissociation constants pK_a and pK_b will have a major influence on the response. The point of the least sensitivity is in general pH_{pzc}, which equals to $0.5(pK_a + pK_b)$. The overall sensitivity increases when the difference ΔpK between pK_a and pK_b is smaller. In that case one type of charged groups already "takes over" when the influence of the other type of charged groups is diminishing. For instance ΔpK = 8, 4, and 2 for SiO_2, Al_2O_3 and Ta_2O_5, respectively [58] and the overall sensitivity indeed increases and becomes more Nernstian, i.e. 59.2 mV difference in ϕ_0 per pH unit, for SiO_2, Al_2O_3 and Ta_2O_5, respectively. These effects are illustrated in six examples in Figure 5.7.

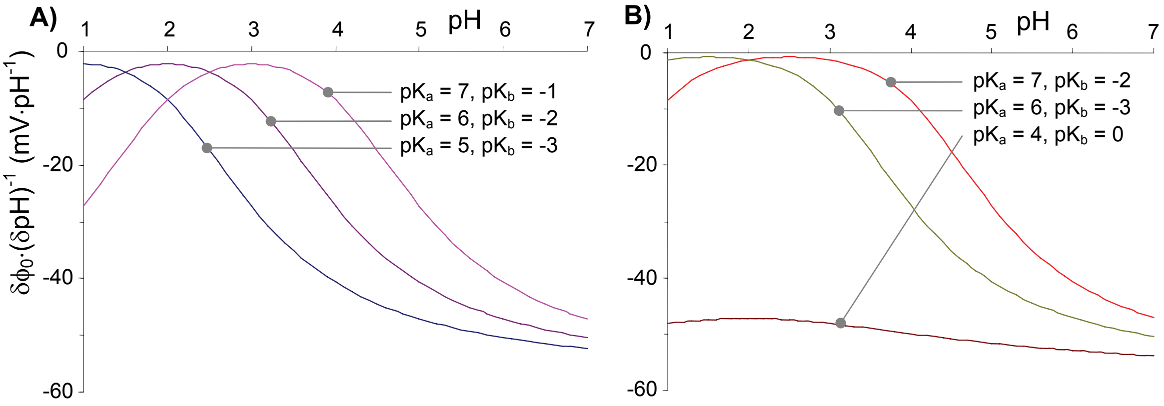

Figure 5.7. The simulated *pH* response of an amphoteric surface for six different values of the dissociation constants; C_0 = 0.1 M, C_H = 20 μF·cm^{-2}, and N_s = 5·10^{18} m^{-2}.

In Figure 5.7A the sensitivity is shown for the original SiO_2 surface, i.e. pK_a = 6 and pK_b = -2, leading to $pH_{pzc} \approx 2$ and $\Delta pK = 8$. Also shown is the effect of shifting both pK values one pK unit, while ΔpK stays 8. In those cases the response has the same shape as the original curve but the point of zero charge shifts to 1 and 3, respectively. In the two upper curves in Figure 5.7B the effect of an increasing ΔpK is shown, resulting in a larger pH regime where the sensitivity is low or even zero and an overall decrease in sensitivity. In the bottom curve the case is shown where pH_{pzc} = 2 as in the case of the original curve in Figure 5.7A but ΔpK has been reduced to 4. This increases the response drastically, which is now almost constant over the complete pH range in the figure.

All these simulation results serve the purpose to analyze and comprehend the pH responses of silicon samples modified with organic monolayers as described in the next section.

5.3 Results and Discussion

5.3.1 Cyclic voltammetry experiments

For use as insulators in FET-based sensors some bias-voltage will be applied over the gate-bulk region in order to give the FET the right settings in practical read-out circuits [51]. This gate-bulk region is the reference electrode-electrolyte-monolayer-silicon structure and some part of the bias voltage will certainly drop over the insulator. It is therefore of importance to know the electrochemical behavior of EIS-structures with organic monolayers as insulators. This paragraph gives the results of cyclic voltammetry experiments both on p-type <100> silicon electrodes modified with C_{12}, C_{16}, C_{22} monolayers and H-terminated samples and n-type <100> silicon electrodes modified with C_{12}, and C_{22} monolayers. The electrolyte consisted of a 1M KNO_3 solution without any additional redox couple. Since KNO_3 is practically inert, the only likely reactions to occur are the oxidation and reduction of water. In Figure 5.8 the measurement results of the first scan are shown for p-type silicon.

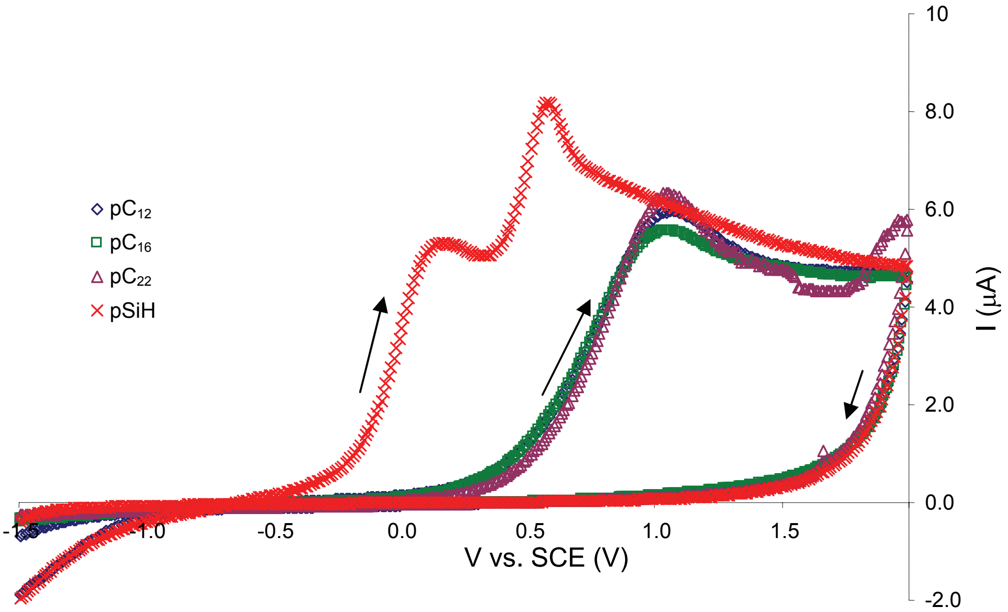

Figure 5.8. Cyclic voltammograms of all tested samples on p-type silicon in 1M KNO_3. The scanrate was 10 mV·s^{-1}. The results for the samples with monolayers are typical from duplo experiments.

At the first scan of the SiH sample a positive currents starts to flow at around -0.75 V vs. SCE. Subsequently a small current peak appears at 0.1 V vs. SCE, followed by a larger peak at 0.5 V vs. SCE. After this peak the current drops gradually and appears to be independent of voltage. In subsequent scans these peaks disappeared and the overall currents were at least one order of magnitude lower. It is known from literature that p-type silicon is easily oxidized in aqueous solutions since the holes which are readily available in p-type silicon, both without any applied bias and at anodic potentials, are needed for the oxidation of water and consequently the oxidation of silicon [31]. The fact that these large currents can be associated with oxide formation was also described in the thesis of Kooij [60]. He performed experiments on H-terminated p-type <100> silicon samples in 1M KCl and he concluded that in the first scan a passivating oxide layer is formed on the electrode surface, which blocks charge transfer in subsequent scans. In his experiments he scanned the voltage from 0 V to 3.0 V vs. SCE at 50 $mV \cdot s^{-1}$ and estimated via the charge transferred in one scan and assuming a same oxide density as a thermal oxide that approximately 1.4 nm of anodic oxide was grown. In this case the estimated charge transported in the anodic region to the pSiH sample was 3.9 $mC \cdot cm^{-2}$ and using the same assumptions as Kooij this equals to approximately 3.1 nm of formed SiO_2 if all oxide obtained via oxidation of water is used for silicon oxidation.

The silicon electrodes modified with organic monolayers of three different chain lengths all showed a positive current onset at approximately 0 V vs. SCE and a current peak at 1.0 V vs. SCE. The current onset, current peak and magnitude all seemed to be independent of monolayer chain length which is in strong contrast with the current-voltage behavior of mercury-monolayer-p-type silicon samples in which a strong current decrease was observed for increasing chain lengths [27]. The results depicted in Figure 5.8 indicate that the monolayer suppresses charge transfer but (partial) oxidation still occurs. This is also indicated by the fact that in subsequent scans always a strong current decrease was observed as was the case for Si-H. The estimated charge transported in the anodic region to the pC_{12} sample was 2.4 $mC \cdot cm^{-2}$ and using the same assumptions as mentioned above this equals to approximately 1.9 nm of formed SiO_2, a reduction of 39% as compared to the SiH samples. In case of samples modified with organic monolayers not all Si-H sites are substituted by Si-C linked alkyl chains. Via simulations it was shown that on Si<111> about 50-55% of all Si-H sites have reacted [61, 62] and it is estimated that on the Si<100> surface about 30-35% has reacted [63]. A large percentage of unreacted Si-H groups thus remains on the surface. If these sites can be approached by water or oxygen they can possibly be oxidized, resulting in such large oxidation peaks as shown in Figure 5.8. In the discussion above it was assumed that all the charge transferred in the anodic current is used to oxidize water and consequently oxidize the silicon surface. The oxidation of the silicon can in this simple case be described by a two step reaction. However, it is also reasonable to assume that not all the oxygen formed via the oxidation of water is used for silicon oxidation but that a part of this will leave the electrode as oxygen gas. The discussion above thus concerns a worst case scenario.

To the best of our knowledge p-type silicon electrodes modified with organic monolayers have not been investigated in literature and this is the first notice of electrochemical behavior of p-type silicon electrodes modified with organic monolayers. Instead, studies of organic monolayers on silicon electrodes are mostly focused on n-type silicon, probably since n-type silicon is less prone to oxidation due to the lack of holes (in the dark) [31] and thus a more stable behavior is maintained in aqueous solutions. For electrochemical voltammetric experiments on n-type silicon electrodes modified with organic monolayers different scenarios are mentioned in literature. Cheng et al. [47] found a strong current decrease for increasing monolayer chain lengths on Si-C_nH_{2n+1} (n = 5, 6, 7, and 8) electrodes in a tetrahedrofuran (THF) electrolyte with redox couple. Bansal and Lewis [41] found for n-type Si-C_nH_{2n+1} (n = 1, 2, 4, and 6) electrodes in an aqueous solution with redox couple for n = 1 and 2 an improving blocking behavior of the electrodes but for n = 4 and 6 a decreasing current blocking behavior as compared to H-terminated silicon electrodes. In [42] they investigated n-type Si-C_nH_{2n+1} (n = 2, 4, 6, 10, 12, and 18) electrodes in an organic solvent with redox couple. For n > 6 they could no longer observe a relation between monolayer chain length and blocking behavior of the monolayer. Yu et al. [44] also investigated n-type Si-C_nH_{2n+1} (n = 2, 6, 10, and 15) electrodes in an organic solvent with redox couple and found a more rectifying behavior of the electrodes for increasing chain lengths, i.e. for increasing chain length the redox couple oxidation peaks were suppressed more as compared to the reduction peaks. Furthermore, they found a very small influence of monolayer chain length on electron transfer rate.

We also performed experiments on n-type silicon electrodes. In Figure 5.9 the first out of five scans made in the dark of silicon electrodes modified with a C_{12} and C_{22} monolayer are shown. Also in the figure are shown the first out of five scans of subsequent measurement under illumination.

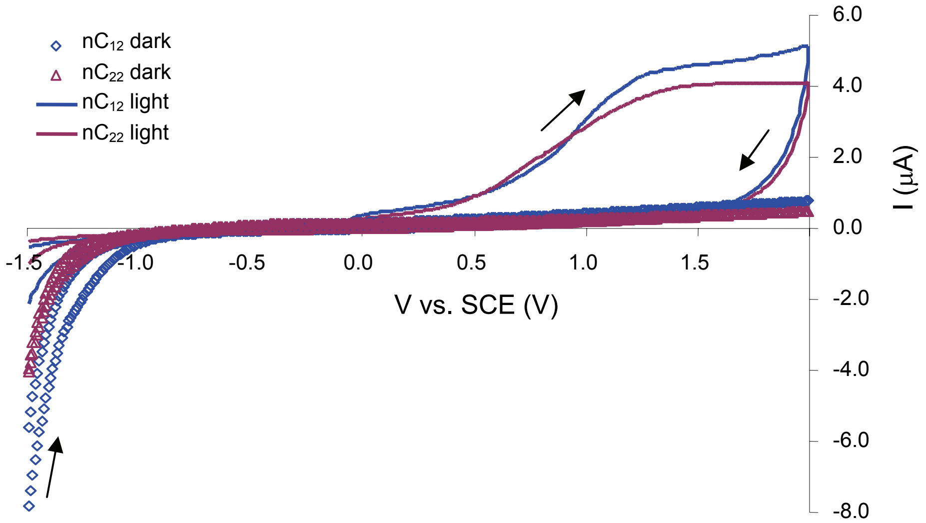

Figure 5.9. Cyclic Voltammograms of all tested samples on n-type silicon in 1 M KNO_3. The scanrate was 10 $mV{\cdot}s^{-1}$.

N-type silicon operated in the dark possesses many free electrons but few holes. This makes n-type silicon reactive in the cathodic regime (the more negative voltages in Figure 5.9) and not very reactive in the anodic regime due to the lack of holes [31]. When the voltage on the electrode is more negative than –1 V vs. SCE, the electrons, readily accumulated at the electrode surface, will be consumed in the reduction process of hydrogen ions and hydrogen gas is thus formed at the electrode. In Figure 5.9 large cathodic currents associated with the reduction of hydrogen ions can be observed for the two electrodes. The currents are smaller for the electrode modified with a C_{22} monolayer as compared to the C_{12} monolayer, indicating that in this case a longer alkyl chain blocks the current more effectively. Due to the lack of holes an anodic oxide on n-type silicon electrodes will not be formed so easily as on p-type silicon [31]. This correlates with the low currents observed in Figure 5.9 in the anodic regime. Also the fact that subsequent scans were far more reproducible on n-type silicon as compared to p-type silicon, i.e. a much lesser percentage current decrease as compared to the first scan, indicates that indeed little anodic oxide is formed. Under illumination, holes are photo generated and now an anodic oxide can be formed under anodic bias conditions [31]. This can be observed in Figure 5.9 where large anodic currents, in the same order of magnitude as for the p-type silicon electrodes, are now observed. The relation between current magnitude and monolayer chain length also holds in this case. Smaller currents flow through the silicon electrode modified with C_{22} monolayer. In subsequent scans under illumination the current dropped at least one order of magnitude as was the case for the p-type silicon electrodes, indicating that an anodic oxide has indeed formed on the surface.

These results indicate that during operation in the anodic regime (partial) oxidation occurs both on p-type silicon electrodes modified with C_{12}, C_{16}, or C_{22} monolayers and on illuminated n-type electrodes modified with C_{12} or C_{22} monolayers. It is reasonable to assume that this oxide layer or spots are very small in thickness. As long as anodic voltages are kept low, this oxide is likely not to grow any further since for thick oxides large electric fields are required due to the fact that ions needed for oxidation have to migrate through the already formed oxide, which acts as blocking layer [31]. However, Si-OH groups at the surface of the formed SiO_2 spots can easily be (de)protonated and this gives rise to a certain *pH* response as explained in section 5.2.2. This can be an unwanted side effect in eventual sensory functions. It is thus stressed again that operation of the device should be performed in the cathodic regime and large anodic voltages should be avoided to keep the silicon surface as non-oxidized as possible.

5.3.2 Capacitance-Voltage experiments

Measurement of capacitance voltage (*C-V*) curves is a standard technique for characterizing the *pH* or *pX* responses of EIS-structures with insulating oxides or insulators with receptors susceptible to species X, respectively [51]. Besides that, *C-V* measurements can reveal important information on the insulator capacitance and any parasitic charges or defects located in the insulator or at the silicon-insulator interface [51]. Some basic theory on *C-V* measurements can also be found in the previous chapter. In order to characterize EIS-structures with organic monolayers as insulators and investigate their *pH* sensitivity, *C-V* measurements were performed on several samples. In Figure 5.10 *C-V* curves are shown for a p-type silicon electrode modified with a C_{22} monolayer, measured at different *pH* values. Such *C-V* curves were typical for most of the tested samples.

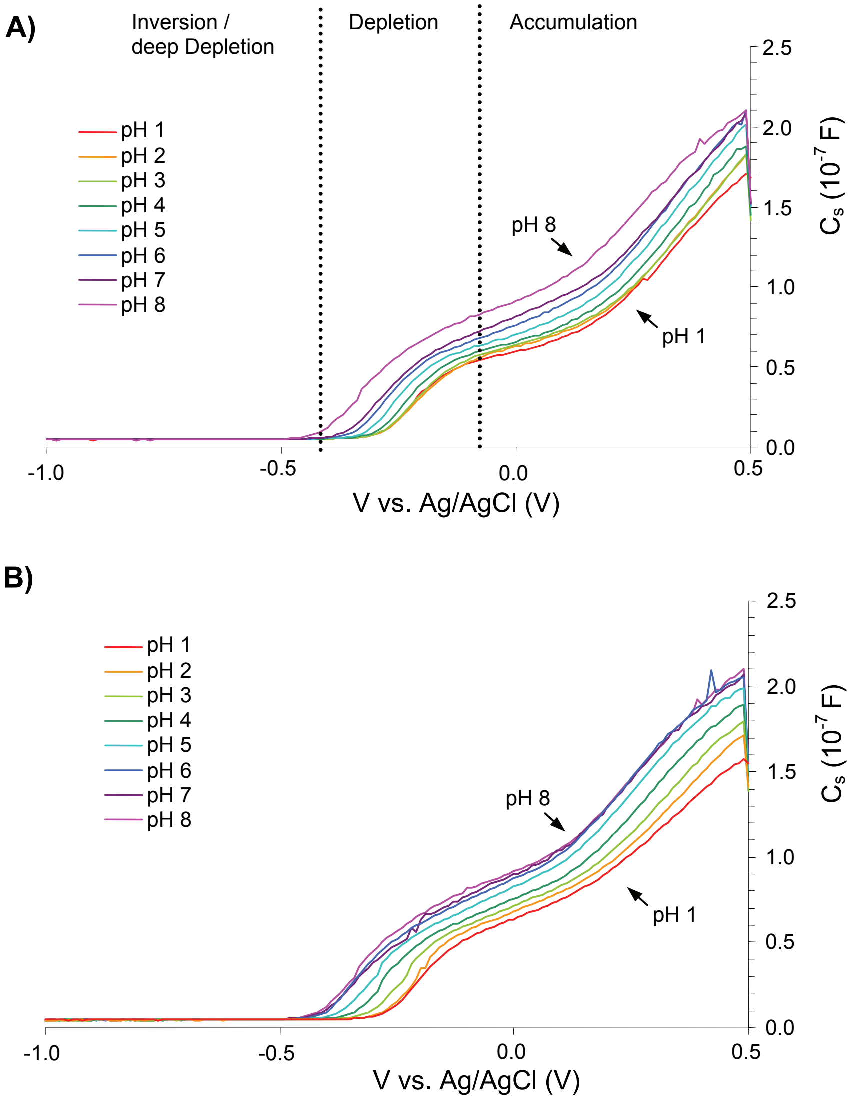

Figure 5.10. Typical high-frequency *C-V* curves of p-type silicon electrodes modified with a C_{22} monolayer. In A) the *C-V* plots are shown for up going *pH* values ranging from 1 to 8 and in B) *C-V* plots are shown for the down going *pH* values ranging from 8 to 1. The background electrolyte was 0.1 M TetraButylAmmonium-Chloride (TBACl) The capacitance values are calculated via a series model (see Chapter 4 for details).

In Figure 5.10A the three operating regimes of the silicon-electrode are indicated, namely inversion, depletion, and accumulation. The regimes are indicated for the plot made at *pH* 8. On the left-hand side the inversion regime is indicated. The capacitance in this regime equals the series circuit of the depletion capacitance (C_{sc}), insulator capacitance (C_{ins}) and electrolyte double layer capacitance (C_{dl}). In equilibrium situations, such as indicated here, C_{sc} has reached a constant value and consequently the total capacitance will also be constant here. In case of non-equilibrium situations the deep depletion situation can occur since C_{sc} will then decrease further for more negative bias voltages, thereby decreasing the total capacitance further as a function of bias voltage. For more positive bias voltages C_{sc} will increase and the total capacitance will now also increase strongly as a function of bias voltage. This depletion regime is indicated in Figure

5.10A roughly between -0.4 and -0.1 V vs. Ag/AgCl. For even higher voltages C_{sc} will be negligibly high and the total capacitance equals the insulator and double layer capacitance. This is the accumulation regime, indicated in Figure 5.10A for voltages higher than -0.1 V vs. Ag/AgCl. *C-V* curves were made to investigate two major properties of the electrodes: 1) the insulator or monolayer properties via the accumulation capacitance and 2) the *pH* responses via the shift along the *V*-axis of the individual *C-V* plots for different *pH* values. Concerning the first point it can be seen in Figure 5.10A that the accumulation capacitances do not reach a constant level but increase as a function of bias voltage. At voltages higher than 0.2 - 0.3 V vs. Ag/AgCl an even sharper increase occurs. Such non-constant capacitances were typical for silicon electrodes modified with organic monolayers and consequently a detailed analysis of the insulator properties and silicon-monolayer interface properties could not be carried out. Concerning the second point it can already be seen in Figure 5.10A and B that the *C-V* curves shift along the *V*-axis at different *pH* values. The curves shift to more negative values for increasing *pH* values (Figure 5.10A) and shift to more positive values for decreasing *pH* values (Figure 5.10B). This can be associated with an increasing negatively charged layer at the insulator-electrolyte interface at increasing *pH*, which is in good agreement with theoretical predicted behavior for SiO_2 as indicated in Figure 5.4.

It was stated before that for a proper determination of the *pH* sensitivity the flatband voltage V_{fb} has to be known. In case of ideal *C-V* curves with constant accumulation capacitances V_{fb} can be determined analytically from these plots [29] but this can not be done in this case. Another possibility to estimate the V_{fb} shifts between the curves is to measure graphically the shifts along the *V*-axis between the curves, provided that the curves are identical irrespective of the *pH* value [51]. There is, however, a trend that the capacitances in accumulation increase for increasing *pH* values. This will be explained below. The third option to determine (the shifts in) V_{fb} is via the use of Mott Schottky plots. This procedure is discussed in detail in the previous paragraph. To illustrate the fact that the capacitance in accumulation does not only increase for increasing voltages but also for increasing *pH*, a calculation has been made in Table 5.1 in order to illustrate this effect.

Table 5.1. Influence of *pH* on the estimation of C_{acc}.

pH	C_{acc} (V = 0 V vs. AgAgCl) [nF]	V_{fb} [V vs. Ag/AgCl]	$\Delta V_{fb} = V_{fb} - V_{fb}$(*pH* 1 up) [V vs. Ag/AgCl]	C_{acc} (V = 0 - ΔV_{fb} V vs. Ag/AgCl) [nF]
1 up	59.6	-0.253	0	59.6
3 up	63.9	-0.257	0.004	63.2
5 up	70.4	-0.291	0.038	66.8
7 up	81.5	-0.333	0.078	72.3
7 down	89.9	-0.380	0.127	73.5
5 down	82.6	-0.342	0.089	70.9
3 down	68.0	-0.276	0.023	69.1
1 down	63.6	-0.242	-0.010	64.5

Table 5.1 gives an overview of the measured capacitance at 0 V vs. Ag/AgCl for 4 different *pH* values at both the up going and down going *pH* sweeps. It can be seen that *C* increases indeed for increasing *pH* values. The shift in V_{fb}, however, has not been taken into account and therefore these values can not be compared since at 0 V vs. Ag/AgCl a shifted curve to the left gives already a higher capacitance (see Figure 5.10A). Therefore, the amount of shift has been calculated via V_{fb} as determined via Mott Schottky plots. The third column lists V_{fb} and the fourth column lists the shift in V_{fb} with respect to V_{fb} measured at *pH* 1 of the up going sweep. In the fifth column C_s has been determined again now taking the V_{fb} shift into account. Still, C_s is higher for higher *pH* values both in the up going and down going sweeps and C_s decreases for decreasing *pH* values. The data in Table 5.1 illustrates that the *C-V* curves for different *pH* values are thus not identical and graphical determination of the *pH* sensitivity is therefore thought to be not correct. The *pH* sensitivity is therefore determined via the Mott Schottky plots, which will be treated in the next paragraph.

The relation between *pH* and accumulation capacitance was not clear to a large degree. In a later stage in this project it was realized that the rather large, hydrophobic cation TBA used in many of the *pH* experiments might be able to adsorb non-specifically to the monolayer, thereby increasing the apparent monolayer thickness and lowering the total insulator capacitance. Possibly, this may even be a *pH* related process. In Appendix A adsorption measurements are shown in which the influence of cation size and hydrophobic nature are investigated. These results indicated that adsorption can occur for the large TBA cation. It is not clear to what degree such adsorption might affect the found *pH* sensitivities. Future measurements are therefore recommended to be carried out with background electrolytes containing smaller cations, such as TetraMethylAmmonium (TMA) or TetraEthylAmmonium (TEA).

5.3.3 Mott Schottky measurements: *pH* responses

In the *C-V* curves in Figure 5.10 it was shown that *pH* sensitivity was present for all silicon electrodes modified with organic monolayers. Analysis of this sensitivity was neither possible via an analytical determination of V_{fb} via the *C-V* data nor via graphical determination of the shifts of the plots. All *pH* sensitivities have therefore been determined via Mott Schottky (C^{-2} vs. V) plots. The theory behind Mott Schottky measurements and analysis has been described in detail in Chapter 4. In Figure 5.11 typical Mott Schottky plots are shown for a p-type silicon electrode modified with a C_{22} monolayer.

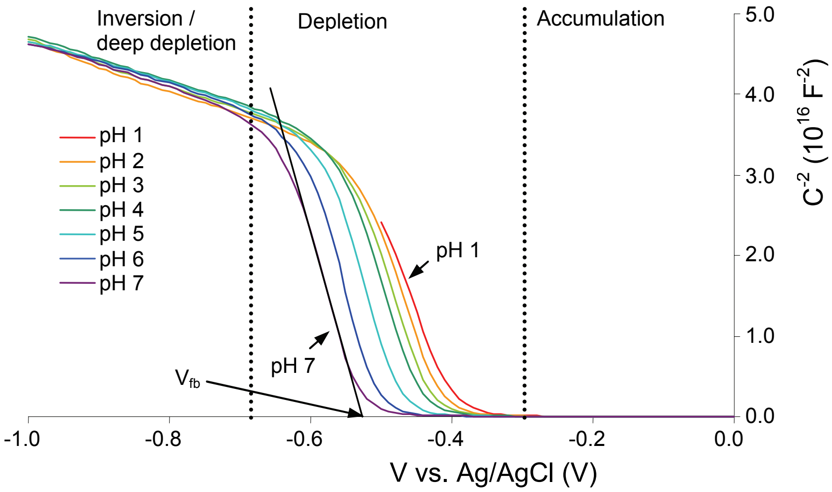

Figure 5.11. Mott Schottky plots for a p-type silicon electrode modified with a C_{22} monolayer. The curves are measured at *pH* values ranging from 1 to 7 in steps of 1 *pH* unit. The *V*-axis intercept of the fit lines renders the flatband voltage V_{fb}.

In Figure 5.11 typical Mott Schottky plots are shown for the tested p-type silicon electrodes. At the onset of depletion linear curves over a 0.1 V wide range are obtained, which all shift along the *V*-axis upon *pH* changes. At approximately -0.5 to -0.6 V vs. Ag/AgCl all curves bend towards a *pH* independent, linear curve with a lower slope. This region can be associated with a deep depletion region, as C_{sc} and thus the total capacitance decrease for more negative potentials and C^{-2} will increase. From the slope of this curve the correct doping values can be obtained but from it no *pH* influence can be derived. The former curves give information on the *pH* sensitivity but nonetheless via the slopes of these lines the wrong values for the doping are found. A discussion on the interpretation of such Mott Schottky plots with double slopes has been given in the previous chapter. It suffices to say that V_{fb} is derived from the curves with the steep slopes since these are shifted upon *pH* changes. However, the doping should be calculated via the slope of the second curve. Via the analysis of the Mott Schottky plots the *pH* sensitivity was calculated. The tested electrodes were p-type silicon with either C_{22} or C_{12} monolayers as insulators. As a reference, electrodes with SiO_2 and SiO_2 coated with a hydrophobic layer of HMDS (HexaMethylDiSilazane) were used. HMDS is normally used as a primer in lithographic processes. It is used here to investigate the influence of reducing the number of active sites on SiO_2 surfaces via treatment with an organic monolayer. The *pH* sensitivities for up going sweeps from *pH* 1 through 7 are given in Figure 5.12.

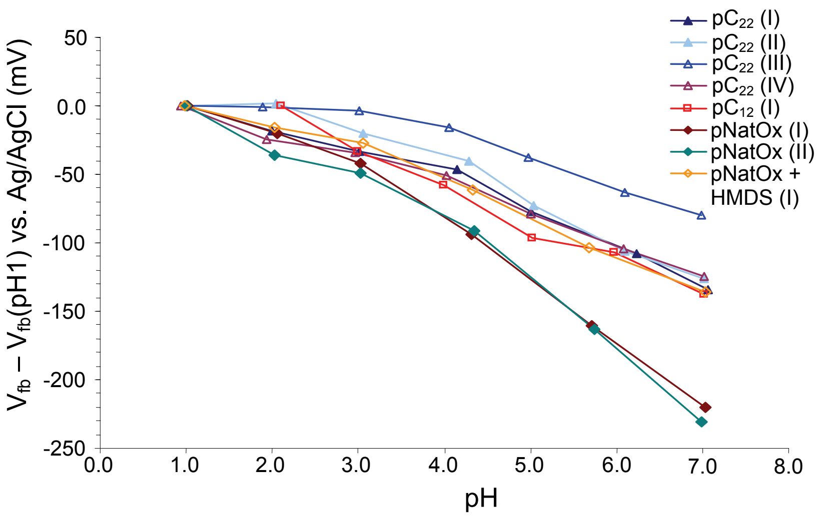

Figure 5.12. *pH* sensitivities of p-type silicon electrodes with a variety of insulators. To provide a better overview all responses start at 0 V vs. Ag/AgCl at *pH* 1, i.e. $V_{fb} - V_{fb}$ (*pH*1) is plotted on the left axis.

The electrodes with SiO_2 insulators give the highest *pH* response, a total of 220 – 231 mV from *pH* 1 through 7. Applying a HMDS coating on top of the SiO_2 surface reduces its sensitivity due to the reduced number of active sites to a very large degree, namely 136 mV over the *pH* 1 through 7 range. The samples modified with the C_{12} and C_{22} monolayers also showed a strong decrease in *pH* sensitivity as compared to samples with bare SiO_2 insulators. This indicates that the monolayer, although densely packed, does not cover the complete silicon surface and that oxide sites, initially present or formed during measurements, can react with the hydrogen ions. The sample with C_{12} monolayer showed a sensitivity of 137 mV in the *pH* 1 through 7 range. The sensitivities of the tested samples with a C_{22} monolayer varied greatly from a mere 79 to 134 mV in the *pH* 1 through 7 range. In the *pH* 4 - 7 range the *pH* sensitivity is quite constant for all samples. In order to give a comparison between the samples this average *pH* sensitivity is given in Table 5.2. Also indicated in this table are the starting values of V_{fb} at *pH* 1.

Table 5.2. *pH* sensitivity in the *pH* 4 - 7 range and V_{fb} values at *pH* 1.

Sample	$dV_{fb}\cdot(dpH)^{-1}$ [mV·pH^{-1}]	V_{fb} at *pH* 1 [mV vs. Ag/AgCl]
pC_{22} (I)	29.3	-396
pC_{22} (II)	31.0	-584
pC_{22} (III)	21.7	-253
pC_{22} (IV)	24.5	-136
pC_{12} (I)	24.8	+368
pNatOx (I)	46.5	+79
pNatOx (II)	53.0	+38
pNatOx + HMDS (I)	27.4	-94

The samples with SiO_2 insulators show the largest *pH* sensitivity. Coating of the SiO_2 with HMDS lowers its sensitivity to 27.4 mV·pH^{-1}. Among the samples with monolayers there is a large spreading between the sensitivities of 21.7 to 31.0 mV·pH^{-1}. Such spreading may be attributed to different degrees of oxide formation or presence at the samples. As will be illustrated below via simulations a relative low number of active surface groups is needed for a noticeable *pH* response (see also Figure 5.4).

It should also be mentioned that the responses caused are assumed to be totally due to (de)protonation of Si-OH sites. However, evidence exists in literature that organic layers can be surface charged via OH$^-$ adsorption onto these layers. Marinova et al. [64] found via electrophoretic mobility measurements of oil droplets in aqueous solutions that OH$^-$ adsorption occurs at the oil-water interface, where the magnitude of the surface potential depends on the *pH*. They stated that the most probable reason for the specific adsorption seems to be hydrogen bonds formation of the OH$^-$ ions with the water molecules in the boundary layer. Grunze and co-workers [65] found that OH$^-$ adsorption plays a crucial role in the molecule to molecule repulsion of methoxy tri(ethylene-glycol)-terminated undecanethiolate monolayers on gold surfaces. Since ethylene-glycol is a nonionic surfactant and adsorption or incorporation of ions into these layers were not very likely, systematic analysis led to the conclusion that OH$^-$ adsorption occurs at these surfaces, resulting in the repelling forces between the molecules. In two other articles [66, 67] they found that the surface potential due to OH$^-$ adsorption at different monolayers, amongst which also an octadecanethiol monolayer on gold which is a chemically inert CH$_3$ – terminated monolayer just as the monolayers tested here, was negative at *pH* values > 4 and positive for *pH* values < 4. It is thus reasonable to assume that OH$^-$ adsorption also occurs at the monolayers tested here since they are no different in (hydrophobic) nature than the layers discussed above. Since the surface potential due to both OH$^-$ adsorption and Si-OH (de)protonation become more negative at higher *pH* values, the two effects, if they occur simultaneously, can not be separated from each other. For *pH* values > 4 both effects lead to negative surface potentials and hence both effects will then lead to a stronger *pH* dependency than was to be expected from the (de)protonation effect of Si-OH groups solely. In fact in Figure 5.12 it can be seen that all samples have an increased *pH* sensitivity in the *pH* 4 – 7 region as compared for the *pH* < 4 region. However, a more detailed investigation on this topic is necessary to draw strong conclusions on the *pH* dependent charging effects occurring at these monolayer surfaces.

The mentioned values of V_{fb} in Table 5.2 at the start of the measurements at *pH* 1 all lie in a moderate and for practical read-out circuits good voltage range and show that no significant contribution of parasitic charges in the insulator and / or silicon-insulator interface are present, which would then lead to drastic V_{fb} shifts [29].

Hysteresis

Hysteresis is an important feature in sensor characterization and provides information on the reliability of the sensor output. Figure 5.12 and Table 5.2 contain the results of up going *pH* sweeps only. Consequent down going *pH* sweeps are very useful to investigate such hysteresis phenomena and also the structure of the silicon-monolayer in terms of integrity and stability. The latter can be visualized as follows: if during the up going *pH* sweep oxide is formed and thereby raising the number of N_s, this will result in a consequently higher *pH* sensitivity in the down going sweep. Figure 5.13 displays the results of the up and down going *pH* sweeps of two samples with a C_{22} monolayer, a sample with native oxide, and a sample with native oxide coated with HMDS.

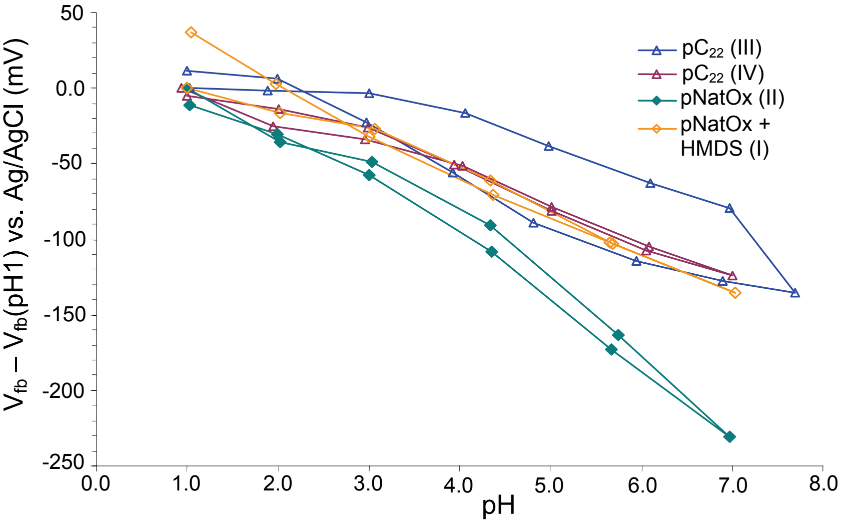

Figure 5.13. *pH* sensitivities for up and down going *pH* sweeps of p-type silicon electrodes with a variety of insulators. To provide a better overview all responses start at 0 V vs. Ag/AgCl at *pH* 1, i.e. $V_{fb} - V_{fb}$ (*pH*1) is plotted on the left axis.

The sample with SiO_2 showed some hysteresis. The maximum deviation between up and down going *pH* points was 19 mV but eventually at *pH* 1 the deviation stays moderate. The sample with SiO_2 - HMDS showed moderate hysteresis between *pH* 3 and *pH* 7. However, for *pH* 2 and 1 in the down going sweep the *pH* sensitivity was equal to the sensitivity at *pH* > 4 and did not decrease as was the case for the up going sweep or the up and down going sweeps of the sample with SiO_2. The reasons for this behavior are unknown. Sample pC_{22} (IV), a sample with a C_{22} monolayer, displayed little hysteresis over the entire *pH* range. The maximum deviation at *pH* 2 was 12.5 mV. If this sample would have been oxidized during the up going *pH* sweep it was expected that the sensitivity would have increased in the down going *pH* sweep, but this was not the case. The sensitivities between *pH* 4 and 7 were 24.5 and 24.0 $mV \cdot pH^{-1}$ for the up going and down going *pH* sweep, respectively. The fact that both sensitivities are almost equal indicates that little change, i.e. little extra oxidation, has occurred at the sample. Sample pC_{22} (III) was measured up to *pH* 8. At *pH* 8 this sample showed a large drift, which causes the apparent high difference between *pH* 7 and *pH* 8. Due to this high difference it looks like there is a large difference between up and down going *pH* sweeps. However, when the sensitivities between *pH* 4 and 7 are calculated these were 21.7 and 23.7 $mV \cdot pH^{-1}$ for the up going and down going *pH* sweep, respectively. A slight increase was observed, indicating a certain amount of extra oxide but nonetheless these sensitivities were lower than for sample pC_{22} (IV). It is expected that also at this sample little extra oxide has been introduced. At the up going *pH* sweep the response was flat between *pH* 1 and 3, but at the down going sweep there was still a response visible in this region. This may be an indication that the dissociation constants pK_a and pK_b of the (de)protonation reactions of Si-OH groups have changed somewhat during the measurements.

In order to quantify the found *pH* responses and thus the possible amounts of oxide in parameters from site binding theory, such as N_s, pK_a, pK_b, and C_{dl} the data has been fitted to routines written in Matlab, according to the model described in section 5.2.2.

Simulations

The simulation data has been manually fitted to the measurement data by varying the four parameters N_s, pK_a, and pK_b and C_{dl} until a good visual fit was obtained. C_{dl} on its turn consists of two capacitors in series, C_H and C_{diff}, as discussed in section 5.2.1. The diffuse layer capacitance, C_{diff}, is considered to be negligibly large since the experiments are performed in an 0.1 M electrolyte. This means that C_{dl} equals the Helmholtz capacitance, C_H. C_H is considered to be constant in electrochemical experiments but nonetheless its value differs in literature from 10-40 $\mu F\cdot cm^{-2}$ at metal electrodes [52] to 3-4 $\mu F\cdot cm^{-2}$ at semiconductor electrodes that are H-terminated [53] or modified with Si-C linked monolayers [45, 50], making C_H and thus C_{dl} an uncertain parameter. The sensitivity depends strongly on C_H (see Equation 5.7); a twofold decrease in C_H has the same effect as a twofold increase in β_{int}. Since β_{int} scales proportionally with N_s (see Equation 5.12) this means also that in this model a twofold decrease in C_H has the same effect as a twofold increase in N_s. This relation between C_H and N_s is illustrated in Figure 5.14, where two fits are depicted for the *pH* response of an electrode with SiO_2.

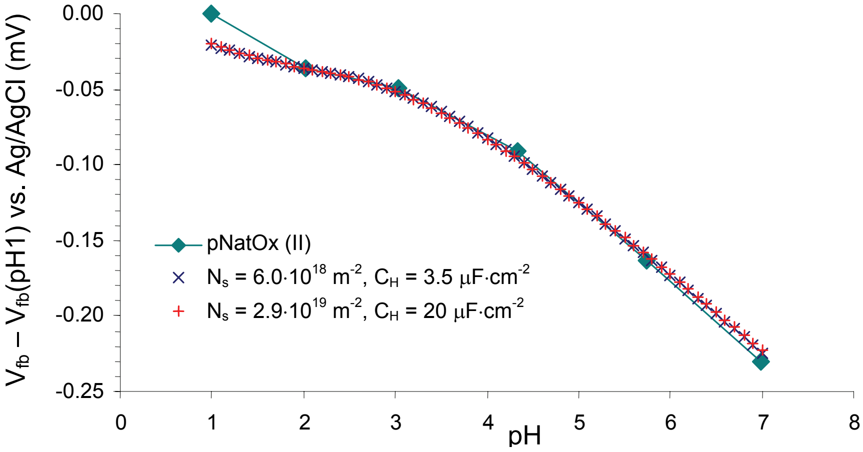

Figure 5.14. *pH* sensitivity data for sample pNatOx (II) with two different fit functions. The fit parameters were pK_a = 6.0 and pK_b = -2.0. N_s was fitted using two different values of C_H as indicated in the graph.

The data was fitted with $C_{H,1} = 20\ \mu F\cdot cm^{-2}$ and $C_{H,2} = 3.5\ \mu F\cdot cm^{-2}$ and similar fits were obtained. Fitting the data with $C_{H,1}$ leads to a very large $N_{s,1} = 2.9\cdot10^{19}\ m^{-2}$ and fitting the data with a lower $C_{H,2}$ a similar fit can be obtained but $N_{s,2}$ had to be lowered in the same degree as $C_{H,2}$ to $6.0 \cdot 10^{18}$ m^{-2}, which is very close to the theoretical value of $5.0 \cdot 10^{18}$ m^{-2} [58]. The latter observation can even be an indication that C_H at silicon electrodes with a layer of SiO_2 should also be lower than the value normally taken from metal electrodes. In conclusion, C_H is an uncertain parameter in the fitting procedure and an over- or underestimation of C_H leads consequently to an over- or underestimation of N_s. Therefore all fits were performed for both limiting values of C_H = 3.5 and 20 µF·cm^{-2} to provide a broad range of N_s values and incorporate the uncertainty in C_H.

An application example of the site binding theory on the data of an electrode modified with a Si-C linked monolayer is shown in Figure 5.15 together with three different fit functions where only the parameter N_s has changed.

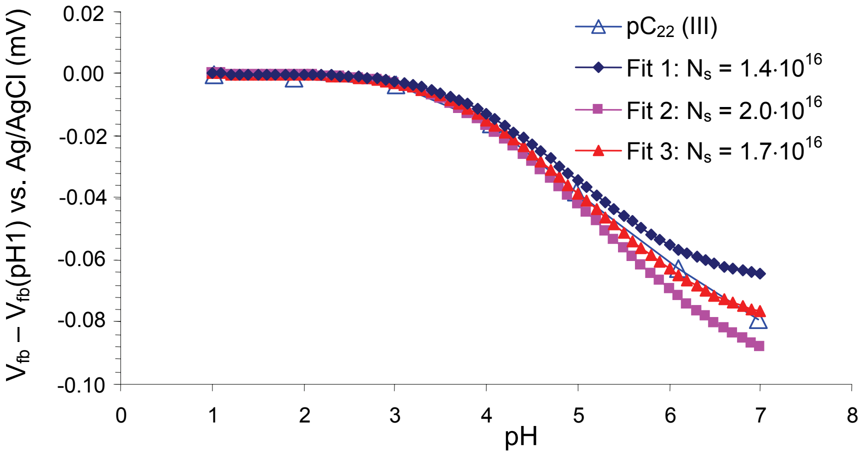

Figure 5.15. *pH* sensitivities for sample pC22 (III) with three different fit functions. The fit parameters were C_H = 3.5 µF·cm^{-2}, pK_a = 4.6 and pK_b = -3.2. N_s was varied as indicated in the graph.

In Figure 5.15 it is clearly indicated that the slope of the sensitivity at higher *pH*s is mainly determined by the number of active groups N_s. Fit function 1 with $N_s = 1.4 \cdot 10^{16}$ m^{-2} has a too low slope as compared to the measurement data. Even saturation occurs for $pH > 6$ so the number of active groups should be higher. Fit function 2 with $N_s = 2.0 \cdot 10^{16}$ m^{-2} has a too high slope so N_s should be lower. Fit function 3 with $N_s = 1.7 \cdot 10^{16}$ m^{-2} (this is a mere 0.34% of the active groups as compared to a pure SiO_2 surface [58] provided C_H = 3.5 µF·cm^{-2}) gives the optimal fit since the slope is equally steep to the slope of the measurement data. This example illustrates how small differences in N_s already result in different responses. A collection of the *pH* responses of tested samples together with their optimal fit functions can be found in Figure 5.16.

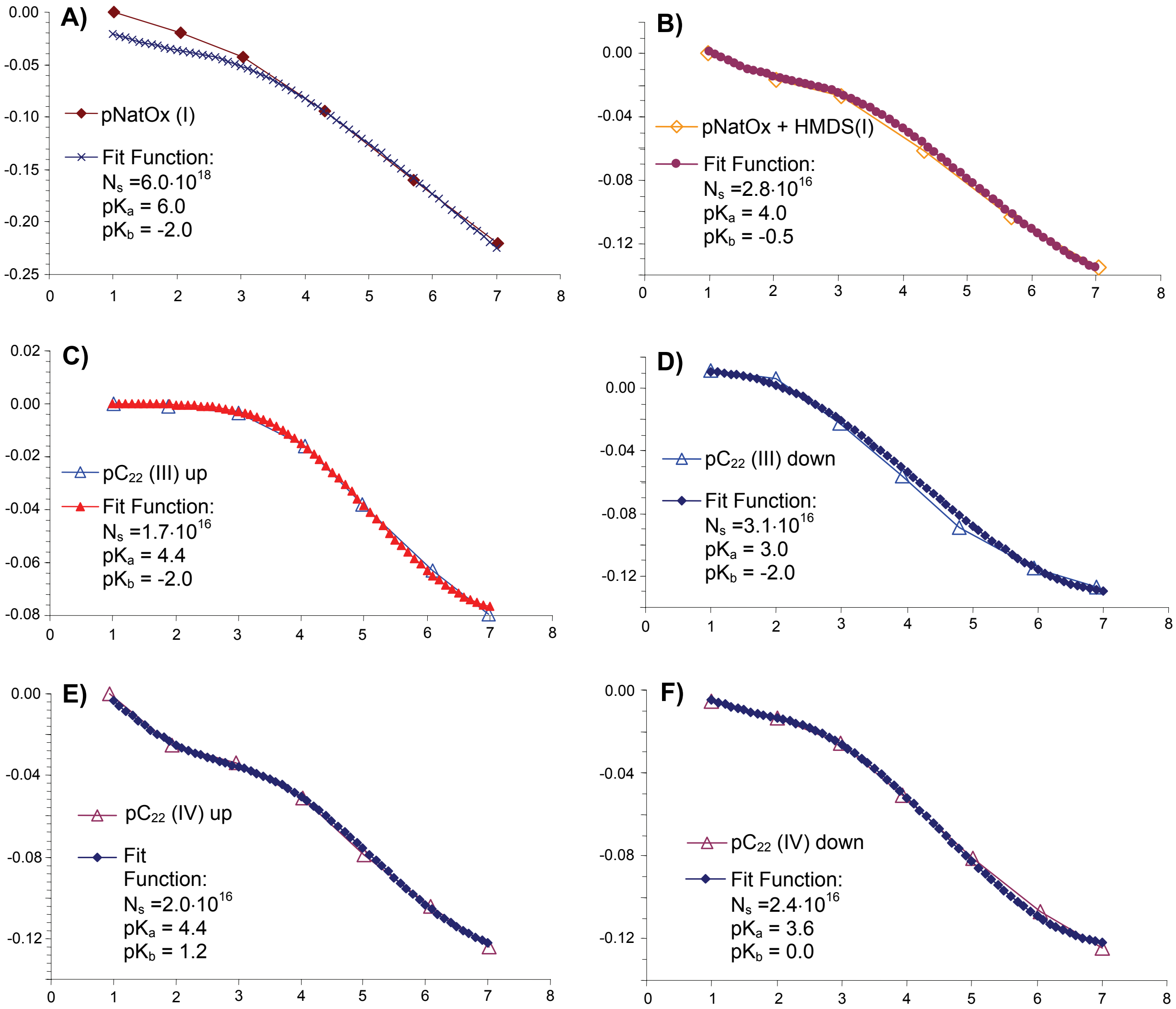

Figure 5.16. *pH* sensitivities and their best fit functions (using C_H = 3.5 μF·cm^{-2}) of 4 different samples. On the Y-axis is plotted: V_{fb} – V_{fb}(*pH1*) vs. Ag/AgCl [V] and on the X-axis the *pH* is plotted. The plots are A) p-type sample with SiO_2 insulator; B) p-type sample with SiO_2 insulator coated with HMDS; C) and D) pC_{22} (III) sample for up an down going *pH* sweep, respectively; E) and F) pC_{22} (IV) sample for up and down going *pH* sweep, respectively.

Good fits were obtained for all samples over the entire, measured *pH* range, demonstrating the versatility of such universal site binding model for different kinds of active surface layers. Although very good fits were obtained, the possible influence of OH^- adsorption process can not be ruled out. However, no direct influence of it could be observed in the measurement data. A theoretical case in which it should be observable is when the number of N_s of Si-OH sites is so low that saturation of charged sites would occur and a consequent lower or no response for the higher *pH* values would be observed according to the model (see Figure 5.6). If OH^- adsorption is then dominant a *pH* response will be measured for the higher *pH* values whereas the fit will only be good for lower *pH* values.

In Table 5.3 an overview is given of all simulation results for both values of C_H.

Table 5.3. The results of the fitting procedure for both C_H = 20 and 3.5 μF·cm^{-2} for several samples.

Sample	Sweep Up / Down	pK_a	pK_b	$N_{s,1}$ [10^{17} groups·m^{-2}] [a]	$N_{s,2}$ [10^{16} groups·m^{-2}] [b]
pC_{22} (I)	Up	4.2	0.5	1.3	2.6
pC_{22} (II)	Up	4.0	-2.0	1.6	3.2
pC_{22} (III)	Up	4.4	-2.0	0.8	1.6
	Down	3.0	-2.0	1.6	3.1
pC_{22} (VI)	Up	4.4	1.2	1.0	2.0
	Down	3.6	0.0	1.2	2.4
pNatOx (I)	Up	6.0	-2.0	$2.9 \cdot 10^2$	$6.0 \cdot 10^2$
pNatOx (II)	Up	6.0	-2.0	$2.9 \cdot 10^2$	$6.0 \cdot 10^2$
pNatOx + HMDS (I)	Up	4.0	0.5	1.4	2.8

[a] calculated using $C_{H,1}$ = 20 μF·cm^{-2}
[b] calculated using $C_{H,2}$ = 3.5 μF·cm^{-2}

On forehand it must be said the there is a large uncertainty in the values of pK_b (fourth column of Table 5.3). This is due to the fact that the influence of pK_b is noticeable for pH values $< pH_{pzc}$, which is for most samples around pH 1 and 2 and there are only one or two measurement points at pH 1 and pH 2 available for the determination of pK_b. Furthermore, the sensitivities are lowest around pH 1 and 2 which also hinders a good determination of pK_b, hence the large spreading in the values of pK_b. The values for N_s and pK_a are determined with more accuracy since more data points were available for these parameters.

In Table 5.3 the relation between the values for C_H and N_s is illustrated again, i.e. $N_{s,2} = N_{s,1} \cdot (C_{H,2} \cdot C_{H,1}^{-1})$. The samples with SiO_2 have a large number of $N_s = 2.9 \cdot 10^{19}$ m^{-2} for $C_{H,1}$ whereas for $C_{H,2}$ a value of $N_s = 6.0 \cdot 10^{18}$ m^{-2} is found, very close to the literature value of $N_s = 5 \cdot 10^{18}$ m^{-2} for pure SiO_2 surfaces [58]. This still higher value of N_s can be ascribed to the more porous nature of electrochemically grown (native) oxide [31] and the consequently higher number of Si-OH groups or alternatively, C_H should even be lower than 3.5μF·cm^{-2}. The values of pK_a =6 and pK_b = -2 are the literature values for SiO_2 surfaces [58].

The sample with SiO_2 surface coated with HMDS showed a large decrease in the number of active groups as can be expected since many OH groups are now bound to the HMDS. N_s dropped to $2.8 \cdot 10^{16}$ m^{-2} (using C_H = 3.5 μF·cm^{-2}), which correlates to only 0.56% of groups remaining as compared to pure SiO_2 surfaces. So few remaining surface groups are thus still able to give a considerable pH response as suspected also from Figure 5.4.

As compared to pure SiO_2 the pK_a value has dropped two units to pK_a = 4 or K_a has increased from $1 \cdot 10^{-6}$ to $1 \cdot 10^{-4}$. This lowering of pK_a was also observed for all samples with Si-C linked, organic monolayers. The values for pK_a for these samples varied between 4 – 4.4 in the up going pH sweep (Table 5.3). To provide more insight in the meaning of this lower pK_a Equation 5.9a has been rewritten to:

$$\frac{\upsilon_{SiO^-}}{\upsilon_{SiOH}} = \frac{K_a}{a_{H_S^+}} \text{ or } \log\left(\frac{\upsilon_{SiO^-}}{\upsilon_{SiOH}}\right) = \log\left(\frac{K_a}{a_{H_S^+}}\right) = pH_s^+ - pK_a \tag{5.9a}$$

A lower pK_a or higher K_a results in a higher amount of surface protons needed to obtain the same mole fraction of Si-O$^-$ groups with respect to the neutral Si-OH groups. Since the concentration of surface protons is directly related to the concentration of bulk protons (see Equation 5.5) a lower pK_a signifies also that a lower bulk pH or more bulk protons are needed to obtain the same mole fraction. In other words, it is harder for the surface to become deprotonated. It is also interesting to note that such a lower pK_a is in line with the process of OH$^-$ adsorption. Since both adsorbed OH$^-$ ions onto the monolayer and Si-O$^-$ groups in oxide spots in the monolayer will create a negative surface charge, it can be expected that these two processes compete with each other, resulting in more protons needed to obtain the same mole fraction of Si-O$^-$ vs. Si-OH groups as compared to bare SiO_2. Furthermore, it must be noted that the pK_a value obtained via fitting is in fact an average pK_a for the whole surface. There are a multitude of amphoteric groups which all have their own dissociation constants. This statistical distribution for the dissociation constants is a function of both space and time. The reason for this is that especially in the case of island formation, groups in the centre of large islands will behave approximately the same as Si-OH groups on a bare silicon oxide surface. Groups close to the organic chains will, however, suffer from a maximal influence of the hydrophobic organic groups. If such islands grow due to further oxidation, the surface conditions also change as a function of time. In conclusion, a proper understanding of the charging phenomena occurring at these samples with organic monolayer would benefit from a detailed study on the atomic scale and since the measurements performed here are in fact bulky, macro-measurements it is hard to distinguish between all possible different phenomena occurring at the surfaces of these samples, such as OH$^-$ adsorption, (de)protonation of Si-OH groups and surface morphology changes due to oxidation.

All pC_{22} samples showed also a strong decrease in the number of active surface groups as compared to pure SiO_2. N_s varied between the samples between $(1.6\text{-}3.2)\cdot10^{16}$ m^{-2} (for C_H = 3.5 µF·cm^{-2}), which corresponds to a mere 0.32 - 0.64% of total active surface groups as compared to pure SiO_2. This indicates that the organic monolayers cover the silicon surface to a very large degree and that only a very small fraction of the surface is in fact covered with oxide spots or islands. The two samples, pC_{22}(III) and (IV), for which also the down going pH sweep was measured, showed a small increase in N_s for the down going sweep (see Table 5.3 and Figure 5.16D and F). In both cases N_s increased to 3.1 and $2.4\cdot10^{16}$ m^{-2} (for C_H = 3.5 µF·cm^{-2}), respectively. This corresponds to 0.48 - 0.62% of active groups as compared to SiO_2 surfaces. The two samples likely showed a small degree of oxidation during the measurements. In both cases the pK_a shifted towards lower values indicating that surface Si-OH deprotonation became more difficult. A physical explanation of these even lower pK_a values is not available and more experiments are needed to understand this phenomenon.

Drift and initial settling

For all samples V_{fb} was measured at multiple points in time per pH to obtain information on initial settling phenomena and drift behavior. There was a large spreading in settling time between the samples with monolayers. Some did not show any settling time and showed very stable behavior of V_{fb}, while others had long settling times. This is illustrated with two examples in Figure 5.17.

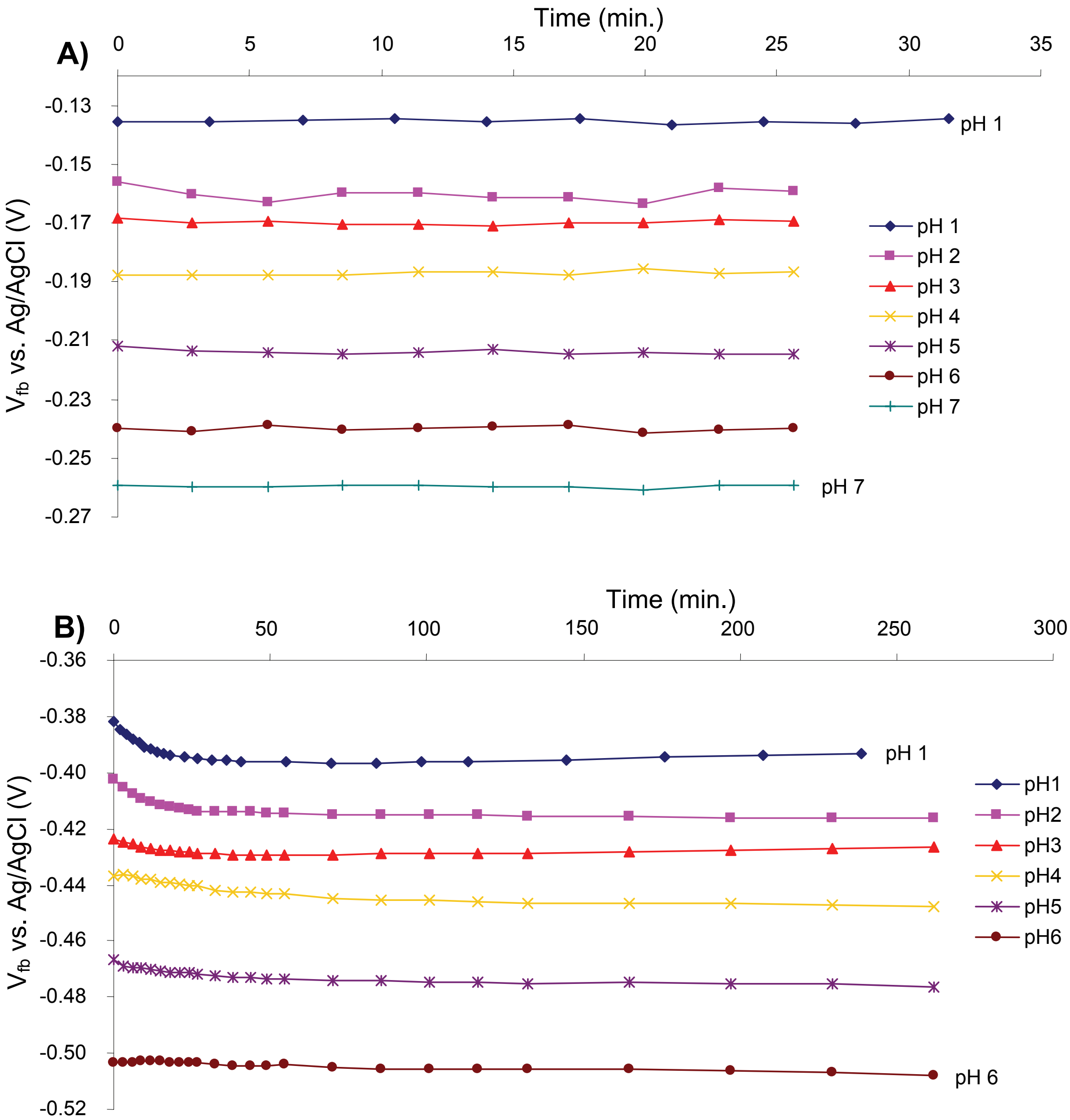

Figure 5.17. V_{fb} vs. time for different pH values. Two samples are shown: A) sample pC_{22} (IV) and B) sample pC_{22} (I). Note the different timescales for the two samples.

Sample pC_{22} (IV) in Figure 5.17A is an example of a sample without any settling time or very short settling times. At each *pH* value the sample was stable from the beginning and showed a very low drift rate during the 30 minutes measurement span. On the other hand, sample pC_{22} (I) shows initial, exponential-like settling times of approximately 30 minutes. This exponential settling time seemed to reduce for higher *pH* values. The physical phenomena causing the difference in settling times are not very clear up till now. The experimental measurement conditions of the two samples were similar so it is plausible that physical differences between the two samples cause the observed deviations between the samples. Perhaps surface states and differences in silicon-monolayer interface properties play a role in the settling behavior. After all, differences up to 450 mV in the starting values of V_{fb} were found for the electrodes with C_{22} monolayers (see Table 5.2), which can also be attributed to different interface charges and properties of the electrodes. In Figure 5.18 the drift behavior is examined in more detail for four different samples.

The sample with SiO_2 showed the largest drift in all three cases. For the two SiO_2 samples the drift was always in the positive direction at *pH* 1 and 2 and in the negative direction at *pH* 3 - 7. The SiO_2 sample with HMDS showed already less drift than the SiO_2 sample in the beginning 30 minutes as if the coverage with HMDS leads to a more stable behavior. Sample pC_{22} (I) showed initial drift (see Figure 5.17B) while sample pC_{22} (IV) hardly showed any initial drifting behavior (see Figure 5.17A). It can be concluded that all samples with monolayers showed more stable behavior than the samples with pure SiO_2. For three samples the long-term drift has also been determined. This is listed in Table 5.4.

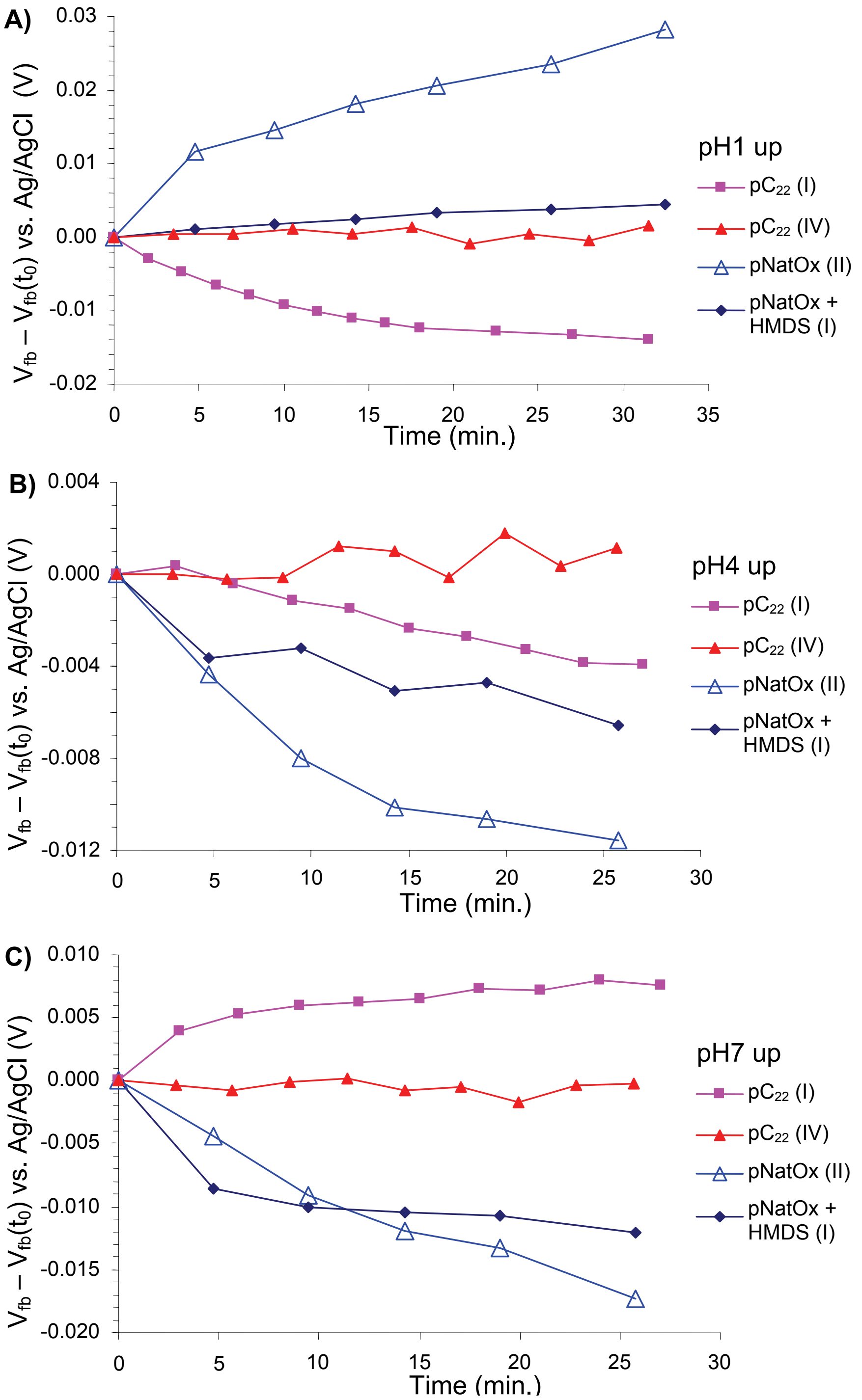

Figure 5.18. V_{fb} vs. time in the initial 30 minutes for four different samples at A) *pH* 1 sweep up, B) *pH* 4 sweep up and C) *pH* 7 sweep up. To provide a better overview all responses start at 0 V vs. Ag/AgCl at t_0, i.e. $V_{fb} – V_{fb}(t_0)$ is plotted on the left axis.

Table 5.4. Long term drift rate in mV·h^{-1} measured between 160 and 260 minutes.

Sample	*pH* 1	*pH* 2	*pH* 3	*pH* 4	*pH* 5	*pH* 6	*pH* 7
pC_{22} (I)	1.43	-0.41	0.78	-0.64	-0.93	-1.47	0.33
pC_{22} (II)	-4.87	-2.90	2.70	-1.32	0.31	0.0	-2.13
pC_{22} (III)	0.93	0.11	-10.07	-1.10	-0.46	-0.57	-1.19

On average sample pC_{22} (II) showed the highest drift albeit that this drift seems to be in random directions. For the other two samples the long-term drift stayed in most cases below 1 mV·h^{-1}. Also in their case the drift seems to be random, i.e. no preferential direction was observed as was the case for the samples with SiO_2 (see Figure 5.18). This is a rather low drift rate when compared with FETs with SiO_2 gates. Matsuo et al. [68] measured the drift of FETs with four different insulators after 10^3 minutes of operation in *pH* 7 solution. They could not determine the drift at SiO_2 ISFETs due to its instability and found a drift rate of 1.0 mV·h^{-1} at FETs with Si_3N_4 gates. Chen et al. [69] found a drift rate of approximately 1 mV·h^{-1} for SiO_2 ISFETs being immersed for ten hours. If one takes into account the simple fabrication routes of these monolayers and the lack of subsequential processing steps normally encountered in oxide gate-insulators the drift rates can be considered quite low. Furthermore, low drift rates indicate that there is a well-established and stable equilibrium between the silicon-monolayer structure on one side and the electrolyte on the other side. The above results are promising for further exploration of such monolayers in FET based devices.

5.4 Conclusions

P- and n-type silicon electrodes modified with unfunctionalized, Si-C linked monolayers, obtained via the surface alkylation of 1-alkenes, have electrochemically been characterized via a number of studies. The primary goal of these studies was to understand the electrochemical behavior of such modified electrodes in aqueous solutions before possibly applying such layers as gate insulators, and thus oxide-replacements, in FET-based sensors.

P-type electrodes and illuminated n-type electrodes modified with organic monolayers both get oxidized under anodic potentials and therefore, high anodic potentials should be avoided. From Mott Schottky measurements it was shown that the amount of oxide initially present and created under operating conditions was low, less than 1% as compared to pure SiO_2 surfaces. This remaining oxide, however, still caused a *pH* sensitivity of circa 25 mV·pH^{-1} in the *pH* 4 - 7 range. All samples with monolayers showed a reduced value of pK_a (4.0 - 4.4) as compared to pure SiO_2 (6.0), indicating more acidic behavior of the remaining Si-OH groups in such monolayers. Long-term drift during Mott Schottky measurements was low, less than 1 mV·h^{-1} in general. The above results clearly are promising for application of such organic monolayers in sensory EIS-structures, albeit that a cross sensitivity towards H^+ should be taken into account. Since such monolayers can be easily chemically modified with a large variety of receptor groups it is expected that a large variety of sensory structures can be created.

5.5 Experimental

5.5.1 Materials.

Silicon <100> 4" wafers (p-type: 5-10 Ω·cm and n-type: 1-10 Ω·cm) from Okmetic, Finland were used. KNO_3 (A.C.S. Reagent, 99+%) and TetraButylAmmoniumHydroxide 40% were purchased via Aldrich and used as received. TetraButylAmmoniumChloride (Fluka; purum, >97%), HexaMethylDiSilazane (HMDS) (Merck, VLSI grade), and Hydrogen Chloride 37% (Riedel – de Haën; extra pure) were used as received. Mesitylene (Fluka, 99%) was distilled and stored on $CaCl_2$. The dried mesitylene was filtered to remove traces of $CaCl_2$. 1-Hexadecene (Sigma, ~99%) and 1-dodecene (Fluka, ≥99%) were distilled at least twice at reduced pressure. Docosene (TCI America, 99+%) was used as received. HF (Fluka, 50% p.a.-plus) was diluted with demineralized H_2O.

5.5.2 Sample preparation.

Back contact fabrication and dicing

The wafers were first cleaned using a standard wafer cleaning (5 min. in 100% HNO_3, copious rinsing in demi water, 10 min. in boiling (69%) HNO_3 at 95°C and again copious rinsing in demi water). The front side was subsequently covered with HMDS and photoresist (Olin 907/12). After that the wafers were pre-baked at 120° C for 30 minutes. Then the wafers received a 1% HF dip to remove the native oxide from the backside. A metal contact was made to the wafer via sputtering. This contact was a 1000nm aluminum layer was directly sputtered. Next, a chromium layer was sputtered onto the aluminum on both type wafers to protect it from being etched in HF prior to monolayer formation. This was followed by an annealing step at 450° C in a N_2 atmosphere. The photo resist was removed with acetone. Finally, the samples were diced into pieces of 10mm x 10mm.

Monolayer fabrication

Cleaning: The samples of which the surface was to be modified with organic monolayers were first wiped with a tissue that was saturated with chemically pure acetone. After that, the samples were sonicated for at least 10 min. in demineralized water. After drying in a stream of nitrogen, the samples were sonicated for at least 10 min. in acetone. Then, the samples were rinsed copiously with acetone and dried in a stream of nitrogen. Subsequently, the samples were placed in an oxygen plasma cleaner (Harrick PDC-32G) for 1 - 5 min. The Si<100> samples were etched in 2.5% aqueous HF for 2 min.

Monolayer preparation: A solution (8-10 mL, 0.1 – 0.4 M) of 1-alkene in mesitylene was placed in a small three-necked flask fitted with a nitrogen inlet, a reflux condenser with a $CaCl_2$ tube, and a stopper. The solution was refluxed for at least 45 min under a flow of nitrogen. Subsequently, a cleaned and freshly etched sample was added to the refluxing solution, while a slow nitrogen flow was maintained. After 2 h the modified sample was removed from the solution and excessively rinsed with distilled PE40/60, EtOH, and CH_2Cl_2, respectively. An overview of the samples used for cyclic voltammetry experiments is given in Table 5.5.

Table 5.5. Properties of the samples used in the cyclic voltammetry experiments.

Sample abbreviation [a]	Dopant type	Monolayer	Contact angle [b] [°]
pC_{22} (A)	p<100>	$-C_{22}H_{45}$	107
pC_{22} (B)	p<100>	$-C_{22}H_{45}$	107
pC_{16} (A)	p<100>	$-C_{16}H_{33}$	100
pC_{16} (B)	p<100>	$-C_{16}H_{33}$	100
pC_{12} (A)	p<100>	$-C_{12}H_{25}$	109
nC_{22} (A)	n<100>	$-C_{22}H_{45}$	105
nC_{12} (A)	n<100>	$-C_{12}H_{25}$	106

[a] = Samples marked with (A) are displayed in Figure 5.8. Samples marked with (B) were measured for reproducibility and showed similar behavior as the (A) samples.

[b] = Errors are ± 1° for the contact angle measurements.

Samples with oxidized surfaces

The samples with SiO_2 insulators were taken from the diced wafers and were cleaned ultrasonically for 10 minutes in demi water and in pure acetone, consecutively. Samples that received a HMDS coating were subsequently put for 20 minutes in demi water at 80° C to activate as many as possible surface OH groups. After that, the samples were put in a beaker with pure HMDS that was covered with parafilm. This beaker was put for 1 hour in an oven at 60° C. Afterwards, the samples were spinned dry.

5.5.3 Instrumentation and settings

Cyclic voltammetry experiments

Samples were placed in a home-made Teflon electrochemical cell. The sample contacted the electrolyte via an O-ring, which left an area open of approximately 0.33 cm^2. All experiments were performed in 1.0 M KNO_3 under continuous argon bubbling through the electrolyte. The sample was connected as the working electrode to a EG&G Princeton Applied Research 273A potentiostat. To the same device, a saturated calomel (SCE) electrode and a platinum electrode were connected as reference electrode and counter electrode, respectively. The potentiostat was computer controlled via a home-made measurement program in Labview. For the measurements under illumination a Schott KL1500 light source at full power was used. Every measurement consisted of 5 consecutive scans from –1.5 V to +2.0 V and back to –1.5 V vs. SCE at a scan rate of 10 $mV{\cdot}s^{-1}$. Such low scan rate was chosen to minimize displacement current due to capacitive charging and to have the device under test in constant equilibrium. Before the start of the scan the sample was kept for 30 seconds at –1.5 V vs. SCE.

Capacitance – Voltage and *pH* titration experiments

The samples were first placed in a separate home-made Teflon sample holder. Via an opening with an O-ring in the holder the sample surface was in contact with the electrolyte. The area of this contacted surface was approximately 0.49 cm^2. This holder was consequently placed in a beaker glass with 65 ml of electrolyte and was connected as the working electrode to a Princeton Applied Research PARSTAT2263 potentiostat, which was computer controlled via the PowerSuite software package. To the potentiostat also an Ag/AgCl (sat'd KCl) electrode and a platinum electrode were connected as reference electrode and counter electrode, respectively. Impedance measurements were performed using a bias voltage sweep from –1.0 V to +0.5 V vs. Ag/AgCl in steps of 10 mV. The amplitude and frequency of the ac-voltage were 10 mV and 10 kHz, respectively. At each *pH* a number of at least 10 scans were performed over at least 30 minutes to a maximum of four and a halve hours to obtain information on settling times and drift. The *pH* was measured just before and right after a measurement sequence with a Ag/AgCl *pH* electrode and a Radiometer PHM83 autocal *pH* meter. The starting solution was 65 ml of 0.1 M TBACl solution to which was added a 260 µl of buffer mixture, containing 0.5 M acetic acid, 0.5 M boric acid, and 0.5 M of orthophosphate acid. This mixture was then set to *pH* 1 via titration with HCl. The *pH* values were varied either by (diluted) TBAOH or by (diluted) HCl. TBACl was originally chosen due to its inert behavior. However, since this is such a large, hydrophobic cation the assumption has arisen that it may in fact adsorb to the hydrophobic, organic monolayer. To be sure that such adsorption does not occur and may introduce unexpected side effects it is recommended to perform future measurements with smaller cations, such as the TetraEthylAmmonium (TEA) and TetraMethylAmmonium (TMA) cations.

5.6 References

[1] A. B. Sieval, A. L. Demirel, J. W. M. Nissink, M. R. Linford, J. H. van der Maas, W. H. de Jeu, H. Zuilhof, E. J. R. Sudhölter, "Highly stable Si-C linked functionalized monolayers on the silicon (100) surface", *Langmuir* **1998**, *14*, 1759.

[2] M. R. Linford, P. Fenter, P. M. Eisenberger, C. E. D. Chidsey, "Alkyl Monolayers on Silicon Prepared from 1-Alkenes and Hydrogen-Terminated Silicon", *Journal of the American Chemical Society* **1995**, *117*, 3145.

[3] M. R. Linford, C. E. D. Chidsey, "Alkyl Monolayers Covalently Bonded to Silicon Surfaces", *Journal of the American Chemical Society* **1993**, *115*, 12631.

[4] A. Bansal, X. L. Li, I. Lauermann, N. S. Lewis, S. I. Yi, W. H. Weinberg, "Alkylation of Si surfaces using a two-step halogenation Grignard route", *Journal of the American Chemical Society* **1996**, *118*, 7225.

[5] C. H. deVilleneuve, J. Pinson, M. C. Bernard, P. Allongue, "Electrochemical formation of close-packed phenyl layers on Si(111)", *Journal of Physical Chemistry B* **1997**, *101*, 2415.

[6] A. B. Sieval, V. Vleeming, H. Zuilhof, E. J. R. Sudhölter, "An improved method for the preparation of organic monolayers of 1-alkenes on hydrogen-terminated silicon surfaces", *Langmuir* **1999**, *15*, 8288.

[7] R. Boukherroub, S. Morin, F. Bensebaa, D. D. M. Wayner, "New synthetic routes to alkyl monolayers on the Si(111) surface", *Langmuir* **1999**, *15*, 3831.

[8] J. M. Buriak, "Organometallic chemistry on silicon and germanium surfaces", *Chemical Reviews* **2002**, *102*, 1271.

[9] A. B. Sieval, R. Linke, H. Zuilhof, E. J. R. Sudhölter, "High-quality alkyl monolayers on silicon surfaces", *Advanced Materials* **2000**, *12*, 1457.

[10] D. D. M. Wayner, R. A. Wolkow, "Organic modification of hydrogen terminated silicon surfaces", *Journal of the Chemical Society-Perkin Transactions 2* **2002**, 23.

[11] S. F. Bent, "Organic functionalization of group IV semiconductor surfaces: principles, examples, applications, and prospects", *Surface Science* **2002**, *500*, 879.

[12] N. Shirahata, A. Hozumi, T. Yonezawa, "Monolayer-derivative functionalization of non-oxidized silicon surfaces", *Chemical Record* **2005**, *5*, 145.

[13] L. J. Webb, N. S. Lewis, "Comparison of the electrical properties and chemical stability of crystalline silicon(111) surfaces alkylated using grignard reagents or olefins with Lewis acid catalysts", *Journal of Physical Chemistry B* **2003**, *107*, 5404.

[14] A. B. Sieval, C. L. Huisman, A. Schonecker, F. M. Schuurmans, A. S. H. van der Heide, A. Goossens, W. C. Sinke, H. Zuilhof, E. J. R. Sudholter, "Silicon surface passivation by organic monolayers: Minority charge carrier lifetime measurements and Kelvin probe investigations", *Journal of Physical Chemistry B* **2003**, *107*, 6846.

[15] W. J. Royea, A. Juang, N. S. Lewis, "Preparation of air-stable, low recombination velocity Si(111) surfaces through alkyl termination", *Applied Physics Letters* **2000**, *77*, 1988.

[16] Q.-Y. Sun, L. C. P. M. d. Smet, B. v. Lagen, M. Giesbers, P. C. Thüne, F. A. Wolf, H. Zuilhof, E. J. R. Sudhölter, "Covalently Attached Monolayers on Crystalline Hydrogen-Terminated Silicon: Extremely Mild Attachment by Visible Light", *Journal of the American Chemical Society* **2005**, *127*, 2514.

[17] N. S. Lewis, "Frontiers of research in photoelectrochemical solar energy conversion", *Journal of Electroanalytical Chemistry* **2001**, *508*, 1.

[18] N. S. Lewis, "Chemical control of charge transfer and recombination at semiconductor photoelectrode surfaces", *Inorganic Chemistry* **2005**, *44*, 6900.

[19] N. Saito, S. Youda, K. Hayashi, H. Sugimura, O. Takai, "Chemical resistivity of self-assembled monolayer covalently attached to silicon substrate to hydrofluoric acid and ammonium fluoride", *Surface Science* **2003**, *532*, 970.

[20] D. Vuillaume, "Nanometer-scale organic thin film transistors from self-assembled monolayers", *Journal of Nanoscience and Nanotechnology* **2002**, *2*, 267.

[21] Q. L. Li, G. Mathur, M. Homsi, S. Surthi, V. Misra, V. Malinovskii, K. H. Schweikart, L. H. Yu, J. S. Lindsey, Z. M. Liu, R. B. Dabke, A. Yasseri, D. F. Bocian, W. G. Kuhr, "Capacitance and conductance characterization of ferrocene-containing self-assembled monolayers on silicon surfaces for memory applications", *Applied Physics Letters* **2002**, *81*, 1494.

[22] E. A. Dalchiele, A. Aurora, G. Bernardini, F. Cattaruzza, A. Flamini, P. Pallavicini, R. Zanoni, F. Decker, "XPS and electrochemical studies of ferrocene derivatives anchored on n- and p-Si(1 0 0) by Si-O or Si-C bonds", *Journal of Electroanalytical Chemistry* **2005**, *579*, 133.

[23] K. M. Roth, A. A. Yasseri, Z. M. Liu, R. B. Dabke, V. Malinovskii, K. H. Schweikart, L. H. Yu, H. Tiznado, F. Zaera, J. S. Lindsey, W. G. Kuhr, D. F. Bocian, "Measurements of electron-transfer rates of charge-storage molecular monolayers on Si(100). Toward hybrid molecular/semiconductor information storage devices", *Journal of the American Chemical Society* **2003**, *125*, 505.

[24] F. Wei, B. Sun, Y. Guo, X. S. Zhao, "Monitoring DNA hybridization on alkyl modified silicon surface through capacitance measurement", *Biosensors & Bioelectronics* **2003**, *18*, 1157.

[25] W. Liao, F. Wei, M. X. Qian, X. S. Zhao, "Characterization of protein immobilization on alkyl monolayer modified silicon(111) surface", *Sensors and Actuators B-Chemical* **2004**, *101*, 361.

[26] W. Cai, J. R. Peck, D. W. van der Weide, R. J. Hamers, "Direct electrical detection of hybridization at DNA-modified silicon surfaces", *Biosensors and Bioelectronics* **2004**, *19*, 1013.

[27] E. J. Faber, L. C. P. M. de Smet, W. Olthuis, H. Zuilhof, E. J. R. Sudhölter, P. Bergveld, A. van den Berg, "Si-C Linked Organic Monolayers on Crystalline Silicon Surfaces as Alternative Gate Insulators", *ChemPhysChem* **2005**, *6*, 2153.

[28] Y. J. Liu, H. Z. Yu, "Alkyl monolayer-passivated metal-semiconductor diodes: Molecular tunability and electron transport", *ChemPhysChem* **2002**, *3*, 799.

[29] D. K. Schroder, *Semiconductor Material and Device Characterization*, 2nd ed., Wiley, New York, **1998**.

[30] E. Yablonovitch, D. L. Allara, C. C. Chang, T. Gmitter, T. B. Bright, "Unusually Low Surface-Recombination Velocity on Silicon and Germanium Surfaces", *Physical Review Letters* **1986**, *57*, 249.

[31] X. G. Zhang, *Electrochemistry of Silicon and its Oxide*, Kluwer Academic Publishers, New York, **2001**.

[32] Y. J. Liu, H. Z. Yu, "Effect of organic contamination on the electrical degradation of hydrogen-terminated silicon upon exposure to air under ambient conditions", *Journal of the Electrochemical Society* **2003**, *150*, G861.

[33] D. Graf, M. Grundner, R. Schulz, L. Muhlhoff, "Oxidation of Hf-Treated Si Wafer Surfaces in Air", *Journal of Applied Physics* **1990**, *68*, 5155.

[34] S. I. Raider, R. Flitsch, M. J. Palmer, "Oxide Growth on Etched Silicon in Air at Room Temperature", *Journal of the Electrochemical Society* **1975**, *122*, 413.

[35] M. Morita, T. Ohmi, E. Hasegawa, M. Kawakami, K. Suma, "Control Factor of Native Oxide-Growth on Silicon in Air or in Ultrapure Water", *Applied Physics Letters* **1989**, *55*, 562.

[36] M. Morita, T. Ohmi, E. Hasegawa, M. Kawakami, M. Ohwada, "Growth of Native Oxide on a Silicon Surface", *Journal of Applied Physics* **1990**, *68*, 1272.

[37] T. Miura, M. Niwano, D. Shoji, N. Miyamoto, "Kinetics of oxidation on hydrogen-terminated Si(100) and (111) surfaces stored in air", *Journal of Applied Physics* **1996**, *79*, 4373.

[38] J. E. Olsen, F. Shimura, "Infrared analysis of film growth on the silicon surface in room air", *Journal of Vacuum Science & Technology A: Vacuum, Surfaces, and Films* **1989**, *7*, 3275.

[39] G. J. Kluth, R. Maboudian, "Oxidation mechanism of the ammonium-fluoride-treated Si(100) surface", *Journal of Applied Physics* **1996**, *80*, 5408.

[40] M. L. W. Vanderzwan, J. A. Bardwell, G. I. Sproule, M. J. Graham, "Mechanism of the Growth of Native-Oxide on Hydrogen Passivated Silicon Surfaces", *Applied Physics Letters* **1994**, *64*, 446.

[41] A. Bansal, N. S. Lewis, "Stabilization of Si photoanodes in aqueous electrolytes through surface alkylation", *Journal of Physical Chemistry B* **1998**, *102*, 4058.

[42] A. Bansal, N. S. Lewis, "Electrochemical properties of (111)-oriented n-Si surfaces derivatized with covalently-attached alkyl chains", *Journal of Physical Chemistry B* **1998**, *102*, 1067.

[43] S. Takabayashi, M. Ohashi, K. Mashima, Y. Liu, S. Yamazaki, Y. Nakato, "Surface structures, photovoltages, and stability of n-Si(111) electrodes surface modified with metal nanodots and various organic groups", *Langmuir* **2005**, *21*, 8832.

[44] H. Z. Yu, R. Boukherroub, S. Morin, D. D. M. Wayner, "Facile interfacial electron transfer through n-alkyl monolayers formed on silicon (111) surfaces", *Electrochemistry Communications* **2000**, *2*, 562.

[45] H. Z. Yu, S. Morin, D. D. M. Wayner, P. Allongue, C. H. de Villeneuve, "Molecularly tunable "organic capacitors" at silicon/aqueous electrolyte interfaces", *Journal of Physical Chemistry B* **2000**, *104*, 11157.

[46] C. J. Barrelet, D. B. Robinson, J. Cheng, T. P. Hunt, C. F. Quate, C. E. D. Chidsey, "Surface characterization and electrochemical properties of alkyl, fluorinated alkyl, and alkoxy monolayers on silicon", *Langmuir* **2001**, *17*, 3460.

[47] J. Cheng, D. B. Robinson, R. L. Cicero, T. Eberspacher, C. J. Barrelet, C. E. D. Chidsey, "Distance dependence of the electron-transfer rate across covalently bonded monolayers on silicon", *Journal of Physical Chemistry B* **2001**, *105*, 10900.

[48] F. Wei, X. S. Zhao, "The capacitance of mixed alkyl monolayers on Si(111) surface", *Thin Solid Films* **2002**, *408*, 286.

[49] P. Allongue, C. H. de Villeneuve, J. Pinson, F. Ozanam, J. N. Chazalviel, X. Wallart, "Organic monolayers on Si(111) by electrochemical method", *Electrochimica Acta* **1998**, *43*, 2791.

[50] P. Allongue, C. H. de Villeneuve, J. Pinson, "Structural characterization of organic monolayers on Si < 111 > from capacitance measurements", *Electrochimica Acta* **2000**, *45*, 3241.

[51] P. Bergveld, A. Sibbald, *Analytical and Biomedical Applications of Ion-Selective Field-Effect Transistors, Vol. XXIII*, Elsevier, **1988**.

[52] A. J. Bard, L. R. Faulkner, *Electrochemical Methods, Fundamentals and Applications*, John Wiley & Sons, **1980**.

[53] G. Oskam, J. C. Schmidt, P. C. Searson, "Electrical Properties of n-Type (III) Si in Aqueous $K_4Fe(CN)_6$ Solution", *Journal of The Electrochemical Society* **1996**, *143*, 2538.

[54] D. E. Yates, S. Levine, T. W. Healy, "Site-binding model of the electrical double layer at the oxide/water interface", *Journal of the Chemical Society, Faraday Transactions 1* **1974**, *70*, 1807.

[55] L. Bousse, *The Chemical Sensitivity of Electrolyte/Insulator/Silicon Structures: Fundamentals of ISFET Operation*, PhD thesis, Universtity of Twente (Enschede), **1982**.

[56] A. v. d. Berg, *Ion Sensors based on ISFETs with Synthetic Ionophores*, PhD thesis, University of Twente (Enschede), **1988**.

[57] R. E. G. van Hal, J. C. T. Eijkel, P. Bergveld, "A novel description of ISFET sensitivity with the buffer capacity and double-layer capacitance as key parameters", *Sensors and Actuators B: Chemical* **1995**, *24*, 201.

[58] R. E. G. van Hal, J. C. T. Eijkel, P. Bergveld, "A general model to describe the electrostatic potential at electrolyte oxide interfaces", *Advances in Colloid and Interface Science* **1996**, *69*, 31.

[59] R. C. Weast, M. J. Astle, W. H. Beyer, *CRC Handbook of Chemistry and Physics*, 65th ed., CRC Press, Boca Raton, Florida, **1984**.

[60] E. S. Kooij, *Silicon: Electrochemistry and Luminescence*, PhD thesis, University of Utrecht (Utrecht), **1997**.

[61] A. B. Sieval, B. van den Hout, H. Zuilhof, E. J. R. Sudhölter, "Molecular Modeling of Alkyl Monolayers on the Si(111) Surface", *Langmuir* **2000**, *16*, 2987.

[62] A. B. Sieval, B. van den Hout, H. Zuilhof, E. J. R. Sudhölter, "Molecular Modeling of Covalently Attached Alkyl Monolayers on the Hydrogen-Terminated Si(111) Surface", *Langmuir* **2001**, *17*, 2172.

[63] A. B. Sieval, *Covalently Bound Organic Monolayers on Hydrogen-Terminated Silicon Surfaces*, PhD thesis, Wageningen University (Wageningen), **2001**, chapter 3, p. 44.

[64] K. G. Marinova, R. G. Alargova, N. D. Denkov, O. D. Velev, D. N. Petsev, I. B. Ivanov, R. P. Borwankar, "Charging of oil-water interfaces due to spontaneous adsorption of hydroxyl ions", *Langmuir* **1996**, *12*, 2045.

[65] H. J. Kreuzer, R. L. C. Wang, M. Grunze, "Hydroxide ion adsorption on self-assembled monolayers", *Journal of the American Chemical Society* **2003**, *125*, 8384.

[66] Y. H. M. Chan, R. Schweiss, C. Werner, M. Grunze, "Electrokinetic characterization of oligo- and poly(ethylene glycol)-terminated self-assembled monolayers on gold and glass surfaces", *Langmuir* **2003**, *19*, 7380.

[67] R. Schweiss, P. B. Welzel, C. Werner, W. Knoll, "Dissociation of surface functional groups and preferential adsorption of ions on self-assembled monolayers assessed by streaming potential and streaming current measurements", *Langmuir* **2001**, *17*, 4304.

[68] T. Matsuo, M. Esashi, "Methods of isfet fabrication", *Sensors and Actuators* **1981**, *1*, 77.

[69] S. C. Chen, Y.-K. Su, J. S. Tzeng, "The fabrication and characterisation of ion-sensitive field-effect transistors with a silicon dioxide gate", *Journal of Physics D: Applied Physics* **1986**, *19*, 1951.

Appendix A

Adsorption measurements of cations

For proper electrochemical measurements the choice for a suitable background electrolyte is important. The background electrolyte should not be chemically reactive with the silicon electrode and furthermore, it should not adsorb or bind non-specifically to the insulator surface. The latter phenomenon could result in worst case into a change of binding dynamics of target species in the solution with functional receptor groups on the insulator surface.

Originally from ISFET technology in the BIOS group TetraButylAmmoniumChloride (TBACl) is chosen as a background electrolyte, because of is large size (diameter ~1 nm) compared to alkaline cations (e.g. potassium (K) and Sodium (Na), which have radii of 0.133 nm and 0.098 nm, respectively) as to prevent diffusion of the cation into the oxide layer. A hypothesis, however, is that because of the large alkyl chains, TBA will be hydrophobic (i.e. lipophillic) and prefers to be in the vicinity of the organic monolayer.

In this appendix the non-specific interaction between cations of different electrolytes and the monolayer surface is treated. With the use of two different techniques, namely Mott Schottky and reflectometry measurements, an electrolyte system with the least number of disadvantages can hopefully be chosen.

First Mott Schottky measurements were performed as to determine a change in flatband potential as a function of TBA concentration. If a higher concentration leads to more accumulated, adsorbed TBA cations on the surface this will consequently lead to a more positively charged surface layer that will shift the flatband voltage, V_{fb}. However, these measurements were not successful and no conclusions could be drawn from them.

Another attempt to investigate cation adsorption was by reflectometry measurements. In a reflectometry measurement a coherent circularly polarized (p- and s- type polarization are equal) laser is pointed at the monolayer. The reflected light is coherently detected by two photo detector arrays (one for the s-type and one for the p-type polarization). The ratio of the two polarization directions is a measure of the number of absorbed particles. The exact relation between the two is determined via a calibration curve. A calibration curve can be determined both experimentally as well as theoretically. Because neither quantitative theory nor calibration experiments were found in literature for this specific experiment, there is no calibration curve. The hypothesis is, however, a qualitative one, which means that we are only interested in a change in reflection (i.e. change in number of absorbed particles) and not in the absolute value of this change.

The samples used for these tests were strips of silicon wafers modified thermally with 1-hexadecene. The samples are placed in a homemade flow-cell. The solutions are flushed through the flow-cell by gravitational and rotor driven hydrodynamics. The different solutions are placed at the same height with respect to the flow-cell to obtain a constant flow through the cell. Waste is removed from the cell by a rotor pump. Three different cations have been used in this study. The TBA cation is the largest cation with four butyl-chains attached to each nitrogen atom. It is also expected to be the most hydrophobic one and thus most prone to adsorb to the monolayer. The TMA cation is the smallest TetraAlkylAmmonium cation with four methyl groups attached to each nitrogen atom. Since it is less hydrophobic than TBA it is expected to give a much lower adsorption, if any, than the TBA cation. Sodium is used as a reference since this cation is very hydrophilic and it is expected that it will show completely no adsorption with monolayer. Measurements are performed on an optical table and inside a darkened cabinet. For the measurements four different solutions are used (see Table 5A.1).

Table 5A.1. Solutions used for reflectometry experiments.

Solution	Composition
B	10 mM NaCl
C	10 mM NaCl + 5 mM TBACl
D	15 mM NaCl
E	10 mM NaCl + 5 mM TMACl

Solution B and D are used as a standard background signal. Solution C and E are used to estimate the absorption of TBACl and TMACl on the monolayer. In Figure 5A.1 the result of the first measurement is shown.

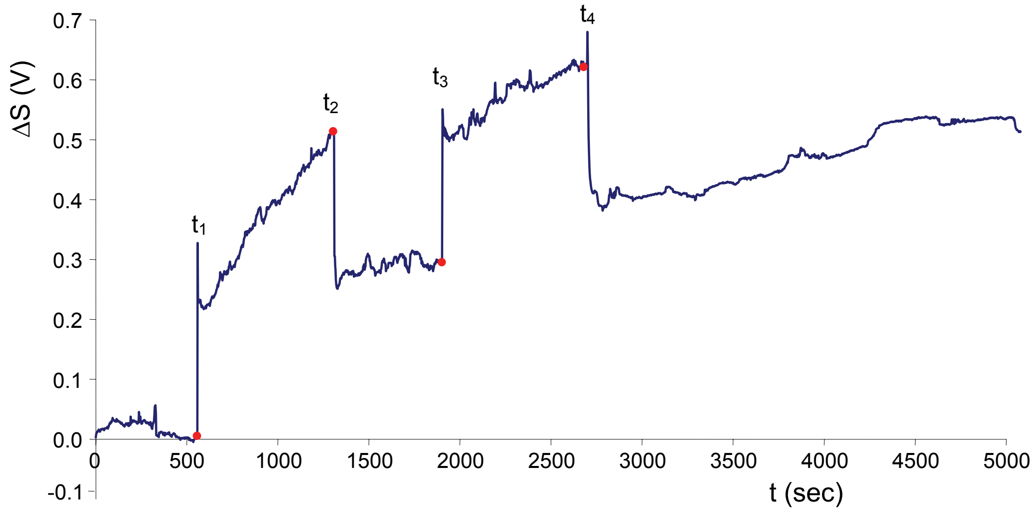

Figure 5A.1. Reflectometry data measured at a <100> silicon sample with C_{16} monolayer for different solutions. The dots with the accompanying numbers represent the following solution replacements: t_1 = B → C, t_2 = C → B, t_3 = B → C, and t_4 = C → B.

In Figure 5A.1 it is obvious that there is a large change in signal when a sodium containing solution is substituted by a solution that contains both sodium and TBA. A problem with this result is, however, that not only the composition of the solution changes, but also the concentration is increased by 50% (which is known to have an influence on the refractive index of the solution, which changes the output signal). Therefore a new experiment has been performed in which the concentration of the solution is kept constant. The result of this experiment is given in Figure 5A.2.

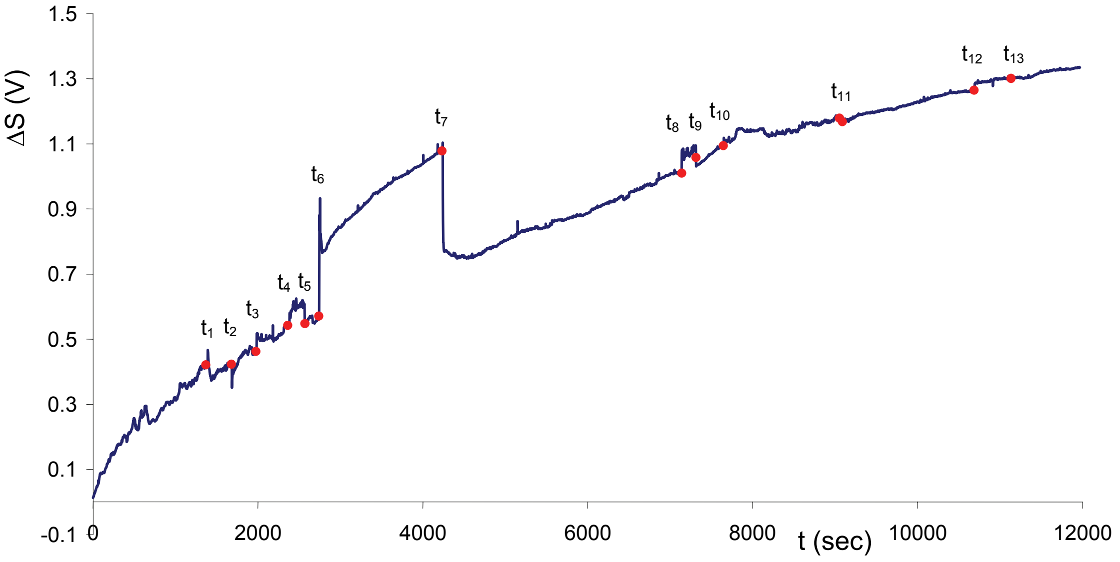

Figure 5A.2. Reflectometry data measured at a <100> silicon sample with C_{16} monolayer for different solutions. The dots with the accompanying numbers represent the following solution replacements: t_1 = B → D, t_2 = D → B, t_3 = D → B, $t_{4,5}$ = change of vessels with electrolytes and consequent opening and closing of cabinet, t_6 = D → C, t_7 = C → D, $t_{8,9}$ = change of vessels with electrolytes and consequent opening and closing of cabinet, t_{10} = D → E, t_{11} = E → D, t_{12} = D → E, and t_{13} = E → D.

In figure 5A.2 it can be observed that the change in signal, caused by a change in concentration of the electrolyte, is negligible in comparison with the signal change caused by a change of cation type (from solely sodium at $t_{1,2,3}$ to sodium and TBA at $t_{6,7}$). In this result again a large signal shift occurs when at t_6 TBA is added to the solution. When TMA is added to the system at t_{11} the signal change is negligible to the response caused by TBA. Another experiment has been performed to verify the results depicted in Figure 5A.2. The result of this last experiment is given in Figure 5A.3.

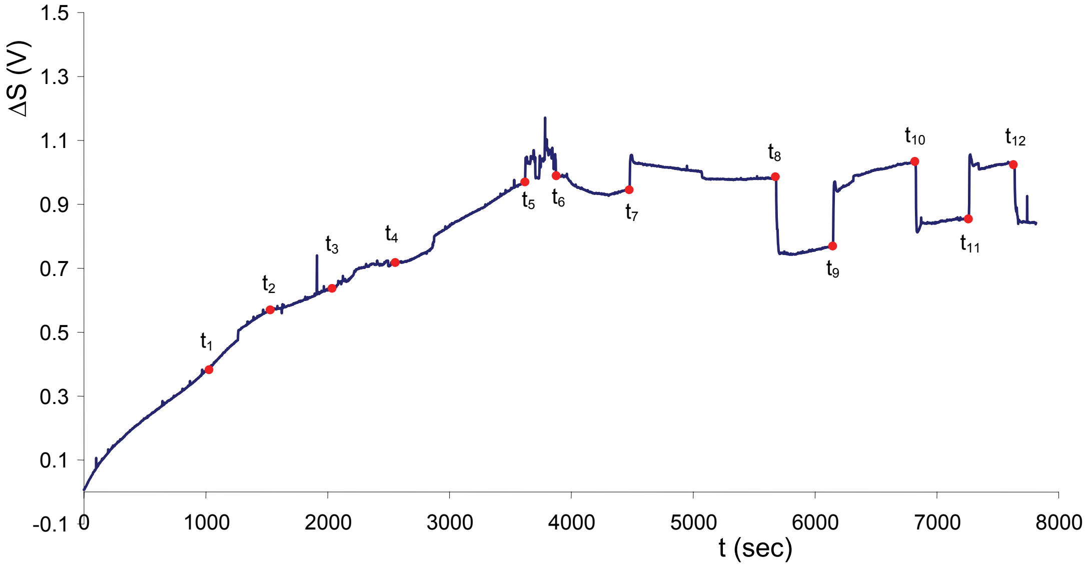

Figure 5A.3. Reflectometry data measured at a <100> silicon sample with C_{16} monolayer for different solutions. The dots with the accompanying numbers represent the following solution replacements: t_1 = D → E, t_2 = E → D, t_3 = D → E, t_4 = E → D, $t_{5,6}$ = change of vessels with electrolytes and consequent opening and closing of cabinet, t_7 = D → C, t_8 = C → D, t_9 = D → C, t_{10} = C → D, t_{11} = D → C, and t_{12} = C → D.

In Figure 5A.3 it can be observed that again changing solutions with solely Na cations to the solution with TMA ($t_{1\text{-}4}$) causes a negligible shift in signal as compared to changing solutions from solely Na to the solution with TBA ($t_{7\text{-}12}$). These reflectometry measurements indicate that indeed TBA absorbs to the monolayer surface, because there is an obvious correlation between signal change and the substitution of the solely sodium containing solution and the solution containing both sodium and TBA. Another observation that can be made from these measurements is that the solution with TMA causes a negligible change in signal as compared to the solution with TBA. However, caution should be maintained when drawing the conclusion from these measurements that TMA does not absorb to the monolayer. The reason for this caution is that TMA is a much smaller cation than TBA and is, therefore, expected to cause a smaller signal change when binding to the surface. Therefore, it is possible that TMA also absorbs to the surface, but is causing a signal change that is of such magnitude that it is smaller than the background noise of the system.

In conclusion, it is recommended that TBACl as a background electrolyte should not be used for electrochemical characterizations of silicon samples modified with organic monolayers since there are indications of TBA adsorption onto these monolayers.

Chapter 6

Ion Sensing using EIS-structures and Hybrid Organic Semiconductor FETs (HOSFETs) with crown ether functionalized, Si-C linked Monolayers

Abstract: This chapter contains a collection of results on ion-sensing measurements with Hybrid Organic Semiconductor FETs (HOSFETs) and EIS-structures with functionalized monolayers. The results are very promising, though not fully conclusive. HOSFETs with unfunctionalized monolayers display *pH* sensitivity, and just like the EIS-structures with unfunctionalized monolayers this is strongly reduced as compared to pure SiO_2 gate insulators. This indicates that despite the good surface coverage of the monolayer still some SiO_2 sites are available. Crown ethers (15-crown-5) are subsequently incorporated in mixed monolayers to obtain functionalities towards Na^+ and K^+ ions. Via measurements on HOSFETs and EIS-structures modified with such monolayers and pure $–C_{10}H_{21}$ monolayers or pure SiO_2 as a reference, the highest sensitivity towards both cations is found for SiO_2, followed by the functionalized monolayers whereas no sensitivity at all for the inert monolayers. The fact that inert monolayers are insensitive towards cations shows the potential of these monolayers in creating sensing structures made from silicon with Si-C linked monolayers. It is reasoned that the poor results of the cation sensing measurements can in fact be attributed to poor binding properties of the chosen receptor and not to deficiencies of the supporting silicon-monolayer device.

6.1 Introduction

Since their introduction more than 35 years ago by Bergveld [1, 2] FET based sensors have contributed a major part to electrochemical and physical sensors [3, 4]. The original Ion Selective FET sensor (ISFET) used a metal oxide or SiO_2 as sensing material and was sensitive towards H^+ [1, 2]. Not long after those first papers many variations arose upon the original concept of the ISFET sensor towards sensing other species in liquids, such as other ions than H^+ (CHEMFET), enzymes (ENFET) and even biochemical substances (BIOFET) [5]. Furthermore, FET based sensors have been developed that operate in other media such that they response to for instance gasses (GASFET) or pressure (PRESSFET) [5]. More recently, a FET based sensor able to measure the concentration of H_2O_2 was developed (^{E}MOSFET), of which the measuring principle was not based on the change of surface potential but on a direct modulation of the gate work function [3].

The most important functional element of the FET based sensors is formed by the Electrolyte-Insulator-Silicon (EIS) structure [4]. This is the electrochemical analogue of the solid-state Metal-Insulator (or Oxide)-Silicon (MIS or MOS) structure [6, 7], which on its turn is the functional element of the MOSFET device. Schematic pictures of both MIS- and EIS-structures are shown in Figure 6.1.

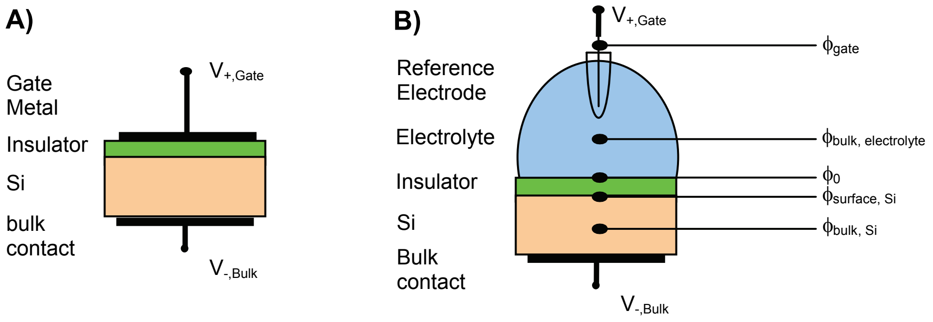

Figure 6.1. Schematic setup of A) a MIS-structure and B) an EIS-structure with a two-electrode connection. Also indicated in B) are the potentials at different locations in the EIS-structure.

EIS-structures can be used as sensory elements due to the fact that the surface layer of the gate insulator (mostly oxides) shows specific interactions with protons in the bulk of the solution. The result of such specific interaction between those protons and charged groups on the insulator surface, i.e. so-called (de)protonation of surface X-OH groups (X = Ta, Al, Si etc.), is depicted in Figure 6.2.

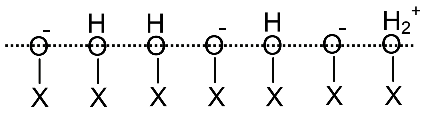

Figure 6.2. Graphical interpretation of (de)protonation of surface X-OH groups (X = Ta, Al, Si etc.).

The *pH* dependent potential on the surface is called ϕ_0 and the potential in the bulk is called ϕ_{bulk}. Since the latter is constant and can be taken zero as a reference, the potential difference between surface and bulk will simply be written as ϕ_0. ϕ_0 is located within the device as depicted in Figure 6.1B and can thus not be determined directly. However, via external connections as shown in Figure 6.1B ϕ_0 can be determined. The characteristic voltage of the EIS-structure is the so-called flatband voltage V_{fb}, which is the externally applied voltage needed to make all energy bands in the silicon flat from bulk to the surface [6]. V_{fb} can be written as Equation 6.1a [4] :

$$V_{fb} = E_{ref} - \phi_0 + \chi_{sol} - \frac{\Phi_{Si}}{q} - \frac{Q_{ins} + Q_{ss}}{C_{ins}} \qquad (6.1a)$$

where E_{ref} is the contribution of the reference electrode; χ_{sol} is the surface dipole potential of the solution; Φ_{Si} is the silicon workfunction; Q_{ins} and Q_{ss} are the insulator charge and surface states charge, respectively and these are zero in ideal cases; C_{ins} is the insulator capacitance. Except for ϕ_0 all the other terms are constant and *pH* independent. Although in the early days of FET based sensor research, surface states were also thought to display a *pH* dependent influence on V_{fb} the work of Diot et al. [8] showed that this was not the case. In the case of MIS-structures the flatband voltage is also a characteristic voltage and can be written simply as in Equation 6.1b [6, 7]:

$$V_{fb} = \frac{\Phi_M}{q} - \frac{\Phi_{Si}}{q} - \frac{Q_{ins} + Q_{ss}}{C_{ins}} \qquad (6.1b)$$

where Φ_M is the gate metal silicon workfunction and the other variables are the same as for Equation 6.1a. Equation 6.1a can in fact be regarded as the adapted from of Equation 6.1b in which the term $\Phi_M \cdot q^{-1}$ term (due to the gate metal) has been replaced by the term E_{ref} - ϕ_0 - χ_{sol} (due to the reference electrode and electrolyte).

The MOS- and EIS-structures can now be incorporated in the FET device and schematic drawings of both MOSFET and ISFET device are drawn together with all relevant electrical connections in Figure 6.3.

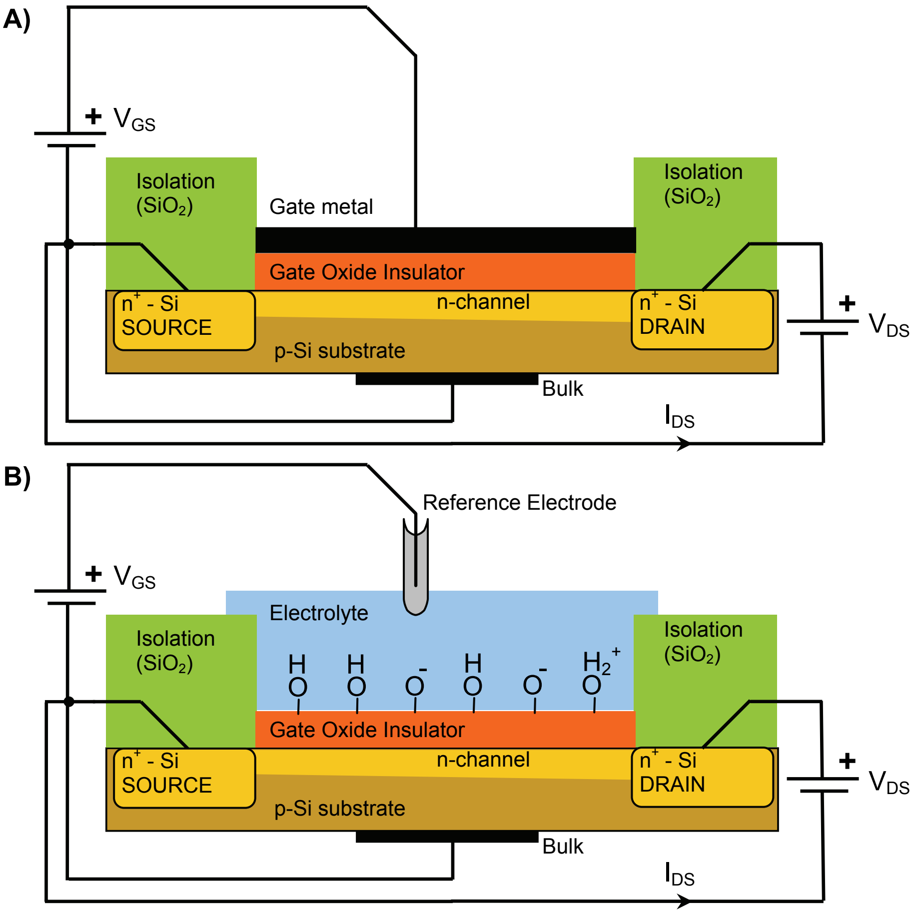

Figure 6.3. Schematic drawings of four terminal n-channel FET devices: A) MOSFET and B) ISFET.

The characteristic voltage of both FET devices is the threshold voltage V_{th} that can be roughly described as the onset voltage of the FET device, i.e. for $V_{GS} > V_{th}$ the channel between source and drain is opened and a source drain current I_{DS} can flow. For both devices the threshold voltage can be written as Equation 6.2 [6]:

$$V_{th} = V_{fb} + \psi_{s,inv} + \frac{Q_{inv}}{C_{ins}} \quad \text{with } Q_{inv} = \sqrt{2q\varepsilon_0\varepsilon_{r,Si}N_A\psi_{s,inv}} \qquad (6.2)$$

where $\psi_{s,inv}$ is the silicon surface potential (see Figure 6.1B) at inversion, which is in general taken to be equal to $2\psi_B = 2kT\cdot q^{-1}\cdot\ln(N_A\cdot n_i^{-1})$ with $2kT\cdot q^{-1}$ being the thermal voltage (25.7 mV at 298 K), N_A is the substrate doping and n_i is the carrier density for intrinsic silicon ($1.45\cdot10^{10}$ cm^{-3}) [6]; Q_{inv} is the charge at the silicon surface at the onset of inversion [6] and C_{ins} is the insulator capacitance; V_{fb} is the flatband voltage as defined above and for MOSFETs and ISFETs the Equations 6.1b and 6.1a should be substituted, respectively.

Finally, the external drain-source current I_{DS} can be written as a function of V_{th}, V_{DS} and V_{GS} as shown in Equation 6.3a (non-saturated or linear mode) and 6.3b (saturated mode):

$$I_{DS} = \mu C_{ins} \frac{W}{L}\left[(V_{GS} - V_{th})V_{DS} - \tfrac{1}{2}V_{DS}^{2}\right] \text{ for } V_{GS} > V_{th} \text{ and } (V_{GS} - V_{th}) > V_{DS} \qquad (6.3a)$$

and

$$I_{DS} = \mu C_{ins} \frac{W}{L}(V_{GS} - V_{th})^{2} = \mu C_{ins} \frac{W}{L}V_{DS}^{2} \text{ for } V_{GS} > V_{th} \text{ and } (V_{GS} - V_{th}) < V_{DS} \qquad (6.3b)$$

where μ is the mobility of electrons (for n-channel FETs) or holes (p-channel FETs), respectively; W is the width of the channel and L is the length of the channel; the rest of the parameters is defined above. For practical use only the operation in the linear mode (Equation 6.3a) is of interest. Upon pH changes only the parameter ϕ_0 will change and by substituting Equations 6.1 and 6.2 in 6.3a an expression of $I_{DS} = A\phi_0 + B$ is obtained where A and B are constants and hence I_{DS} has become a simple function of ϕ_0. In practical read out circuitry, however, the output is given as a voltage V_{out} which is a direct function of ϕ_0 [3, 4].

In this project an alternative gate insulator is proposed, namely a Si-C linked organic monolayer, which replaces the inorganic oxide insulators. Examples of thus created EIS-structures and the characterizations thereof can be found in Chapters 4 and 5. The FET based sensor with such organic insulator is the latest acquisition in the list of FET sensor family and is called the Hybrid Organic Semiconductor FET (HOSFET) [9]. A schematic overview of a thus created sensor is depicted in Figure 6.4.

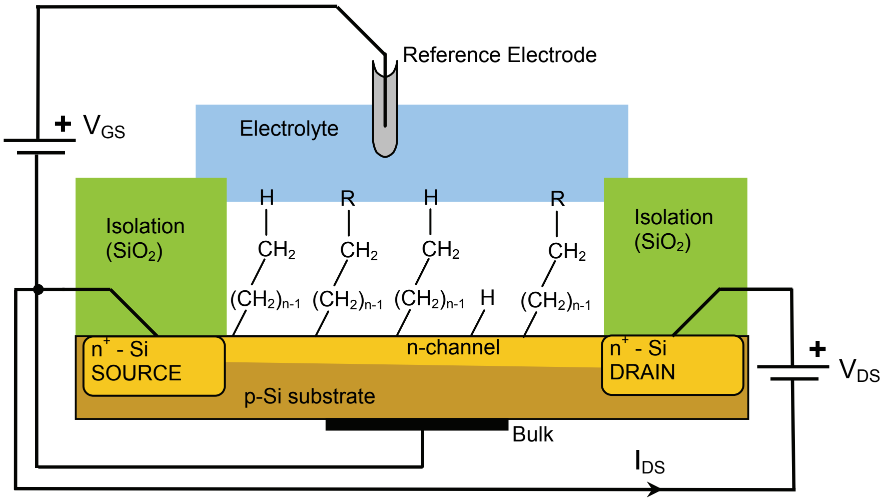

Figure 6.4. Schematic drawing of a four terminal n-channel HOSFET device. The gate insulator has been replaced by a Si-C linked monolayer, which can be easily functionalized with desired end groups R.

Figure 6.4 implies that the operating principle remains exactly the same as the ISFET. The theoretical advantages of using Si-C linked monolayers instead of oxide insulators are amongst others:

1) Si-C linked monolayers on both <100> and <111> silicon form densely packed layers and inhibit oxidation of the underlying silicon. The surface morphology of these layers can be atomically tuned, i.e. the layers are equally flat or rough as the initial H-terminated silicon surface [10, 11]. Furthermore, chemically inert monolayers are obtained when methyl-terminated monolayers are used, whereas a H-terminated silicon surface gets oxidized in air and in water, resulting in a chemically active surface layer.
2) Such monolayers can easily be functionalized [11] via organic chemistry. Numerous functionalities can be attached to the alkyl chains ranging from DNA, antibodies and proteins to ferrocene groups, gold nanoparticles and crown ethers [12]. This is in contrast to CHEMFETs with inorganic gate insulators, which consist often of complex, stacked sensing structures, necessary to create other functionalities than H^+ sensitive layers [4].
3) The chemistry of monolayer formation is very simple as compared to clean room made gate insulators. Monolayer formation requires merely wet-bench chemistry. The temperatures stay quite low (maximum of 160° C for thermally activated alkylation reactions [13]) as compared to clean room made insulators. Furthermore, no additional process step is required after monolayer formation whereas inorganic insulators require often annealing and curing steps after the initial deposition or growing step [14].
4) Besides these advantages in the chemical domain also advantages are expected with respect to the noise and detection limit of the HOSFET as compared to the ISFET. Since such nm-thin insulators are used the overall insulator capacitance C_{ins} increases as compared to the capacitance of inorganic insulators of which the thickness is in general in the order of 100 nm. A higher capacitance will lead to an increase of the field-effect and considering Equation 6.3a also an increase in sensitivity would then be expected. In practical ISFET read-out circuitry, however, I_{DS} is not the output parameter. Instead the circuit's output is a feed-back voltage that is directly proportional to the actual surface charge on the insulator ϕ_0 [3, 4]. Hence, increasing C_{ins} does not lead to an increase in sensitivity but it does have a beneficial influence on the detection limit and noise behavior of the FET. After all, any small change in ϕ_0 can more easily be detected.

To our best knowledge no article has been published yet that reports results on FET sensors with Si-C linked organic monolayers as gate insulator, such as the HOSFET depicted in Figure 6.4. On the other hand recent examples can be found in literature in which FET devices with functionalized monolayers onto intermediate (mostly oxide or nitride) layers were characterized. The target species are either simply H^+ [15], or complex biological, molecular complexes as enzymes [15] and DNA [16-18]. The latter has even been determined without the use of a reference electrode [17].

EIS-structures as derived from the HOSFET in Figure 6.4 have been shown to be able to serve as electrochemical sensory structures as reported in literature. However, target species have so far been limited to complex species like DNA only [19, 20]. As is the case for DNA detection via FET sensors a proper theoretical understanding and explanation of the measured signals upon DNA hybridization is still lacking and the reported results in terms of sensor signal and hybridization time vary significantly in literature as was discussed by Poghossian et al. [18]. They considered many factors that can influence the eventual output signal of FETs sensitive towards DNA. Thus, given the large number of factors influencing the eventual output signal, DNA does not seem to be the most suitable species to verify the operation of EIS-structures and HOSFETs with Si-C linked monolayers as gate insulators. It is preferred to verify the sensing behavior via simple ion-detection measurements to keep the theoretical basis describing the behavior orderly and provide easy comparison with the behavior of ISFETs and CHEMFETs. So far results on specific detection of simple ions, Na^+, Ca^{2+} via EIS-structures based on the HOSFET are still absent, so from literature it can not be unambiguously concluded that direct sensing of ions is possible with such EIS-structures. On the other hand, the results of Flink et al. [21] are very promising; they showed that devices with similar functionalized monolayers as the ones used here, except that they are bound to gold surfaces, could be used to detect alkali-ions, thereby showing that binding events do occur and can be detected at devices with such monolayers tested in aqueous solutions.

In this chapter two main topics are treated. Firstly, an attempt has been made to electrically characterize HOSFETs with aluminated gate contacts made via evaporation. Secondly, ion sensing via HOSFETs and EIS-structures with functionalized, organic monolayers is treated in detail. These Si-C linked monolayers had either methyl (CH_3) or crown ether (15-crown-5) modified end groups. Examples of such monolayers are depicted in Figure 6.5.

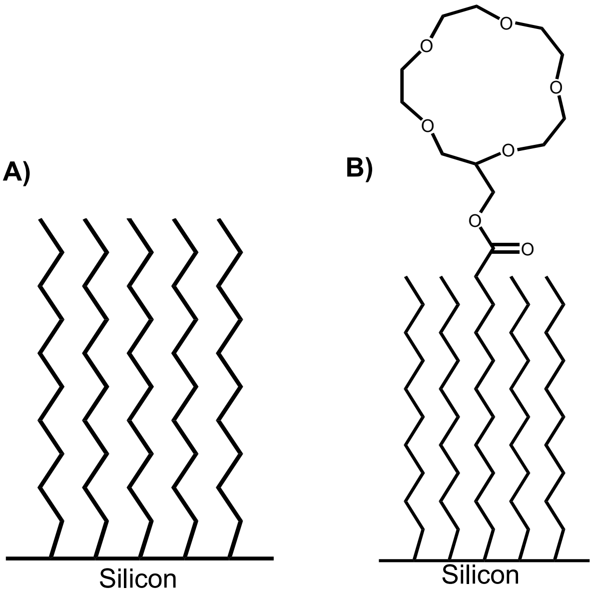

Figure 6.5. Schematic drawings of the monolayers tested in this chapter: A) unfunctionalized ($-CH_3$ terminated) monolayer; B) Monolayer of which part of the end groups of the chains have been functionalized with a crown ether (15-crown-5) group.

In the theory section of this chapter the site binding theory as discussed in Chapter 5 is adapted to describe and simulate the response of neutral carriers towards cations such as binding of alkali-ions by crown ethers (see Figure 6.5B). The results and discussion section starts with the electrical characterization of solid state HOSFETs with aluminated gate contacts in section 6.3.1. These have been measured to test the monolayers in practical solid-state devices and compare their behavior with Si-H gate insulators and native oxide and 70nm-thick, thermal oxides. In section 6.3.2 the electrochemical measurements on HOSFETs with unfunctionalized (i.e. methyl terminated) monolayers are treated. The results are compared with measurements on EIS-structures with similar monolayers as discussed in Chapter 5 and with ISFETs of the same type. In section 6.3.3 the electrochemical measurements on HOSFET with crown ether (15-crown-5 terminated) monolayers are treated in order to test receptor groups which are sensitive to other species than H^+. These are complemented with simulations and measurements on EIS-structures with the same monolayers. Next the conclusions are given followed by the experimental section.

6.2 Theory

The universal site binding model was introduced and discussed in detail in Chapter 5. In this section it is generalized to a model that describes the binding of a positively charged ion I^+ to a neutral receptor ligand L via a single complexation reaction with one dissociation constant, such as alkali ions binding to a crown ether. As a starting point serves the general expression of the site binding theory (Equation 5.7) which is repeated in Equation 6.4:

$$\frac{\delta\phi_0}{\delta pX_B} = -2.303\frac{kT}{q}\alpha, \text{ where } \alpha = \frac{1}{\frac{2.303kTC_{dl}}{q^2\beta_{\text{int}}}+1} \tag{6.4}$$

where the sensitivity is defined as the change in surface potential $\delta\phi_0$ upon a change in bulk species X_B and characterized by a single parameter α which on its turn depends on the intrinsic buffer capacity β_{int} of the surface and the capacitance of the electrical double layer in the electrolyte C_{dl}.

The precise control of the surface density of functional groups at the organic monolayer is a great potential in sensor technology for creating layers with precisely desired functionalities. Monolayers with functionalities are created via a reaction of the surface with a mixture of two 1-alkenes in a certain molar ratio. One of these 1-alkenes is an inert alkyl chain and the other has an end group that can be further functionalized with desired sensing moieties. It was shown that the initial molar ratio of the two 1-alkenes is also observed in the monolayer [22]. The percentage of functionalized alkyl chains shows thus a one on one relation with the initial percentage of functional 1-alkenes. In the simulations this percentage has to be rewritten to the receptor density $N_{S,receptor}$ [groups·m^{-2}], which can be estimated in the following way. All measurements are performed on <100> oriented silicon and this orientation will be used as starting point. The number of surface atoms on <100> oriented silicon is $6.78 \cdot 10^{14}$ atoms·cm^{-2} [23]. It is estimated that 61% of these surface atoms reacts with a 1-alkene [24], which leads to $4.14 \cdot 10^{14}$ alkyl-chains per cm^2. If for instance 20% of the surface is modified with functionalized alkenes, this will lead to $8.3 \cdot 10^{13}$ receptor groups per cm^2 or $8.3 \cdot 10^{17}$ receptor groups per m^2, whereas 50% functionalized alkyl chains lead to a receptor density of $2.1 \cdot 10^{14}$ receptor groups per cm^2 or $2.1 \cdot 10^{18}$ receptor groups per m^2. In contrast, for a SiO_2 surface N_S is $5 \cdot 10^{18}$ m^{-2} and for Ta_2O_5 surfaces N_s is even $1 \cdot 10^{19}$ m^{-2} [25]. A large N_S is favored for creating a good response (see Chapter 5, section 5.2). Such high values of N_S as for oxides can unfortunately not be reached (theoretically) via a functionalization of (planar) monolayers but for percentages of functional groups above 20% N_S is in the same order of magnitude as for SiO_2 so well measurable responses can be expected. Besides $N_{S,receptor}$ also the dissociation constants play of course a very important role in the eventual response.

6.2.1 Site binding theory for EIS-structures with Si-C linked, crown ether functionalized monolayers

In this subsection a site binding model for the specific binding of cations with crown ethers is described. This model is based on the affinity a specific cation has for a crown ether. Only [*B*] and β_{int} have to be adapted with respect to the original site binding theory. The reason for this is that site binding for functionalized monolayers with crown ethers is driven by other reactions and thus other dissociation constants.

As a start [*B*] is described using the dissociation constants of the occurring site-binding reactions given in Equation 6.5.

$$\left[L_{I^+}\right] \rightleftharpoons [L] + I^+ \tag{6.5}$$

where L represents the ligands (i.e. crown ethers) and I^+ represents the specific ions that are to be sensed. Variables between square brackets represent surface bound species. Via the activity constants of the different species, the dissociation constant of Equation 6.5 can be determined. This is illustrated in Equation 6.6.

$$\frac{\upsilon_{[L]} a_{I_S^+}}{\upsilon_{[LI^+]}} = K_{I^+} \tag{6.6}$$

where υ represents the activity constants for surface species, $a_{I_S^+}$ is the activity of the species to be sensed and the K_{I+} value is a tabulated intrinsic dissociation constant. Concerning the notation of K_{I+} it must be said that in literature it is common to use the stability constant K or K_S, which is the reciprocal of K_{I+} [26, 27]. Here it is chosen to use K_{I+} to maintain consistency with the general site binding model in Chapter 5. In general, however log(K) is given in literature and in those cases comparison is easy since log(K) = pK_{I+}.

The next parameter is the number of active crown ether groups, $N_{S,crown}$, which is determined by the number of neutral and positively charged sites. This is illustrated in Equation 6.7.

$$N_{s,crown} = \upsilon_{[L]} + \upsilon_{[LI^+]} \tag{6.7}$$

Combining and rewriting Equations 6.6 and 6.7 gives [B] as a function of just K_{I+}, $a_{I_s}{}^+$ and $N_{s,crown}$ (Equation 6.8).

$$[B] = N_{S,crown}\left(-\frac{\upsilon_{[LI^+]}}{\upsilon_{[L]} + \upsilon_{[LI^+]}}\right) = N_{S,crown}\left(-\frac{a_{I_S^+}}{a_{I_S^+} + K_{I^+}}\right) \tag{6.8}$$

To determine the response as a function of the above defined parameters, β_{int} defined as [B] differentiated as a function of in this case pI_S, has to be calculated. The result is given in Equation 6.9.

$$\beta_{\text{int}} = N_{S,crown}\, 2.303 \frac{a_{I_S^+} K_{I^+}}{\left(a_{I_S^+} + K_{I^+}\right)^2} \tag{6.9}$$

With these two newly defined parameters, [B] and β_{int}, the model is adapted to describe the pI response of a functionalized monolayer with cation sensitive groups. The number of functionalized groups ($N_{S,crown}$) is an input parameter of this model and can be calculated via the method described in the beginning of section 6.2.

Next the simulation results of the site binding model for cation binding in crown ethers are presented to predict and explain future results of samples of which the surface has been modified with crown ethers.

First, the influence of the dissociation constant (i.e. the reciprocal of the affinity constant of the specific cation for the crown ethers) on the number of charged and neutral groups at 25% of crown ether surface groups is simulated in Figure 6.6.

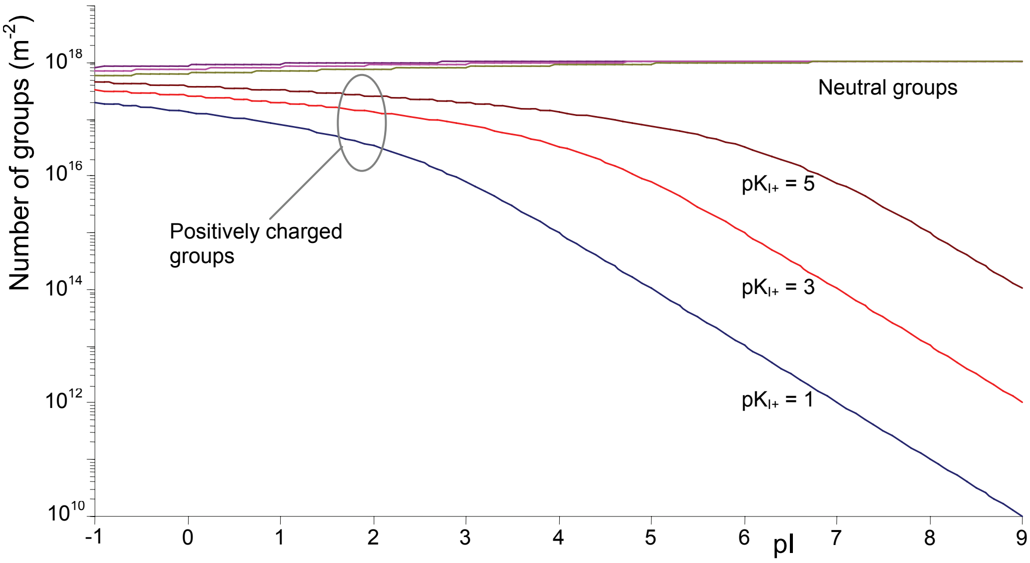

Figure 6.6. Simulated number of active surface groups as a function of the specific ion concentration. $N_{S,Crown}$ = $1.03 \cdot 10^{18}$ m^{-2} (25% coverage). Note that both the horizontal and the vertical axis are logarithmic.

In Figure 6.6 it can be observed that the number of positive groups decrease rapidly for pI > 4. It should be noted on forehand, however, that this decrease is probably not causing a high sensitivity because of the low number of charged groups (i.e. a low number of groups causes a low β_{int} (Equation 6.9) and hence a low sensitivity (see Equation 6.4 in which pX_B should be replaced by pI_B).

Second, the pI responses, for different dissociation constants pK_{I+} and different surface densities (10% and 25%) of crown ether groups, are simulated and given in Figure 6.7.

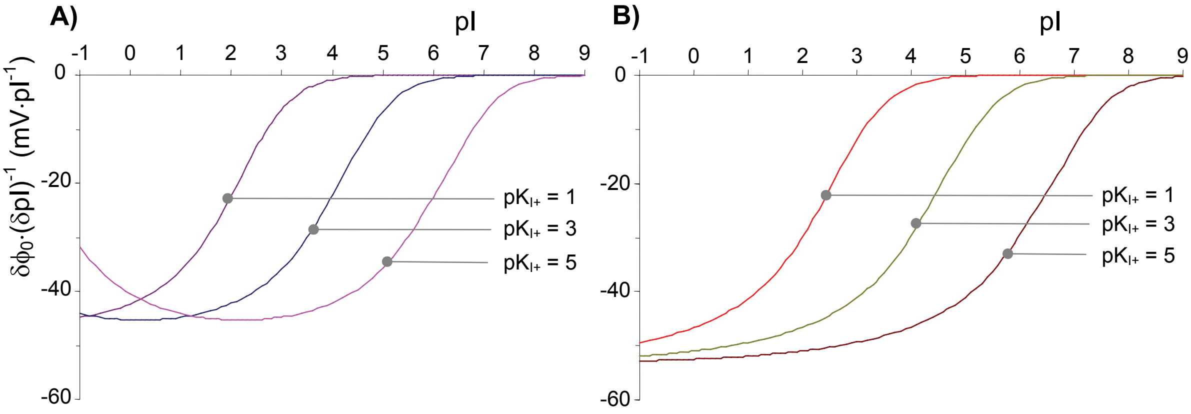

Figure 6.7. Simulated sensitivity as a function of the concentration of a specific cation for three different dissociation constants: A) 10% ($N_{s,crown}$ = $4.14 \cdot 10^{17}$ m^{-2}) and B) 25% ($N_{s,crown}$ = $1.03 \cdot 10^{18}$ m^{-2}) groups.

In Figure 6.7 it can be seen that the lower the dissociation constant (and thus the higher pK_{I+}) the higher the sensitivity for small concentrations. This result can be intuitively grasped by realizing that the dissociation constant is the reciprocal of the affinity constant. Another important observation is that the sensitivity increases for a larger number of crown ether groups. This observation can be better seen in the next simulation in Figure 6.8.

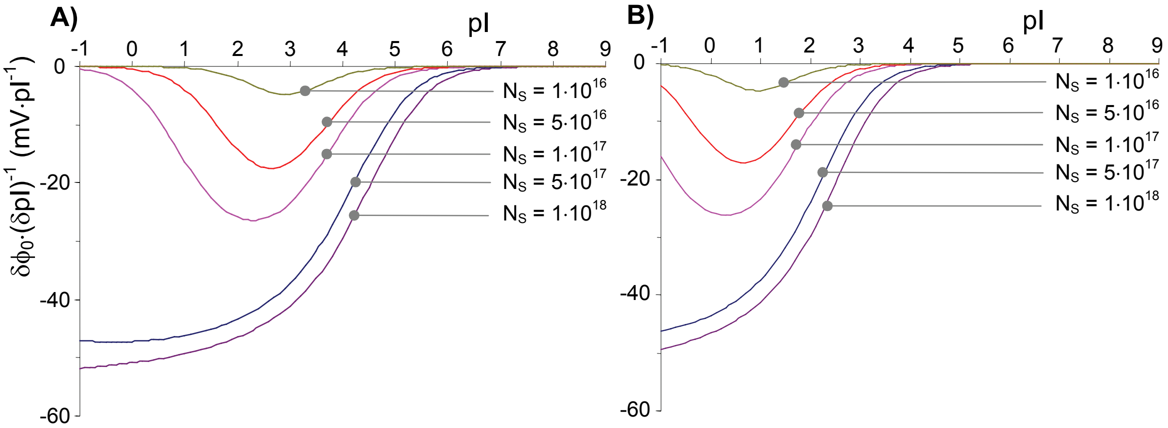

Figure 6.8. Sensitivity for the concentration of the specific ion for different number of surface groups $N_{s,crown}$ (m^{-2}) for A) $pK_I^+ = 3$ and B) $pK_I^+ = 1$.

In Figure 6.8 it can be observed that for a low density of surface groups ($N_{s,crown} \leq 1.10^{17}$ m^{-2}) even saturation occurs. Saturation can be explained by the fact that all available crown ethers have formed a complexion. So increasing the concentration of the specific ion does not lead to an increase in ϕ_0. In Figure 6.8B it is illustrated that no response is expected for $pI > 4$, i.e. concentrations less than 100 μM, if $pK_{I+} = 1$, irrespective of the number of surface groups.

In the simulation the proposed functionalized samples operate well (i.e. have a response) with both 10% ($N_{s,crown} = 4.14.10^{17}$ m^{-2}) and 25% ($N_s = 1.03.10^{18}$ m^{-2}) crown ether groups on the surface. However, no guarantees can be made to the sensitivity at real samples because there is a little information in literature on affinity constants for specific cations binding to surface bound crown ether groups in aqueous solutions.

6.2.2 Enthalpy and other binding related considerations on specific cationic complexation at crown ethers bound to surfaces

As mentioned in the previous subsection, crown ethers can form complexes with specific cations. The interaction between the crown ether and the cation is based on an electrostatic interaction between the positively charged cation and the negatively polarized oxygen atoms inside the crown ether. Because nature strives for the energetically most efficient situation, it is interesting to take a look at the difference in enthalpy of the total system before and after complexation of the cation with the crown ether. In this project an aqueous solution is used which has the consequence that the cations will be hydrated. Before a cation will form a complex with the crown ether, it will first have to lose its hydration shell. Considering enthalpy, it should thus be energetically more favorable for the cation to form a complex with the crown ether, than to have a hydration shell. Hydration enthalpy values of ions as well as complexation enthalpy values in anhydrous solutions are very well tabulated in literature [28, 29]. In Figure 6.9 an energy diagram is given for the complexation of a hydrated sodium ion with a crown ether.

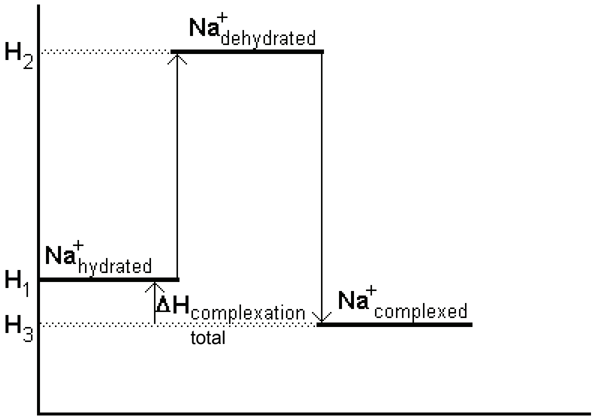

Figure 6.9. Enthalpy considerations for the complexation of a hydrated sodium ion and a crown ether. The ratio of enthalpies depicted here is random and not to scale.

Via the difference in enthalpy between hydration and complexation it can be determined if it is energetically favorable (only enthalpy considerations) for a cation to lose its hydration shell and to form a complexion with the crown ether. In Equation 6.10 this difference is defined.

$$\Delta H_{complexation,total} = H3 - H1 = (H3 - H2) - (H1 - H2) = \Delta H_{hydration} - \Delta H_{complexation} \qquad (6.10)$$

where $\Delta H_{complexation,total}$ [J] is the total difference in enthalpy from hydration to complexion. $\Delta H_{complexation}$ [J] and $\Delta H_{hydration}$ [J] are respectively the difference in enthalpy for the complexation of a dehydrated cation and the difference in enthalpy for the hydration process. In this project sodium ions ought to be complexed in a 15-crown-5 ether. According to [29] the hydration enthalpy, $\Delta H_{hydration}$, for sodium ions at 298 K is $-3.9\cdot10^5$ J.mol^{-1}. The complexation enthalpy for sodium ions with 15-crown-5 ethers is at 298 K approximately $-5\cdot10^5$ J.mol^{-1} [28]. With these values $\Delta H_{complexation,total}$ can be approximated at -100 kJ.mol^{-1}. The negative sign means that, when only considering enthalpy, it is energetically more favorable for the sodium ion to dehydrate and form a complex with the 15-crown-5 ether.

According to literature [28, 30, 31] the ring size of a crown ether is an important parameter in determining the selectivity of the ether for a specific cation over interfering cations present in the solution. This observation can be intuitively understood when considering the fact that nature strives for cations to have a certain number of negative sites in close proximity. When the ring is too small the cation will be sterically hindered to get in close proximity with negative oxygen sites, when the size is too large the cation can not be in close proximity with all oxygen sites, but only with a few of them. According to [31] crown ethers sometimes have a higher affinity than expected by the ratio of the ring size and the cation diameter, because cations can also be sandwiched by multiple crown ethers. Although this sandwich complex is a phenomenon in solutions with mobile crown ethers, two fairly immobile crown ethers with a spacing of approximately the same size as an interfering cation can have a high affinity for this interfering cation too as was shown by Flink et al. [32]. Therefore it is important to look at the distance between surface bound crown ethers. In [23] the spacing of surface atoms at <100> oriented silicon is tabulated as 0.543 nm. As explained in the beginning of section 6.2 the crown ethers can assumed to be evenly distributed across the surface and the degree of coverage by the monolayer is 61% [24]. Say that 10%, 20%, or 50% of the alkyl chains is functionalized with a crown ether, neighboring crown ethers are then separated on average by 8.90 nm, 4.45 nm or 1.78 nm, respectively. The diameter of interfering cations, of which it is reasonable to believe that they are present in the electrolyte in sufficient amounts to interfere with the measurement, is only in the order of magnitude of several hundred picometers. Therefore, the probability that sandwich complexes will form at surface bound crown ethers is remotely small and is expected not to occur.

6.3 Results and Discussion

It is noted on forehand that the HOSFETs used for solid-state, electrical characterization are FETs on planar chips according to a standard FET design of the BIOS group (University of Twente) [4]. These FETs are not packaged and measurements on them are performed "on-chip". All FETs used for electrochemical, titration measurements are performed with fully processed and packaged single FETs. These FETs were developed, packaged and delivered by Sentron (Roden, the Netherlands). The gate areas of all these FETs were etched open during the processing of the wafers so they could be modified with organic monolayers after they were packaged. Further details can be found in section 6.5.

6.3.1 Electrical characterization of solid state HOSFETs with aluminum gates

In Chapters 2 and 3 MIS-structures were successfully characterized with mercury as gate metal. However, in order to go to practical MIS-devices and MISFETs solid, preferably clean room compatible, gate metals should be applied. Aluminum is the most obvious choice as it is also widely used in the fabrication of CMOS Integrated Circuits [14]. The group of Vuillaume successfully characterized MIS-structures of n- and p-type silicon with $–C_{18}H_{37}$ monolayers with evaporated Al gate contacts [33, 34]. These devices showed outstanding electrical properties and the monolayers did not seem to be damaged by the evaporation of the metal. Detailed information on evaporating conditions and device yield, however, were not mentioned by the authors. In our case, planar FET devices were fabricated using the standard design from the BIOS group. In total two wafers were fabricated from which four types of FETs were obtained.

On one wafer the FETs had a thick (70 nm) thermal gate oxide and these FETs were used as reference. On the other wafer the gates of the FETs were etched open and the gates of these FETs were later modified, resulting in FETs of the other three types, with either -$C_{16}H_{33}$ organic monolayer, native oxide or an H-terminated surfaces. Characterization was carried out with a Semiconductor Parameter Analyzer via the measurement of $I_{DS} - V_{GS}$ and $I_{DS} - V_{DS}$ curves. Also the leakage currents ($I_{GS} - V_{GS}$) were measured. More details can be found in section 6.5.

$I_{DS} - V_{GS}$ and $I_{DS} - V_{GS}$ characteristics

In Figure 6.10 both the typical $I_{DS} - V_{DS}$ and $I_{DS} - V_{GS}$ curves of FETs with four types of gate insulators are shown. The results are typical of at least 5 different FETs per type.

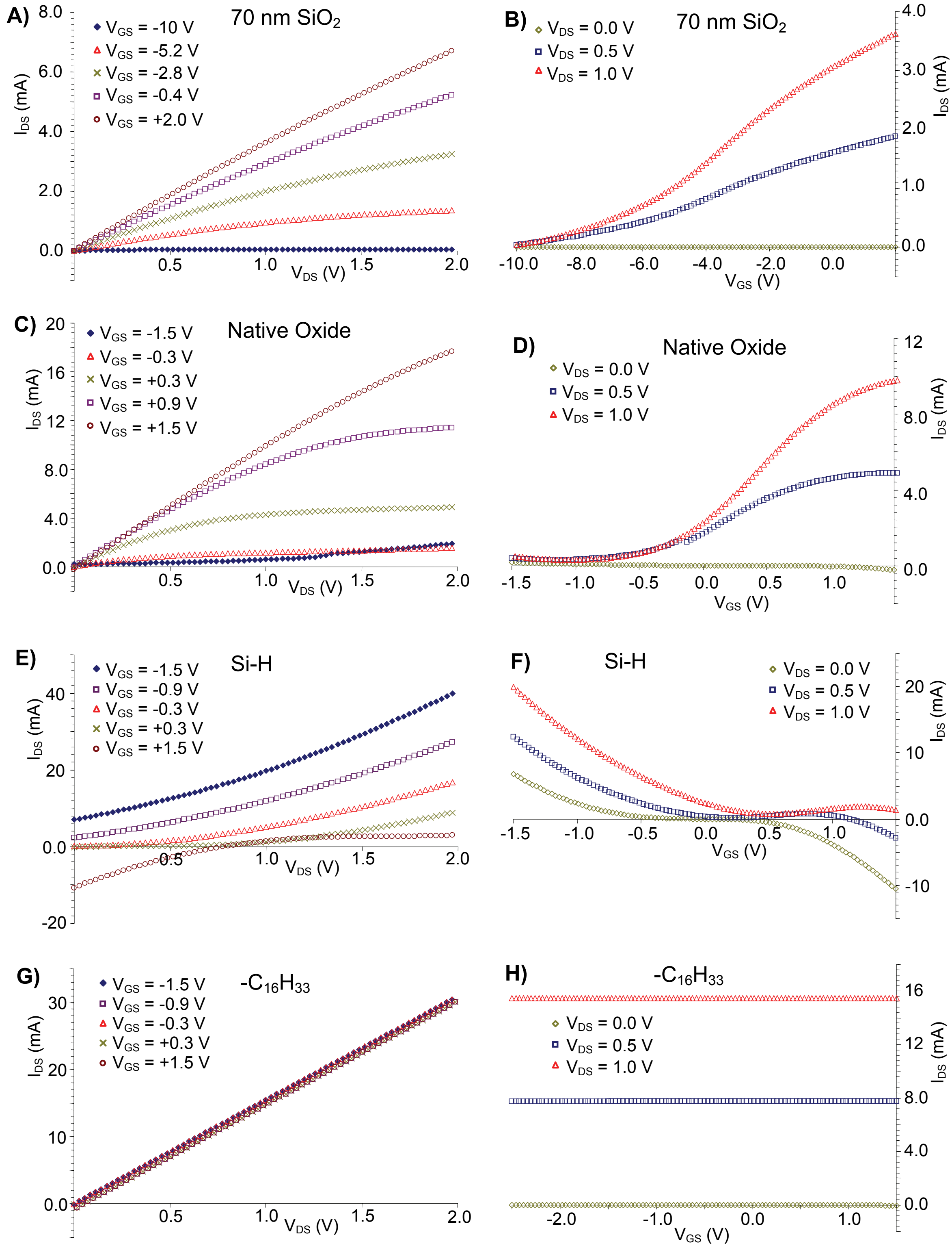

Figure 6.10. Typical $I_{DS} – V_{DS}$ (left-hand side) and $I_{DS} – V_{GS}$ (right-hand side) plots of FETs with insulators of A,B) thermal SiO_2; C,D) native oxide; E,F) H-terminated Si; G,H) $–C_{16}H_{33}$ monolayer.

The results for the reference FETs with thermal oxides (Figures 6.10A and B) are in accordance with theory. Making V_{GS} more positive leads to the formation of a deeper n-type inversion in the channel (see Figure 6.3A) and hence a larger current I_{DS} can flow. The threshold voltage of these FETs was calculated via a graphical determination. For the FET operated in the saturation regime ($V_{GS} - V_{th} < V_{DS}$) Equation 6.3b is valid and a plot of $\sqrt{I_{DS}}$ vs. V_{GS} should be a straight line with the V-axis being the threshold voltage [7]. The threshold voltages for these FETs with thermal oxide were all in the range of -11.9 through -13.3 V.

The results of the reference FETs with native oxide (Figures 6.10C and D) as insulator varied. About 50% of the FETs showed behavior like the one in Figures 6.10C and D, which is clear FET behavior just like the FETs with thermal oxides as gate insulators. The behavior of the other FETs could hardly be controlled via V_{GS}. I_{DS} values were much larger for these FETs and nearly independent of V_{GS}. The threshold voltage could not be properly derived for all these FETs.

The plots of the reference FETs with the gate metal deposited directly onto the H-terminated bulk silicon (Figures 6.10E and F) were heavily distorted. This distortion is due to the large leakage currents through the gate (discussed in the next paragraph). It can be seen, however, that there is still visible influence of the field effect, i.e. by changing V_{GS} also I_{DS} changes.

In case of the FETs with organic insulators (Figures 6.10G and H) there appears to be no influence of the field effect (V_{GS}) at all. In Figure 6.10H I_{DS} is solely a function of V_{DS} irrespective of V_{GS}. It is expected that FETs with such organic monolayers should give at least better results than FETs with H-terminated gate insulators. It is therefore reasoned that during fabrication of the monolayer the devices were fatally damaged. This will be clarified in the next paragraph on gate leakage current measurements.

Gate leakage current ($I_{GS} - V_{GS}$) characteristics

In Figure 6.11 the gate leakage current vs. gate voltage ($I_{GS} - V_{GS}$) curves of FETs with four types of gate insulators are shown. The results are representative of at least 5 different FETs per type.

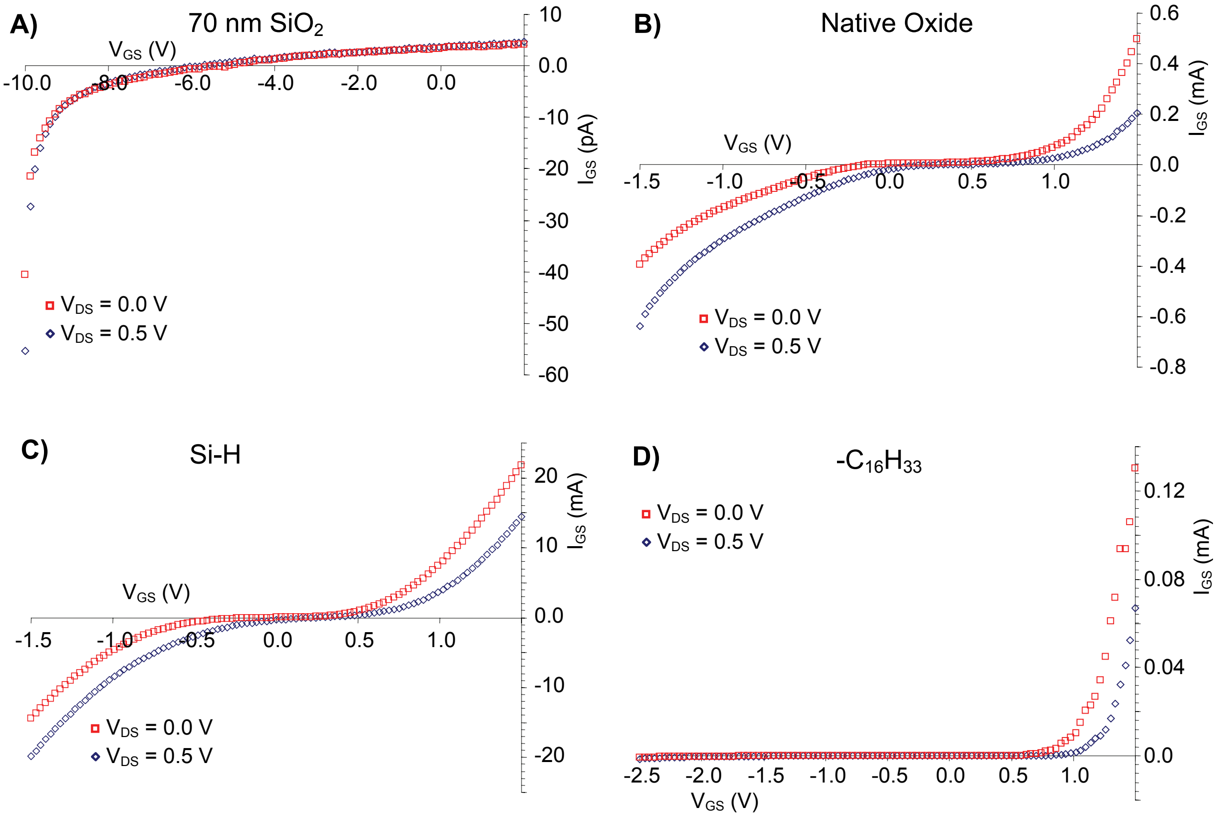

Figure 6.11. Gate leakage current vs. gate voltage ($I_{GS} - V_{GS}$) curves for V_{DS} = 0.0 V and 0.5 V of FETs with four different gate insulators: A) thermal SiO_2; B) native oxide; C) H-terminated Si; D) $-C_{16}H_{33}$ monolayer. Note the different scales on the current-axis: in A) I_{GS} is expressed in pA and in B-D) I_{GS} is expressed in mA.

The leakage currents through the 70 nm SiO_2 insulators (Figure 6.11A) are very low with a maximum of approximately -50 pA at -10 V. The leakage currents through the native oxide insulators (Figure 6.11B) are symmetrical in shape and much higher up to approximately +/- 0.5 mA at +/- 1.5V, showing that native oxide is a poor insulator. This is even worse in the case of the H-terminated silicon as gate insulator (Figure 6.11C). In that case the leakage currents show also a symmetrical shape but the currents are nearly two orders of magnitude higher as compared to the FETs with native oxide insulators. In case of the organic alkyl insulator the currents do not have a symmetrical shape around 0 V but instead show a Schottky-like diode behavior with the highest current density of approximately 0.1 mA observed at +1.5 V. These values are lower than found at native oxide and H-terminated Si insulators. However, the shape of the plots in Figure 6.11D is opposite to the expected shape as can be explained as follows. In Figure 6.4 it can be seen that source and bulk are interconnected and that in an $I_{GS} - V_{GS}$ measurement the structure looks like: gate metal | monolayer | p-type bulk silicon | bulk contact with the gate positively biased with respect to the bulk silicon. This situation is similar to the MIS-structures of p-type silicon characterized in Chapter 2. In that case also Schottky diode behavior was observed except the plots were reversed with respect to Figure 6.11D. This gives rise to the possibility that in fact metal | monolayer | n-type silicon | bulk contact structures have been measured in case of the FETs with organic alkyl insulators. This may even be possible because before the gate has been modified with an alkyl monolayer, the native oxide has to be etched via HF etching. In case of the FETs with organic monolayers this has been done via etching for 2 minutes in a 2.5% HF solution and this may have led to an over etching of the gate area, exposing parts of the n^+ source and drain regions. These are subsequently modified with an alkyl monolayer and also become covered with the Al gate metal. In that case the FET channel has been short-circuited since the current can flow directly form drain through the monolayer to the gate metal and then again through the monolayers into the source region. This is illustrated in Figure 6.12A. In Figure 6.12B the *J* - *V* curves are shown from the Hg| $C_{16}H_{33}$ | p-type and n-type Si MIS-structures of Chapter 2 to show that Figure 6.11D indeed represents data of a Schottky diode with n-type silicon.

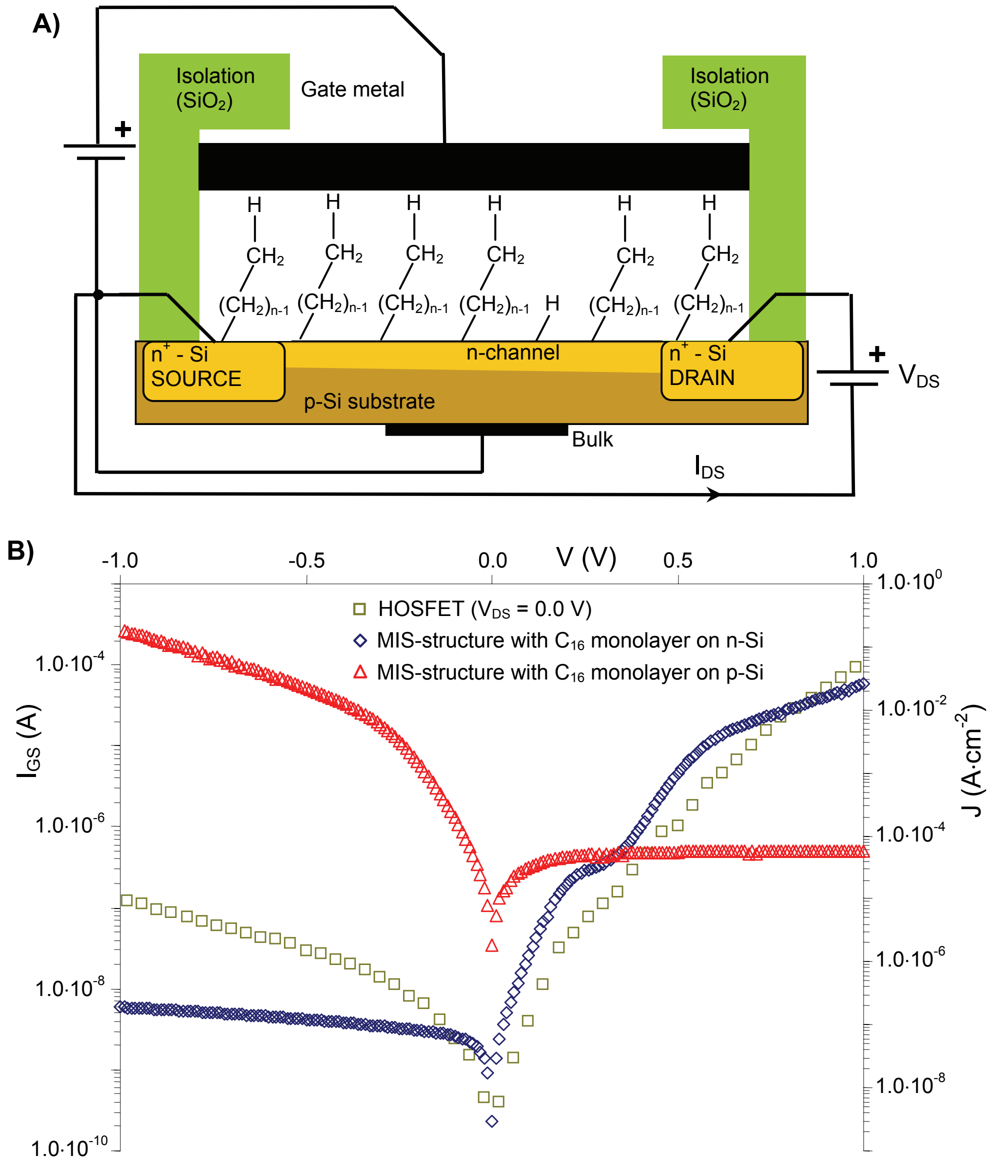

Figure 6.12. A) Schematic picture of a HOSFET with (exaggerated and not to scale) over etched gate area, resulting in a short-circuited channel region. B) I_{GS} – V_{GS} data (left axis) of HOSFET with C_{16} monolayer as gate insulator and *J* - *V* data (right axis) of MIS-structures with C_{16} monolayer on n- and p-type silicon.

It must be noted that the data in Figure 6.12B can only be qualitatively compared and not quantitatively. The data of the MIS-structures are current densities and the data of the HOSFET are plain currents since the area through which the current flows is not precisely known. From the figure it is nonetheless plain to see that the current data of the HOSFET resembles a Schottky diode of n-type silicon. This observation also correlates with the data of Figures 6.10G and H; the linear relation between I_{DS} and V_{DS} in Figure 6.10G implies the behavior of a resistor and a device like Figure 6.12A fits this theory.

The fact that the FETs with H-terminated silicon as gate insulator are not short-circuited may be attributed to the fact that those gate areas were etched in more diluted HF solutions for shorter times and consequently the source and drain regions may not have been exposed. These FETs were etched for 1 minute in 1% HF solution vs. 2 minutes in 2.5% HF for the FETs with organic insulators.

Finally, it is noticed that although it seems that the FETs with monolayers are short-circuited, this doesn’t imply that similar phenomena occur at the packaged HOSFETs described in the upcoming paragraphs since these were other FETs with other designs (see section 6.5). In fact all those HOSFETs could be properly read out in the FET amplifier, which would not have been possible in case of short-circuited FETs.

6.3.2 *pH* responses of HOSFETs with unfunctionalized, organic monolayers

Chapter 5 contains a detailed analysis of the *pH* responses of EIS-structures with unfunctionalized, organic monolayers, whereas in this section the focus is on the *pH* responses of HOSFETs (see Figure 6.4) based on those EIS-structures. The results here are compared with the responses of the EIS-structures in Chapter 5. In Figure 6.13 two up and down going titration curves are shown for two HOSFETs, which had unfunctionalized ($-C_{16}H_{33}$) monolayers as gate insulators. It was expected that these HOSFETs showed a reduced *pH* sensitivity as compared to SiO_2 ISFETs (also shown in Figure 6.13A).

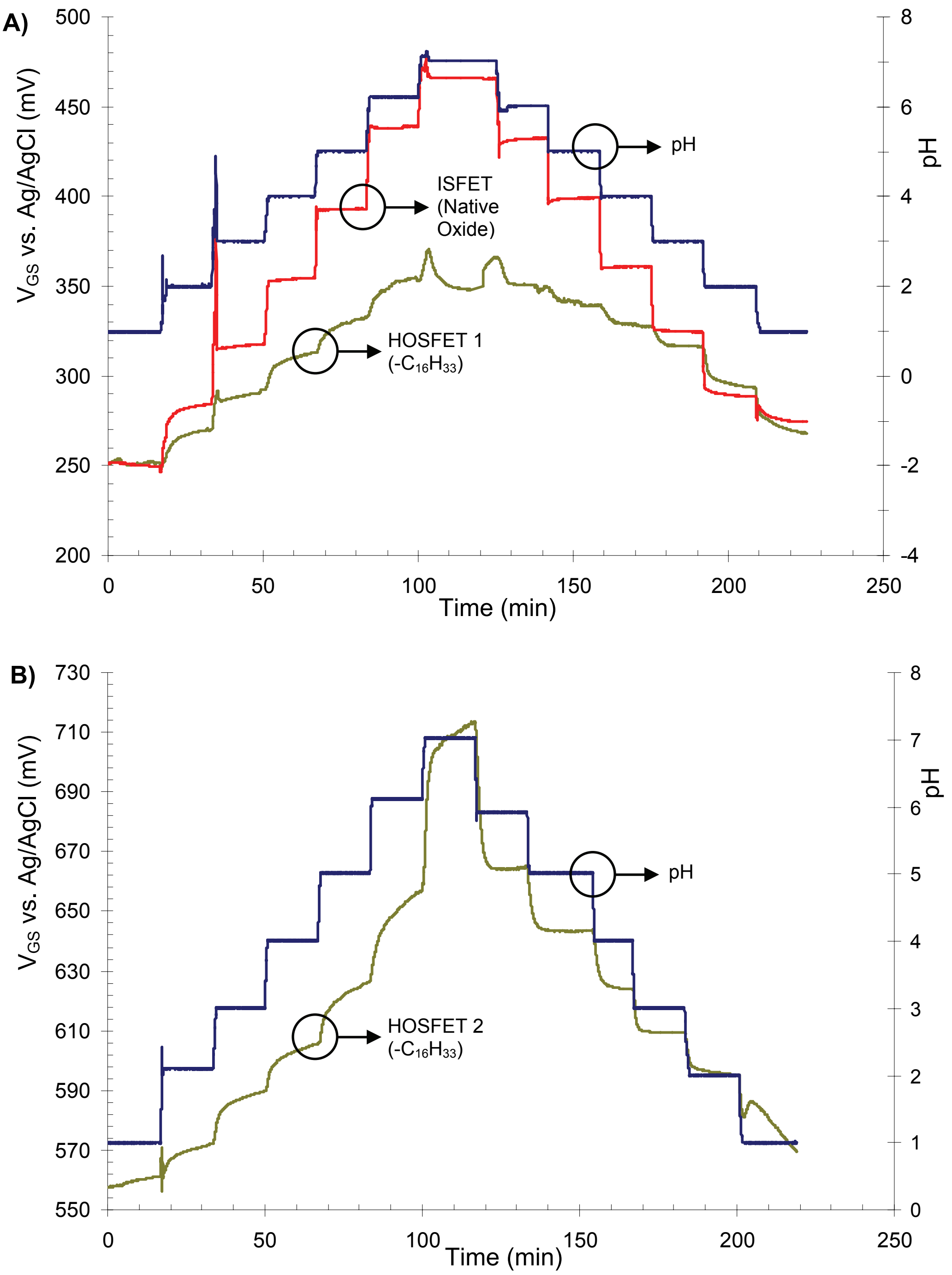

Figure 6.13. Titration curves from *pH* 1 through 7 and back to 1 of A) simultaneously measured HOSFET 1 with $-C_{16}H_{33}$ monolayer as gate insulator and ISFET with native oxide as gate insulator; B) HOSFET number 2 with $-C_{16}H_{33}$ monolayer as gate insulator. To the V_{GS} data of HOSFET 1 1.2 V was added to let the starting values of HOSFET and ISFET coincide. The real starting value of HOSFET 1 was -950 mV vs. Ag/AgCl.

The response of HOSFET 1 in Figure 6.13A displays an unexpected dip at *pH* 7 and returned to a higher value at approximately 120 minutes. Since this phenomenon occurred only once and only at this HOSFET it is considered as an artifact of which the origin is so far unknown. HOSFET 2 in Figure 6.13B also gave an unexpected response at from *pH* 6 to *pH* 7 and also from *pH* 7 back to *pH* 6. The response was here much higher than at the other *pH* values. Also for this observation no clear answer can be given. It can in no way be correlated to the data in Chapter 5. Besides these unexpected phenomena a number of clear trends are visible in Figure 6.13. First of all, all FETs show a response towards *pH* changes. The ISFET clearly displays a higher sensitivity than HOSFET 1 in Figure 6.13A, which is in accordance with the results of Chapter 5. HOSFET 1 has a total response of 116 mV over 6 *pH* units whereas the ISFET has a response of 216 mV in the same *pH* range.

Another feature concerns the drift and settling times. The ISFET clearly has a quick response with undershoot in the response for low *pH* (< 3) values and overshoot at high *pH* (> 4) values. Both HOSFETs always displayed undershoot and a slower response time as compared to the ISFET. The responses have exponential shapes, resembling responses often observed for systems dominated by diffusion processes. Diffusion as dominant process in HOSFET responses is, however, not directly expected. Since the monolayers are so thin site binding reactions are expected to occur almost instantaneously. On the other hand, also at the EIS-structures long (up to 30 minutes), exponential-like settling behavior was observed at some of the EIS–structures with unfunctionalized monolayers (Chapter 5, Figure 5.17). In those cases settling times varied and no clear reasons were at hand to explain the variations. The drift at the HOSFETs seemed to be sweep direction dependent. In the up going sweep the drift seemed to be higher than for the down going sweep.

Since the drift rate of the HOSFETs was high the *pH* responses or sensitivity could not be determined in a straightforward way. Therefore a measurement routine was used based on the following calculations. Each measurement took 1000 seconds; the starting value t_{start} of the response at a certain *pH* starting at time x000 was defined as the average value of the data between x200 and x400 seconds, since the initial settling times always had passed after 200 seconds; the end t_{end} of the response at a certain *pH* starting at time x000 was defined as the average value of the data between x750 and x950 seconds. A response at a certain *pH* Y is then defined as $t_{start,\,Y} - t_{end,\,Y\text{-}1}$ and the drift at *pH* Y is defined as $t_{end,\,Y} - t_{start,\,Y}$. Subsequently, the *pH* responses have been determined and are displayed in Table 6.1 for each *pH* step.

Table 6.1. *pH* responses upon single *pH* steps for the two HOSFETs and single ISFET.

pH step	ΔV_{GS} (HOSFET 1) [mV vs.Ag/AgCl]	ΔV_{GS} (HOSFET 2) [mV vs.Ag/AgCl]	ΔV_{GS} (ISFET) [mV vs.Ag/AgCl]
1 → 2	14.3	8.8	31.5
2 → 3	18.8	15.6	32.7
3 → 4	18.9	13.4	36.4
4 → 5	16.4	17.0	38.4
5 → 6	19.5	24.5	44.8
6 → 7	- [a]	52.9	26.8
7 → 6	-13.7	-47.9	-33.9
6 → 5	-6.6	-21.0	-33.6
5 → 4	-9.8	-18.9	-38.5
4 → 3	-10.6	-14.6	-35.7
3 → 2	-19.8	-13.0	-34.7
2 → 1	-20.8	-12.5	-12.1

[a] data not available de to measurement artifact.

Apart from the data between *pH* 6 and 7 the two HOSFETs show low *pH* responses, which are comparable with the EIS-structures in Chapter 5 (see for instance Table 5.2). Those EIS-structures showed a *pH* sensitivity varying from 20 – 30 mV·pH^{-1} in the *pH* 4 – 7 range. In most cases the sensitivity of the HOSFETs was lower than 20 mV·pH^{-1}. The ISFET with native oxide as insulator showed a much higher response > 30 mV·pH^{-1} for all cases except from *pH* 2 → 1. Values of *pH* sensitivities mentioned in literature for ISFETs with SiO_2 gates are 37 – 48 mV·pH^{-1} for *pH* < 7 [35], 40 mV·pH^{-1} [36], and even hardly a *pH* response around *pH* 2 up to a maximum of 45 mV·pH^{-1} [25]. The values for the ISFET are in nearly all the cases in close agreement with the literature data. The deviation with theory and the data in Chapter 5 for the EIS-structures with SiO_2 insulators is that at these ISFETs there is no influence of the point of zero charge. The sensitivity stays quite constant over the entire *pH* range apart from the data of *pH* 2 → 1. Nonetheless, comparing the data of the ISFET with the HOSFET indicates that at least some kind of gate surface modification has occurred. Unfortunately, modification of the gates of these HOSFETs cannot be verified with any kind of surface characterization technique (water contact angle measurements, AFM, X-ray reflectivity, etc.) since the gate size is too small. So it cannot be determined if the gate modification has succeeded in the same way as for the EIS-structures, of which the modification could be perfectly verified.

Next, the amount of drift has been calculated via the method mentioned above. The results are depicted in Figure 6.14.

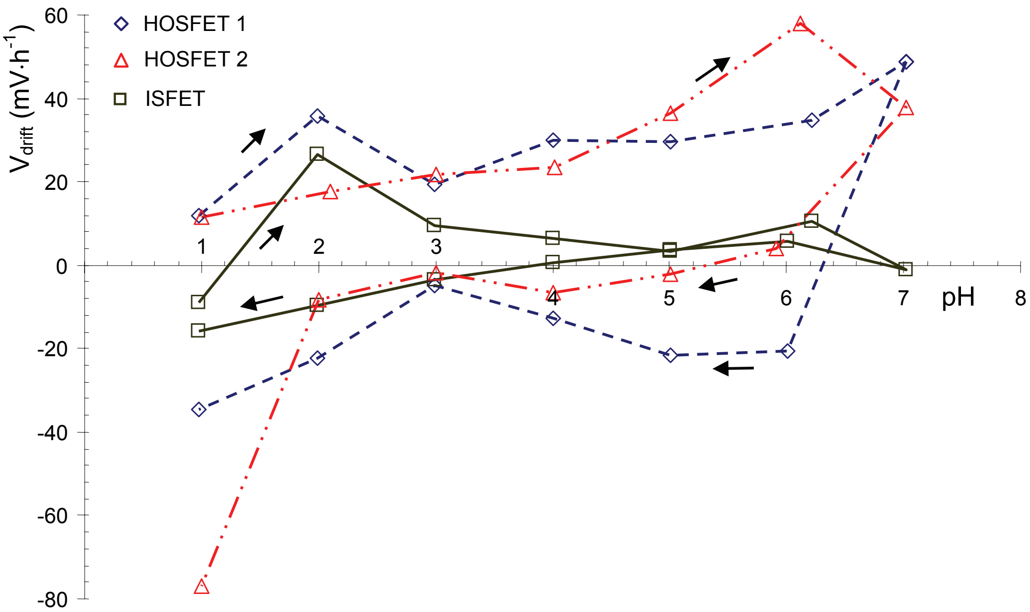

Figure 6.14. Drift data expressed in mV per hour of the two HOSFETs and one ISFET. The results of the up going and down going sweeps are indicated with arrows.

The ISFET had less drift than the two HOSFETs. The drift rate of the two HOSFETs is around 20 mV·pH^{-1}, which can be regarded very high, almost one order of magnitude higher than EIS-structures with similar monolayers, which had in general drift values much lower than 2 mV·pH^{-1} (see Chapter 5, Table 5.4). In case of a HOSFET the total device is of course more complex and therefore more causes can be present that increase the drift of the device, especially since these devices were made from existing FETs that are not (yet) optimized for modification with organic monolayers. The drift of all 3 FETs was in general sweep direction dependent; for up going *pH* sweeps the drift was in positive direction and for down going *pH* sweeps the drift was in negative direction. More research is needed to test such HOSFET devices. First of all, it should be verified if the gate surface modification via the alkylation reaction succeeds and second it needs to be verified if the design of the used FET shows any unwanted components, materials of process steps, which can negatively affect the monolayer incorporation.

6.3.3 Alkali-ion responses of HOSFETs and EIS-structures with crown ether terminated, organic monolayers

To test the ion-sensing abilities of HOSFETs and EIS-structures with organic monolayers it is desired to anchor to these monolayers receptor groups that are sensitive to other ions than H$^+$ and should also have no or very little cross sensitivity towards H$^+$. Crown ethers may be a suitable candidate for this task. Crown ethers were discovered in the mid-1960's by Charles Pedersen [37, 38] and have since than drawn a lot of attention. They provide potentially good candidates to serve as receptor groups in chemical sensors since they show selective binding of cations, such as Na^+, K^+ etc., which depends on the chemical composition of the crown. The chemistry behind crown ethers has been extensively described in literature [28, 30, 39]. The focus in this section is on the sensing behavior of HOSFETs and EIS-structures modified with monolayers that have functional crown ether groups of the 15-crown-5 (see Figure 6.5B). This crown ether should, given its hole-size, be sensitive towards Na^+ ions [27]. However, in literature it was shown that this crown ether was more sensitive towards complexation with K^+ than Na^+ ions as determined both in methanol as a solvent [26, 27, 30, 39] or in water as a solvent [27, 39]. It must be noted that such data was determined for free crown ethers in a solution and not for fixed crown ethers on monolayers as in this case. Nonetheless, it is expected that the trend of K^+ being more easily complexed by this crown ether remains valid. Flink et al. [21, 32, 40] showed that indeed sensing structures could be created via functionalized monolayers with crown ethers on gold surfaces and they also found the highest sensitivity towards K^+ for the 15-crown-5 [32, 40]. Given the reasons above it was decided that in the trial measurements of HOSFETs modified with such crown ethers first the sensitivity towards K^+ was determined. The titration results for a HOSFET with a monolayer with 10% 15-crown-5 groups simultaneously measured with an ISFET with native oxide insulator are shown in Figure 6.15. In contrast to the measurements reported on HOSFETs so far, these measurements were performed in a flow-cell, which enabled us to switch easily between solutions from high to low concentrations (see section 6.5 for details).

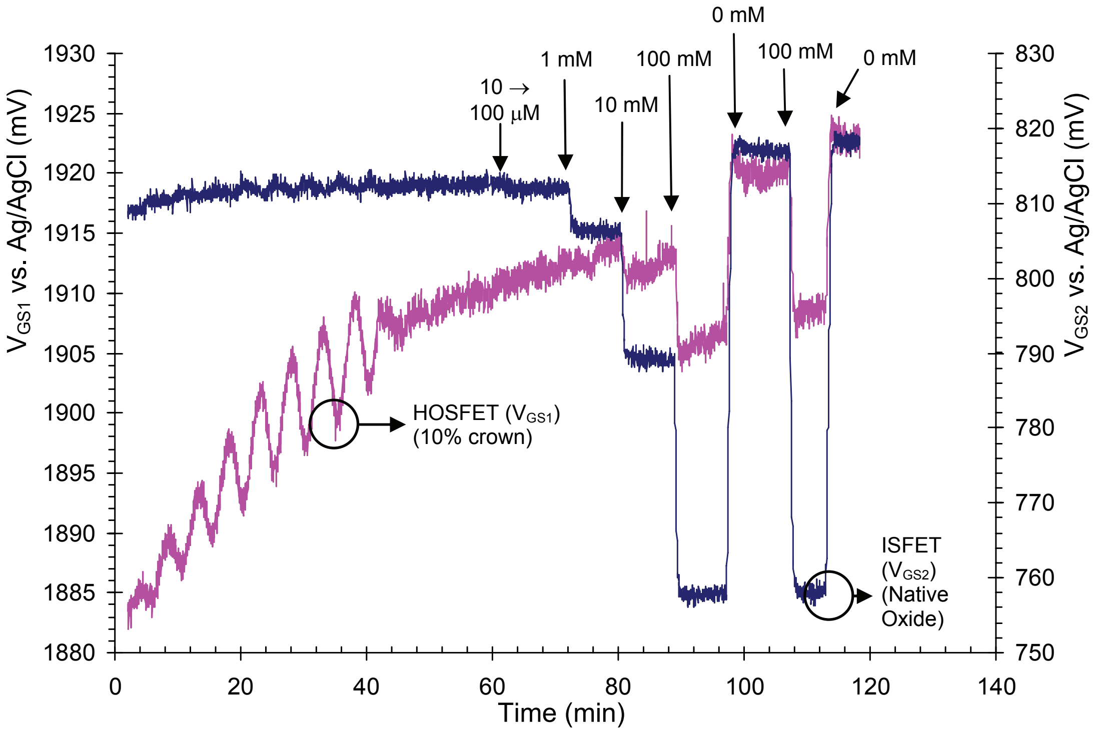

Figure 6.15. Responses of simultaneously measured HOSFET (10% crown ether) and ISFET (SiO_2) upon different K^+ concentrations with the *pH* fixed at 7. A change in K^+ concentration is indicated with an arrow.

The oscillations visible until 45 minutes are due to oscillations in the automated temperature controller, which was unstable until that time (see section 6.5 for details). It is remarkable to see that as both FETs were exposed to the same temperature oscillations, the HOSFET gave a larger signal change upon these temperature changes as compared to the ISFET. Why the HOSFET is more sensitive towards temperature changes is not clear and was also not the main interest of this test. The span of the V_{GS}- axis of the HOSFET is 50 mV and of the ISFET is 80 mV. It is obviously visible that the ISFET gives a much larger signal change towards changes in [K^+]. Furthermore, the ISFET already gives a noticeable change in output signal at the change from 10 μM to 100 μM K^+, whereas the HOSFET started to give a noticeable response at 10 mM. The magnitudes of the responses of both FETs have been summarized in Table 6.2

Table 6.2. Responses upon [K^+] changes for the HOSFET with 10% crown ether and the ISFET.

[K^+] step	ΔV_{GS1} (HOSFET) [mV vs.Ag/AgCl]	ΔV_{GS2} (ISFET) [mV vs.Ag/AgCl]
0 → 10 μM	+1.0	0.0
10 → 100 μM	+1.6	-0.8
0.1 → 1 mM	+0.6	-5.8
1 → 10 mM	-1.8	-17.1
10 → 100 mM	-6.6	-31.6
100 → 0 mM	+14.0	+59.4
0 → 100 mM	-11.7	-58.8
100 → 0 mM	+14.1	+60.1

Table 6.2 confirms the observations described above. Especially, the changes in [K^+] from 100 mM to 0 mM and vice versa are very illustrative. The ISFET gives here a signal change of approximately 60 mV whereas the HOSFET gives a change in signal of approximately 10 – 15 mV. The data for the ISFET is by the way in accordance with data from the literature. It is known that SiO_2 shows sensitivity towards both Na^+ and K^+. In [36] it was shown that ISFETs with SiO_2 insulators were more sensitive towards K^+ than towards Na^+ at *pH* 7. The response was -31 mV upon a [K^+] step from 10 mM to 100 mM and the total response from 0 mM to 100 mM was -55 mV. These values are both in close comparison with the data in Table 6.2. Matsuo et al. measured the response from [Na^+] and [K^+] steps only from 0 to 1 M at *pH* 7. Their ISFETs were more sensitive towards Na^+ (30 – 50 mV) than towards K^+ (20 – 30 mV). This data is already lower than the data depicted here for [K^+] steps from 0 to 100 mM. The differences could be due to preparation of the oxides.

Since no surface characterization techniques could be applied to check if the chemical modification of the HOSFET gate succeeded, the precise origin of the low responses remained at first unclear. On one hand, the results may be explained by low affinity of the crown towards alkali-ions on the other hand the results may be due to an unsuccessful gate modification. To rule out the latter cause, the experiments have been repeated on EIS-structures with monolayers with 10% and 25% crown ethers. As a reference EIS-structures with native oxide and unfunctionalized monolayers are used. The latter should theoretically be completely inert towards both Na^+ and K^+. The measurements were performed in the same way as the EIS-structures measured in Chapter 5. The responses were determined via Mott Schottky measurements (see Chapters 4 and 5). Both the responses towards Na^+ and K^+ were measured. The typical results of the reference samples (SiO_2 and $–C_{10}H_{21}$ insulators) of Na^+ and K^+ titrations are depicted in Figure 6.16. These titrations were performed by increasing the concentration K^+ or Na^+ a ten-fold at fixed time-intervals.

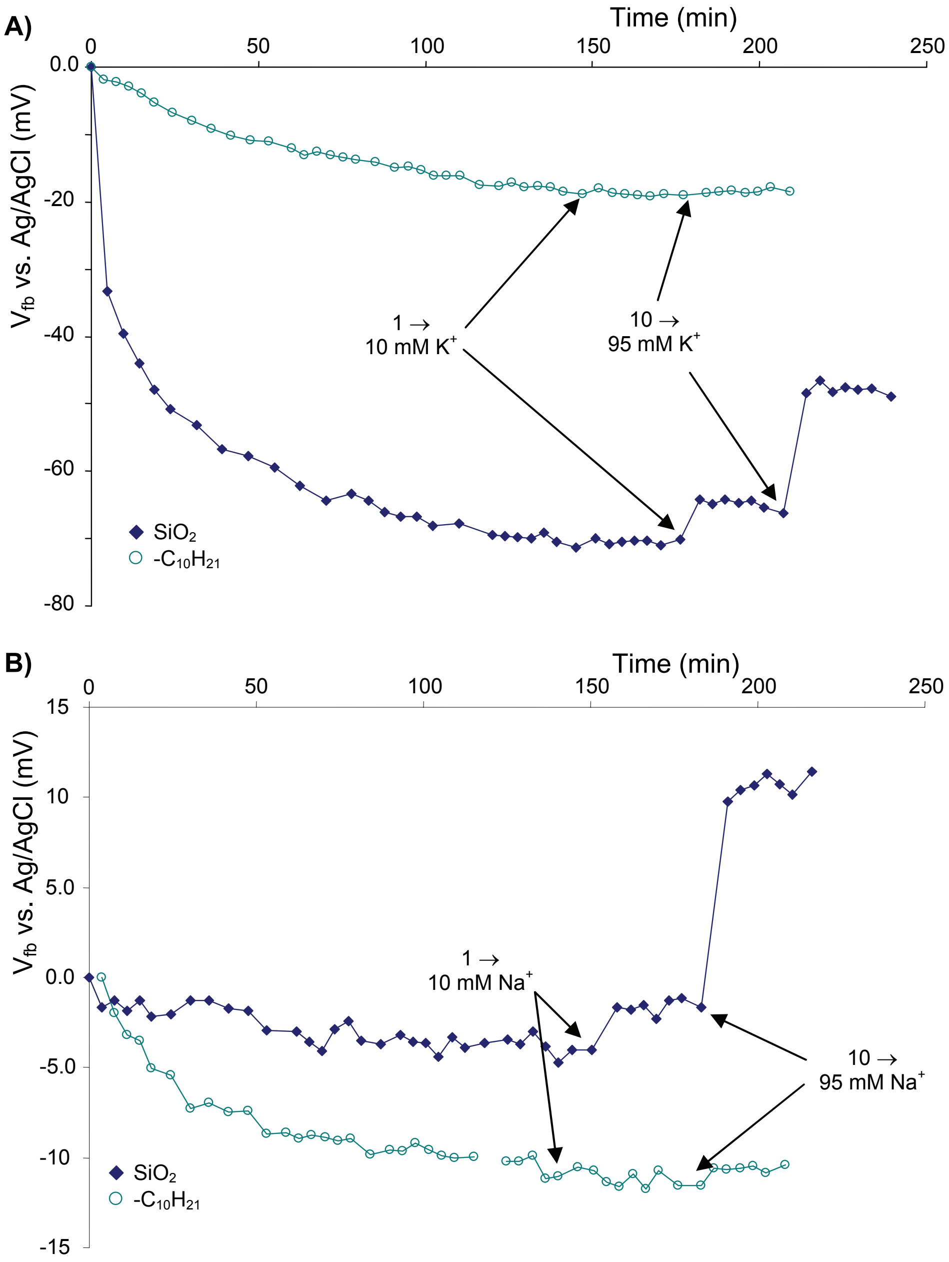

Figure 6.16. Typical A) K^+ and B) Na^+ responses of EIS-structures with SiO_2 and $–C_{10}H_{21}$ insulators. Only the steps for concentrations of 10 mM and 95 mM are indicated with arrows in the graph.

The samples with unfunctionalized monolayers were indeed completely insensitive towards both K^+ (Figure 6.16A) and Na^+ (Figure 6.16B). The samples with SiO_2 showed, just like the ISFETs with SiO_2 insulators, a noticeable response towards both K^+ (Figure 6.16A) and Na^+ (Figure 6.16B). Overall the responses of the EIS-structure with SiO_2 were lower than measured at the ISFET above; the responses were not noticeable for concentrations smaller than 10 mM. However, the trend was the same; the response for K^+ was higher than the response towards Na^+ (note the different scales in the figures). These measurements indirectly imply that there is a very low amount of oxide present at the samples with unfunctionalized monolayers. It could be expected that if there was a considerable amount of oxide at these samples that they should have given a response due to this oxide but this was clearly not the case.

Next, the typical responses of two EIS-structures with monolayers with 10% and 25% crown ether terminated end groups towards K^+ and Na^+ are depicted in Figure 6.17.

Obviously, all samples displayed sensitivity towards both K^+ and Na^+. Also in these cases responses were visible only for concentrations of 10 mM or higher. The response for K^+ was higher than the response towards Na^+ (note the different scales in the figures). To quantitatively compare the data the responses have been calculated and are summarized for all samples for the K^+ responses and Na^+ responses in Table 6.3.

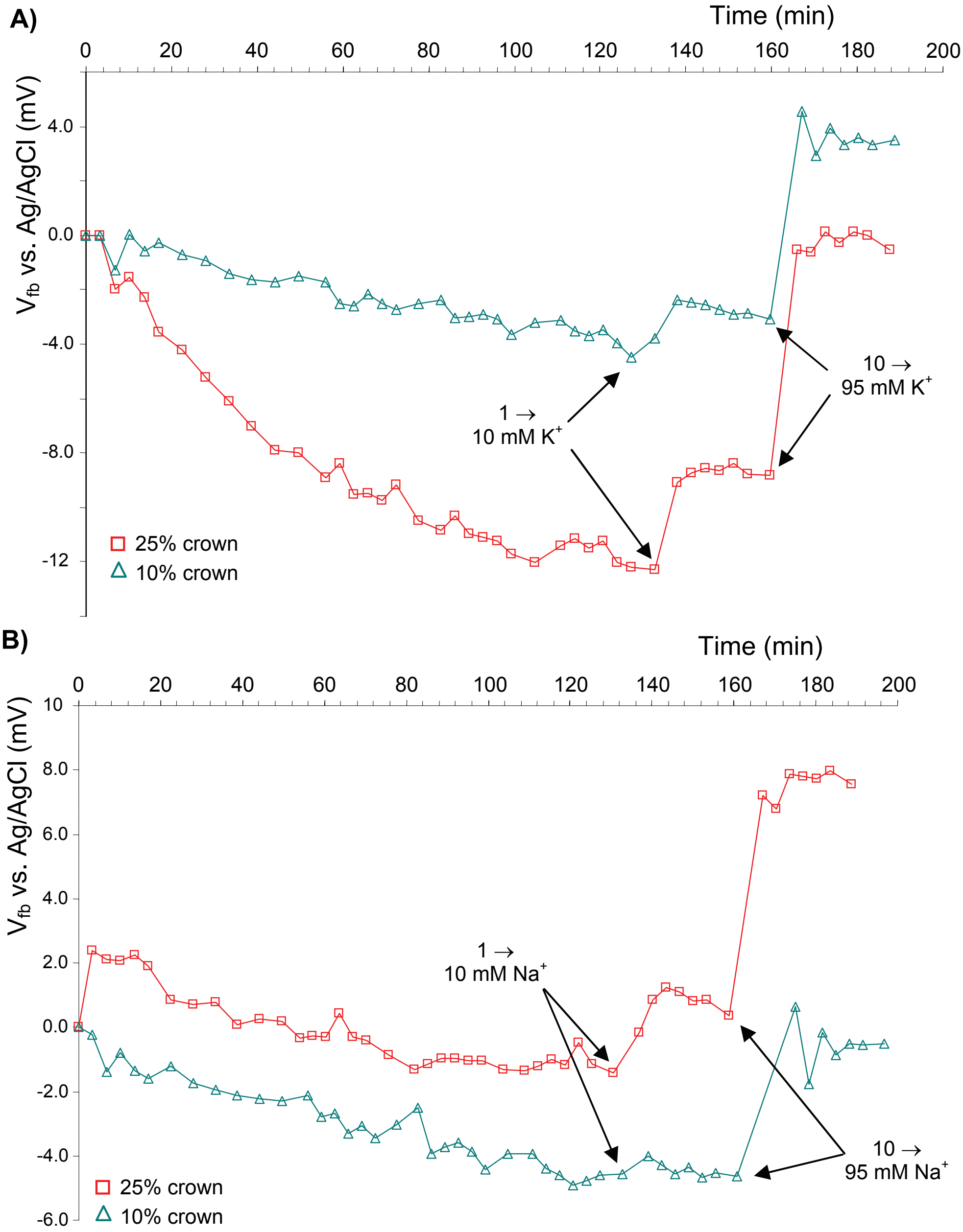

Figure 6.17. Typical A) K^+ and B) Na^+ responses of EIS-structures with monolayers as insulators with 10% or 25% crown ether. Only the steps for concentrations of 10 mM and 95 mM are indicated with arrows.

Table 6.3. Responses upon $[K^+]$ and $[Na^+]$ changes for all tested EIS-structures.

[cation] step	ΔV_{fb} $(-C_{10}H_{21})$ [mV vs.Ag/AgCl]	ΔV_{fb} (SiO_2) [mV vs.Ag/AgCl]	ΔV_{fb} (10% crown) [mV vs.Ag/AgCl]	ΔV_{fb} (25% crown) [mV vs.Ag/AgCl]
1 → 10 µM K^+	< 1	6	4	2
10 → 95 µM K^+	< 1	18	9	10
1 → 10 µM Na^+	< 1	2.5	< 1	< 1
10 → 95 µM Na^+	< 1	11.5	8	4

Table 6.3 demonstrates some clear features. The sensitivity towards K^+ was higher for all samples, apart from the samples modified with -$C_{10}H_{21}$ which were insensitive towards both tested ions. The sensitivity of the samples with SiO_2 was higher both for K^+ and Na^+ than of the samples with crown ethers. Furthermore, no direct influence on crown ether density was observed in both measurements. Since the magnitude of the sensitivity of the samples with crown ethers is in between those of the samples with SiO_2 and the samples with –$C_{10}H_{21}$ it might even be hypothesized that SiO_2 could be responsible for the response of the samples with crown ethers if the amount of SiO_2 in these samples was to be higher than at the samples with -$C_{10}H_{21}$ monolayers. Two arguments are now given that oppose this hypothesis. Firstly, it is expected that the mixed monolayer of functionalized and unfunctionalized chains does not have a negative influence on the packing density as compared to a monolayers of 100% unfunctionalized alkyl chains. This was demonstrated for mixed monolayers derived from 1-alkenes and esterified 1-alkenes with trifluoro ethyl groups as end groups [22]. The second argument is explained in detail in the up coming paragraph.

In a later stage in this project it was realized that the choice to use the 15-crown-5 crown ether was not the most suitable to demonstrate ion-sensing of EIS-structures modified with Si-C linked monolayers. The few data on the pK_{K+} and pK_{Na+} values that could be found in literature of complexation of this crown ether with both tested ions in *aqueous* solutions showed that these values are very low for K^+ complexation and even lower for Na^+ complexation. In the first paper it was measured via the Ion Exchange Method that $pK_{K+} = 0.76$ and $pK_{Na+} = 0.67$ [39, 41]. In another paper it was determined via emf measurements that $pK_{K+} = 0.6$ and $pK_{Na+} < 0.3$ [27]. Since most complexation constants are determined via measurements in non-polar *organic* solvents (mostly methanol) one can get a distorted image. The complexation constants are in these cases 3 or more orders of magnitude higher since the crown doesn't have to compete with the dehydrations process of the ions in the water [27]. In Figures 6.7 and 6.8 simulations were shown in which the influence of pK_{I+} was visualized. For $pK_{I+} = 1$ already low sensitivities were expected. The data from literature implies that in practice the situation will even be worse as was indeed found. In summary, the responses upon K^+ and Na^+ as measured by the HOSFETs and EIS-structures with organic monolayers with 15-crown-5 functional groups are most probably caused by the crown ether and not by any residual SiO_2 at these samples. Instead, the low responses are due to the low complexation constants of this crown ether in aqueous solutions. To obtain better results the use of 18-crown-6 is proposed. Based on its crown-size it should demonstrate the highest affinity towards K^+ [27]. This is confirmed in literature, where values for $pK_{K+,\ (18\text{-crown-6})}$ are all in the range of 1.83 – 2.29 as reviewed in the first paper [39] and a value of $pK_{K+,\ (18\text{-crown-6})} = 2.06 \pm 0.04$ was found in the second paper [27]. Furthermore, the cross sensitivity towards Na^+ is much lower as compared to the 15-crown-5, $pK_{Na+,\ (18\text{-crown-6})}$ are all in the range of 0.40 – 1.44 (of which most of the values were < 1) as reviewed in the first paper [39] and a value of $pK_{Na+,\ (18\text{-crown-6})} < 0.3$ was found in the second paper [27]. Such an increase in pK_{K+} is expected to make a large difference in the sensitivities. In Figures 6.7 and 6.8 the simulations for $pK_{I+} = 2$ are expected to be in between the lines for $pK_{I+} = 1$ and 3 which predicts a large increase in sensitivity as compared for $pK_{I+} < 1$. It is hypothesized that the use of the 18-crown-6 in HOSFETs and EIS-structures will demonstrate sensitivities higher than those of samples with pure SiO_2 thereby confirming the ion-sensing abilities of functionalized monolayers on silicon surfaces.

6.4 Conclusions

In this chapter a number of studies on the Hybrid Organic Semiconductor FET (HOSFET) were shown. Concerning the solid-state characterization of HOSFETs with metallized (Al) gate contacts no solid conclusions can be given since the HOSFETs were most likely short-circuited due to an over-etching of the gate area at the HF-etch step thereby exposing the source and drain region. After the metallization step the channel is then effectively short-circuited.

The results of the ion-sensing measurements of HOSFETs with unfunctionalized monolayers and mixed monolayers with receptors were very promising, though not fully conclusive. HOSFETs with unfunctionalized monolayers displayed *pH* sensitivity, and just like the EIS-structures with unfunctionalized monolayers this was strongly reduced as compared to pure SiO_2 gate insulators. This indicates that despite the good surface coverage of the monolayer still some SiO_2 sites are available. To exclude the influence of H^+ cross sensitivity due to Si-OH sites, crown ethers (15-crown-5) were incorporated in mixed monolayers to obtain functionalities towards Na^+ and K^+ ions. The initial measurements on thus functionalized HOSFETs showed a very low sensitivity towards K^+ ions as compared to reference ISFETs with SiO_2 gate insulators. Consecutive measurements were performed with EIS-structures modified with such monolayers and as a reference pure $-C_{10}H_{21}$ monolayers or pure SiO_2. The highest sensitivity towards both cations was found for the samples with SiO_2, followed by the functionalized monolayers and then no sensitivity at all for the inert monolayers. The results of the samples modified with crown ethers were similar to the data determined via the HOSFETs. It was concluded that the low affinity of the 15-crown-5 towards both K^+ and Na^+ in aqueous solutions was responsible for the low responses and not any residual oxide in the monolayers. It was postulated that the choice for the 18-crown-6 should lead to much better results since its affinity towards K^+ is at least a ten-fold higher than in case of the 15-crown-5.

The fact that inert monolayers are insensitive towards cations shows the potential of these monolayers in creating sensing structures made from silicon with Si-C linked monolayers. Although the actual results of the cation sensing measurements were not as good as hoped, the results are nonetheless very promising. After all, it was reasoned that the poor results could in fact be attributed to poor binding properties of the chosen receptor and not to deficiencies of the supporting silicon-monolayer device. The proof of ion-sensing of such silicon electrodes modified with functionalized, Si-C linked monolayers is expected to be confirmed with the use of an 18-crown-6 crown ether as receptor group.

6.5 Experimental

6.5.1 Solid state HOSFETs with aluminum gates

Sample preparation

For this study two different wafers were used. Wafer 1 contained already processed ISFETs with 70 nm SiO2 gate oxide (type A). On wafer 2 (4" p-type, <100> oriented, ρ = 5-10 Ω·cm from Okmetic, Finland) ISFETs were processed according to the standard NMOS process of the BIOS-group (University of Twente) [4]. The difference with the original design was the exclusion of the gate insulator fabrication step. The gate oxide consisted now merely of native oxide. Subsequently on the aluminum source, drain and bulk contacts a layer of Ti/Pt was sputtered in order to create a protective layer over these contacts for the fabrication process of the monolayer in which an HF etching step is necessary. Afterwards both wafers were diced into pieces of 12 mm x 24 mm in such a way that every piece contained 24 FETs. From wafer 2 three types of FETs were made: FETs with native oxide insulators (type B), Si-H terminated silicon as insulator (type C), and a $–C_{16}H_{33}$ monolayer as insulator (type D).

Samples of type D were made via etching (2 min in 2.5% HF), followed by a thermal procedure (2 h reflux in a 0.5 M solution of 1-hexadecene in mesitylene) [13]. Afterwards the sample was rinsed excessively with distilled PE 40/60, EtOH, and CH_2Cl_2, respectively. Modified samples were stored under vacuum.

Prior to metal evaporation the chips with FETs of type B and C were cleaned ultrasonically for 5 minutes in demi water and acetone, consecutively. Then they were placed for 2 minutes in an oxygen plasma cleaner (Harrick PDC-002). Chips of type C were subsequently etched in 1% HF for 40 seconds. The backside of the chips which contained also native oxide turned hydrophobic after approximately 30 seconds. Assuming that the native oxide at the gate was of similar thickness this indicated that a Si-H surface was formed. These chips were then rinsed thoroughly with demi water and spinned dry. Chips with FETs of types A and D were processed as received.

Chips of all 4 types were put in a home-made holder which was placed in the carousel of the evaporation apparatus. Since the carousel rotated continuously during evaporation, the angle varied between 5 – 39° from the crucible's center, relative to the vertical axis of the system. Evaporation started after reaching $< 1\cdot10^{-6}$ mbar base pressure. The deposition rate was estimated to be 12 $Å\cdot s^{-1}$. After the deposition a lithographic mask was applied, and the parts with exposed aluminum (complete area apart from the gate) were etched in commercially available aluminum etchant (acetic acid, nitric acid, and phosphoric acid). A close-up of a resulting chip is depicted in Figure 6.18.

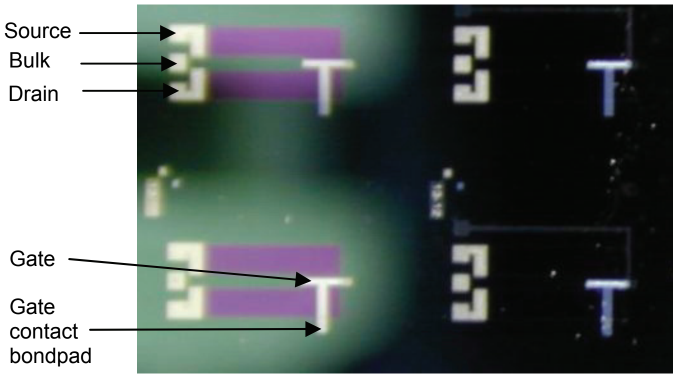

Figure 6.18. Close up of 4 identical FETs of a chip with aluminated gate contact. The left-hand side FETs are illuminated and hence their source and drain regions are visible.

Electrical characterization and settings

The chips were placed on a manual probe station (Cascade model 11000) and each FET was contacted via 4 pins. These were attached to a Hewlett Packard 4156C Semiconductor Parametric Analyzer. Via a low leakage switch mainframe the analyzer was connected to a PC, from where the setup was controlled via the Metrics software package ICS. The bulk and source were interconnected. The following settings were applied for the measurements of:

$I_{DS} - V_{GS}$ and $I_{GS} - V_{GS}$: V_{GS} sweep from -10 to 2.0 V with steps of 120 mV at different values of V_{DS} of 0.0, 0.25, 0.50, 0.75, and 1.0 V (type A) or V_{GS} sweep from -1.5 to 1.5 V with steps of 30 mV at different values of V_{DS} of 0.0, 0.25, 0.50, 0.75, and 1.0 V (types B, C, and D). In all cases I_{DS} and I_{GS} (leakage currents) were measured simultaneously.

$I_{DS} - V_{DS}$: V_{DS} sweep from 0 to 2.0 V with steps of 28.6 mV at different values of V_{GS} of -10, -7.6, -5.2, -2.8, -0.4, and 2.0 V (type A) or V_{DS} sweep from 0 to 2.0 V with steps of 28.6 mV at different values of V_{GS} of -1.5, -0.9, -0.3, 0.3, 0.9, and 1.5 V (types B, C, and D).

6.5.2 HOSFETs and EIS-structures for ion-sensing measurements

Sample preparation of the HOSFETs

The HOSFETs (Sentron, PEI packaging, see Figure 6.19) were used as received, since they cannot go along with piranha solutions or plasma cleaner conditions. The gate – in all cases 18-19 x 600 micrometer – was etched by applying a small drop of 2.5% HF. After 2 min the HF solution was removed and the FETs were rinsed extensively with ultra pure water and dried under a stream of nitrogen. This drying step is essential since the PEI packaging remains wet. Subsequently, the FETs were modified photochemically [22, 42] in a cylindrical vial that was equipped with a flat bottom. The HOSFET was placed upside down and a 447 nm double bore lamp (Jelight Company Inc., Irvine, CA, model: 84-247-2 (447 nm) was placed under the vial (Figure 6.19). After 15 h of irradiation, the HOSFETs were rinsed with PE40/60, EtOH, and PE40/60, respectively. CH_2Cl_2 was not used since partially halogenated solvents can attack PEI. After flushing with N_2 the HOSFETs were sealed under vacuum and stored in dark until electrical characterization.

1 = SiO_2
2 = Isolation
3 = Metal layer
4 = Isolation
5 = Glue / resin
6 = PolyEtherImide (PEI)

Figure 6.19. Schematic representation of the FETs designed by Sentron (left). Photo of the set-up used in the photochemical modification of the gate of a FET (right). The FET is placed upside down in order to illuminate the gate with the penlight that is positioned just under the vial.

Via this process three types of HOSFETs were prepared using a) 1 ml of neat 1-hexadecene, b) solution of 1 ml of 20% 10-undecylenic acid methyl ester (compound 6.1, see Figure 6.20) and 80% 1-decene in mesitylene (total alkene concentration 1.0 M) and c) solution of 10% undecenoyloxymethyl-15-crown-5 (compound 6.2, see Figure 6.20) mixed with 90% 1-decene in mesitylene (total alkene concentration 1.0 M).

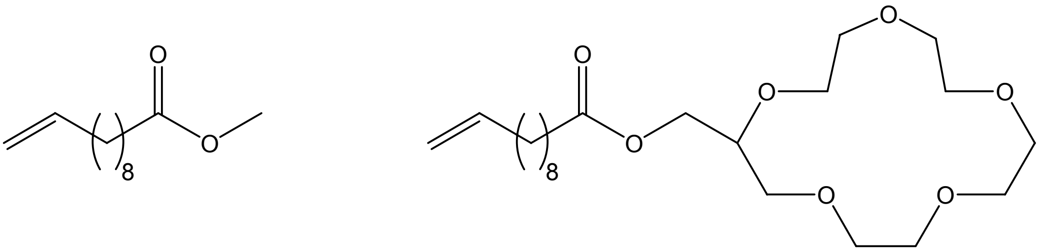

Figure 6.20. Structures of (left) 10-undecylenic acid methyl ester (compound 6.1) and (right) undecenoyloxymethyl-15-crown-5 (compound 6.2).

Sample preparation of EIS-structures with crown ether functionalized monolayers

Details on wafer type and the fabrication of the back contact and the dicing of the wafers into pieces of 10 mm x 10 mm is described in Chapter 5, section 5.5.2. The samples were first sonicated for 10 minutes in demineralized water. Then the samples were wiped with a tissue that was saturated with chemically pure acetone. After that, the samples were sonicated for at least ten minutes in acetone. Then the samples were placed in an oxygen plasma cleaner (Harrick PDC-32G) for 10 minutes. Subsequently, the samples were etched with 2.5% HF for 2 minutes and after that the monolayers were prepared via a thermal procedure (2h reflux; 0.2 M solution) [13]. In this section two different mixed monolayers have been studied: 10 and 25% of compound 6.2 (see Figure 6.20) was mixed with 90 and 75% of 1-decene, respectively. Monolayers prepared from 100% 1-decene were used as a reference. After the monolayer preparation the samples were rinsed excessively with distilled PE 40/60, EtOH, and CH_2Cl_2, respectively. Modified samples were stored under vacuum.

Measurement setups and settings

In case of the HOSFETs with unfunctionalized monolayers the set-up in Figure 6.21 was used:

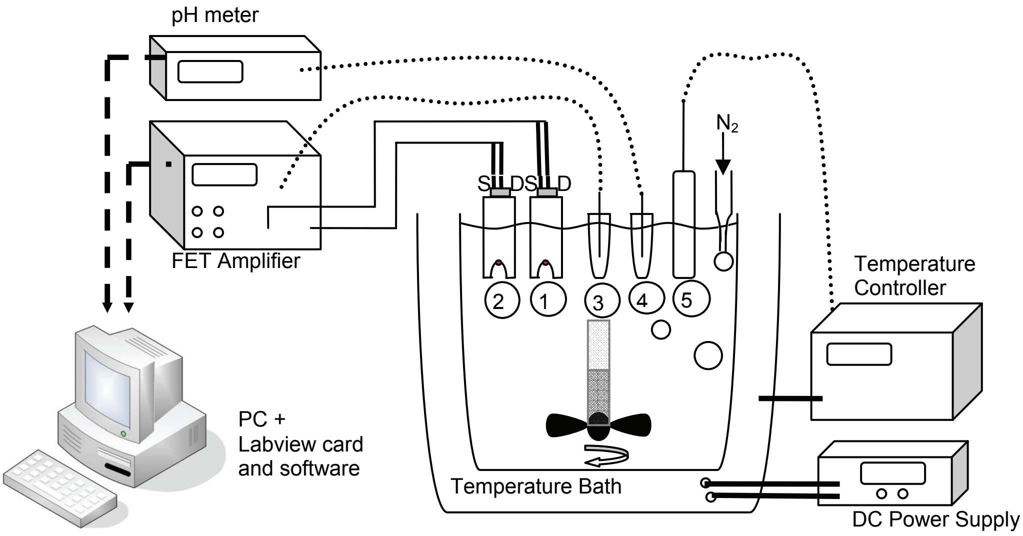

Figure 6.21. Schematic drawing of the HOSFET measurement set-up. The numbers denote the following items: 1 = HOSFET, 2 = reference FET, 3 = Ag/AgCl (sat'd KCl) reference electrode, 4 = pH electrode, and 5 = pT100 temperature sensor.

The electrode bath consists of a 100 ml beaker glass tightly packed in a temperature bath. On top of the glass a cover (not shown in picture) is placed in which the electrodes and FETs can be inserted. The cover also incorporates a stirrer in the middle which is used to continuously stir the fluid. Both FETs are connected to a FET amplifier [3, 4]. The output voltage of such amplifier is directly related to the change in surface potential ϕ_0 due to pH changes. The reference electrode is used to contact the gate of the FET and bias the liquid. The pH is continuously measured with a pH meter (PHM83 autocal pH meter, Radiometer). Both pH meter and FET amplifier are connected (sometimes via an additional multimeter) to a LABVIEW sampling board and read out by a LABVIEW controlled software program.

The electrolyte consisted of 65 ml, 0.1 M solution of TetraButylAmmonium Cloride (TBACl) (Fluka; purum, >97%) to which 260 μl of buffer mixture (0.5 M acetic acid, 0.5 M boric acid, and 0.5 M orthophosphate acid) was added. Titrations are carried out with (diluted) HCl (Riedel – de Haën; extra pure) and (diluted) TetraButylAmmonium Hydroxide (TBAOH) (Aldrich; ~ 40% in water). The temperature is kept constant at 25 ± 0.1° C. To prevent as much of the influence of oxygen as possible, nitrogen is continuously blown through the liquid. The FETs are operated at fixed Drain-Source current $I_{DS} = 100$ μA and voltage $V_{DS} = 0.60$ V.

The following measurement protocol is used. A pH sweep was started at pH 1 and then increased to pH 7 and afterwards returned to pH 1. The pH step size was approximately 1 pH unit and the measurement time at each pH value was approximately 1000 seconds. This was long enough to both monitor the FET response and to a lesser degree the short-term drift behavior.

For the HOSFETs with crown ether functionalized monolayer a new titration set-up had been built in the form of a flow-cell (see Figure 6.22). This enabled us to quickly change between solutions and perform easily up and down going titration that were otherwise not possible for ions other than H^+.

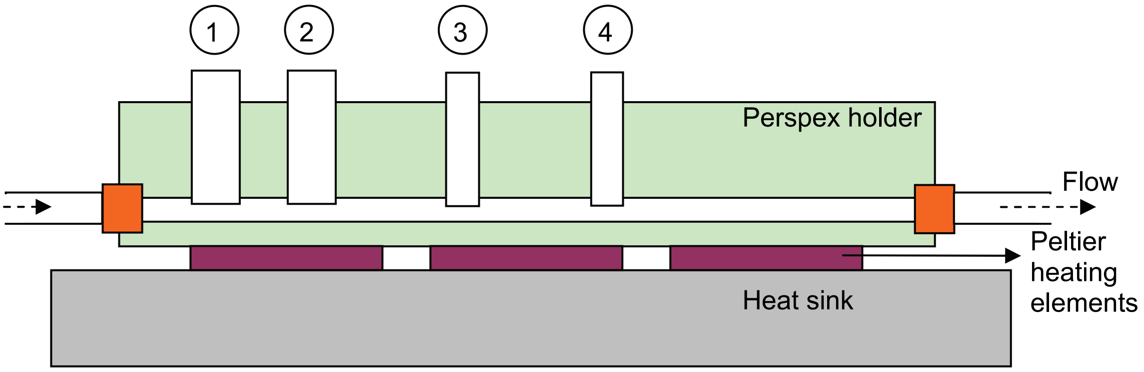

Figure 6.22. Schematic drawing of part of the HOSFET flow-cell set-up. The numbers denote the following items: 1 = HOSFET, 2 = reference FET, 3 = Ag/AgCl (sat'd KCl) reference electrode, and 4 = pT100 temperature sensor.

In this set-up a HOSFET is placed together with a reference FET or another HOSFET in the perspex holder in which a smooth channel has been carefully drilled. Also inserted in the holder are a reference electrode and a temperature sensor to measure the temperature in the flow channel. The perspex holder is placed on Peltier heating elements that are on a heat sink with heat conducting grease smeared between them. The Peltier elements are connected to a computer controlled temperature controller (TCM, Electron Dymamics Ltd.). The controller was set to the PI (Proportional and Integration) modus with parameters: $P = 50$ and $T_i = 100$ s. In this way a very stable temperature of 25 ± 0.1° C was maintained in the channel. To the inlet channel two manually operated valves were connected in order to facilitate quick and easy switching between solutions. The flasks with solutions were placed at elevated positions with respect to the flow-cell using gravity as driving force for the liquid flow.

A total of 6 solutions were prepared with KCl (Aldrich; 99+%, A.C.S. Reagent) concentrations varying from 0 to 0.1 M. As a background electrolyte TetraEthylAmmonium Chloride (Fluke; purum, ≥ 98%) was used. The reasons to go to the TEA^+ instead of the bigger TBA^+ cation are based on the indications that TBA^+ may adsorb to the monolayer (Chapter 5, appendix A). It is expected that a smaller cation like TEA^+ will not adsorb. This is supported by the work of Flink et al. on electrochemical measurements on crown ether functionalized monolayers bound to gold surfaces. They did not observe any adsorption phenomena on their crown ethers or monolayers [32, 40]. The total concentration (ionic strength) of KCl and TEACl was kept constant, i.e. [KCl] + [TEACl] = 0.14 M. Furthermore, a phosphate buffer (10 mM) was added to all solutions to keep all solutions at *pH* 7. The *pH* was adjusted with (diluted) HCl (Riedel – de Haën; extra pure) and (diluted) TetraEthylAmmonium Hydroxide (TEAOH) (Aldrich; purum, ~ 40% in water). The measurements started with $[K^+] = 0$ M and at fixed time intervals a ten fold increase in KCl concentration (starting at 10 μM) was led to the flow cell.

In case of the measurements on the EIS-structures with crown ether functionalized monolayers the following set-up was used. The samples were first placed in a separate home-made Teflon sample holder. Via an opening with an O-ring in the holder the sample surface was in contact with the electrolyte. The area of this contacted surface was approximately 0.49 cm^2. This holder was placed in a beaker glass with 65 ml of electrolyte and was connected as the working electrode to a Princeton Applied Research PARSTAT2263 potentiostat, which was computer controlled via the PowerSuite software package. To the potentiostat also an Ag/AgCl (sat'd KCl) electrode and a platinum electrode were connected as reference electrode and counter electrode, respectively. The beaker glass and electrodes were placed in home-made thermostat bath which was kept constant at 25 ± 0.1° C using a similar controller and the same settings as described for the HOSFETs. Per titration point multiple Mott Schottky measurements (in fact impedance measurements) were performed using a bias voltage sweep from 0.0 V to –1.0 V vs. Ag/AgCl in steps of 10 mV. The amplitude and frequency of the ac-voltage were 10 mV and 10 kHz, respectively. At the first titration point 12 measurements over 45 minutes were done; at consecutive titration points 7 measurements over 30 minutes were done. The flatband voltage V_{fb} and doping N_A were obtained from each data set via the computer program Matlab in which an automatic extraction routine was incorporated (Chapter 4, appendix D).

The titrations were performed in such a way that the same KCl (Aldrich; 99+%, A.C.S. Reagent) concentrations were used at each titration point as in case of the HOSFET measurements described above with the exception of the highest KCl concentration which was now 95 mM instead of 100 mM and the total ionic strength which was now higher, i.e. [KCl] + [TEACl] = 0.351 M. Also a phosphate buffer (10 mM) at *pH* 7 was added to the solutions. After the titration was completed the sample holder and electrodes were thoroughly rinsed with demi water and in clean glass ware the same titrations were repeated under the same conditions with NaCl (Merck; p.a.) instead of KCl.

6.6 References

[1] P. Bergveld, "Development, Operation, and Application of the Ion-Sensitive Field-Effect Transistor as a Tool for Electrophysiology", *IEEE Transactions on Biomedical Engineering* **1972**, *BME-19*, 342.

[2] P. Bergveld, "Development of an Ion-Sensitive Solid-State Device for Neurophysiological Measurements", *IEEE Transactions on Biomedical Engineering* **1970**, *BME-17*, 70.

[3] P. Bergveld, "Thirty years of ISFETOLOGY - What happened in the past 30 years and what may happen in the next 30 years", *Sensors and Actuators B-Chemical* **2003**, *88*, 1.

[4] P. Bergveld, A. Sibbald, *Analytical and Biomedical Applications of Ion-Selective Field-Effect Transistors, Vol. XXIII*, Elsevier, **1988**.

[5] P. Bergveld, "The impact of MOSFET-based sensors", *Sensors and Actuators* **1985**, *8*, 109.

[6] S. M. Sze, *Semiconductor Devices: Physics and Technology*, Wiley, New York, **1985**.

[7] D. K. Schroder, *Semiconductor Material and Device Characterization*, 2nd ed., Wiley, New York, **1998**.

[8] J. L. Diot, J. Joseph, J. R. Martin, P. Clechet, "pH dependence of the Si/SiO2 interface state density for EOS systems : Quasi-static and AC conductance methods", *Journal of Electroanalytical Chemistry* **1985**, *193*, 75.

[9] E. J. R. Sudhölter, H. Zuilhof, A. B. Sieval, L. C. P. M. de Smet, G. M. Visser, P. Bergveld, W. Olthuis, E. J. Faber, patent EP 1 363 122 A1, **2003**

[10] M. R. Linford, P. Fenter, P. M. Eisenberger, C. E. D. Chidsey, "Alkyl Monolayers on Silicon Prepared from 1-Alkenes and Hydrogen-Terminated Silicon", *Journal of the American Chemical Society* **1995**, *117*, 3145.

[11] A. B. Sieval, R. Linke, H. Zuilhof, E. J. R. Sudhölter, "High-quality alkyl monolayers on silicon surfaces", *Advanced Materials* **2000**, *12*, 1457.

[12] L. C. P. M. de Smet, *Covalently Bound Organic Monolayers on Silicon Surfaces: Visible Light Attachment, Characterization and Electrical Properties*, PhD thesis, Wageningen University (Wageningen), **2006**, chapter 1, p. 3.

[13] A. B. Sieval, V. Vleeming, H. Zuilhof, E. J. R. Sudhölter, "An improved method for the preparation of organic monolayers of 1-alkenes on hydrogen-terminated silicon surfaces", *Langmuir* **1999**, *15*, 8288.

[14] J. D. Plummer, M. D. Deal, G. P.B., *Silicon VLSI Technology, Fundamentals, Practice and Modeling*, Prentice Hall, New Yersey, **2000**.

[15] D. Niwa, K. Omichi, N. Motohashi, T. Homma, T. Osaka, "Organosilane self-assembled monolayer-modified field effect transistors for on-chip ion and biomolecule sensing", *Sensors and Actuators B-Chemical* **2005**, *108*, 721.

[16] P. Estrela, A. G. Stewart, F. Yan, P. Migliorato, "Field effect detection of biomolecular interactions", *Electrochimica Acta* **2005**, *50*, 4995.

[17] D.-S. Kim, Y.-T. Jeong, H.-J. Park, J.-K. Shin, P. Choi, J.-H. Lee, G. Lim, "An FET-type charge sensor for highly sensitive detection of DNA sequence", *Biosensors and Bioelectronics* **2004**, *20*, 69.

[18] A. Poghossian, A. Cherstvy, S. Ingebrandt, A. Offenhausser, M. J. Schoning, "Possibilities and limitations of label-free detection of DNA hybridization with field-effect-based devices", *Sensors and Actuators B-Chemical* **2005**, *111*, 470.

[19] W. Cai, J. R. Peck, D. W. van der Weide, R. J. Hamers, "Direct electrical detection of hybridization at DNA-modified silicon surfaces", *Biosensors and Bioelectronics* **2004**, *19*, 1013.

[20] F. Wei, B. Sun, Y. Guo, X. S. Zhao, "Monitoring DNA hybridization on alkyl modified silicon surface through capacitance measurement", *Biosensors & Bioelectronics* **2003**, *18*, 1157.

[21] S. Flink, F. C. J. M. van Veggel, D. N. Reinhoudt, "Sensor functionalities in self-assembled monolayers", *Advanced Materials* **2000**, *12*, 1315.

[22] Q.-Y. Sun, L. C. P. M. de Smet, B. van Lagen, A. Wright, H. Zuilhof, E. J. R. Sudhölter, "Covalently Attached Monolayers on Hydrogen-Terminated Si(100): Extremely Mild Attachment by Visible Light", *Angewandte Chemie International Edition* **2004**, *43*, 1352.

[23] X. G. Zhang, *Electrochemistry of Silicon and its Oxide*, Kluwer Academic Publishers, New York, **2001**.

[24] A. B. Sieval, *Covalently Bound Organic Monolayers on Hydrogen-Terminated Silicon Surfaces*, PhD thesis, Wageningen University (Wageningen), **2001**, chapter 3, p. 44.

[25] R. E. G. van Hal, J. C. T. Eijkel, P. Bergveld, "A general model to describe the electrostatic potential at electrolyte oxide interfaces", *Advances in Colloid and Interface Science* **1996**, *69*, 31.

[26] G. W. Gokel, D. M. Goli, C. Minganti, L. Echegoyen, "Clarification of the Hole-Size Cation-Diameter Relationship in Crown Ethers and a New Method for Determining Calcium Cation Homogeneous Equilibrium Binding Constants", *Journal of the American Chemical Society* **1983**, *105*, 6786.

[27] H. K. Frensdorff, "Stability Constants of Cyclic Polyether Complexes with Univalent Cations", *Journal of the American Chemical Society* **1971**, *93*, 600.

[28] G. W. Gokel, *Crown Ethers and Cryptands*, Royal Society of Chemistry, Cambridge, **1991**.

[29] R. C. Weast, M. J. Astle, W. H. Beyer, *CRC Handbook of Chemistry and Physics*, 65th ed., CRC Press, Boca Raton, Florida, **1984**.

[30] G. W. Gokel, W. M. Leevy, M. E. Weber, "Crown ethers: Sensors for ions and molecular scaffolds for materials and biological models", *Chemical Reviews* **2004**, *104*, 2723.

[31] K. Suzuki, K. Sato, H. Hisamoto, D. Siswanta, K. Hayashi, N. Kasahara, K. Watanabe, N. Yamamoto, H. Sasakura, "Design and synthesis of sodium ion-selective ionophores based on 16-crown-5 derivatives for an ion-selective electrode", *Analytical Chemistry* **1996**, *68*, 208.

[32] S. Flink, B. A. Boukamp, A. van den Berg, F. C. J. M. van Veggel, D. N. Reinhoudt, "Electrochemical detection of electrochemically inactive cations by self-assembled monolayers, of crown ethers", *Journal of the American Chemical Society* **1998**, *120*, 4652.

[33] C. Miramond, D. Vuillaume, "1-octadecene monolayers on Si(111) hydrogen-terminated surfaces: Effect of substrate doping", *Journal of Applied Physics* **2004**, *96*, 1529.

[34] S. Kar, C. Miramond, D. Vuillaume, "Properties of electronic traps at silicon/1-octadecene interfaces", *Applied Physics Letters* **2001**, *78*, 1288.

[35] T. Matsuo, M. Esashi, "Methods of isfet fabrication", *Sensors and Actuators* **1981**, *1*, 77.

[36] S. C. Chen, Y.-K. Su, J. S. Tzeng, "The fabrication and characterisation of ion-sensitive field-effect transistors with a silicon dioxide gate", *Journal of Physics D: Applied Physics* **1986**, *19*, 1951.

[37] C. J. Pedersen, "Cyclic Polyethers and Their Complexes with Metal Salts", *Journal of the American Chemical Society* **1967**, *89*, 2495.

[38] C. J. Pedersen, "Cyclic Polyethers and Their Complexes with Metal Salts", *Journal of the American Chemical Society* **1967**, *89*, 7017.

[39] R. M. Izatt, K. Pawlak, J. S. Bradsha, R. L. Bruening, "Thermodynamic and Kinetic Data for Macrocycle Interaction with Cations and Anions", *Chemical Reviews* **1991**, *91*, 1721.

[40] S. Flink, F. C. J. M. van Veggel, D. N. Reinhoudt, "Recognition of cations by self-assembled monolayers of crown ethers", *Journal of Physical Chemistry B* **1999**, *103*, 6515.

[41] The K_s values in literature are the reciprocal values of the K_{I+} values as defined in the model we are using (Equation 6.6). However, their logarithmic values can be easily compared by realizing that $\log(K_s) = pK_{I+}$.

[42] Q.-Y. Sun, L. C. P. M. de Smet, B. van Lagen, M. Giesbers, P. C. Thune, J. van Engelenburg, F. A. de Wolf, H. Zuilhof, E. J. R. Sudhölter, "Covalently Attached Monolayers on Crystalline Hydrogen-Terminated Silicon: Extremely Mild Attachment by Visible Light", *Journal of the American Chemical Society* **2005**, *127*, 2514.

Chapter 7

Conclusions and Recommendations

Abstract: In this final chapter some overall conclusions are drawn followed by a reiteration of the conclusions of the preceding chapters. Subsequently, a number of recommendations are given for future research.

7.1 Conclusions

Overall, this research project has reached a promising stage. In Chapters 2 and 3 it was shown that the electronic properties of MIS-structures with organic monolayers as insulators on both n-type and p-type silicon were remarkably good. The leakage currents through these structures scaled in a direct manner with the monolayer chain length; the number of interface charges was very low and monolayers derived from 1-alkynes were superior as compared to monolayers derived from 1-alkenes. From the electronic point of view, organic monolayers covalently bound to silicon offer a promising insulating and passivating material for hybrid molecule-silicon electronics. Moreover, given the numerous possibilities for chemical modification of the properties of the organic monolayers and the formation of true silicon-organic molecule interfaces, we believe that such layers are very promising for future nano-dimensioned silicon devices.

In order to measure *pX* responses in the electrochemical domain of EIS-structures with (un)functionalized monolayers the Mott Schottky measurements were proposed since the commonly used methods to investigate these *pX* responses could not be applied. This has proven to be a successful method for determining the *pH* responses of EIS-structures with unfunctionalized monolayers. It was shown that minute traces of SiO_2 (< 1% of active sites as compared to pure SiO_2 surfaces) were present at unfunctionalized monolayers, which still give a considerable *pH* response. Nonetheless, the results are promising for application of such monolayers in sensory EIS-structures, albeit that cross sensitivity towards H^+ should be taken into account.

The results of the ion-sensing measurements of HOSFETs with unfunctionalized monolayers and mixed monolayers with receptors were very promising, though not fully conclusive. HOSFETs with unfunctionalized monolayers displayed *pH* sensitivity in the same order as the EIS-structures with unfunctionalized monolayers, indicating that despite the good surface coverage of the monolayer still some SiO_2 sites are available. Crown ethers (15-crown-5) were incorporated in mixed monolayers in both HOSFETs and EIS-structures to obtain functionalities towards Na^+ and K^+ ions. The highest sensitivity towards both cations was found for the samples with SiO_2, followed by the functionalized monolayers and then no sensitivity at all for the inert monolayers. It was concluded that the low affinity of the 15-crown-5 towards both K^+ and Na^+ in aqueous solutions found for both HOSFETs and EIS-structures modified with monolayers with that receptor, was responsible for the low responses and not any deficiencies of the supporting silicon-monolayer device. The fact that inert monolayers are insensitive towards cations shows the potential of these monolayers in creating sensing structures made from silicon with Si-C linked monolayers. For completeness, the conclusions per chapter are reiterated below.

Chapter 2

Organic monolayers ($-C_nH_{2n+1}$, n = 10, 12, 16, and 22) covalently bound to p- and n-type silicon were successfully characterized via *J-V* and C-V measurements and the results were compared with H-terminated samples and samples with 2 nm SiO_2. It was demonstrated that all layers showed insulating behavior and behaved as Schottky diodes. All monolayers on n-type silicon and monolayers > C_{12} on p-type silicon showed better insulating properties than SiO_2.

Results from *J-V* measurements for p-silicon samples showed that the effective barrier height $q\phi_{eff}$ increased clearly as a function of monolayer thickness. Not only the effective barrier height is affected by the chain length, but also the series resistance R_s was strongly affected in an exponential way. Samples of n-type silicon modified with alkyl monolayers did not display this clear dependence. It was found that $q\phi_{eff}$ increased for nC_{10} and nC_{12} as compared to nSiH and $nSiO_2$, but a decrease was found for the longer chains. An unambiguous explanation for this phenomenon can as of yet not be given and has to be further investigated. Organic alkyl monolayers on n-type silicon form more ideal diodes than these monolayers on p-type silicon.

Results from *C-V* measurements showed typical metal-semiconductor *C-V* behavior for SiH, SiO_2, C_{10}, and C_{12} covered silicon. For C_{16} and C_{22} layers a plateau in accumulation was observed and this indicated the formation of a real capacitance. Analysis of this plateau yielded the dielectric constant, which varied from 1.7 ± 0.1 to 2.8 ± 0.2. Mott Schottky analysis gave similar values for the flatband voltage for different chain lengths apart from pC_{10} samples. This suggests similar interface properties for all investigated monolayers other than pC_{10}. For the C_{16} and C_{22} layers the amount of fixed charge has been evaluated. This gave remarkably low values of fixed charge density for monolayers on p-type silicon ($\sim 6 \cdot 10^{11}$ cm^{-2}) as compared to samples on n-type silicon ($\sim 3 \cdot 10^{12}$ cm^{-2}). Evaluation of the tunneling constant β gave higher values for n-type silicon, $\beta = 0.58\text{-}1.30$ Å^{-1}, as compared to p-type silicon, $\beta = 0.43\text{-}0.46$ Å^{-1} excluding the pC_{10} samples. This confirms that holes tunnel more efficient as compared to electrons.

From stability measurements it was shown that the *J-V* characteristics stayed intact for all samples. For all n-type silicon samples the current in depletion had increased, whereas for p-type silicon the current in depletion had decreased. The capacitance in accumulation had increased in all cases, indicating that ε_r of the insulator may have increased due to oxidation. For p-type silicon samples V_{fb} shifted, following a clear trend, for subsequent measurements towards more negative values. This is in line with oxidation, which usually involves the incorporation of net positive charges. For n-type silicon samples V_{fb} did not shift in a clear way and no conclusions could be drawn from that data, other than that changes have taken place given the changed *J-V* and *C-V* curves.

From the above results we conclude that from the electronic point of view, organic monolayers covalently bound to silicon offer a promising insulating and passivating material for molecular electronic devices. Moreover, given the numerous possibilities for chemical modification of the properties of the organic monolayers and the formation of true silicon-molecule interfaces, we believe that such layers are very promising for future nano-dimensioned silicon devices.

Chapter 3

An electrical study on the influence of molecule type (1-octadecene/1-octadecyne) and silicon substrate orientation (<100>/<111>) has been carried out on Hg | C_{18} monolayer | n-type silicon structures. Both *J-V* and *C-V* measurements have been performed and repeated a number of times to investigate the reproducibility of the samples. The outcome was compared with XPS measurements. A number of clear trends were observed from both *J-V* and *C-V* results. The current densities of the samples modified with alkynes were at least two times lower than those modified with alkenes. The effective barrier heights were approximately 0.08 eV higher for the samples modified with alkynes as compared to those modified with alkenes, indicating a better quality of silicon-monolayer interface for the former. Also the series resistance was significantly higher for the samples modified with alkynes. The values of ε_r of the monolayer made from 1-alkynes were significantly lower than those made from 1-alkenes, indicating a higher degree of oxide present at the monolayers of 1-alkenes. The values of the flatband voltage were approximately 0.1 V more positive for the samples modified with alkynes with respect to those modified with alkenes, which may be again attributed to a higher degree of oxide present at the latter. Concerning the substrate orientation, no clear influence of this was observed in both *J-V* and *C-V* results. This apparent lack of influence of substrate orientation on device behavior and silicon-monolayer interface properties as compared to a SiO_2 insulator is quite remarkable. Nonetheless, this can be seen as a proof for the broad usability of these monolayers in creating stable devices with the desired, precisely tunable interface properties.

The results of the XPS measurements correlated with the differences observed between monolayers made of 1-alkynes or 1-alkenes. More oxygen was present at the monolayers made from 1-alkenes. However, XPS showed that the C_{18} monolayers on Si <111> contained overall more oxygen as compared to all Si <100> samples. This finding could not be correlated in any way to the findings from the electrical characterization and a clear explanation for this is so far not known.

In conclusion, XPS and electrical characterizations provide a powerful combination to determine the electronic properties of such MIS-structures with organic insulators. This study showed via both methods the preferred use of 1-alkynes over 1-alkenes in creating metal-insulator-silicon devices. The ease of fabrication together with the outstanding electrical properties shows the potential applications of the monolayers made from 1-alkynes in hybrid molecular-silicon electronics. Furthermore, given the numerous possibilities for chemical modification of such layers the properties of such electronic devices can be precisely tuned.

Chapter 4

This chapter showed an overview of theoretical and practical considerations on Mott Schottky measurements for use in the characterization of the sensory responses of EIS-structures with thin insulators. In EIS-structures the sensory response is measured via a change of the so-called flatband potential V_{fb} upon a change in stimulus, such as *pH*. In most cases relative measurements are concerned, so not the absolute value of V_{fb} is of interest, but instead ΔV_{fb}. Three methods were mentioned for determining the *pH* sensitivity at EIS-structures. Two of them involve the *C-V* curves as starting point, namely a graphical method in which upon *pH* changes the shifts of the *C-V* curves along the *V*-axis are measured and the second one involves an analytical determination of V_{fb} from ideal *C-V* curves. However, in case of nm-thin insulators *C-V* curves are often distorted, thereby making it impossible to derive the sensory response via the two mentioned methods. A third method, Mott Schottky measurements, was proposed as an alternative to derive the sensory response. The three methods have been tested on ideally behaving EIS-structures with thick insulators. The resulting *pH* sensitivity was similar for all three methods, indicating the validity of all three methods. Since there were on forehand no reasons or indications why this Mott Schottky method should not work on EIS-structures with thin insulators, it was decided that the sensitivities of EIS-structures with thin insulators could be properly analyzed via this method.

Also discussed were the non-idealities encountered during Mott Schottky measurements on EIS-structures of p-type silicon with nm-thin insulators, such as organic monolayers. The first non-ideality concerned frequency dependency of the slopes and *V*-axis intercepts. This made it impossible to derive the absolute value of V_{fb}. The second non-ideality concerned double slopes in the Mott Schottky plots giving rise to two possible flatband voltages and two possible doping values. When the silicon entered depletion a very steep slope (slope 1) appeared over a small voltage regime of approximately 0.1 V. When the silicon got further depleted the slope became less steep and this continued over a very large voltage range (slope 2) that was associated with a deep depletion situation of the electrode. Via slope 2 the proper doping values could be derived but V_{fb} derived from this slope was insensitive and not related to different analytes. From slope 1, on the other hand, V_{fb} showed a clear and realistic dependence on the different analytes. Since the region of slope 1 can be associated with the surface region of the silicon electrode it is expected to be the most sensitive to changes in *pH* and it is thus plausible to use this region as basis for the calculation of the sensitivities.

It is concluded that Mott Schottky measurements provide a good tool for investigating the *pH* responses at EIS-structures with thin insulators. The non-idealities are constant at single frequency measurements and not sensitive towards different analytes and therefore the proper sensory response can still be derived via slope 1 from relative measurements. Via slope 2 the doping can be derived as a routine check.

Chapter 5

P- and n-type silicon electrodes modified with unfunctionalized, Si-C linked monolayers, obtained via the surface alkylation of 1-alkenes, have electrochemically been characterized via a number of studies. The primary goal of these studies was to understand the electrochemical behavior of such modified electrodes in aqueous solutions before possibly applying such layers as gate insulators, and thus oxide-replacements, in FET-based sensors.

P-type electrodes and illuminated n-type electrodes modified with organic monolayers both get oxidized under anodic potentials and therefore, high anodic potentials should be avoided. From Mott Schottky measurements it was shown that the amount of oxide initially present and created under operating conditions was low, less than 1% as compared to pure SiO_2 surfaces. This remaining oxide, however, still caused a *pH* sensitivity of circa 25 $mV·pH^{-1}$ in the *pH* 4 - 7 range. All samples with monolayers showed a reduced value of pK_a (4.0 - 4.4) as compared to pure SiO_2 (6.0), indicating more acidic behavior of the remaining Si-OH groups in such monolayers. Long-term drift during Mott Schottky measurements was low, less than 1 $mV·h^{-1}$ in general. The above results clearly are promising for application of such organic monolayers in sensory EIS-structures, albeit that a cross sensitivity towards H^+ should be taken into account. Since such monolayers can be easily chemically modified with a large variety of receptor groups it is expected that a large variety of sensory structures can be created.

Chapter 6

In this chapter a number of studies on the Hybrid Organic Semiconductor FET (HOSFET) were shown. The results of the ion-sensing measurements of HOSFETs with unfunctionalized monolayers and mixed monolayers with receptors were very promising, though not fully conclusive. HOSFETs with unfunctionalized monolayers displayed *pH* sensitivity, and just like the EIS-structures with unfunctionalized monolayers this was strongly reduced as compared to pure SiO_2 gate insulators. This indicates that despite the good surface coverage of the monolayer still some SiO_2 sites are available. To exclude the influence of H^+ cross sensitivity due to Si-OH sites, crown ethers (15-crown-5) were incorporated in mixed monolayers to obtain functionalities towards Na^+ and K^+ ions. The initial measurements on thus functionalized HOSFETs showed a very low sensitivity towards K^+ ions as compared to reference ISFETs with SiO_2 gate insulators. Consecutive measurements were performed with EIS-structures modified with such monolayers and as a reference pure $-C_{10}H_{21}$ monolayers or pure SiO_2. The highest sensitivity towards both cations was found for the samples with SiO_2, followed by the functionalized monolayers and then no sensitivity at all for the inert monolayers. The results of the samples modified with crown ethers were similar to the data determined via the HOSFETs. It was concluded that the low affinity of the 15-crown-5 towards both K^+ and Na^+ in aqueous solutions was responsible for the low responses and not any residual oxide in the monolayers. It was postulated that the choice for the 18-crown-6 should lead to much better results since its affinity towards K^+ is at least a ten-fold higher than in case of the 15-crown-5.

The fact that inert monolayers are insensitive towards cations shows the potential of these monolayers in creating sensing structures made from silicon with Si-C linked monolayers. Although the actual results of the cation sensing measurements were not as good as hoped, the results are nonetheless very promising. After all, it was reasoned that the poor results could in fact be attributed to poor binding properties of the chosen receptor and not to deficiencies of the supporting silicon-monolayer device. The proof of ion-sensing of such silicon electrodes modified with functionalized, Si-C linked monolayers is expected to be confirmed with the use of an 18-crown-6 crown ether as receptor group.

7.2 Recommendations for future research

In this section a number of recommendations are given, which are divided in four different topics.

Choice of substrate, molecule type and preparation

In Chapter 3 a study has been described on the influence of the substrate orientation (<100> vs. <111>) and molecule from which the monolayer was derived (1-alkyne vs. 1-alkene) on the electronic properties. Via electrical characterization it was shown that the monolayers derived from 1-alkynes had superior properties as compared to the monolayers derived from 1-alkenes. This correlated to the findings of the XPS measurements showing that a higher amount of oxide was present in the samples with monolayers derived from 1-alkenes. One the other hand no distinction was found in the electronic behavior of the two surface orientations whereas via XPS measurements is was found that the monolayers on Si <111> contained overall more oxygen as compared to all Si <100> samples. Such study has up to now never been performed in the electrochemical domain, the eventual working domain of HOSFETs with such monolayers. The electrochemical studies described in this thesis were limited to thermally prepared [1] monolayers derived from 1-alkenes on <100> silicon. It may be interesting to know if the findings of Chapter 3 also hold in electrochemical environments or if the use of a certain crystal orientation or molecule type gives better stability (lower tendency towards oxidation) and has better electronic properties (lower amount of defects). It is known from literature that the amount of defects has a large influence on the leakage currents through such structures [2]. Furthermore, the amount of surface defects and surface roughness also plays a role in the oxidation dynamics [3]. If measurements are required in the alkaline regime ($pH > 7$) the <111> surface orientation is preferred since it is less susceptible towards etching than the <100> surface orientation [3]. Concerning the point of surface roughness it appears that the <111> surface may also be best suited since it has atomically flat terraces on the scale of ~ 10^2 by ~ 10^4 nm^2 [4, 5]. To find out the best suitable surface orientation electrochemical characterization like the ones described in Chapter 5 are recommended for a range of samples with varying surface orientations and molecule type. An important point of attention for the eventual surface roughness is the preparation of the H-terminated surfaces [5] and the miscut angle of the wafers.

HOSFET lay-out

In Chapter 6 a number of electrochemical measurements on fully packaged HOSFETs were presented. As mentioned, the measurement results should be interpreted with care as there were a number of uncertain parameters in these HOSFETs. After the HOSFET was packaged the gate area had still to be modified with a monolayer. Since the size of the gate was so small it could not be verified with standard surface characterization tools if the modification had succeeded. Also the influence of the presence of the package materials on the eventual monolayer quality remains unsure. It is therefore recommended to start the modification on planar chips with a series of FETs just as the ones described in section 6.3.1. The gate dimensions should then be increased to such dimensions that surface modification tools, such as XPS, X-ray reflectivity and AFM, can be applied to check and validate the modification process. A point of attention in the standard ISFET chip lay-out is that the source and drain regions become exposed when the chips are put in HF solution prior to the monolayer surface modification step. The source and drain regions are now fabricated via Chemical Vapor Deposition (CVD) and subsequent in-diffusion at 1100° C. This can lead to widening of the source and drain regions due to sideward diffusion of the dopant atoms as illustrated in Figure 7.1.

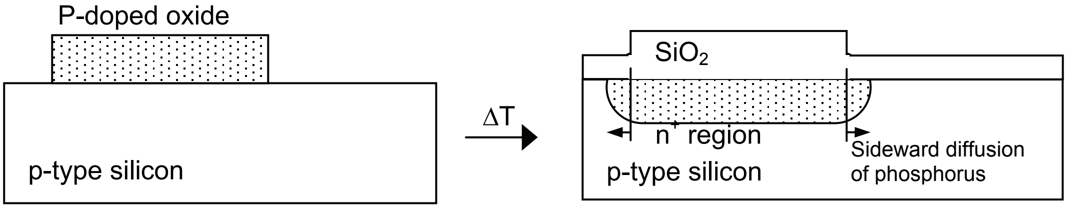

Figure 7.1. Schematic view of the manufacturing of the source and drain region. First a phosphorus doped oxide is made via Chemical Vapor Deposition and after thermal treatment the phosphorus diffuses into the silicon where it forms the n^+ region.

The sideward diffusion of the phosphorus can lead to an earlier exposure of parts of the source and drain regions than expected when the gate oxide is etched in HF. It is thus desired to have a better defined source and drain region. It is recommended to create these via Ion Implantation, which offers a more precise control of the dimensions of the source and drain areas.

Measurements set-ups

A good, practical and easy to operate measurement set-up is recommended when testing multiple chips using a large number of solutions. The testing of the HOSFETs should be done preferably as early in the fabrication process as possible, i.e. on-chip. In that case a droplet of electrolyte should only be in contact with the gate and a precise placement of the droplet is thus required, which may be possible via a Reference electrode clamped in a tube via O-rings. By pressing on the reference electrode the electrolyte is carefully dosed.

Eventually, it can be desired to test an array of HOSFETs at the same time. The gates of each HOSFET can be modified with different functionalized groups creating thus a multi-sensor array. A flow-cell may be a good option to test such arrays and the set-up described in section 6.5.2 may provide a good starting-point. In Figure 7.2 a drawing of a possible set-up for an array of FETs is illustrated.

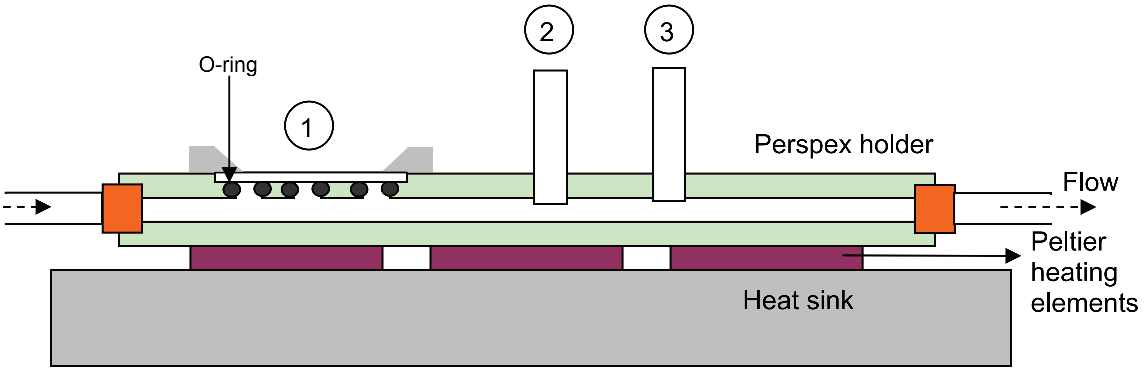

Figure 7.2. Schematic drawing of a flow-cell set-up for an array of HOSFETs. The numbers denote the following items: 1 = Chip with array of HOSFETs, 2 = Ag/AgCl (sat'd KCl) reference electrode, and 3 = pT100 temperature sensor.

The FETs are placed on O-rings that define the contacted gate area. The source, drain and bulk contact of each individual FET can be made via spring contacts. In this way a set-up can be created which offers flexibility and easiness in experimental handling.

Receptor groups for functionalized monolayers

There are a number of things that have to be taken into consideration when choosing a suitable receptor for functionalized monolayers. First of all, the cross-sensitivity towards H^+ due to Si-OH sites makes H^+ receptors quite unpractical. Second, the affinity of a receptor towards a desired ion or species should be high enough to guarantee a good measurable sensor output. In case of the 15-crown-5 receptors described in section 6.3.3 this information was not known when the receptor was chosen and the affinity towards Na^+ and K^+ were both too low to give practical output signals. It is expected that the 18-crown-6 receptor is more suitable since it has a much higher affinity towards K^+ than the 15-crown-5 [6]. A third point of attention is the density of receptor groups. In case of oxides the density of X-OH sites can be $5 \cdot 10^{18}$ m^{-2} for SiO_2 up to $1 \cdot 10^{19}$ m^{-2} for Ta_2O_5 [7]. Such high number cannot be reached for receptor groups in planar monolayers. It was estimated that the receptor density in a monolayer with 50% functional groups on <100> silicon is approximately $2 \cdot 10^{18}$ m^{-2} (see Chapter 6, section 6.2). This is expected to give still a good measurable response. However, if it is desired to increase the response it might be an option to distribute the receptors also in height and thus create a 3D receptor network. In this way the receptor density can be increased. Finally, the fourth point of attention is the length of the inert alkyl chains. These chains should not be too low as it may be expected that charge compensation can occur due to ions of the opposite charge. In such cases no measurable output signal is expected. This is illustrated in Figure 7.3

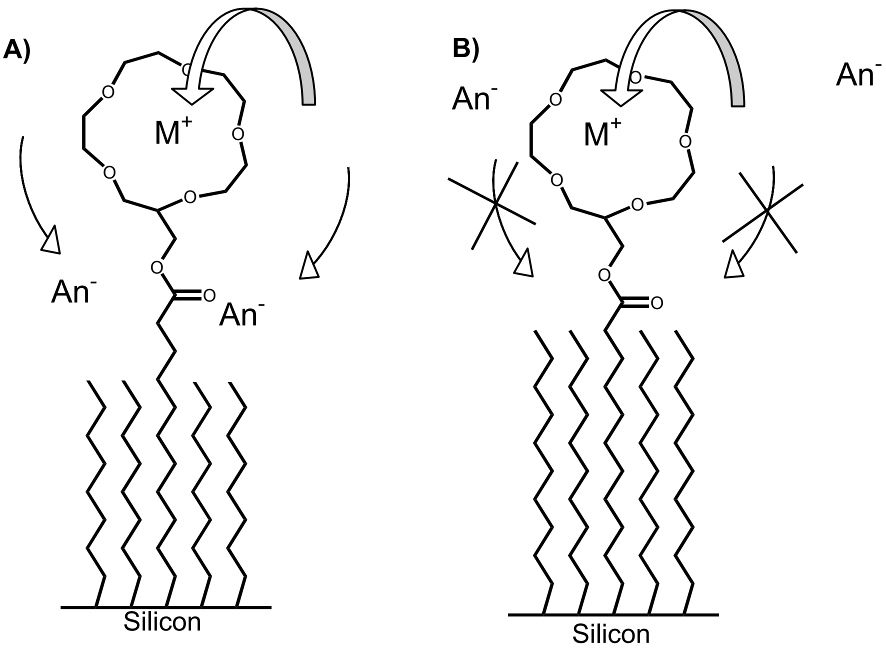

Figure 7.3. A) Charge compensation via anions (An$^-$) upon cation (M$^+$) binding in a crown ether due to too short inert chains. In B) charge compensation is physically not possible due to the long inert chains.

7.3 References

[1] A. B. Sieval, V. Vleeming, H. Zuilhof, E. J. R. Sudhölter, "An improved method for the preparation of organic monolayers of 1-alkenes on hydrogen-terminated silicon surfaces", *Langmuir* **1999**, *15*, 8288.

[2] S. R. Morrison, *Electrochemistry at Semiconductor and Oxidized Metal Electrodes*, Plenum Press, New York, **1980**.

[3] X. G. Zhang, *Electrochemistry of Silicon and its Oxide*, Kluwer Academic Publishers, New York, **2001**.

[4] G. S. Higashi, R. S. Becker, Y. J. Chabal, A. J. Becker, *Comparison of Si(111) Surfaces Prepared Using Aqueous-Solutions of NH_4F Versus HF, Vol. 58*, **1991**.

[5] D. D. M. Wayner, R. A. Wolkow, "Organic modification of hydrogen terminated silicon surfaces", *Journal of the Chemical Society-Perkin Transactions 2* **2002**, 23.

[6] R. M. Izatt, K. Pawlak, J. S. Bradsha, R. L. Bruening, "Thermodynamic and Kinetic Data for Macrocycle Interaction with Cations and Anions", *Chemical Reviews* **1991**, *91*, 1721.

[7] R. E. G. van Hal, J. C. T. Eijkel, P. Bergveld, "A general model to describe the electrostatic potential at electrolyte oxide interfaces", *Advances in Colloid and Interface Science* **1996**, *69*, 31.

Summary

Since their introduction in 1993 the class of covalently bound organic monolayers on oxide free silicon surfaces have found their way to multiple application fields such as passivation layers in solar cells, masking layers in lithographic processing, insulating films in hybrid molecule-silicon electronics, and memory devices. Furthermore, these monolayers can easily be functionalized with a large variety of receptor groups or sensing moieties, thereby forming a new promising material for incorporation in sensory devices such as FET based sensors. In this thesis an overview is given of the electrical and electrochemical characterization of silicon based devices, such as Metal-Insulator-Silicon (MIS) structures, Electrolyte-Insulator-Silicon (EIS) structures and the newly proposed Hybrid Organic Semiconductor FET (HOSFET), with either functionalized or unfunctionalized monolayers incorporated.

After a general introduction in Chapter 1 on the two main topics, Si-C linked monolayers and FET based sensors, a study is presented in Chapter 2 on the influence of silicon surface modification via Si-C_nH_{2n+1} (n = 10, 12, 16, and 22) monolayer-based devices on p-type <100> and n-type <100> silicon. This has been done via the formation of MIS-structures using a mercury probe. From current density - voltage (*J-V*) and capacitance - voltage (*C-V*) measurements a large number of relevant parameters describing the electrical behavior of these devices are derived, amongst others the effective barrier height, the flatband voltage, and the silicon-monolayer fixed charge density. It is shown that the *J-V* behavior of these MIS-structures can be precisely tuned via the monolayer thickness. A similar flatband voltage, independent of monolayer thickness, is found, indicating similar properties for all Si-monolayer interfaces. Furthermore, low values of fixed charges are found for monolayers on p-type silicon ($\sim 6 \cdot 10^{11}$ cm^{-2}). From stability measurements, performed on two separate occasions after months of storage in open air, it is shown that the *J-V* curves stay intact for all samples irrespective of their chain length. For p-type silicon the flatband voltage shifts to more negative values over time, indicating the built in of extra positive charges, which is associated with some oxide formation. The results for devices modified with organic monolayers were superior to devices with SiO_2 insulators of similar thickness.

In a follow-up study presented in Chapter 3 the influences of both the type of monolayer molecule (1-alkene/1-alkyne) and substrate orientation (<100>/<111>) are investigated via Si-$C_{18}H_{37}$ devices on n-type silicon. It is found that 1-alkynes, which are able to make 2 Si-C bonds, have superior insulating properties as compared to 1-alkenes, which make only a single Si-C bond and lead probably to more easily (re)oxidation of remaining surface Si-H bonds. No noticeable influence of substrate orientation is found. XPS measurements confirm the higher degree of oxidation at samples of both substrates with monolayers made from 1-alkenes.

However, in contrast to findings from electrical characterization XPS measurements also show an overall higher amount of oxide on <111> samples as compared to <100> samples. The results from both studies suggest that Si-C linked monolayers, preferably 1-alkynes, on flat silicon may be a viable material for future, hybrid molecular-silicon devices.

Chapter 4 focuses on a measurement method for determining the sensory responses of EIS-structures. Normally, these are determined via capacitance – voltage (*C-V*) curves. However, in case of nm-thin insulators, such as Si-C linked monolayers, *C-V* curves are often distorted, which makes it impossible to derive the sensory response in a straightforward way. Via the proposed method, Mott Schottky measurements, it is still possible to derive the sensory response as was shown and verified via measurements on EIS-structures with thick and thin insulators. The non-idealities encountered during Mott Schottky measurements are also discussed as well as how to deal with these non-idealities.

The work described in Chapter 5 focuses on the electrochemical behavior and characterization of Si-C linked, organic monolayers in EIS-structures prior to incorporation in full sensors. It is shown that p-type silicon electrodes modified with $-C_nH_{2n+1}$ (n = 12, 16, and 22) monolayers become (partially) oxidized when operated under anodic bias voltages. Similar electrodes of n-type silicon, unless illuminated, do not show oxidative behavior but the formation of hydrogen gas is observed for large cathodic potentials. Oxide formation can lead to a sensitivity of the modified electrode towards *pH* changes due to (de)protonation of Si-OH groups. This is investigated via titration experiments, subsequential data analysis via Mott Schottky analysis and data fitting using a site-binding model to compare such monolayers with pure SiO_2 layers and SiO_2 layers modified with HMDS. All samples display *pH* sensitivity. In case of samples with Si-C linked monolayers the amount of Si-OH groups is estimated to be merely 0.32 - 0.64 % of a pure SiO_2 insulator. The pK_a value of all samples with monolayers (4.0 - 4.4) is lowered as compared to pure SiO_2 (6.0) indicating a more acidic behavior of the Si-OH groups as compared to pure SiO_2. Values for the long-term drift of approximately 1 $mV \cdot h^{-1}$ are found for samples with organic monolayers.

Chapter 6 contains a collection of results on ion-sensing measurements with Hybrid Organic Semiconductor FETs (HOSFETs) and EIS-structures with functionalized monolayers consisting of mixed monolayers of crown ether (15-crown-5) functionalized and inert monolayers. As a reference HOSFETs and EIS-structures with neat $-C_{10}H_{21}$ monolayers or pure SiO_2 have been used. Via Na^+ and K^+ titration measurements on the above mentioned devices the highest sensitivity towards both cations has been found for SiO_2, followed by the functionalized monolayers whereas no sensitivity at all has been found for the inert monolayers. The fact that inert monolayers are insensitive towards cations shows the potential of these monolayers in creating sensing structures made from silicon modified with Si-C linked monolayers. The low responses of the HOSFETs and EIS-structures with functionalized monolayers can most likely be attributed to poor binding properties of the chosen receptor and not to deficiencies of the supporting silicon-monolayer device.

Samenvatting

Covalent gebonden organische monolagen op oxidevrije silicium oppervlakken hebben sinds de introductie in 1993 hun weg gevonden in meerdere toepassingen. Die toepassingen zijn passivatielagen in zonnecellen, maskerlagen in lithografische processen, isolerende films in hybride molecuul-silicium elektronica en elektronische geheugens. Bovendien kunnen deze lagen eenvoudig gefunctionaliseerd worden met een grote verscheidenheid aan receptorgroepen. Hierbij wordt een veelbelovend materiaal gevormd voor toepassing in sensoren waaronder de klasse van de op FET gebaseerde sensoren. In dit proefschrift wordt een overzicht gegeven van de elektrische en elektrochemische karakterisatie van op silicium gebaseerde structuren. Dat zijn Metaal-Isolator-Silicium (MIS) structuren, Electroliet-Isolator-Silicium (EIS) structuren en de hier geïntroduceerde Hybrid Organic Semiconductor FET (HOSFET) waarbij allen gemodificeerd zijn met gefunctionaliseerde dan wel met ongefunctionaliseerde monolagen.

Na een algemene inleiding in Hoofdstuk 1, wordt in Hoofdstuk 2 de invloed behandeld van silicium oppervlakmodificatie van Si-C_nH_{2n+1} (n = 10, 12, 16 en 22) structuren op p-type <100> en n-type <100> silicium. Dit is gebeurd door het vormen van MIS-structuren met behulp van een kwikprobe. Door metingen van zowel stroomdichtheid-spanning (*J-V*) als capaciteit-spanning (*C-V*) relaties zijn de nodige relevante parameters afgeleid die het elektronische gedrag van deze structuren beschrijven: de effectieve barrièrehoogte, de vlakkebandspanning en de vaste ladingsdichtheid in het silicium-monolaag grensvlak. Er is aangetoond dat het *J-V* gedrag van deze MIS-structuren precies afgestemd kan worden door de ketenlengte van de monolaag. De vlakkebandspanning is gelijk voor alle structuren, ongeacht de ketenlengte. Dit duidt op gelijke eigenschappen van alle silicium-monolaag grensvlakken. Bovendien is een zeer lage vaste ladingsdichtheid ($\sim 6\cdot10^{11}$ cm^{-2}) gevonden bij monolagen op p-type silicium. Via stabiliteitsmetingen wordt duidelijk dat de *J-V* plots stabiel blijven voor alle samples, ongeacht ketenlengte. Bij p-type silicium verschuift de vlakkebandspanning in de tijd naar meer negatievere waarden, hetgeen oxidevorming impliceert. De resultaten voor structuren met monolagen waren superieur in vergelijking met SiO_2 isolatoren van gelijke dikte.

In het daarop volgende Hoofdstuk 3 worden de invloeden van zowel het type monolaag molecuul (1-alkene/1-alkyne) als de substraatoriëntatie (<100>/<111>) onderzocht via Si-$C_{18}H_{37}$ structuren op n-type silicium. Aangetoond wordt dat 1-alkynen, die 2 Si-C bindingen kunnen maken, betere isolerende eigenschappen hebben dan 1-alkenen, die slechts één enkele Si-C binding maken, hetgeen waarschijnlijk leidt tot een gemakkelijkere oxidatie van overgebleven Si-H bindingen. Er is geen merkbare invloed van substraatoriëntatie waargenomen. XPS-metingen bevestigen het hogere gehalte oxide op structuren van beide oriëntaties gemodificeerd met monolagen van 1-alkenen. In tegenstelling tot de bevindingen met de elektrische metingen is echter via XPS aangetoond dat voor alle structuren op <111> oppervlakken de hoeveelheid oxide hoger ligt dan op de <100> oppervlakken. De resultaten van beide studies tonen aan dat Si-C gelinkte monolagen, bij voorkeur gemaakt van 1-alkynen, op vlak silicium een veelbelovend materiaal vormen voor toekomstige hybride molecuul-silicium apparaten.

In Hoofdstuk 4 wordt een meetmethode behandeld voor het bepalen van *pH* responsies van EIS-structuren. Deze worden gewoonlijk bepaald via *C-V* curven. In het geval van nm-dunne isolatoren, zoals Si-C gelinkte monolagen, zijn deze *C-V* curven vaak dusdanig vervormd dat de responsies daaruit niet meer eenduidig zijn af te leiden. Via de voorgestelde methode, Mott Schottky metingen, blijkt het wel mogelijk te zijn deze responsies te bepalen, zoals aangetoond via metingen aan EIS-structuren met zowel dikke als dunne isolatoren. Tevens worden de niet-idealiteiten, zoals waargenomen tijdens Mott Schottky metingen, behandeld.

In Hoofdstuk 5 worden het elektrochemische gedrag en de karakterisering behandeld van EIS-structuren met ongefunctionaliseerde, Si-C gelinkte monolagen. Het blijkt dat p-type silicium gemodificeerd met $-C_nH_{2n+1}$ (n = 12, 16 en 22) monolagen (gedeeltelijk) oxideert als deze met een anodische biasspanning aangestuurd wordt. Soortgelijke elektrodes van (onbelicht) n-type silicium oxideren niet, maar hier ontstaat waterstofgasontwikkeling bij het aansturen met een hoge kathodische spanning. Oxidevorming kan resulteren in een *pH* gevoeligheid bij zulke elektrodes vanwege het (de)protoneren van (gevormde) Si-OH groepen. Dit laatste is verder onderzocht via titratie-experimenten, data analyse en het data fitten d.m.v. een site-binding model teneinde het gedrag van zulke monolagen te vergelijken met pure SiO_2 lagen en SiO_2 lagen gemodificeerd met HMDS. Alle structuren vertonen een *pH* gevoeligheid. Voor de structuren met Si-C gelinkte monolagen wordt het gehalte Si-OH groepen geschat op slechts 0.32 - 0.64 % van een pure SiO_2 isolator. De pK_a waarde van alle structuren met monolagen (4.0 - 4.4) is lager dan van puur SiO_2 (6.0), hetgeen duidt op een zuurder gedrag van die Si-OH groepen in vergelijking met puur SiO_2. Waarden voor de lange termijn drift zijn ongeveer 1 $mV \cdot h^{-1}$ voor alle structuren met monolagen.

Hoofdstuk 6 bevat de resultaten van ionmetingen met HOSFETs en EIS-structuren met gefunctionaliseerde monolagen bestaande uit gemengde monolagen van kroonether (15-crown-5) gefunctionaliseerde en inerte monolagen. Als referentie zijn getest HOSFETs en EIS-structuren met pure $-C_{10}H_{21}$ monolagen en puur SiO_2. Via Na^+ en K^+ titratiemetingen op bovengenoemde structuren is de hoogste gevoeligheid voor beide cationen gevonden voor SiO_2, gevolgd door de gefunctionaliseerde monolagen, terwijl de inerte monolagen helemaal geen gevoeligheid vertonen. Deze laatste bevinding toont de mogelijkheden tot het maken van sensorstructuren van silicium met Si-C gelinkte monolagen. De lage gevoeligheden van de HOSFETs en EIS-structuren met gefunctionaliseerde monolagen zijn hoogstwaarschijnlijk veroorzaakt door de slechte bindingseigenschappen van de gekozen receptor en niet door enige tekortkomingen van de onderliggende silicium-monolaag structuur.

Gearfetting

Kovalint ferbûne organyske monolagen op oksydefrije silisium oerflakken hawwe sûnt de yntroduksje yn 1993 harren wei fûn yn in ferskaat oan tapassingen. Dat binne passivitaasjelagen yn sinnesellen, maskerlagen yn litografyske prosessen, isolearjende films yn hybride molekuul-silisium-elektroanika en elektroanyske ûnthâlden. Boppedat kinne dizze lagen ienfâldich funksjonalisearre wurde mei in grut ferskaat oan resepsjegroepen. Hjirby wurdt in materiaal mei gâns ûnthjit foarme foar tapassing yn sensoaren mei dêrûnder de klasse fan de op FET basearre sensoaren. Yn dit proefskrift wurdt in oersjoch jûn fan de elektryske en elektrogemyske karakterisearring fan op silisium basearre struktueren. Dat binne Metaal-Isolator-Silisium (MIS) struktueren, Elektrolyt-Isolator-Silisium (EIS) struktueren en de hjir yntrodusearre Hybrid Organic Semiconductor FET (HOSFET) wêrby't alle modifisearre binne mei funksjonalisearre as wol mei ûnfunksjonalisearre monolagen.

Nei in algemiene ynlieding yn Haadstik 1, wurdt yn Haadstik 2 de ynfloed behannele fan silisium oerflakmodifikaasje fan Si-C_nH_{2n+1} (n = 10, 12, 16 en 22) struktueren op p-type <100> en n-type <100> silisium. Dit is bard troch it foarmjen fan MIS-struktueren mei help fan in kwikprobe. Troch mjittingen fan sawol de streamtichtheid-spanning (*J*-*V*) as kapasiteit-spanning (*C*-*V*) relaasjes binne de nedige relevante parameters ôflaat dy't it elektroanyske gedrach fan dizze struktueren beskriuwe: de effektive barrièrehichte, de flakkebânspanning en de fêste ladingstichtheid in it silisium-monolaach grinsflak. Der is oantoand dat it *J*-*V* gedrach fan dizze MIS-struktueren presys ôfstimd wurde kin troch de ketenlingte fan de monolaach. De flakkebânspanning is lyk foar alle struktueren, nettsjinsteande de ketenlingte. Dat tsjut op like eigenskippen fan alle silisium-monolaach grinsflakken. Boppedat is in tige lege fêste ladingstichtheid ($\sim 6{\cdot}10^{11}$ sm^{-2}) fûn by monolagen op p-type silisium. Troch stabiliteitsmjittingen wurdt dúdlik dat de *J*-*V* plots stabyl bliuwe foar alle samples, nettsjinsteande keatlinglingte. By p-type silisium ferskoot de oerflaktespanning yn de tiid nei mear negativere wearden, itjinge oksydefoarming ymplisearret. De resultaten foar struktueren mei monolagen wienen superieur yn ferliking mei SiO_2 isolatoaren fan likense dikte.

Yn it dêrnei folgjende Haadstik 3 wurde de ynfloeden fan sawol it type monolaach molekuul (1-alkene/1-alkyne) as de substraatoriïntaasje (<100>/<111>) ûndersocht mei Si-$C_{18}H_{37}$ struktueren op n-type silisium. Oantoand wurdt dat 1-alkynen, dy't 2 Si-C biningen meitsje kinne, bettere isolearjende eigenskippen hawwe as 1-alkenen, dy't mar ien inkelde Si-C bining meitsje, itjinge wierskynlik laat ta in maklike oksydaasje fan oerbleaune Si-H biningen. Der is gjin merkbere ynfloed fan substraatoriïntaasje waarnommen. XPS mjittingen befêstigje it hegere gehalte oksyde op struktueren fan beide oriïntaasje modifisearre mei monolagen fan 1-alkenen. Yn tsjinstelling ta de befiningen mei de elektryske mjittingen is lykwols mei XPS oantoand dat foar alle struktueren op <111> oerflakken de hoemannichte oksyde heger leit as op de <100> oerflakken. De resultaten fan beide stúdzjes litte sjen dat Si-C linkte monolagen, by foarkar makke fan 1-alkynen, op flak silisium in materiaal mei gâns ûnthjit foarmje foar takomstige hybride molekuul-silisium apparaten.

Yn Haadstik 4 wurdt in mjitmetoade behannele foar it fêststellen fan *pH* responsys fan EIS-struktueren. Dizze wurde ornaris bepaald mei *C-V* kurven. Yn it gefal fan nm-tinne isolatoaren, lykas Si-C linkte monolagen, binne dizze *C-V* kurven faak sa ferfoarme dat de responsys dêrút net mear op ienderlei wize ôf te lieden binne. Troch de útstelde metoade, Mott Schottky mjittingen, blykt it wol mooglik te wêzen dizze responsys fêst te stellen, lykas oantoand troch mjittingen oan EIS-struktueren mei sawol dikke as tinne isolatoaren. Tagelyk wurde de net-idealiteiten, lykas waarnommen by Mott Schottky mjittingen, behannele.

Yn Haadstik 5 wurde it elektrogemyske gedrach en de karakterisearring behannele fan EIS-struktueren mei ûnfunksjonalisearre, Si-C linkte monolagen. It docht bliken dat p-type silisium modifisearre mei -C_nH_{2n+1} (n = 12, 16 en 22) monolagen (foar in part) oksydearret as dizze mei in anodyske biasspanningen oanstjoerd wurdt. Soartgelikense elektroden fan (ûnbeljocht) n-type silisium oksydearje net, mar hjir ûntstiet wetterstofgasfoarming by it oanstjoeren mei in hege katodyske spanning. Oksydefoarming kin resultearje yn in *pH* gefoeligens by sokke elektrodes fanwege it (de)protonearjen fan (foarme) Si-OH groepen. Dit lêste is fierder ûndersocht mei titrasy-eksperiminten, data analyze en it datafitten t.m.f. in site-bining model mei it doel it gedrach fan sokke monolagen te ferlykjen mei suvere SiO_2 lagen en SiO_2 lagen modifisearre mei HMDS. Alle struktueren litte in *pH* gefoeligens sjen. Foar de struktueren mei Si-C linkte monolagen wurdt it gehalte Si-OH groepen skat op 0.32 - 0.64 % fan in suvere SiO_2 isolator. De pK_a wearde fan alle struktueren mei monolagen (4.0 - 4.4) is leger as fan suver SiO_2 (6.0), wat tsjut op in soerder gedrach fan dy Si-OH groepen yn ferliking mei suver SiO_2. Wearden foar de lange termyn drift binne likernôch 1 $mV \cdot h^{-1}$ foar alle struktueren mei monolagen.

Haadstik 6 befettet de resultaten fan ionmjittingen mei HOSFETs en EIS-struktueren mei funksjonalisearre monolagen besteande út mingde monolagen fan kroaneter (15-crown-5) funksjonalisearre en inerte monolagen. As referinsje binne test HOFSETs en EIS-struktueren mei suvere -$C_{10}H_{21}$ monolagen en suver SiO_2. Troch Na^+ en K^+ titrasymjittingen op boppeneamde struktueren is de heechste gefoeligens foar beide kationen fûn foar SiO_2, folge troch de funksjonalisearre monolagen, wylst de inerte monolagen hielendal gjin gefoeligens sjen lieten. Dizze lêste fêststelling lit de mooglikheid sjen foar it meitsjen fan sensorstruktueren fan silisium mei Si-C linkte monolagen. De lege gefoeligens fan de HOFSETs en EIS-struktueren mei funktionalisearre monolagen is nei alle gedachten feroarsake troch de minne biningseigenskippen fan de keazen reseptor en net troch hokker tekoartkommings dan ek fan de ûnderlizzende silisium-monolaach struktuer.

Dankwoord

Dan komt nu het belangrijkste onderdeel van het proefschrift: het dankwoord. Promoveren doe je (gelukkig) niet alleen hoewel de gevoelsbelevenis soms zo wel kan zijn. Ik had mezelf niet dit boekje zien schrijven zonder de hulp en steun van vele mensen en ik zal hier dan ook een poging wagen om velen daarvan persoonlijk te bedanken. Merk je dat je niet wordt genoemd dan is er geen sprake van kwade opzet en dus zeg ik nu op voorhand: bedankt iedereen!

Allereerst wil ik mijn promotor Albert van den Berg bedanken voor alle vrijheid en coaching gedurende deze periode. Je hebt me altijd scherp gehouden, niet alleen door je hoge energieniveau, maar vooral door het einddoel niet uit het oog te verliezen en me te wijzen op al te vage of theoretische invalshoeken die ik wel eens poogde in te slaan. Als theoretische graver schrok praktisch denken me in het begin erg af. Evenwel aan het eind merk ik toch dat praktisch en resultaatgericht denken best handig zijn om tot een tastbaar resultataat te komen; bedankt daarvoor. Mijn promotor van het eerste jaar Piet Bergveld wil ik ook graag bedanken voor de begeleiding in dat jaar en later tijdens gebruikerscommissievergaderingen of als je langskwam op de woensdag. Je originele invalshoeken en aansporing om het vooral eerst maar eens simpel te proberen waren een verrijking voor mijn kijk op techniek (en soms ook op mensen); tige tank! Mijn dagelijks begeleider en assistent promotor Wouter Olthuis wil ik ook graag bedanken voor de degelijke ondersteuning gedurende de afgelopen vier jaar. Je deur stond altijd open en je was altijd bereid om al mijn ideeën, resulaten en tegenslagen aan te horen. Je laat iedereen altijd helemaal in zijn waarde en geeft iedereen de vrijheid. Dat het een hele kunst is om daar mee om te kunnen gaan, heb ik ook moeten leren in die vier jaar. Gelukkig slaagde je erin me altijd weer terug op aarde krijgen; enorm bedankt voor alles. Ik hoop wel dat ik je ooit nog enthousiast kan maken voor muziek van na 1750.

Louis de Smet (Wageningen Universiteit) wil ik hartelijk danken voor een leuke en leerzame samenwerking en niet te vergeten de gastvrijheid (en die van je huisgenoten) tijdens mijn verblijven in Wageningen. Hoewel het niet meeviel om de werelden van chemie en elektrotechniek samen te brengen en het voor mij zeker een x aantal maanden heeft geduurd om de taal van chemici te doorgronden, heb ik het uiteindelijk als absolute meerwaarde ervaren om twee schijnbaar vreemde werelden te verenigen. Zo zijn er zeer leuke resultaten uit dit project gekomen; het geheel is meer dan de som der delen. Ook Han Zuilhof en Ernst Sudhölter wil ik hartelijk danken voor hun nimmer aflatende enthousiasme en ondersteuning in dit project. Ik hoop dat we in de toekomst op dezelfde voet verder zullen gaan.

Dan komen nu eindelijk de andere Bioboys & -girls; ik heb de BIOS groep als een bijzonder prettige omgeving ervaren. Het is niet een groep waar iedereen weggestopt zit in zijn eigen kamer en eens per jaar voor een gezamenlijk uitje elkaar eens verbaasd tegenkomt maar een dynamische groep waarin behalve hard werken, gezelligheid en onderlinge interactie altijd aanwezig zijn en zo de juiste mix van inspanning met ontspanning verkregen wordt. Allereerst wil ik bij naam de lunch- en wandelvrienden Sebastiaan (pc goeroe) Herber, Erik (ErikK) Krommenhoek en Koen van Delft dank zeggen voor hun dagelijks stipte (12:15 precies) doorbreken van de ochtend en het plezierig inluiden van de middagen met allerlei vooral niet werkgerelateerde gesprekken. Sebastiaan en Erik ook nog bedankt voor het beantwoorden van al mijn vragen op chemie- en computergebeid. Mijn kamergenoten (in chronologische volgorde) Björn Timmer, Dorothee (Doro) Hermes, Dragana Mijatovic en meest recente aanwinst Georgette ("mag de radio aan?") Salieb ben ik zeer dankbaar voor de plezierige sfeer op kamer 6240. Speciale dank gaat uit naar Doro voor het gezelligheidsstreven buiten werkuren door het organiseren van allerlei evenementen. Johan ("alles kan gemaakt worden van silicium, glas of plastic") Bomer ben ik dankbaar voor al zijn hulp op technisch vlak. In dit project werden mijn twee linkerhanden gelukkig ruimschoots gecompenseerd door jouw kunde om allerlei exotische wafers, houders en apparaten te maken; heel erg bedankt daarvoor. Ad ("alles kan gemaakt worden met elektronica, het liefst met maar 1 opamp") Sprenkels dank ik voor zijn hulp op elektronisch gebied en voor alle gesprekken al dan niet over elektronica. Jan Eijkel (het sociale bindmiddel binnen de groep) wil ik graag bedanken voor zijn immer luisterend oor en eerlijke respons en niet te vergeten de invoering van de "vrijdagmiddagpraatjes", een uitgelezen kans om elkaar beter te leren. Heiko (KABOEM) van der Linden dank ik voor de lol in de eerste jaren in de groep en daarbuiten (p.s. het EL gebouw staat er nog steeds). Sjouke (KABOEM^2) Hornstra en Ton Jenneboer ben ik dank verschuldigd voor de computerondersteuning. Hermine en Ida dank ik voor het op tijd invullen van lastige formulieren en alle administratieve ondersteuning. Zonder de hulp en steun van twee afstudeerstudenten, Wilrike Groeneveld en Wouter Sparreboom was dit proefschrift niet zo dik geworden. Ik ben jullie veel dank verschuldigd voor jullie inzet en wens jullie veel succes in de toekomst, al dan niet als AIO. De rest van de (ex-) medewerkers mag natuurlijk niet vergeten worden: Han, Joke, Monica, Celio, Severine, Regina, Roald, Anil, Jacob, Woitek, Jurjen, Patrick, Wim, Kevin, Lingling, Ana, Floor, Egbert, Paul, Jan v. N., Gabriël, Ton V., Rob en Annie, dank jullie wel.

Ook buiten de vakgroep hebben talloze mensen op de universiteit bijgedragen tot een fijne sfeer tijdens mijn verblijf op de universiteit. Allereerst wil ik Ed Droog noemen; je deur (en componentenbak ook gelukkig) was altijd open. Je stond altijd klaar om mensen even tussendoor te helpen of voor de gek te houden; bedankt voor allebei. Cora Salm, Marcel Weusthof en Henk de Vries van vloer 3 worden bedankt voor hun hulp bij de metingen uit Hoofdstuk 2 en 3. De cleanroom smurfen Samantha en Marjon dank ik voor de spontane en gezellige lunchafspraken; tevens wil ik graag de rest van de cleanroom staf bedanken voor hun hulp en begeleiding bij mijn weg door de cleanroom. Voor de wat meer oorverdovende en pijngrens overschrijdende afleiding zorgden Willem ("beat the drums, not eat ...") Vos, Raymond ("I'm sailing...") Oudeboon en Paul (Hendrix) Bonsma, aangevuld met ondergetekende bassist tot de band Whipp'm; met veel plezier heb ik met jullie in de pauzes gejamd en geoefend, ik hoop dat er nog een keer een reünie komt. Van de vakgroep SMI wil ik graag Alexander, Martin en Mink bedanken voor gezellige afleiding. Mink wil ik graag extra bedanken voor de wandelingen in de pauzes, eet-, praat- en stapavonden en andere afleidingen die het leven in Enschede meerwaarde geven. Van de Universiteit Utrecht wil ik graag Harold Philipsen en John Kelly bedanken voor de gastvrijheid en hulp tijdens een aantal weken dat ik daar metingen verrichtte. De leden van de gebruikerscommissie wil ik graag bedanken voor hun ondersteuning en input. Marcel Grote Gansey, Henk van Halen, Jan van der Tuin, Erik Hartholt en Luuk Salverda (Sentron) dank ik voor hun hulp en inzet bij de HOSFET gerelateerde zaken.

Buiten de universiteit om zijn er ook veel mensen geweest die het leven in Enschede opvrolijkten en voor de broodnodige afleiding zorgden. De Campuslaan 35 (harde kern) groep bestaande uit Wim, Hans-Willem (HW), Rob, Jiri, Arjen, Pieter, Ilse en later aangevuld met Otto hebben van het wonen en leven in Enschede een onvergetelijke gebeurtenis gemaakt; ontzettend bedankt allemaal.

Als Enschede wat te klein werd bevonden vond ook buiten Enschede de nodige afleiding plaats. Hiervoor zijn o.a. verantwoordelijk een clubje mensen uit de Friese klei, Leeuwarden om precies te zijn. Tineke, Rufus, Hans, Jeroen en Mirjam, Arnold en Miranda, Hedzer en Astrid, Rene en Esther, Jouke en Sjoukje heel erg bedankt voor jullie belangstelling en vriendschap.

Zonder muziek zou mijn leven er heel wat saaier hebben uitgezien en er zijn een aantal muzikanten die samen met mij de nodige dBs wilden produceren: allereerst is er MADCAP uit Leeuwarden bestaande uit Roeland (Roel), Roman (Ro), Erwin (de "H") en Martijn (Dijkstraal); jongens ontzettend bedankt voor alle lol in de oefenruimte en daarbuiten, vaak aangevuld met Trudy, Antonia, Reinus, Marten en ander gespuis. In Enschede kwam er later Sixer bestaande uit Leo (ik "mod" alles), Arjan (Da Voice), Gwen (de high-energy DJ), Gert-Jan (Trashmaster, alias grootkanselier van Twente) en Wim(my Hendrix); jongens en dame ontzettend bedankt voor de dinsdagavond afleiding en lol met zijn allen. Gauw eens wat optredens regelen.

Anna en de familie Solowska wil ik heel graag bedanken voor de immer aanwezige gastvrijheid en warmte die ik altijd heb mogen ervaren in Wageningen, Utrecht en Polen.

Natuurlijk mag zeker niet mijn familie ontbreken. Mijn ouders Rients en Dineke en broer Chris wil ik enorm bedanken voor hun onvoorwaardelijke steun die ik al heel mijn leven heb mogen ontvangen. Eigenlijk zijn woorden niet toereikend genoeg om dat te beschrijven ...

De afsluitende woorden zijn bedoeld voor mijn lieve vriendin Amber, de mooiste combinatie die tussen Nederland en Egypte ontstaan kan; hoewel ik je nu bijna twee jaar ken, heb je me al meer laten zien van het leven dan ik in heel mijn studie plus promotietijd heb geleerd. Inhoudelijk begreep je vaak geen snars van wat ik deed en daar ben ik ook heel blij om; er bleef zo namelijk altijd een andere wereld over waar ik bij jou in kon vertoeven. Ik beloof je dat ik nu iets meer tijd over heb in de weekenden en ik dank je voor al je liefde en geduld.

Erik

Curriculum Vitae

Erik Faber is geboren op 24 maart 1976 te Leeuwarden in Nederland. Nadat hij aldaar in 1994 het V.W.O had doorlopen, begon hij aan de studie Elektrotechniek bij de Noordelijke Hogeschool Leeuwarden. Gedrurende deze opleiding liep hij twee stages: van september 1996 tot en met januari 1997 aan het Kernfysisch Versneller Instituut te Groningen en van februari 1997 tot en met juni 1997 bij de Shell Rafinaderiet te Fredericia, Denemarken. In Groningen werkte hij mee aan een hoogfrequent versterker voor het detecteren van ionenbundels; in Denemarken werkte hij mee aan meerdere opdrachten, waaronder een onderzoek naar een zelfstandig foutdetectiesysteem voor dubbel uitgevoerde sensoren in oliepijpleidingen. Van februari 1998 tot en met juni 1998 verrichte hij zijn afstudeeronderzoek bij Friesland Coberco Dairy Foods te Leeuwarden. Zijn werk bestond uit vooronderzoek naar een barcodesysteem voor interne en externe goederen-transporten.

Na het behalen van het HTS-diploma in 1998 vervolgde hij de studie in de elektrotechniek via een kopstudie aan de Universiteit Twente. Tijdens deze opleiding nam hij deel aan een studiereis in november-december 2000 naar Japan, Taiwan en Singapore, en daarna verrichtte hij van februari 2001 tot en met januari 2002 zijn afstudeeronderzoek bij de leerstoel biosensoren, onder leiding van de voormalige leerstoelhouder prof. P. Bergveld en dr. W. Olthuis. Het afstudeeronderzoek bestond uit het verbeteren van interface electronica voor het uitlezen van een Ta_2O_5 geleidbaarheidssensor.

Van februari 2002 tot en met januari 2006 trad hij als promovendus in dienst bij de leerstoel biosensoren aan de Universiteit Twente. Hij verrichtte hier onder leiding van prof. Van den Berg en dr. W. Olthuis onderzoek naar de elektrische en electrochemische karakterisering van de Hybrid Organic Semiconductor FET (HOSFET). De resultaten van dat werk zijn beschreven in dit proefschrift.